

On the Regulation of Chromosome Segregation in Human Cells

-

Implications of Bub1 Kinase Inhibition During Cell Division

Inauguraldissertation

zur Erlangung der Würde eines Doktors der Philosophie
vorgelegt der
Philosophisch-Naturwissenschaftlichen Fakultät
der Universität Basel

von

Anna Pauline Baron
aus Deutschland
Basel, 2015

Originaldokument gespeichert auf dem Dokumentenserver der Universität
Basel edoc.unibas.ch

Dieses Werk ist unter dem Vertrag „Creative Commons Namensnennung-Keine
kommerzielle Nutzung-Keine Bearbeitung 3.0 Schweiz“ (CC BY-NC-ND 3.0 CH)
lizenziiert. Die vollständige Lizenz kann unter creativecommons.org/licenses/by-nc-nd/3.0/ch/ eingesehen werden.



Namensnennung-Keine kommerzielle Nutzung-Keine Bearbeitung 3.0 Schweiz
(CC BY-NC-ND 3.0 CH)

Sie dürfen: Teilen — den Inhalt kopieren, verbreiten und zugänglich machen

Unter den folgenden Bedingungen:



Namensnennung — Sie müssen den Namen des Autors/Rechteinhabers in der von ihm festgelegten Weise nennen.



Keine kommerzielle Nutzung — Sie dürfen diesen Inhalt nicht für kommerzielle Zwecke nutzen.



Keine Bearbeitung erlaubt — Sie dürfen diesen Inhalt nicht bearbeiten, abwandeln oder in anderer Weise verändern.

Wobei gilt:

- **Verzichtserklärung** — Jede der vorgenannten Bedingungen kann **aufgehoben** werden, sofern Sie die ausdrückliche Einwilligung des Rechteinhabers dazu erhalten.
- **Public Domain (gemeinfreie oder nicht-schützbarer Inhalte)** — Soweit das Werk, der Inhalt oder irgendein Teil davon zur Public Domain der jeweiligen Rechtsordnung gehört, wird dieser Status von der Lizenz in keiner Weise berührt.
- **Sonstige Rechte** — Die Lizenz hat keinerlei Einfluss auf die folgenden Rechte:
 - Die Rechte, die jedermann wegen der Schranken des Urheberrechts oder aufgrund gesetzlicher Erlaubnisse zustehen (in einigen Ländern als grundsätzliche Doktrin des **fair use** bekannt);
 - Die **Persönlichkeitsrechte** des Urhebers;
 - Rechte anderer Personen, entweder am Lizenzgegenstand selber oder bezüglich seiner Verwendung, zum Beispiel für **Werbung** oder Privatsphärenschutz.
- **Hinweis** — Bei jeder Nutzung oder Verbreitung müssen Sie anderen alle Lizenzbedingungen mitteilen, die für diesen Inhalt gelten. Am einfachsten ist es, an entsprechender Stelle einen Link auf diese Seite einzubinden.

Genehmigt von der Philosophisch-Naturwissenschaftlichen Fakultät auf Antrag
von

Prof. Dr. Erich A. Nigg

Prof. Dr. Christoph Handschin

Basel, den 10. November 2015

Prof. Dr. Jörg Schibler
Dekan

Table of Contents

1. Summary	1
2. Introduction	5
2.1 The Cell Cycle.....	6
2.1.1 <i>Mitosis</i>	10
2.1.2 <i>Cell Cycle Checkpoints</i>	12
2.2 The Spindle Assembly Checkpoint	15
2.2.1 <i>Molecular basis of the mitotic checkpoint</i>	16
2.2.2 <i>Cell fates after a SAC-mediated cell cycle arrest</i>	20
2.3 The Mechanism of Chromosome Alignment.....	21
2.4 Chromosome Cohesion – Hold and Release.....	24
2.5 Mitotic Kinases – Regulation by Phosphorylation.....	27
2.5.1 <i>Budding uninhibited by benzimidazole (Bub1)</i>	30
2.5.2 <i>Mitotic kinase inhibitors as anti-cancer agents</i>	33
2.6 Phosphoproteomics	35
2.7 Quantification of Phosphorylated and Unphosphorylated Peptides	36
2.7.1 <i>DDA – Data dependent acquisition</i>	38
2.7.2 <i>Directed Mass Spectrometry</i>	39
2.7.3 <i>Targeted Mass Spectrometry</i>	40
2.7.4 <i>Higher stage fragmentation of the neutral loss peaks</i>	42
3. Results	45
3.1 Probing the catalytic functions of Bub1 kinase using small molecule inhibitors BAY-320 and BAY-524	47
3.1.1 <i>Aim of the project</i>	47
3.1.2 <i>Introduction</i>	48
3.1.3 <i>The inhibitors BAY-320 and BAY-524 specifically inhibit Bub1 kinase in vitro and in vivo</i>	50
3.1.4 <i>Inhibition of Bub1 kinase activity</i>	55
3.1.5 <i>Catalytic activity of Bub1 regulates Shugoshin localization and chromatid cohesion</i>	61
3.1.6 <i>Bub1 inhibition affects the CPC</i>	64
3.1.7 <i>Bub1 and Haspin inhibition have an additive effect on CPC recruitment to centromeres</i>	70
3.1.8 <i>Bub1 inhibition produces minor effects on SAC signaling in HeLa or RPE1 cells</i>	74
3.1.9 <i>Bub1 inhibition does not significantly interfere with chromosome congression</i>	82
3.1.10 <i>Bub1 inhibition sensitizes HeLa cells to clinically relevant doses of Paclitaxel</i>	86

3.2	Evaluation of data-dependent and –independent mass spectrometric workflows for sensitive quantification of proteins and phosphorylation sites	90
3.2.1	<i>Aim of the Project</i>	90
3.2.2	<i>Author contributions</i>	90
3.2.3	<i>First-author publication</i>	92
3.2.4	<i>Supporting Information</i>	109
4.	General Discussion & Outlook	127
4.1	BAY-320 and BAY-524: novel tools to probe Bub1 function	129
4.1.1	<i>Validation of BAY-320 and BAY-524 as Bub1 inhibitors</i>	130
4.1.2	<i>Impact of Bub1 inhibition on mitotic progression</i>	131
4.1.3	<i>Bub1 inhibition and its potential therapeutic influence</i>	134
4.1.4	<i>Future prospects</i>	135
4.2	The evolution of phospho-peptide quantification	136
5.	Material and Methods	139
5.1	Preparation of BAY-320 and BAY-524 inhibitors	141
5.2	Determination of IC ₅₀ -concentrations	141
5.3	Kinase selectivity profiling	141
5.4	In vitro kinase assay	141
5.5	Cell Culture.....	142
5.6	Transient plasmid transfection and siRNA-mediated protein depletion	143
5.7	Fluorescence-activated cell sorting	143
5.8	Cell extracts and sample preparation for Western blot analysis	143
5.9	Histone Isolation	144
5.10	Antibodies.....	144
5.11	Immunofluorescence microscopy, image processing, quantification and live cell imaging	145
5.12	Colony Formation Assay	146
5.13	rAAV-mediated gene targeting	147
6.	Appendix	149
6.1	Abbreviations	151
7.	References	155
	Curriculum Vitae	185
	Acknowledgements	187

1. Summary

The maintenance of correct chromosome number (euploidy) during cell division is essential for health. Loss of euploidy is observed in most cancers and is linked to tumorigenesis. During mitosis, a highly conserved surveillance mechanism termed 'spindle assembly checkpoint' safeguards correct chromosome segregation by delaying anaphase onset until all chromosomes are properly bi-oriented on the spindle apparatus. The kinase Bub1 functions in the spindle assembly checkpoint and in chromosome congression, but the impact of its catalytic activity on these function remains controversial.

Here we present a thorough characterization of two novel small-molecule ATP-competitive inhibitors of Bub1 kinase, BAY-320 and BAY-524, to demonstrate potent Bub1 kinase inhibition both *in vitro* and in intact cells. We compared the cellular phenotypes of Bub1 kinase inhibition in HeLa and RPE-1 cells with those of protein depletion, indicative of catalytic or scaffolding functions, respectively. We demonstrate that Bub1 inhibition resulted in the persistence of chromosome arm cohesion. Furthermore, Bub1 inhibition affected chromosome association of Shugoshin and the chromosomal passenger complex, without abolishing global Aurora B function. Bub1 cooperates with Haspin on CPC localization, as inhibition of both kinases showed an additive effect. But for all that, Bub1 kinase inhibition exerted only minor effects on mitotic progression, chromosome alignment or spindle checkpoint function. In striking contrast, Bub1 depletion impaired all the mentioned mitotic processes, arguing that Bub1 largely operates as a scaffolding protein.

Although, Bub1 inhibition seems to have little influence in mitotic fidelity, BAY-320 and BAY-524 treatment sensitized cells to low doses of Paclitaxel, resulting in remarkable impairment of chromosome segregation and cell proliferation.

These findings are relevant to our understanding of Bub1 kinase function and the prospects of targeting Bub1 for therapeutic applications.

2. Introduction

Cancer is characterized by an alteration in the strict regulation of cell division. Cancer cells reproduce at a much higher rate than their normal counterparts. A deregulated cell cycle results in the failure to repair DNA damage before the cell progresses to mitosis or in the failure to segregate chromosomes faithfully. Furthermore these cells do not respond correctly to internal and external signals that regulate cell cycle progression.

So far, the most effective cancer treatment strategies aim at the induction of aberrant mitoses leading to a controlled cell death of highly proliferative cancer cells. These treatments very often have deleterious side effects.

Protein phosphorylation controls many aspects of cell cycle regulation or more precisely cell division. The specific inhibition of mitotic protein kinases marks a new attempt to tackle aberrant cell division. Thus, the development of specific small molecule inhibitors along with the further understanding of the complex regulation processes involved in cell division mark new opportunities to improve cancer therapies.

2.1 The Cell Cycle

Cells have the remarkable attribute to create copies of themselves, defining them as the smallest and simplest form of solitary life, like unicellular bacteria and yeasts. Multi-cellular organisms arise from one single founder cell. Countless complex sequences of cell divisions transform that single cell into diverse communities of cells, which form the various tissues and organs that comprise a fully developed and functional individual. The cell cycle is a highly regulated and coordinated process that consists of a series of events that take place in a cell, which eventually lead to its duplication and division into two equal daughter cells.

In 2001, the identification of key molecules, which coordinate the cell cycle in all eukaryotic organisms, was awarded with the Noble Prize in Physiology or

Medicine to Leland Hartwell, Tim Hunt and Paul Nurse. The three scientists together have enabled an understanding at the molecular level of how the cell is driven from one phase to the next during division (Nasmyth, 2001).

To produce two identical daughter cells, the DNA of each chromosome must be faithfully replicated and then carefully segregated into the two daughter cells. Ergo, each daughter cell contains the entire genome. In addition, cells also duplicate their macromolecules and organelles by simply dividing them and therefore grow in order to keep their original cell size after division. Hence, cells need to coordinate their growth and division. In eukaryotes this process is organized into four sequential stages: G_1 (gap phase 1), S (synthesis phase) and G_2 (gap phase 2) that comprise together interphase and M (mitotic) phase consisting of mitosis and cytokinesis. During interphase, the cell continues to grow, accumulates nutrients, replicates its DNA and prepares for its division. The genetic material is replicated during S (synthesis) phase, resulting in duplicated chromosomes, called sister chromatids that must be equally segregated. DNA is allowed to duplicate once and only once per cell cycle. Additional time to grow is provided by the gap phases, G_1 and G_2 . Here, the cell can decide whether the environmental conditions are suitable for propagation. G_1 corresponds to the interval between mitosis and DNA replication, in which the cell is metabolically active and continuously grows. In G_2 , DNA replication is completed and the cell continues to grow and to synthesize proteins needed for mitosis. If the environment is unfavorable the cell may extend the time spend in G_1 or enter a quiescent state, called G_0 . The cell does not proliferate unless appropriate extracellular signals trigger this process. Most proteins, RNAs, macromolecules even organelles are synthesized throughout interphase and their high-copy numbers allow their simple distribution, respectively their fragmentation (Morgan, 2007). During M phase the cell segregates its genome and cytoplasmic content equally on to two daughter cells with cytokinesis as a final step. M phase is usually a very brief period in the cell cycle compared to interphase, which can

take up to 90-95 % of the cycle time (Cooper and Hausman, 2013). The protein machinery that governs the precise execution of cell cycle events is under strict control of a regulatory network. This system acts as a timer programming the molecular events in the right order and for the time until a preceding event is completed. Hence, all cell cycle events are ordered and directional, meaning it is impossible to reverse the cycle. The regulatory drivers of the cell cycle are cyclins and cyclin-dependent kinases (Cdks) (Figure 1). Cyclins are the regulatory or activating subunits of Cdks and once a cyclin/Cdk complex is activated, it phosphorylates target proteins and thereby changes their enzymatic activity, their location or their interaction with other proteins. Cdks are constitutively expressed whereas cyclin levels oscillate in a cyclical fashion throughout the cell cycle. Their expression is triggered by transcription and proteasome-dependent degradation in response to external and internal molecular signals, so that different cyclin/Cdk pairings are active at specific points. (Morgan, 2007; Lodish et al., 2012; Alberts et al., 2014).

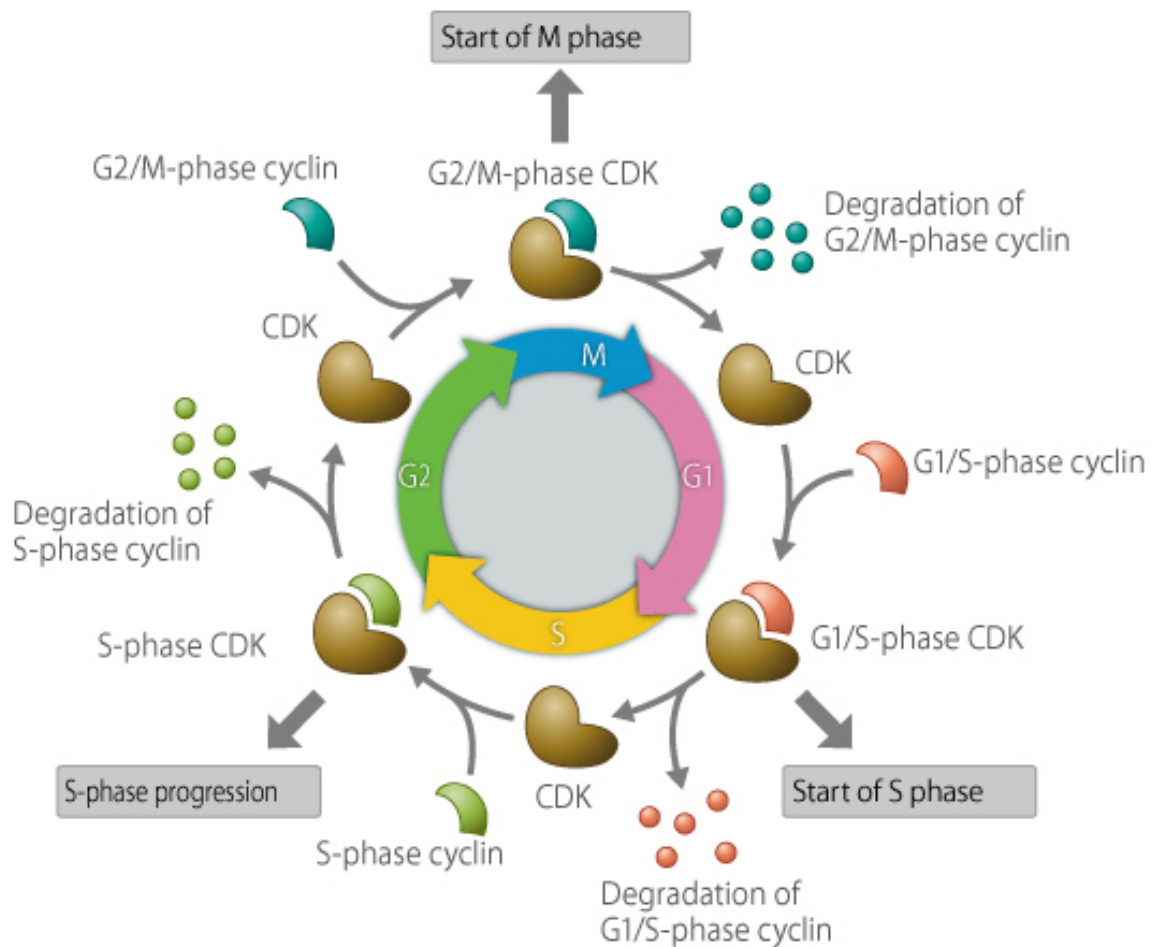


Figure 1: Cyclin-Cdk complexes play a central role in cell cycle progression. The function of cyclin-Cdks is to run the cell cycle smoothly, and these are therefore called “cell cycle engines.” Cyclins are proteins that vary in quantity throughout the cell cycle. Each cyclin is rapidly synthesized during a specific phase of the cell cycle and is again promptly degraded down after it serves its purpose. Inactivation, activation of cyclin-Cdk1 complexes allows the transition from one cell cycle phase to the other. Adapted from (CSLS, The University of Tokyo, 2011).

Specifically, there are several types of G₁/S-phase cyclins and G₁/S-phase Cdks. Cyclin D-Cdk4/6 complex and the cyclin E-Cdk2 complex are representative examples of G₁/S-phase cyclin-Cdk complexes, which function at the start of the S phase. G₂/M-phase cyclin and G₂/M-phase Cdk (cyclin B-Cdk1 complex) function at the start of M phase and induce nuclear membrane breakdown and chromosome formation when activated.

2.1.1 Mitosis

*“Where a cell arises, there must be a previous cell,
just as animals can only arise from animals and plants from plants”
Rudolf Virchow, 1858*

Mitosis is usually referred to as the last stage of the mammalian cell cycle and also visually the most spectacular. In 1882, Walter Flemming was the first cytologist to describe chromosome behavior and their distribution during the cell cycle (Paweletz, 2001). A process he called *mitosis*, according to the Greek word for ‘thread’. Surprisingly, already back then the process of cell division could be described in great detail and has since then been a source of great fascination.

Mitosis encompasses the time in which sister chromatids are segregated equally on to two daughter cells. Regarding the regulation of mitosis by the oscillation of cyclin levels, mitosis can be divided in two major parts. During mitotic entry an abrupt increase in Cdk activity triggers the phosphorylation of a variety of proteins leading to the assembly of the mitotic spindle, the priming of the chromatin to sister chromatid pairs and their attachment to the mitotic spindle. In the second half of mitosis, Cdk activity decreases thereby initiating the separation of sister chromatids, the subsequent division into two daughter cells and hence exit from mitosis (Morgan, 2007).

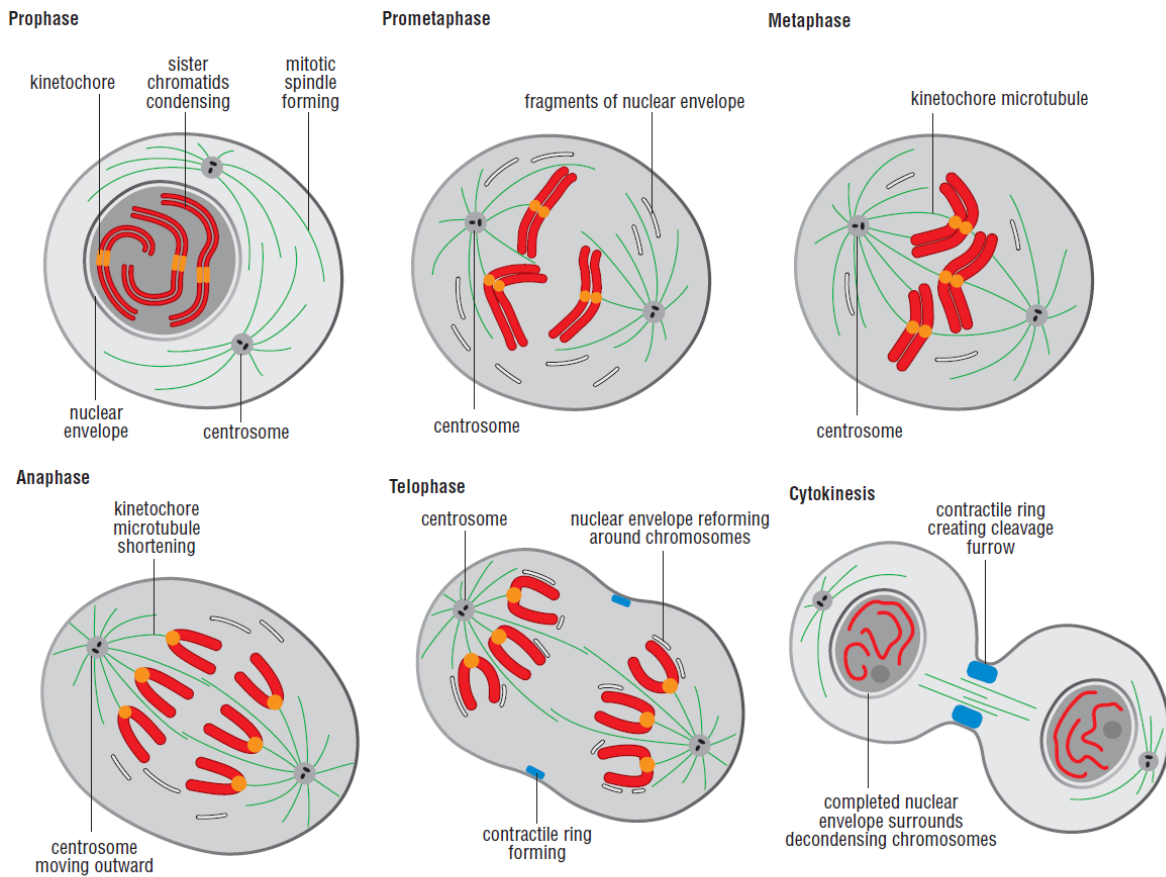


Figure 2: Events of mitosis. Depicted are the six morphologically distinct mitotic phases: Prophase, Prometaphase, Metaphase, Anaphase and Telophase. Mitosis is followed by cytokinesis. Adapted from (Morgan, 2007).

The process of mammalian nuclear division is further split into six distinct phases that can be distinguished based on cell morphology (Figure 2) (Pines and Rieder, 2001; Scholey et al., 2003). During ‘prophase’, the replicated interphase chromatin condenses into chromosomes, each comprising two sister chromatids held together by a ring-like centromeric protein complex, called cohesin. The centrosomes (main microtubule organizing centers, MTOCs), which have been duplicated during S phase, begin to separate and move towards the opposite ends of the cell and start to nucleate highly dynamic microtubules (MTs) to initiate mitotic spindle assembly. Nuclear envelope breakdown (NEBD) signals the beginning of ‘prometaphase’. The biopolar spindle forms, and MTs are now able to invade nuclear space and make contact with chromosomes. Moreover, a

specialized proteinaceous structure situated on both sister chromatids, called kinetochore (KT), assembles adjacent to the centromeric region (Cheeseman and Desai, 2008). During a highly dynamic and stochastic process KTs are captured by MTs emanating from opposing spindle poles and serve as anchors. When all chromosomes have become stably attached by a biopolar attachment between KTs and MTs, they begin to congress at the center of the cell. 'Metaphase' is the state when all chromatids are bipolar attached and aligned at the cell equator, the so-called metaphase plate (Walczak et al., 2010). The cells await the signal to separate. After a brief delay, during which the connection between sister-chromatids is resolved, 'anaphase' is initiated. Here, sister chromatids are pulled apart towards opposite spindle poles by the shortening of kinetochore MTs. Separation is further accelerated as the poles move further apart from each other towards the cell cortex. During 'telophase' the spindle disassembles and a new nuclear envelope reassembles around each set of decondensing chromatids, completing the formation of two daughter nuclei. The cleavage furrow begins to ingress, constricting the spindle midzone. Cell division is completed as cytokinesis occurs (Barr and Gruneberg, 2007). The central spindle compresses to form a compact midbody and contraction of an actin-myosin II-based ring-like structure beneath the plasma membrane leads to furrow ingression. Finally abscission takes place resulting in the formation of two new genetically identical daughter cells (Pines and Rieder, 2001; Lodish et al., 2012; Cooper and Hausman, 2013; Alberts et al., 2014).

2.1.2 Cell Cycle Checkpoints

"Normal cells obey strict rules. Divide only when told. Die rather than misbehave."

Dr. Andrew Murray, 2005

Director of the Center of Genomic Research

Harvard University

The ultimate goal of the cell cycle is to produce duplicates of each cell's DNA and to divide the cell and its content evenly between the two resulting daughter cells. Successful progression through the cell cycle requires control mechanisms. A tight network, including three major regulatory transitions or checkpoints, controls this cycle. These checkpoints function as molecular brakes to block progression, giving 'STOP and GO' signals, namely the G₁/S- or restriction-point, the G₂/M- or DNA damage checkpoint and the spindle assembly checkpoint (SAC) at the metaphase-to-anaphase transition. Accordingly, the control system monitors and dictates progression through the cycle. The next step is not triggered unless the cell is prepared and has met the needed requirements (Hartwell and Weinert, 1989; Alberts et al., 2014). These checkpoints respond to feedback loops and information received from the processes they control. Thus, they are able to sense defects that occur during essential processes like DNA replication. It is monitored if the environment is suitable and whether all cell cycle stages occur in the appropriate order. If a defect or a delay is sensed, a cell cycle arrest is induced and the cell gets more time to repair or to meet the needed prerequisites, respectively (Malumbres and Barbacid, 2009). To achieve this, eukaryotic cells have evolved molecular control mechanisms, involving post-translational modification and targeted degradation. The master regulator of the cell cycle control system is a family of kinases known as Cdks. They are associated with their regulatory subunits, cyclins. Different complexes are formed and activated at different stages of the cell cycle. Their activity oscillates during the cell cycle and cyclin levels are regulated by transcription and proteasome-dependent degradation throughout the cell cycle, so that different cyclin/Cdk pairings are active at specific points (Vermeulen et al., 2003). The activity of cyclin/Cdk complexes is most often deregulated in cancers, due to genetic or epigenetic changes in Cdks, their regulators or upstream mitogenic pathways (Vermeulen et al., 2003; Malumbres and Barbacid, 2009).

The first checkpoint is located at the end of G₁ phase, just before entry into S

phase (restriction point). During progression through G_1 the cell senses internal and external conditions and decides whether it should divide, delay division, or enter a resting stage (G_0). If the checkpoint is passed the cell is committed to a new round of the cell cycle and the cell activates cyclin/Cdk-dependent transcription which promotes entry into S phase (Bertoli et al., 2013). After the decision has been made to progress past the restriction point, cyclin D levels rise and form a complex with Cdk4 and Cdk6. Phosphorylation of target proteins and the transcriptional activation of downstream targets eventually activates cyclin E/Cdk2 that promote the G_1/S transition eventually. The cyclin E/Cdk2 complex promotes an 'all or nothing' switch from which the cell cannot return (Skotheim et al., 2008). During S phase, DNA is being replicated and in G_2 the cell undergoes rapid growth and gets prepared for mitosis. At the G_2/M or DNA damage checkpoint, the cell ensures that all necessary prerequisites for cell division have been met and eventually triggers the G_2 -to-M phase transition.

The G_2/M transition is mediated by the activation of the cyclin B/Cdk1 complex. Cyclin B/Cdk1 activity depends on the dephosphorylation of two residues in the ATP-binding site of Cdk1 (Thr 15 and Tyr 15) by the phosphatase Cdc25 that overcomes the inhibitory phosphorylation by the two kinases Wee1 and Myt1 (Nigg, 2001; Donzelli and Draetta, 2003; Perdiguero and Nebreda, 2004). The activated cyclin B/Cdk1 complex as well as rising cyclin B levels guide the cell subsequently towards the entry of mitosis.

The third checkpoint, called SAC, present at the metaphase-to-anaphase transition, monitors proper chromosome segregation. During mitosis sister chromatid cohesion must be maintained until all chromosomes are correctly aligned at the cell equator. Only then chromosome segregation can be initiated. Defects may provoke unequal inheritance of the genetic information that may facilitate tumor progression by accumulating numerical chromosomal aberrations (CIN). The SAC is dependent on cyclin B activity and Securin, an inhibitor of Separase, which is responsible for cleaving sister-chromatid cohesion prior to

segregation (Musacchio and Salmon, 2007).

The SAC and its regulation will be discussed in detail in the following chapter (2.2 *The Spindle Assembly Checkpoint*).

2.2 The Spindle Assembly Checkpoint

In 1991, two parallel screens in *Saccharomyces cerevisiae* first discovered the SAC and several of its signaling components (Hoyt et al., 1991; Li and Murray, 1991). The key components were the MAD (mitotic-arrest deficient) genes for Mad1, Mad2 and Mad3 and the BUB (budding uninhibited by benzimidazole) genes for Bub1 and Bub3. If mutated, cells bypassed the ability to arrest in mitosis in response to spindle poisons. Later these genes were found to be conserved in eukaryotes (Musacchio and Salmon, 2007). With the exact mechanism being unknown at first, laser ablation and micromanipulation experiments demonstrated that a mitotic delay is mediated by an inhibitory signal capable of being generated by single unattached KT (Rieder et al., 1995; Li and Nicklas, 1995). Since then, the SAC has been identified as a surveillance mechanisms that delays anaphase onset until correct bipolar attachment of chromosomes to MTs emanating from opposing spindle poles has been achieved (Lara-Gonzalez and Taylor, 2012; Musacchio and Salmon, 2007; Vleugel et al., 2012). The KT represents the catalytic platform to generate the SAC signal. Thus most checkpoint proteins are highly enriched at unattached KTs to generate the 'wait' signal but are absent from properly attached KTs (Li and Nicklas, 1995; Musacchio and Hardwick, 2002; Cleveland et al., 2003; Pinsky and Biggins, 2005; Musacchio and Salmon, 2007). Cells, which have an altered or artificially inactivated checkpoint, undergo precocious mitotic exit in the presence of unattached or incorrectly attached chromosomes and are therefore prone to missegregation events. These errors can lead to aneuploidy (abnormal number of chromosomes) or genetic instability,

which are a hallmark of cancer (Weaver and Cleveland, 2006; Kolodner et al., 2011).

The downstream target of the SAC is the anaphase promoting complex/cyclosome (APC/C), an E3 ubiquitin ligase that targets proteins for proteolytic degradation (Chang and Barford, 2014; Pines, 2011). Activation of the APC/C is governed by its co-factor Cdc20. Active APC/C^{Cdc20} triggers exit from mitosis and sister-chromatid segregation via degradation of Cyclin B and Securin, (Peters, 1999). Cyclin B degradation inactivates Cdk1, the master mitotic kinase. Securin is a stoichiometric inhibitory binding partner of Separase, a cysteine protease that cleaves cohesin complexes (Pines, 2006). The SAC itself catalyzes the formation of an inhibitory complex that prevents Cdc20 from activating the APC/C, thereby stabilizing Cyclin B and Securin and blocking the transition from meta- to anaphase (Lara-Gonzalez et al., 2012).

2.2.1 Molecular basis of the mitotic checkpoint

The SAC includes the core proteins Mad1, Mad2, Bub1, Bub1, BubR1 (human ortholog of yeast Mad3), Mps1, Aurora B (Lara-Gonzalez et al., 2012; Musacchio and Salmon, 2007), however the KT itself is comprised by more than 80 different proteins (Cheeseman and Desai, 2008; Santaguida and Musacchio, 2009). It is widely known that Bub1 is localizing to unattached KTs in early prophase and is there required to recruit the majority of downstream SAC effectors, including Mad1, Mad2, Bub3 and BubR1 (Meraldi et al., 2004; Perera et al., 2007; Johnson et al., 2004; Sharp-Baker and Chen, 2001). At the unattached KT the molecular inhibitor of the APC/C is formed, the so-called mitotic checkpoint complex (MCC) that is needed for the sequestration of Cdc20 and consists of BubR1, Bub3, Mad2 and Cdc20 (Chao et al., 2012; Kulukian et al., 2009; Sudakin et al., 2001) (Figure 3).

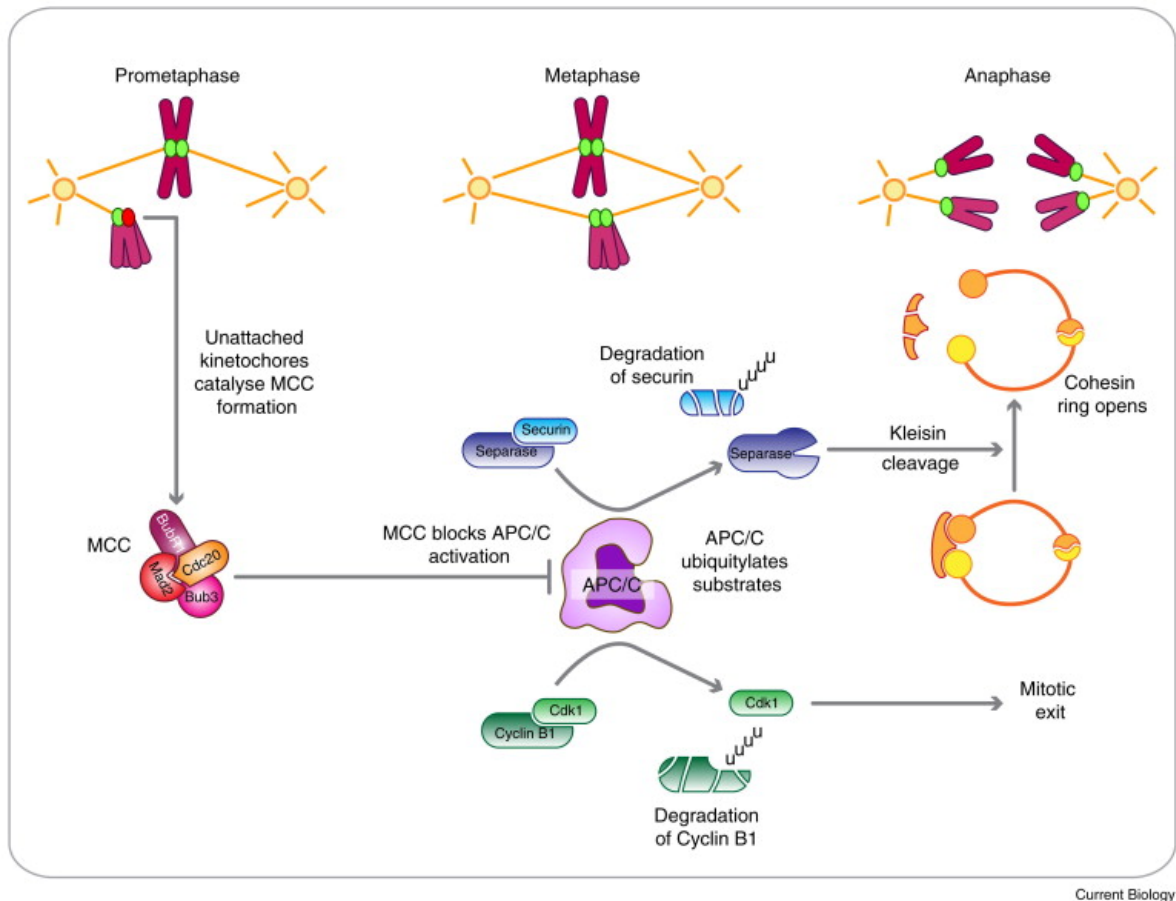


Figure 3: Molecular basis of the SAC. During early mitosis (prometaphase) the unattached kinetochore (green) catalyzes the formation of the MCC, composed of BubR1, Bub3, Mad2 and Cdc20. This complex formation leads to the inhibition of the APC/C. Once bi-orientation is achieved, the generation of the MCC is stopped, releasing Cdc20 that can now activate the APC/C. This leads to the ubiquitylation of cyclin B and Securin and thus their degradation. Securin is an inhibitor of Separase, which in turn cleaves the Scc1 kleisin subunit of cohesin. This allows ring opening and sister-chromatid separation. Meanwhile, degradation of cyclin B1 inactivates Cdk1, leading to mitotic exit. Adapted from (Lara-Gonzalez and Taylor, 2012).

The current model for the formation includes the ‘Mad2 template model’ (De Antoni et al., 2005; Mapelli et al., 2007). Mad2 can adopt two distinct conformations, an inactive ‘open’ conformer and an active ‘closed’ conformer that is able to bind Cdc20. According to the model, KT-bound Mad1 binds open-Mad2 (o-Mad2) and catalyzes its conversion from the open to the closed state (c-Mad2). This conversion stabilizes the heterodimer and equips it with a prion-like activity, by further inducing the same conversion in soluble O-Mad2. This process is called

conformational dimerization (Mapelli et al., 2006). The formation and maintenance of the MCC is also dependent on the kinase Mps1. Mps1 phosphorylates so-called MELT motifs (Met-Glu-Leu-Thr) on the KT protein Knl1, which acts as an anchor for Bub3:Bub1 and Bub3:BubR1 complexes (Krenn et al., 2014; London et al., 2012; Overlack et al., 2015; Primorac et al., 2013; Sheppard et al., 2012; Vleugel et al., 2013; Yamagishi et al., 2012). The cMad2:Cdc20 complex is then primed to bind BubR1:Bub3 and forms a heterotetramer (Fang, 2002; Davenport et al., 2006; Nilsson et al., 2008) that is bound to the APC/C and acts as a pseudosubstrate (Sudakin et al., 2001; Wang et al., 2011; Morrow et al., 2005). Although Mad2 is needed for the initial step of MCC generation, Mad2 might only play a subordinate role in APC/C inhibition as it is sometimes only a substoichiometric component of the MCC and is thought to rather promote the interaction between BubR1 and Cdc20 (Nilsson et al., 2008; Kulukian et al., 2009; Westhorpe et al., 2011). New evidence is emerging that BubR1 interferes with substrate binding either by inducing a conformational change on the APC/C or by directly occupying the substrate/activator binding site (Lara-Gonzalez et al., 2012; Buschhorn et al., 2011; da Fonseca et al., 2011).

As a single KT is able to generate a stable wait signal even for several hours (Rieder et al., 1995), the question arises how SAC signaling of a single KT is amplified to levels that arrest cells in mitosis. A first notion was that the SAC signal is an all-or-nothing response in which a threshold for the initiation of the wait signal has to be met (Collin et al., 2013). However, it has been shown that the amount of MCC generated and thus the strength with which the APC/C is inhibited, correlates with the number of unattached KTs (Dick and Gerlich, 2013).

The rapid establishment of the SAC signal depends on positive-feedback loops between several mitotic kinases. As already mentioned Mps1, localizes to unattached KTs and recruits Bub1/Bub3 dimers, which in turn recruit other SAC effectors like Mad1, Mad2 and BubR1 (Lara-Gonzalez and Taylor, 2012; Vleugel et al., 2012; Nijenhuis et al., 2013). Bub1 together with Haspin, triggers Aurora B

localization at the inner centromere by phosphorylating histones H2A and H3 (Kawashima et al., 2007; Kelly et al., 2010; Yamagishi et al., 2010). Aurora B feeds back to Mps1 and stimulates its further recruitment to KTs (Nijenhuis et al., 2013; Saurin et al., 2011) whereas Mps1 further enforces its influence on Aurora B (Jelluma et al., 2008; van der Waal et al., 2012). This cascade ensures rapid and robust MCC activity.

Despite its key function in mitosis, the SAC already operates during interphase. A recent study proposes that not only positive feedback-mechanisms fuel a rapid establishment of the SAC signal but that nuclear pore complexes (NPCs) can act as scaffolds for MCC generation instead of KTs (Rodriguez-Bravo et al., 2014). This pre-made wait signal allows the cell to initiate a wait signal before NEBD and thus before the KT is assembled to generate a KT-based SAC signal. Additionally this pre-mitotic wait signal allows correction of erroneous attachments that are not sensed by the SAC (Rodriguez-Bravo et al., 2014) (merotelic attachments, see chapter 2.3 *The Mechanism of Chromosome Alignment*).

Stable bi-orientation of all sister-chromatids silences the SAC and the cell is able to initiate the metaphase to anaphase transition. This silencing is governed by several mechanisms. As the SAC signal is dependent on the enrichment of SAC effectors on the unattached KT, effectors get depleted from the KT as soon as stable attachment is sensed and tension increases between KTs (Lara-Gonzalez et al., 2012). This 'stripping' of SAC components, mostly Mad1:Mad2 complexes, is mediated via the minus-end directed microtubule motor dynein (Gassmann et al., 2010; Howell et al., 2001). However, this pathway does not contribute directly to the disassembly of cytoplasmic inhibitors, which is required for the release of Cdc20. An antagonist of the SAC is p31^{comet}. Overexpression of this protein causes a SAC override while its depletion delays anaphase onset (Westhorpe et al., 2011; Mapelli et al., 2006; Fava et al., 2011). p31^{comet} binds Mad2 at the dimerization interface and thus prevents the recruitment and conversion of open-Mad2 (Mapelli et al., 2006; Fava et al., 2011; Jia et al., 2011; Lara-Gonzalez et al., 2012).

Since phosphorylation is a key driver of mitotic events, it is reasonable to argue that also phosphatases contribute to SAC silencing and there is evidence that PP1 (protein phosphatase 1) plays an important role in reverting phosphorylation at least in yeast (Vleugel et al., 2012).

2.2.2 Cell fates after a SAC-mediated cell cycle arrest

As previously mentioned, cell cycle checkpoints can arrest cells at different stages during progression, as response to DNA damage, spindle abnormalities or unfavorable environmental conditions. Usually a cell re-enters or continues the cycle after this stop-signal has been extinguished, e.g. after DNA damage repair or stable chromosome bi-orientation. However, if the damage cannot be repaired, the cell cannot stay in an infinite arrest. A variety of subsequent fates after a prolonged arrest are possible. One likely fate is cell death (apoptosis) that is marked by cell shrinkage, chromatin condensation, nuclear fragmentation and blebbing of the plasma membrane (Elmore, 2007). Apoptosis can be induced by the cell cycle control system in response to aberrant mitoses (Vitale et al., 2011). Apoptosis due to a prolonged mitotic arrest is mediated via Caspase-9, which is normally inhibited by cyclin B/Cdk1 (Allan and Clarke, 2007). During a prolonged arrest cyclin B is slowly degraded due to an unsatisfied SAC, thereby releasing the inhibition of Caspase-9 and leading towards an exit from mitosis via cell death (Gascoigne and Taylor, 2008). Another possible fate is the exit of mitosis with or without division and the return to interphase, a process known as 'slippage' (Brito and Rieder, 2006; Gascoigne and Taylor, 2008). A model has been proposed, illustrating that the cell fate is determined by two competing networks that include cell death initiation pathways and cell exit from mitosis due to cyclin B degradation (Gascoigne and Taylor, 2008). Both networks have thresholds and depending on which threshold is reached first, either death or exit is induced.

However the rate of slippage or death can differ within and between populations (Gascoigne and Taylor, 2008).

2.3 The Mechanism of Chromosome Alignment

During mitosis, replicated sister chromatids are aligned at the cell equator in metaphase and are subsequently segregated into two daughter cells. This process requires the establishment of stable KT-MT attachments and a wide variety of proteins are needed for generating these connections and to induce dynamics that foster proper chromosome alignment.

A simple but fundamental model, the ‘search and capture’ model described in 1986, tries to explain the complex mechanism of chromosome attachment and alignment (Kirschner and Mitchison, 1986). This model postulates that capture is initiated by MTs that are nucleated at MTOCs and that undergo growth and shortening (MT catastrophe) and search the cytoplasmic space for chromosomes. Those MTs get selectively stabilized once they reach their targets, the KT region. The mono-oriented chromosome oscillates close to the pole it is attached to, until it gets caught by the opposite pole. Since this process reflects a stochastic behavior, full capture of all chromosomes can take some time (Guo et al., 2013). However, this attractive model does not account sufficiently for a realistic timing of chromosome capture (Wollman et al., 2005). Since this model relies on the action of centrosomes that act as MTOCs, another model proposes an acentrosomal nucleation of MTs, which spontaneously adopt a spindle-like structure. This model is called the ‘self-assembly’ model (Heald et al., 1996; Guo et al., 2013). Here, nucleation is dependent on a RanGTP gradient around chromosomes that is generated by chromatin association with the guanine nucleotide exchange factor (GEF) RCC1 (Li et al., 2003).

Indeed, the SAC should only be silenced once all sister chromatids are attached in a bipolar fashion, an arrangement that is described as ‘amphitelic’ attachment (**Figure 4**). Since the generation of kinetochore-microtubule (KT-MT) attachments is a stochastic process, erroneous attachments can be formed. These incorrect attachments can generate lagging chromatids and chromosome missegregation in anaphase. ‘Monotelic’ attachments are characterized by the attachment of only a single KT to MTs and represents a normal condition in prometaphase. In addition, MTs emanating from one pole might become attached to both sister KTs of a single chromosome resulting in ‘syntelic’ attachment. ‘Merotelic’ attachments are characterized by single KTs that are captured by MTs from opposite poles. Hence one chromatid gets pulled towards both directions and can create a lagging chromosome (Morgan, 2007; Gregan et al., 2011).

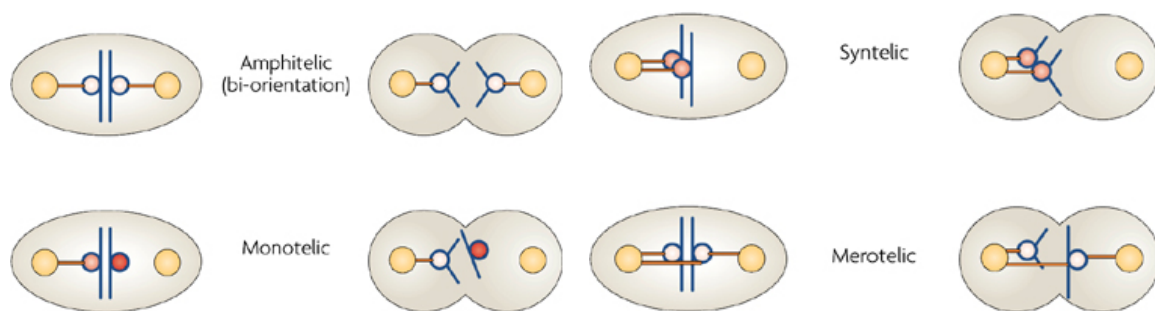


Figure 4: Attachments states that occur during mitosis. Monotelic attachment is a normal condition during prometaphase before bi-orientation. In syntelic attachment, both sisters are connected to the same pole. Merotelic attachments occur when one KT is captured from both poles. Adapted from (Musacchio and Salmon, 2007).

The SAC is activated by monotelic and syntelic attachments, as those KT-MT attachments are not fully stabilized due to low tension (Nezi and Musacchio, 2009; Pinsky and Biggins, 2005). In contrast, merotelic attachments produce sufficient tension and are not sensed by the SAC and can lead to chromosome missegregation and aneuploidy (Gregan et al., 2011). However, in both cases

Aurora B plays a central role in correcting these erroneous attachments (Hauf et al., 2003; Lampson et al., 2004; Knowlton et al., 2006; Lampson and Cheeseman, 2011). This attachment error correction mechanism is executed via active destabilization in order to provide a new opportunity to reach bi-orientation (Lampson et al., 2004). Aurora B is a member of the chromosomal passenger complex (CPC), together with Borealin, INCENP and Survivin (Carmena et al., 2012). The CPC is involved in several processes of mitosis due to its dynamic localization, including chromosome cohesion at chromosome arms, the regulation of KT-MT attachments, the SAC at the centromeric/KT region and cytokinesis at the spindle midzone and the midbody (Carmena et al., 2012). The centromeric localization of the CPC is dependent on two histone phosphorylations mediated by the kinases Haspin and Bub1 (Yamagishi et al., 2010).

During prometaphase, the CPC corrects erroneous attachments by phosphorylating the positively charged N-terminal tail of the Ndc80-Hec1 complex in the KMN network. The N-terminal tail interacts with the negatively charged C-terminal tail of tubulin, which weakens KT-MT interactions (Cheeseman et al., 2006; DeLuca et al., 2006; Ciferri et al., 2008; Guimaraes et al., 2008). Moreover, Aurora B regulates the activity and the recruitment of the kinesin-13 microtubule depolymerase MCAK through phosphorylation (Lan et al., 2004; Andrews et al., 2004; Zhang et al., 2007; Tanno et al., 2010). However, so far it is not completely known how inhibition of MCAK facilitates error-correction (Carmena et al., 2012). Bi-oriented chromosome pairs are exposed to pulling forces from both opposite poles. This generates tension and leads to an increase of the inter-kinetochore space. This spatial separation of Aurora B from its substrates at the outer KT reduces phosphorylation by Aurora B and thus increases stability of bi-oriented attachments (Liu et al., 2009). Hence, Aurora B is able to target KTs that are not under full tension and can destabilize erroneous KT-MT attachments until bi-orientation is achieved.

Alongside with attachment error correction, MT motor-mediated

movement of chromosomes during mitosis contributes to proper alignment (Cheeseman and Desai, 2008; Kops et al., 2010). KTs are able to bind MTs laterally and this facilitates chromosome alignment by rapid poleward movement. This movement is mediated by the minus end-directed motor dynein (Yang et al., 2007) and the plus-end directed motor CENP-E (McEwen et al., 2001; Putkey et al., 2002). Whereas dynein promotes poleward movement to increase the probability of end-on KT capture at a place where a lot of MTs are present, CENP-E moves chromosomes from the polar region to the cell equator, which is necessary for congression (Yang et al., 2007; Kapoor et al., 2006).

2.4 Chromosome Cohesion – Hold and Release

In bacteria, chromosome segregation occurs almost at the same time as DNA replication. However in eukaryotes, large genomes can only be segregated with a gap phase between S and M phase, to ensure chromosome condensation and proper preparation for cell division (Nasmyth et al., 2000). During S phase the genome of a cell is being replicated and sister chromatid cohesion is established, which permits delayed chromosome segregation. This connection between sister chromatids needs to be maintained until metaphase to ensure their bi-orientation. Only then sister chromatids are separated from each other. Sister chromatid cohesion allows sustaining this connection despite emerging pulling forces from spindle MTs that attach to KTs to achieve bi-orientation. Cohesion also gives information about which chromatids should be separated during cell division, making sure that each emerging daughter cell is genetically identical. Premature sister chromatid segregation either triggers the SAC, as no stable KT MT attachments can be formed, or leads to premature division and aneuploid daughter cells (Peters and Nishiyama, 2012).

Cohesion is mediated by ring complexes of cohesin that consist of Smc1 (structural maintenance of chromosomes 1), Smc3, Scc1 (sister chromatid cohesion 1) and Scc3/SA (stromal antigen) (Nasmyth and Haering, 2009; Anderson et al., 2002; Haering et al., 2002). Interactions between Smc1, Smc3 and Scc1 form a tripartite ring structure that embraces chromatin (Gruber et al., 2003; Ivanov and Nasmyth, 2005; Haering et al., 2008). The fourth cohesin subunit Scc3/SA directly binds Scc1, which is needed to recruit other proteins that stabilize sister chromatid cohesion (Peters and Nishiyama, 2012).

Cohesin associates with chromatin during G₁ phase and is dependent on ATP hydrolysis followed by a ring opening (Peters and Nishiyama, 2012). During G₁, cohesin only wraps one single chromatid but during DNA replication the ring complexes encircle both chromatids and become cohesive (Losada, 2014). The establishment of cohesion requires the acetylation of Smc3 by Eco1 (Zhang et al., 2008). It was suggested that this acetylation process stabilizes cohesin on DNA by blocking ATP hydrolysis and hence ring opening (Peters and Nishiyama, 2012). Furthermore, after acetylation of Smc3, Sororin is recruited via Pds5 (Nishiyama et al., 2010). Sororin stabilizes cohesion by antagonizing the cohesin release factor Wapl, as Sororin and Wapl compete for the binding with Pds5 (Schmitz et al., 2007). In the absence of Sororin, Wapl-Pds5 dissociates cohesion from chromatin (Gandhi et al., 2006; Kueng et al., 2006).

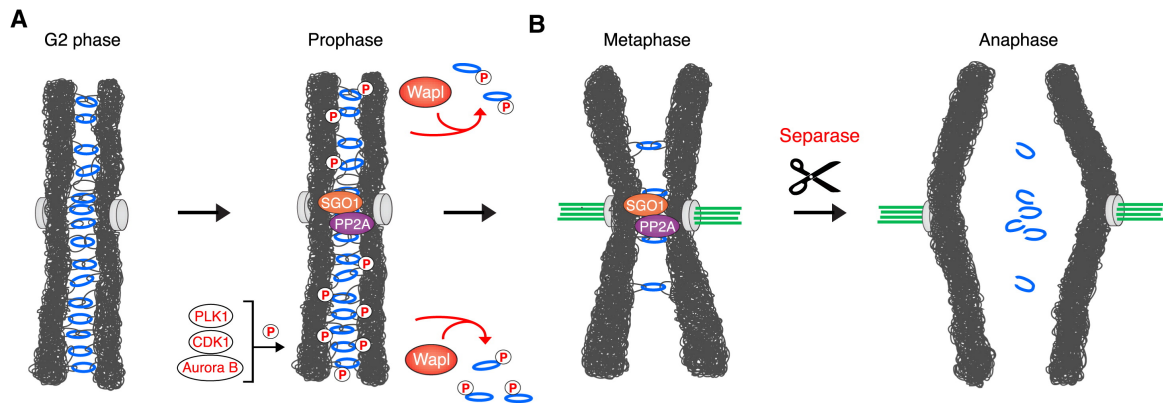


Figure 5: Two distinct pathways remove Cohesin during mitosis. (A) The initial removal of cohesion is dependent on Cdk1, Plk1 and Aurora B activity. The phosphorylation of various proteins allows removal of cohesin from chromosome arms. Centromeric cohesion is protected by Sgo1, which recruits phosphatase PP2A. PP2A counteracts phosphorylation that preserves the cohesin ring structure at the centromere. (B) When the SAC is silenced centromeric cohesion gets removed by Separase, thereby triggering sister chromatid separation. Adapted from (Haarhuis et al., 2014).

In eukaryotes, two distinct pathways release cohesin from chromatin (Figure 5). During prophase cohesin complexes are removed from sister chromatid arms, by a mechanism called the ‘prophase pathway’ (Waizenegger et al., 2000). This pathway is dependent on the action of three mitotic kinases. Cdk1 and Aurora B phosphorylate Sororin, which in turn drives its dissociation from Pds5. Subsequently Wapl is able to bind Pds5 and to unload cohesin (Nishiyama et al., 2013). Additionally, Plk1 phosphorylates the Scc3/SA subunit and triggers the dissociation of the cohesin ring (Sumara et al., 2002; Lenart et al., 2007). However, a small portion of cohesion at centromeres is maintained. This protection of cohesion is executed by a protein called Shugoshin (Sgo). Sgo recruits the phosphatase PP2A and thereby counteracts the Plk1-mediated phosphorylation of Scc3/SA (Kitajima et al., 2006; Liu et al., 2013b). The remaining cohesion is only removed after bi-orientation has been achieved in metaphase. The Scc1 subunit is cleaved by Separase, a protease that is activated after the SAC is satisfied and the APC/C ubiquitylates its inhibitor Securin (Hauf et al., 2001).

2.5 Mitotic Kinases – Regulation by Phosphorylation

The coordinated process that eventually leads to the irreversible separation of sister chromatids during mitosis needs a tightly regulated control and execution system. Several kinases are acting side by side during mitosis and sometimes even collaborate with each other, adding complexity to the system.

The major mitotic kinase is Cdk1 in conjunction with its activator cyclin B (Morgan, 2007). Active Cdk1 mediates various cellular reorganizations at mitotic entry and is involved in almost all processes until metaphase, while at the same time prevents late mitotic events, through inhibitory phosphorylation. Substrates at early mitosis include proteins involved in the regulation of NEBD, centrosome separation, spindle assembly, chromosome condensation and Golgi dynamics (Lodish et al., 2012; Alberts et al., 2013; Morgan, 2007). To ensure the activity of Cdk1/cyclinB is maintained during early mitosis, Cdc25C phosphatase counteracts the inhibitory phosphorylation on Cdk1 (Sebastian et al., 1993). The timed activation of the APC/C^{Cdc20} at metaphase results in the degradation of cyclin B and the shutdown of Cdk1 activity. Phosphatases like PP2A or Cdc14 seem to counteract Cdk1 function at the onset of anaphase (Wurzenberger and Gerlich, 2011). The removal of the inhibitory impact of Cdk1 on late mitotic processes, allows for example the formation of the central spindle or furrow ingression, regulated by Prc1 or Mklp1 (Wurzenberger and Gerlich, 2011). Thus the transition from metaphase to anaphase and mitotic exit is mainly driven by the inactivation of cyclin B/Cdk1 and by the proteolysis of components required for Cdk1 activity.

Mps1 (monopolar spindle 1) is a serine/threonine/tyrosine kinase located at the apex of mitotic checkpoint signaling. Several studies have shown the absolute requirement for Mps1 in the SAC (Liu et al., 2003; Stucke et al., 2002; Tighe et al., 2008; Liu and Winey, 2012). Mps1 fosters directly or indirectly the recruitment of a vast number of checkpoint components, like Bub1, BubR1, Cdc20, Mad1, Mad1 and Plk1 (Lan and Cleveland, 2010; Maciejowski et al., 2010; Santaguida et al.,

2010; Sliedrecht et al., 2010). Cells lacking Mps1 exit mitosis prematurely with unaligned chromosomes, leading to aneuploid progeny. Moreover, it has been shown that the MCC is already formed in interphase to allow cells to arrest in early prophase before a functional KT is build to emit a stop signal. This initial interphase MCC formation is dependent on Mps1 (Rodriguez-Bravo et al., 2014; Maciejowski et al., 2010). Mps1 has additional functions in chromosome congression and error correction of KT-MT attachments that are dependent on Aurora B activity (Jelluma et al., 2010). Efficient Mps1 recruitment to KTs is fueled by Aurora B. Inhibition of Aurora B delays the activation of Mps1, however it is not needed to maintain Mps1 activity (Saurin et al., 2011). Despite its ubiquitous functions in the SAC, only few substrates of Mps1 have been identified, including Mps1 itself, Plk1, Borealin and Knl1 (Dou et al., 2011; Schubert et al., 2015b; Jelluma et al., 2008; Yamagishi et al., 2012).

Aurora B kinase is a member of the CPC, which also contains three non enzymatic proteins Borealin, INCENP and Survivin (Carmena et al., 2012). Beside its function in chromosome alignment (see chapter 2.3 *The Mechanism of Chromosome Alignment*), Aurora B is also involved in the establishment of the SAC signal, chromosome cohesion, cleavage furrow ingression and cytokinesis. This reflects a very dynamic localization of this kinase. Inhibition of the kinase compromises the checkpoint and leads to exit from mitosis without cytokinesis (Ditchfield et al., 2003; Hauf et al., 2003). The spatiotemporal activity of Aurora B is tightly regulated by its main counteracting phosphatase PP1 via dephosphorylating Aurora B substrates as well as reducing the activating autophosphorylation on Aurora B (Liu et al., 2010; Emanuele et al., 2008; Honda et al., 2003)

Plk1 (Polo-like kinase 1) is key a regulator of mitotic progression (Petronczki et al., 2008; Schubert and Nigg, 2013). The N-terminal domain of Plk1 contains a kinase domain, whereas the C-terminal domain features two highly conserved polo-box domains (PBD). These form a phosphopeptide binding pocket that

mediate the recruitment of Plk1 to proteins that have been primed by phosphorylation (Elia et al., 2003). This kinase supports amongst others the maturation of the centrosome and bipolar spindle formation (Petronczki et al., 2008; Kishi et al., 2009). Furthermore, Plk1 is involved in the removal of cohesin from chromosome arms by phosphorylating Scc3/SA, in a process called the 'the prophase pathway' (Waizenegger et al., 2000). In prometaphase, levels of Plk1 are especially high on KTs. Later on Plk1 localizes to the central spindle in anaphase and to the midbody in telophase (Petronczki et al., 2008). KT-based function of Plk1 is most probably the formation of stable KT-MT attachments (Hanisch et al., 2006a; Lenart et al., 2007; Santamaria et al., 2007) whereas Plk1 fuels spindle elongation and the execution of proper cytokinesis at the end of mitosis (Taylor and Peters, 2008). Cells devoid of Plk1 activity enter a robust checkpoint-mediated mitotic arrest and display monopolar spindles and KTs with normal levels of Mad2 (Lenart et al., 2007; Santamaria et al., 2007). This indicates dispensability for Plk1 in checkpoint signaling. Surprisingly, Plk1 shares a similar motif preference as Mps1 (Dou et al., 2011; Santamaria et al., 2011). It has been recently shown that Plk1 is able to strengthen the establishment of the SAC signal and to maintain it by acting synergistically with Mps1. However, this attribute is usually masked by its other function, mainly bipolar spindle formation (Schubert et al., 2015b; Espeut et al., 2015).

BubR1 (Budding Uninhibited by Benzimidazoles Related 1) also contains a C-terminal kinase domain whereas its counterpart in yeast, Mad3, has lost this domain (Bolanos-Garcia and Blundell, 2011; Li and Murray, 1991). The protein has been proposed to be a pseudokinase, with its kinase domain acting as protein structure stabilizer but otherwise being dispensable in vertebrates (Suijkerbuijk et al., 2012b). Thus, the main function of BubR1 lies in the formation of the MCC (Lara-Gonzalez et al., 2012; Bolanos-Garcia and Blundell, 2011) and chromosome alignment via PP2A recruitment (Foley et al., 2011; Suijkerbuijk et al., 2012a; Kruse et al., 2013; Xu et al., 2013).

Those kinases are only a selection of enzymes active during mitosis. The next chapter will focus on a specific mitotic kinase, called Bub1.

2.5.1 Budding uninhibited by benzimidazole (Bub1)

Bub1 was one of the first initially identified and characterized components of the SAC (Farr and Hoyt, 1998; Taylor and McKeon, 1997; Musacchio and Salmon, 2007). Bub1 is a serine-threonine protein kinase and is one of the first checkpoint proteins that binds to unattached KTs in early prophase (Jablonski et al., 1998). The protein structure can be generally divided into three distinct domains. A N-terminal domain that contains 3 tetratricopeptide repeats (TPR). Approximately the first 300 residues are sufficient for KT recruitment (Taylor and McKeon, 1997; Taylor et al., 1998). Then, a Bub3-binding domain (or Gle2-binding domain, GLEBS, residues 240-280) that ensures binding to Bub3 throughout the cell cycle (Hardwick et al., 2000; Larsen et al., 2007; Roberts et al., 1994; Taylor et al., 1998) via binding to a 7-bladed β -propeller structural domain of Bub3 (Larsen and Harrison, 2004; Larsen et al., 2007). And a C-terminal kinase domain (residues 784-1085) (Kang et al., 2008).

Bub1 recruitment to unattached kinetochores

Mutations in the Bub3-binding domain prevent KT localization of Bub1 (Klebig et al., 2009) and it is suggested that this interaction might be necessary for efficient KT recruitment (Overlack et al., 2015). The recruitment of the Bub1:Bub3 complex to the nascent KT is mediated via Knl1 and Mps1 kinase. Knl1 acts as a scaffold, with several MELT-based (Met-Glu-Leu-Thr) short sequences that serve as docking sites when phosphorylated by Mps1 (London and Biggins, 2014; Sheppard et al., 2012; Vleugel et al., 2013; Yamagishi et al., 2012; Zhang et al., 2014; Overlack et al., 2015; Primorac et al., 2013). Additionally, Bub1 directly interacts

with the KI1 (Lys-Ile) and KI2 motifs in the N-terminus of Knl1 via its TPR motifs (Krenn et al., 2014; Kiyomitsu et al., 2011; Bolanos-Garcia and Blundell, 2011). This interaction is supposed to enhance MELT-mediated recruitment of Bub1, however it was also shown that mutations in the TPR domain do not affect Bub1 recruitment to KT (Krenn et al., 2014; 2012; Lara-Gonzalez et al., 2012). Moreover, a recent study gives insight into the regulation of KT residency of Bub1. It has been shown that Bub1 localization at KT is dynamic and dependent on Bub1 autophosphorylation (Asghar et al., 2015).

Mitotic functions of Bub1

Bub1 mediates several processes during mitosis. It gets recruited to unattached KTs, where the anaphase-wait-signal is generated and gets released once bi-orientation is achieved. At the KT, Bub1 mediates the recruitment of core checkpoint effectors, such as Mad1, Mad2, BubR1 and Bub3 and this recruitment marks an important step for all downstream signaling of the SAC (Boyarchuk et al., 2007; Johnson et al., 2004; Klebig et al., 2009; Meraldi and Sorger, 2005; Rischitor et al., 2007; Sharp-Baker and Chen, 2001; Overlack et al., 2015). Recent data in *Caenorhabditis elegans* even report a direct interaction between Bub1 and Mad1 (Moyle et al., 2014). Depletion of Bub1 by RNAi (Meraldi and Sorger, 2005) or BUB1 knock-out (Perera et al., 2007) leads to checkpoint malfunction. In addition, Bub1 has been shown to phosphorylate Cdc20, adding an extra level of APC/C inhibition (Kang et al., 2008; Tang et al., 2004a). However, this phosphorylation event remains controversial, since kinase-dead (KD) mutants are able to support the spindle checkpoint (Perera and Taylor, 2010; Klebig et al., 2009). Thus, the molecular consequences of Cdc20 phosphorylation remain to be shown. While studies in yeast and frog show a requirement of Bub1 kinase activity in KT function, it is believed that Bub1 acts as a non-catalytic scaffold for the checkpoint in mammals (Fernius and Hardwick, 2007; Rischitor et al., 2007; Sharp-Baker and Chen, 2001; Johnson et al., 2004; Boyarchuk et al., 2007; Overlack et al.,

2015). In particular, in yeast, mouse and human cells Bub1 kinase activity was reported to be important for chromosome alignment but dispensable for SAC signaling (Fernius and Hardwick, 2007; Warren et al., 2002; Klebig et al., 2009; Perera and Taylor, 2010; Ricke et al., 2012).

In addition to targeting SAC effectors to the unattached KT, Bub1 is also required for the KT targeting of the kinesin CENP-E (Johnson et al., 2004; Sharp-Baker and Chen, 2001), which has been proposed to promote bi-orientation via various pathways (Kim et al., 2010; Schaar et al., 1997; Iemura and Tanaka, 2015). It has been shown that Bub1 is promoting stable KT-MT end-on attachment and thus chromosome bi-orientation (Johnson et al., 2004; Klebig et al., 2009; Meraldi and Sorger, 2005; Windecker et al., 2009). This function can be either exerted via CENP-E or via Bub1-dependent phosphorylation of H2A. Phosphorylation of H2A at T120 provides a recruitment platform for Sgo1 and thus the CPC via a direct interaction with Borealin (Yamagishi et al., 2010; Kawashima et al., 2010; Tsukahara et al., 2010). It has been shown that interference with Bub1 leads to impaired PP2A and Aurora B recruitment to centromeres (Tang et al., 2006; Ricke et al., 2012), most presumably due to the lack of pT120-H2A and reduced CPC levels. Thus, the reported errors in chromosome alignment in Bub1-deficient cells (Johnson et al., 2004; Meraldi and Sorger, 2005; Perera et al., 2007; Jeganathan et al., 2007; Klebig et al., 2009) could be a result of dephosphorylated Aurora B substrates, since ectopic tethering of the CPC recues chromosome alignment (Ricke et al., 2012). This can also be underlined by the fact that Bub1 overexpression results in Aurora B hyperactivation and increased numbers of chromosome segregation errors (Ricke and van Deursen, 2011). Taken together, although Bub1 kinase activity seems to be not directly involved in SAC signaling, a secondary impact via Aurora B, fueling into the Mps1-Aurora B feedback loop, might still be possible.

As previously mentioned, the Bub1-dependent phosphorylation of T120-H2A focuses Sgo proteins to the KT where it protects centromeric cohesin from

being cleaved prematurely (Kawashima et al., 2010; Tang et al., 2004b; 2006). In Bub1 depleted cells, Sgo is relocated to chromosome arms and causes a persistent cohesion of mitotic chromosomes in together with a loosening of centromeric cohesion (Kitajima et al., 2005). It is suggested that the decrease of centromeric cohesion could perturb chromosome bi-orientation due to insufficient tension between sister-chromatids. However, evidence is still missing (Kitajima et al., 2005).

2.5.2 Mitotic kinase inhibitors as anti-cancer agents

Minor missegregation events can promote tumorigenesis, whereas severe aneuploidy is usually followed by cell death (Holland and Cleveland, 2009). Apoptosis, mitotic catastrophe and hyperploid progression are usually the desired outcomes of chemotherapy, as they eventually kill proliferating cancer cells. It has been shown that shutting down the SAC by RNAi causes apoptosis in cancer cells (Kops et al., 2004; Michel et al., 2004). Therefore, tackling the SAC for cancer therapeutics seems plausible. Traditional anti-mitotic drugs include MT toxins. However, their side effects and toxicity limit their usage in clinics (Gascoigne and Taylor, 2008). A recent study showed that tumor cells are more sensitive to low doses of Paclitaxel if mild chromosome segregation errors are induced by the reduction of essential mitotic checkpoint proteins than normal human fibroblasts (Janssen et al., 2009). The combination of SAC inhibition and clinical doses of Paclitaxel increased the amount of cell death and shows a new path to selectively kill cancer cells by raising aneuploidy to intolerable levels.

The development of small-molecule inhibitors for mitotic kinases for example bears a new advantage towards MT toxins, as those can also affect non-dividing cells (Schmit and Ahmad, 2007; Figueroa-Masot et al., 2001). The advantages of targeting mitotic kinases are their active expression in proliferating

cells, thus quiescent cells should not be affected. Families of mitotic kinases have usually very specific target sites for chemical inhibition and most often their deregulation is linked to uncontrolled proliferation (Schmit and Ahmad, 2007).

In the following, some of the most important mitotic kinase inhibitors are listed that are currently used in research (Table 1).

Table 1: Selection of inhibitors that target mitotic kinases.

Kinase	Functions	Inhibitor(s)	References
Cdk1	mitotic entry, early spindle assembly, NEBD breakdown, chromosome condensation, chromosome cohesion, etc.	RO-3306	(Vassilev et al., 2006)
Mps1	spindle checkpoint, interphase MCC formation, chromosome alignment	Reversine	(Santaguida et al., 2010)
Aurora B	chromosome cohesion, spindle checkpoint, chromosome alignment, central spindle assembly, cytokinesis	ZM-447439, Hesperadin	(Ditchfield et al., 2003; Hauf et al., 2003)
Plk1	centrosome maturation, mitotic spindle formation, SAC establishment, chromosome cohesion, central spindle elongation, cleavage furrow ingression, cytokinesis	ZK-Thiazolidinone (TAL), BI-2536	(Santamaria et al., 2007; Lenart et al., 2007)
Haspin	CPC recruitment, chromosome alignment, chromosome cohesion,	5-iodotubercidin (5-ITu)	(De Antoni et al., 2012)
Bub1	spindle checkpoint, chromosome alignment, chromosome cohesion	2OH-BNPP1, BAY-320, BAY-524	(Kang et al., 2008), this study

2.6 Phosphoproteomics

Phosphorylation is one of the most prominent and wide spread post-translational modifications (PTMs) of proteins and a key regulator of their function. Reversible phosphorylation regulates a huge variety of cellular processes and it is therefore crucial to gain a fundamental understanding of this process. For instance, protein phosphorylation can increase or decrease a protein's biological activity, stabilize it or mark it for destruction, facilitate or inhibit subcellular translocations or initiate or disrupt protein-protein interactions (Cohen, 2002). Taking the constant availability of ATP into account, phosphorylation represents a simple, fast and flexible tool in eukaryotic cells for initiation of various processes. Hence, monitoring phosphorylation sites helps to elucidate regulation mechanisms and it is a prerequisite for characterizing upstream kinases according to their substrate specificities and substrate sequence motifs.

Phosphorylation is often a substoichiometric event since not all copies of a given protein are usually present in the phosphorylated state. Therefore complete phosphorylation profiling remains a challenge. There are different approaches to determine phosphorylation sites. One can use computer algorithms (Trost and Kusalik, 2011) to predict potential phosphorylation sites based on the consensus recognition motif of known protein kinases, or based on known phosphorylation sites in a homologous protein. Also the use of phospho-specific antibodies with high sensitivity can give a hint on the time-point when a protein is phosphorylated, however the availability is a huge limitation factor. In the past, 2-D phospho-peptide mapping with ^{32}P labeling (van der Geer and Hunter, 1994; Nagahara et al., 1999) combined with site directed mutagenesis or Edman sequencing (Berg et al., 2015) has been most often the method of choice. Nowadays people move to a mass spectrometry (MS) based approach (Dephoure et al., 2013), which allows fast and sensitive identification of low abundant sites including peptide sequence analysis and the exact localization in the protein.

Due to their substoichiometric phosphorylation, phospho-peptides are usually under-represented in a peptide sample, due to an excess of unphosphorylated peptides. Therefore prior to LC-MS/MS analysis, phosphorylated peptides have to be enriched to increase the number of identifications (Fíla and Honys, 2012). To date, many different enrichment strategies exist like performing immunoprecipitation (IP) or more advanced techniques like the enrichment of phosphorylated peptides using TiO₂-beads or immobilized metal affinity chromatography (IMAC). Metal oxides, like titanium dioxide (TiO₂) beads have a high specific affinity to organic phosphates in solution and exhibit high mechanical, chemical, and thermal stability and are currently the most used resin material (Ozlu et al., 2010). Suitable modifiers should be able to exclude or compete with the binding of non-phosphorylated peptides to TiO₂ beads. 2,5-dihydroxy benzoic acid (DHB), phthalic acid, glycolic acid, and lactic acid have proven to be efficient additives (Larsen et al., 2005; Thingholm and Larsen, 2009).

2.7 Quantification of Phosphorylated and Unphosphorylated Peptides

It is not only important to identify proteins and their phosphorylation sites but also to give quantitative information about the extent and the dynamic changes in their abundance. This also simplifies the identification of possible upstream kinases. However, the precise quantification of low abundance proteins remains a challenging task (Domon and Aebersold, 2010). In the past conventional data-dependent acquisition (DDA) mass spectrometry (MS) workflows have been the method of choice for protein quantification, however they have become more and more outdated due to limits in sensitivity, sequencing speed and their dynamic range (Sandhu et al., 2008; Michalski et al., 2011). Protein quantification in combination with DDA workflows has been tackled by two main approaches. Stable isotope labeling by amino acids in cell culture (SILAC) (Ong et al., 2003;

Chen et al., 2015) or label-free quantification (Wong and Cagney, 2010; Bantscheff et al., 2007). SILAC uses the incorporation of 'heavy' labeled amino acids into one or more of the samples being studied. The differentially labeled samples are then cross-compared to each other. Unlabeled and labeled samples can be simply combined prior to mass spectrometric (LC-MS) analysis. Labeled proteins with stable isotopes have shifted mass-to-charge (m/z) ratios in mass spectra compared to their natural, non-labeled counterparts but are otherwise identical in all respects (Ong et al., 2003; Chen et al., 2015). A disadvantage of this method is inefficient labeling, the need for cultivable cells and high costs. Moreover, to monitor low abundant proteins or phosphorylation events it is still required to enrich the protein of interest and/or to perform phospho-peptide enrichment, respectively (Ibarrola et al., 2003). However, enrichment procedures on pull-down samples have proven to very difficult (data not shown).

Label-free quantification also aims at the relative quantification of two or more samples on the basis of the assumption that conditions with sufficient data redundancy and identical peptides across different MS experiments can be compared (Wong and Cagney, 2010). This can be achieved either by comparing the mass spectrometric signal intensity of peptide precursor ions of a protein of interest or by comparing the number of acquired fragment spectra (spectral counts) that match to a peptide/protein (Wong and Cagney, 2010; Bantscheff et al., 2007).

In the last years ambitious efforts have been made in order to establish acquisition methods (directed and targeted work-flows) that allow the usage of labeled internal standards for the quantification of a selected set of proteins of interest and that overcome the limiting factors of DDA-driven workflows (Schmidt et al., 2008; Jaffe et al., 2008; Savitski et al., 2010; Picotti et al., 2009).

In the following sections different MS approaches are shortly discussed that have been validated in regard of peptide and phospho-peptide quantification during this study (Figure 6).

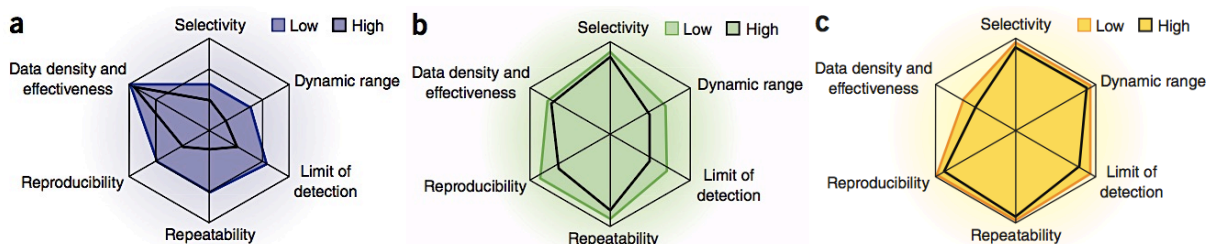


Figure 6: Performance profiles of the discovery (shotgun) (a), directed (b) and targeted (c) proteomic method. ‘High’ and ‘Low’ refer to sample complexity. Adapted from (Domon and Aebersold, 2010).

2.7.1 DDA – Data dependent acquisition

A universally applicable proteomic method is generally described as data dependent acquisition (DDA), shotgun proteomics, or discovery-based strategy (Figure 7). Here, peptides are eluted from a liquid chromatography (LC) setup and are converted to gas phase ions by electrospray ionization. The masses of the ions produced in the ion source are recorded generating a full mass spectrum that comprises all precursors that elute at a given time. This spectrum is generally referred to as survey scan (MS^1). In order to identify the peptide, information from parent masses and fragmented ions are needed. Those are generated by fragmentation of the parent ion (process is part of Tandem MS or MS/MS). During the DDA mode, a fixed number of precursor ions detected in the survey scan, are automatically selected according to pre-determined and user-defined criteria, usually on the basis of their signal intensity in the survey scan (data-dependent). These precursor ions are automatically selected, isolated and subjected to fragmentation by collision-induced dissociation (CID) and a full fragment-ion mass spectrum is generated (MS^2) (Domon and Aebersold, 2010; Blackburn and Goshe, 2009). The interpretation of the MS^2 spectra allows amino acid sequence identification and together with parent-ion data, peptide identification is possible (Gillette and Carr, 2013).

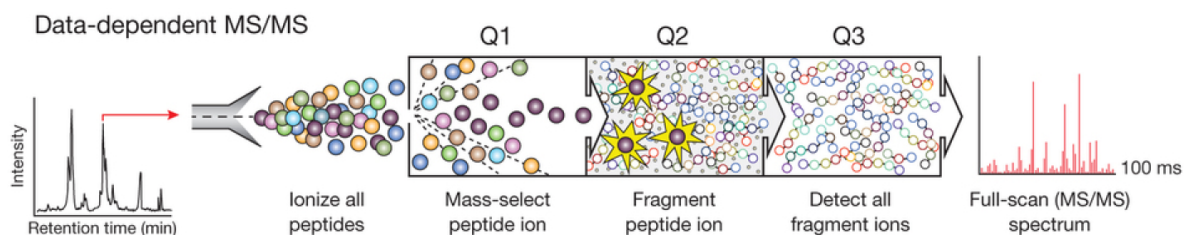


Figure 7: DDA – Data dependent acquisition. At any given point of the chromatographic separation, hundreds of peptides are eluting. A full-scan MS spectrum is acquired but only a fixed number of precursor ions, usually with the highest intensities are selected for fragmentation. Adapted from (Gillette and Carr, 2013).

DDA analysis is not suitable for characterizing whole proteomes, as one big limitation of this approach is the discrimination against peptides of low abundance (Schmidt et al., 2008). MS¹ signals for low abundant peptides as for example post-translational modified peptides are most often not detected because of significant background noise (Sherrod et al., 2012). Also the amount of available precursor ions exceeds the number of product ion scans (Schmidt et al., 2009). Moreover, high intensity precursor ions are being oversampled in regard to the total number of peptides. Hence, directed and targeted approaches have been developed to overcome these sampling limitations.

2.7.2 Directed Mass Spectrometry

Directed proteomics circumvents the bias of automatically selecting high abundant and high intensity precursor ions, as it is the case for data dependent acquisition (DIA, data-independent acquisition) (see previous chapter). A predetermined set of peptide ions that are detected in a survey scan is selected for fragmentation, allowing the analysis of low intensity precursor ions. In a first analysis, survey scans are generated and features (mass-to-charge ratio, m/z ; retention time t_R) or peptides of interest are selected from this initial experiment

for an inclusion list. This information is then used for a second experiment during which the selected precursors of interest are chosen for fragmentation as soon as their mass (m/z) is detected in the survey scan. This means the MS^2 acquisition mode is performed in DDA mode but the precursor mass selection takes into account the additional constraints of the inclusion list (Figure 8) (Domon and Aebersold, 2010). This hypothesis-driven MS technique is applied on rapidly scanning mass spectrometers with high accuracy precursor ion measurement (hybrid linear ion trap/Orbitrap) (Schmidt et al., 2009). This provides the advantage that MS^2 analyses can be focused on non-redundant and information-rich precursor ions, which provides increased depth of analysis (Schmidt et al., 2008).

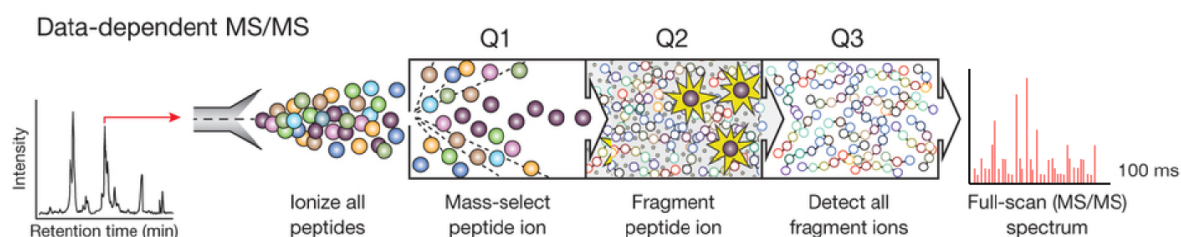


Figure 8: Directed Mass Spectrometry. A full-scan MS spectrum is acquired, however, precursor ion fragmentation takes place by taking additional constraints of an inclusion list into account during precursor mass selection. Hence full MS^2 spectra of selected precursor ions are detected. Adapted from (Gillette and Carr, 2013).

2.7.3 Targeted Mass Spectrometry

Targeted experiments also take previously acquired data into account when generating MS^2 spectra and are hence also a DIA strategy. In this case a set of predetermined product ions from precursor ions that are anticipated but not

necessarily detected in a survey scan, are being observed (Domon and Aebersold, 2010).

This workflow is generally used with selected reaction monitoring (SRM) and is based on a reference spectrum that allows the identification of an analyte using only a few selected fragment ions instead of the entire set of the MS² fragmentation spectrum (Gillette and Carr, 2013). These experiments are usually carried out on triple quadrupole instruments (QqQ) that have two mass filters. In a SRM experiment a precursor ion of a particular mass is selected in the first stage of a tandem mass spectrometer (Q₁, mass filter). This precursor ion is then selected for fragmentation (q₂). However, only selected fragment ions are then detected (Q₃, mass filter) (Figure 9) (Lange et al., 2008). A precursor ion and its specific fragment ion are referred to as transitions (precursor-fragment pairs). Relative quantification is achieved by relating the fragment ion intensities (peak areas) to the corresponding signals of isotopically labeled reference peptides of identical sequence that are spiked in as concentration standards (Domon and Aebersold, 2010). SRM can therefore be used to generate a calibration curve for absolute quantification (Gillette and Carr, 2013). Pseudo-SRM (pSRM) does not focus on single selected fragment ions but records a full MS² spectrum for each monitored peptide.

Both SRM and pSRM have become increasingly popular as they are suitable for quantification and due to the focused setup of these methods and their high resolution further increase in specificity is achieved (Gallien et al., 2012; Peterson et al., 2012).

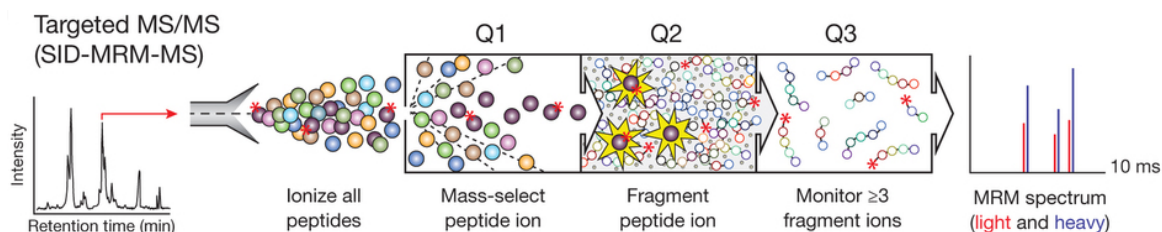


Figure 9: Targeted Mass spectrometry. During targeted experiments first proteotypic peptides uniquely representing proteins of interest are predefined from a prior experiment together with their most informative fragment ions. Those preselected peptides are selected for fragmentation (Q1 and Q2) and only fragment ions of interest are selected for detection (Q3). During pSRM all generated fragment ions of the targeted peptide are being detected. Quantification is achieved via the usage of synthetic peptides containing stable-isotope labels can be spiked in as standards (asteriks). Comparison of labeled standards and unlabeled peaks provides relative and up to absolute quantification of the endogenous analyte. Adapted from (Gillette and Carr, 2013).

2.7.4 Higher stage fragmentation of the neutral loss peaks

A common feature of the fragmentation of phospho-peptides is the neutral loss of phosphoric acid during CID of phosphorylated precursor ions if phosphorylated at serine or threonine. This loss leads to information poor MS² spectra that are dominated by the neutral loss peak that is found 80 or 98 Da lower than the precursor mass (Boersema et al., 2009). These frequent loss peaks translate into reduced intensities of sequence informative ions and most often mask peptide-specific fragment ions that are required for identification and quantification of phospho-peptides (Villén et al., 2008; Ulintz et al., 2009; Palumbo et al., 2008). Hence, this causes a general decline in MS² spectra quality. This limitation can be circumvented by isolation of the neutral loss fragment and a following second fragmentation step, called higher stage fragmentation or high-resolution higher energy collision dissociation (HCD) (Schmidt et al., 2009; Olsen et al., 2007). Once these ions are detected, they get isolated and can be either automatically selected for MS³ (in non-targeted approaches), or be manually assigned (targeted analysis) for MS³ on a subsequent LC/MS analysis (Steen et al.,

2006). This leads to a highly more selective and efficient backbone-fragmentation and therefore results in more sequence informative fragments. Another extension of MS³ acquisition is multi stage activation (MSA). This method is also used for the further analysis of neutral phospho loss peaks, however this is done without an additional isolation cycle. Hence, the initial MS² ions are trapped together with the product ions of the neutral loss fragment thereby generating a composite spectrum (Ulitz et al., 2009) (Figure 10).

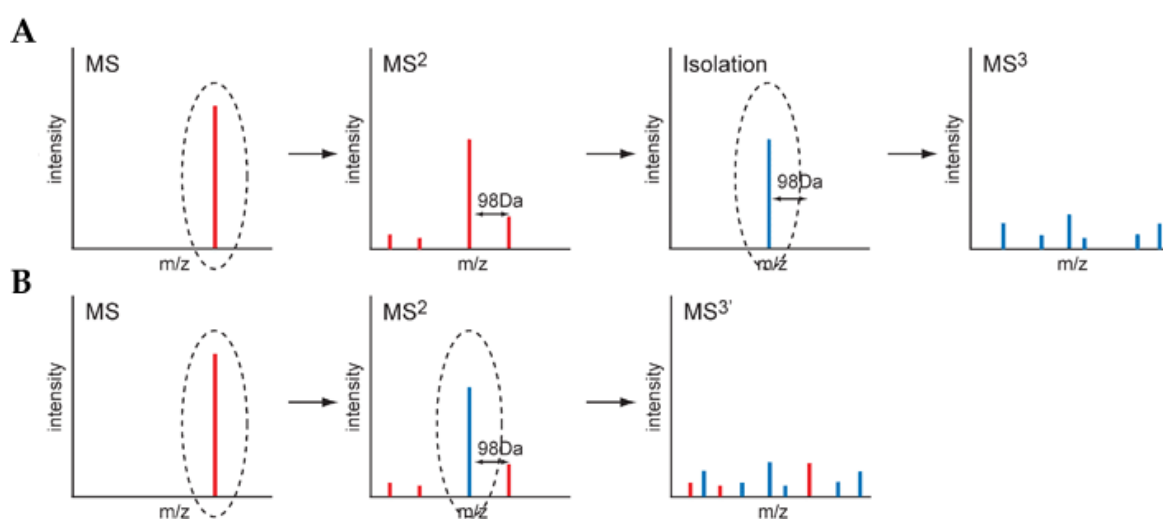


Figure 10: Neutral loss of phospho-peptides during fragmentation. (A) During MS² analysis of phospho-peptides very often the resulting fragments display a dominant neutral 2loss peak that corresponds to the loss of phosphoric acid and that only provide poor MS² spectra quality. If a neutral loss peak is detected, it gets isolated and is reselected for a second round of fragmentation yielding information-rich MS³ data. (B) During multistage activation a dominant neutral loss peak has been detected and gets reselected for a second round of fragmentation but retains the informative fragments from the precursor ion. Hereby the isolation step between MS² and MS³ is eliminated, producing structurally informative ion spectra with fragments from both collision events. Adapted from (Rogers and Foster, 2009).

3. Results

3.1 Probing the catalytic functions of Bub1 kinase using small molecule inhibitors BAY-320 and BAY-524

3.1.1 Aim of the project

Bub1 is a dual function kinase in mitosis: it is part of the SAC signaling network that monitors the metaphase-to-anaphase transition and it contributes to the mechanism of chromosome alignment. Despite of vast evidence on Bub1 specific function during mitosis, the role of its kinase activity function is still under debate.

While studies in yeast and *Xenopus laevis* share no consensus on whether kinase activity of Bub1 is needed (Fernius and Hardwick, 2007; Rischitor et al., 2007; Sharp-Baker and Chen, 2001) or not (Yamaguchi et al., 2003), the common comprehension of Bub1 function in SAC signaling in mammals goes without its kinase activity (Ricke et al., 2012; Perera and Taylor, 2010; Klebig et al., 2009). Still, studies propose a direct involvement of Bub1 catalytic activity on APC/C inhibition.

The ultimate aim of this study was to examine the role of Bub1 kinase activity during mitotic progression, and by doing so to shed more light upon the requirement of Bub1 kinase activity for SAC signaling.

The foundation and starting point of the presented work was the recent availability of two Bub1 inhibitors designed and synthesized by BAYER Pharma AG. BAY-320 and BAY-523, two small molecule inhibitors, allowed the specific inhibition of Bub1 *in vitro* and *in vivo* and thus gave the advantage to distinguish scaffold and catalytic functions with temporal resolution.

3.1.2 Introduction

The maintenance of euploidy during cell division is important for survival and development of all organisms. During mitosis of higher eukaryotes, a highly conserved surveillance mechanism termed SAC, safeguards correct chromosome segregation by delaying anaphase onset. The attachment and orientation of chromosomes within the mitotic spindle is sensed at kinetochores (KTs), proteinaceous structures located at mitotic centromeres. Until full chromosomal alignment is achieved, KTs relay a 'wait signal' through the generation of a diffusible inhibitor of the ubiquitin ligase APC/C, termed MCC (Musacchio, 2011; Foley and Kapoor, 2013; Sacristan and Kops, 2015). The formation of MCC critically depends on the assembly of several protein kinases at KTs, including Aurora B, Monopolar spindle 1 (Mps1) and Budding uninhibited by benzimidazoles 1 (Bub1) (Santaguida et al., 2011; Jelluma et al., 2010; Meraldi and Sorger, 2005). These in turn regulate both correct KT-MT attachment and SAC activity. Once chromosome bi-orientation is achieved through stable KT-MT attachments, the SAC is silenced through MT-dependent removal of checkpoint components as well as local phosphatase activity; this allows APC/C-driven degradation of several mitotic proteins, including Securin and Cyclin B, and results in the onset of chromatid separation and mitotic exit (Funabiki and Wynne, 2013).

The serine/threonine kinase Bub1, along with Bub3, is one of the first proteins to accumulate at unattached KTs (Jablonski et al., 1998), governed by Mps1-dependent phosphorylation of MELT motifs on the KMN complex member KNL-1 (Yamagishi et al., 2012; London et al., 2012; Shepperd et al., 2012; Vleugel et al., 2013; Overlack et al., 2015). At KTs, Bub1 is then thought to regulate a variety of processes, including chromosome cohesion, KT-MT interactions and SAC function through the recruitment of additional factors, notably Sgo1, CENP-E, CENP-F, BubR1, Aurora B kinase, Mad1 and Mad2 (Kitajima et al., 2005; Liu et al.,

2013a; Taylor and McKeon, 1997; Meraldi and Sorger, 2005; Perera et al., 2007; Klebig et al., 2009). In particular, depletion of Bub1 was reported to interfere with chromosome alignment as well as mitotic arrest (Meraldi and Sorger, 2005; Perera et al., 2007; Klebig et al., 2009), but the importance of Bub1 catalytic activity for mitotic progression remains controversial. While studies in yeast and frog show a requirement of Bub1 kinase activity for KT function, it is believed that in mammals Bub1 primarily acts as a non-catalytic scaffold (Fernius and Hardwick, 2007; Rischitor et al., 2007; Sharp-Baker and Chen, 2001; Johnson et al., 2004; Boyarchuk et al., 2007; Overlack et al., 2015). In particular, Bub1 kinase activity was reported to be important for chromosome alignment but dispensable for SAC signaling (Ricke et al., 2012; Perera and Taylor, 2010; Klebig et al., 2009).

Here we present a thorough characterization of two novel small-molecule ATP-competitive inhibitors of Bub1 kinase. We show that BAY-320 and BAY-524 act as potent inhibitors of human Bub1 *in vitro* and *in vivo*. By comparing phenotypes provoked by Bub1 kinase inhibition and Bub1 protein depletion we are able to differentiate between catalytic and non-catalytic functions of Bub1. We demonstrate that Bub1 catalytic activity is required for chromosome arm resolution and the establishment of centromeric Sgo pools. Moreover, Bub1 kinase activity regulates the chromosomal localization of Aurora B and the CPC. In this function, Bub1 cooperates with Haspin, and chemical inhibition of both Bub1 and Haspin kinases show an additive effect. In striking contrast, Bub1 catalytic activity is largely dispensable for chromosome alignment and SAC function, arguing that Bub1 largely operates as a scaffolding protein. However, even though Bub1 inhibition per se exerts only minor effects on mitotic fidelity, BAY-320 and BAY-524 treatment sensitizes cells to low doses of Paclitaxel, resulting in remarkable impairment of chromosome segregation and cell proliferation.

3.1.3 The inhibitors BAY-320 and BAY-524 specifically inhibit Bub1 kinase *in vitro* and *in vivo*

The chemical synthesis of small molecule inhibitors against Bub1 has recently been described (Hitchcock et al., 2013). In this study we used the two compounds 2-[5-cyclopropyl-1-(4-ethoxy-2,6-difluorobenzyl)-4-methyl-1H-pyrazol-3-yl]-5-methoxy-N-(pyridin-4-yl)-pyrimidin-4-amine and 2-[1-(4-ethoxy-2,6-difluorobenzyl)-5-methoxy-4-methyl-1H-pyrazol-3-yl]-5-methoxy-N-(pyridin-4-yl)pyrimidin-4-amine, abbreviated as BAY-320 and BAY-524, respectively (Figure 11).

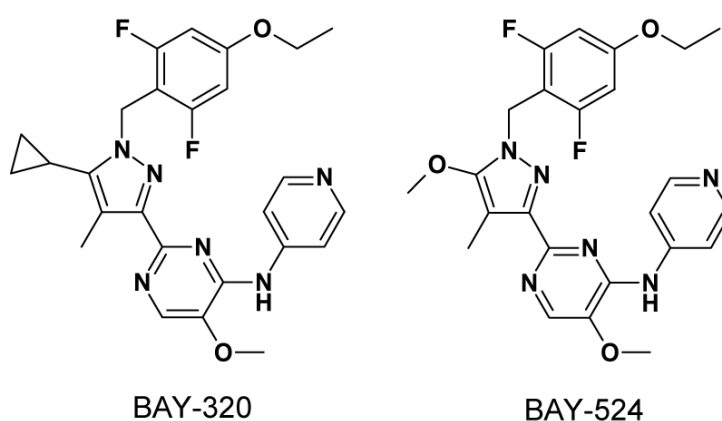


Figure 11: Chemical structures of ATP-competitive inhibitors BAY-320 and BAY-524.

When assayed *in vitro* in presence of 2 mM ATP, both compounds inhibited the catalytic domain of recombinant human Bub1 (amino acids 704-1085) with an IC_{50} of 680 ± 280 nM and 450 ± 60 nM, respectively (Table 2).

Table 2: IC₅₀ profile of BAY-320 and BAY-524. (Data by courtesy of BAYER Pharma AG)

	MW [g/mol]	Bub1 kinase inhibition (2 mM ATP)		HeLa proliferation		HeLa proliferation (3 nM Paclitaxel)		A375 pro- liferation	A375 proliferation (3 nM Paclitaxel)
		IC50	SD	IC50	SD	IC50	SD	IC50	IC50
BAY-320	492.5	6.8E-07	2.8E-07	4.0E-06	1.4E-06	6.7E-07	2.7E-07	3.6E-06	4.0E-07
BAY-524	482.5	4.5E-07	6.0E-08	8.1E-06	1.2E-06	6.4E-07	5.9E-07	nd	nd

concentrations are depicted in M

When tested against a panel of 222 protein kinases, BAY-320 showed only modest cross reactivity with other kinases, even when used at a concentration of 10 μ M (Table 3). *In vitro* inhibition of Bub1 by BAY-320 and BAY-524 was demonstrated by monitoring both Bub1 autophosphorylation and phosphorylation of human histone H2A on threonine 120 (Thr120), the best characterized physiological substrate (Kawashima et al., 2010) (Figure 12).

Table 3: Kinase-selectivity profile of BAY-320. Percentage of residual kinase activity at 10 μ M BAY-320 is shown. (Data by courtesy of BAYER Pharma AG)

Kinase	Activity*	Kinase	Activity*	Kinase	Activity*
Abl(h)	98	Flt4(h)	50	PDK1(h)	124
ACK1(h)	108	Fms(h)	76	PhK γ 2(h)	38
ALK(h)	60	Fyn(h)	91	Pim-1(h)	56
ALK4(h)	82	GCK(h)	79	Pim-2(h)	119
Arg(h)	78	GRK5(h)	99	Pim-3(h)	112
ARK5(h)	85	GRK6(h)	102	PKA(h)	141
ASK1(h)	86	GRK7(h)	96	PKB α (h)	93
Aurora-A(h)	105	GSK3 α (h)	148	PKB β (h)	57
Aurora-B(h)	99	GSK3 β (h)	209	PKB γ (h)	47
Axl(h)	91	Haspin(h)	47	PKC α (h)	102
Blk(m)	48	Hck(h)	110	PKC β I(h)	97
Bmx(h)	122	HIPK1(h)	105	PKC β II(h)	96
BRK(h)	72	HIPK2(h)	81	PKC γ (h)	100
BrSK1(h)	70	HIPK3(h)	102	PKC δ (h)	99
BrSK2(h)	108	IGF-1R(h)	50	PKC ϵ (h)	106
BTK(h)	130	IKK α (h)	115	PKC η (h)	101
CaMKI(h)	41	IKK β (h)	107	PKC ζ (h)	100
CaMKII β (h)	84	IR(h)	84	PKC μ (h)	107
CaMKII γ (h)	106	IRR(h)	99	PKC θ (h)	88
CaMKI δ (h)	54	IRAK1(h)	105	PKD2(h)	90
CaMKII δ (h)	89	IRAK4(h)	74	PKG1 α (h)	89
CaMKIV(h)	77	Itk(h)	103	PKG1 β (h)	82
CDK1/cyclinB(h)	68	JAK2(h)	206	Plk1(h)	127
CDK2/cyclinE(h)	76	JAK3(h)	146	Plk3(h)	112
CDK3/cyclinE(h)	92	JNK1 α 1(h)	89	PRAK(h)	102

CDK5/p35(h)	119	JNK2 α 2(h)	92	PRK2(h)	96
CDK6/cyclinD3(h)	80	JNK3(h)	46	PrKX(h)	65
CDK7/cyclinH/MAT1(h)	99	KDR(h)	82	PTK5(h)	224
CDK9/cyclin T1(h)	104	Lck(h)	32	Pyk2(h)	113
CHK1(h)	113	LIMK1(h)	95	Ret(h)	102
CHK2(h)	56	LKB1(h)	105	RIPK2(h)	85
CK1 γ 1(h)	114	LOK(h)	76	ROCK-I(h)	79
CK1 γ 2(h)	120	Lyn(h)	58	ROCK-II(h)	93
CK1 γ 3(h)	97	MAPK1(h)	94	Ron(h)	80
CK1 δ (h)	104	MAPK2(h)	95	Ros(h)	92
CK2(h)	96	MAPKAP-K2(h)	77	Rse(h)	131
CK2 α 2(h)	110	MAPKAP-K3(h)	85	Rsk1(h)	72
CLK2(h)	115	MEK1(h)	96	Rsk2(h)	55
CLK3(h)	90	MARK1(h)	92	Rsk3(h)	99
cKit(h)	79	MELK(h)	58	Rsk4(h)	79
CSK(h)	76	Mer(h)	38	SAPK2a(h)	102
c-RAF(h)	78	Met(h)	62	SAPK2b(h)	103
cSRC(h)	111	MINK(h)	50	SAPK3(h)	105
DAPK1(h)	56	MKK4(m)	108	SAPK4(h)	106
DAPK2(h)	62	MKK6(h)	100	SGK(h)	63
DCAMKL2(h)	140	MKK7 β (h)	136	SGK2(h)	64
DDR2(h)	81	MLCK(h)	50	SGK3(h)	46
DMPK(h)	110	MLK1(h)	82	SIK(h)	121
DRAK1(h)	50	Mnk2(h)	89	Snk(h)	101
DYRK2(h)	94	MRCK α (h)	117	SRPK1(h)	103
eEF-2K(h)	156	MRCK β (h)	89	SRPK2(h)	102
EGFR(h)	75	MSK1(h)	47	STK33(h)	92
EphA1(h)	87	MSK2(h)	81	Syk(h)	64
EphA2(h)	114	MSSK1(h)	103	TAK1(h)	106
EphA3(h)	59	MST1(h)	84	TAO1(h)	74
EphA4(h)	88	MST2(h)	51	TAO2(h)	74
EphA5(h)	119	MST3(h)	33	TAO3(h)	80
EphA7(h)	89	mTOR(h)	100	TBK1(h)	102
EphA8(h)	116	MuSK(h)	55	TGFBR1(h)	98
EphB2(h)	106	NEK2(h)	97	Tie2 (h)	46
EphB1(h)	140	NEK3(h)	61	TLK2(h)	94
EphB3(h)	93	NEK6(h)	118	TrkA(h)	37
EphB4(h)	102	NEK7(h)	85	TrkB(h)	149
ErbB4(h)	128	NEK11(h)	83	TSSK1(h)	93
FAK(h)	89	NLK(h)	89	TSSK2(h)	95
Fer(h)	90	p70S6K(h)	50	Txk(h)	46
Fes(h)	91	PAK2(h)	89	ULK2(h)	94
FGFR1(h)	66	PAK4(h)	94	ULK3(h)	102
FGFR2(h)	102	PAK5(h)	120	WNK2(h)	84
FGFR3(h)	143	PAK6(h)	95	WNK3(h)	91
FGFR4(h)	134	PAR-1B α (h)	103	VRK2(h)	104
Fgr(h)	143	PASK(h)	44	Yes(h)	100
Flt1(h)	40	PDGFR α (h)	102	ZAP-70(h)	120
Flt3(h)	97	PDGFR β (h)	99	ZIPK(h)	56

* % residual kinase activity at 10 μ M BAY-320

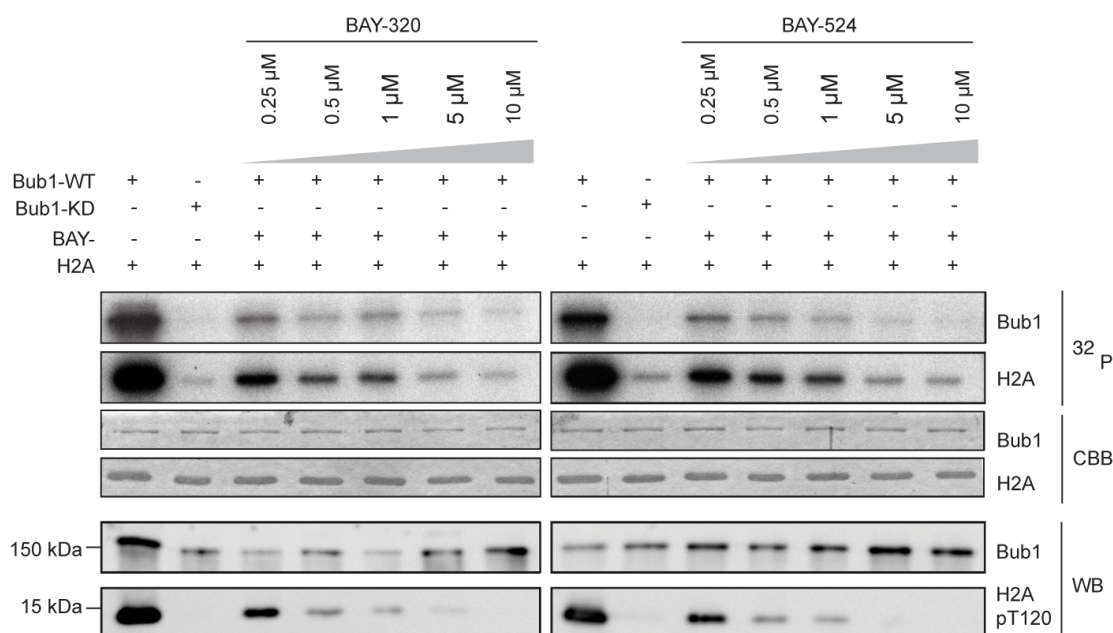


Figure 12: BAY-320 and BAY-524 inhibit Bub1 kinase *in vitro*. *In vitro* kinase assays showing dose-dependent inhibition of Bub1 kinase activity towards histone H2A. Assays were performed by mixing human wild-type (WT) or kinase-dead (KD) LAP-Bub1, ectopically expressed in and purified from mitotic HEK 293T cells, with recombinantly expressed histone H2A as a substrate, γ - 32 P-ATP and increasing doses of the Bub1 inhibitors BAY-320 and BAY-524. After 30 min at 30°C, reactions were stopped and analyzed by gel electrophoresis. Bub1 autophosphorylation and H2A phosphorylation were visualized by autoradiography (32 P) and protein levels were monitored by Coomassie brilliant blue staining (CBB). Histone H2A-T120 phosphorylation (pT120-H2A) was detected by phospho-antibody probing of Western blots (WB) and Bub1 was monitored as control.

To test whether BAY-320 and BAY-524 also inhibit Bub1 in intact cells, increasing doses of inhibitors were applied to mitotically synchronized HeLa and hTERT-RPE1 (RPE1) cells, and phospho-histone H2A-Thr210 staining at KTs was monitored by immunofluorescence (Figure 13). These studies revealed that near-maximal inhibition of Bub1 could be achieved by using BAY-320 at 3 μ M and BAY-524 at 7 μ M; these concentrations were therefore used for long-time treatment (>10 h) in all future experiments on intact cells. At concentrations of 10 μ M or above, both inhibitors increasingly caused inhibition of cell proliferation and cell death (data not shown).

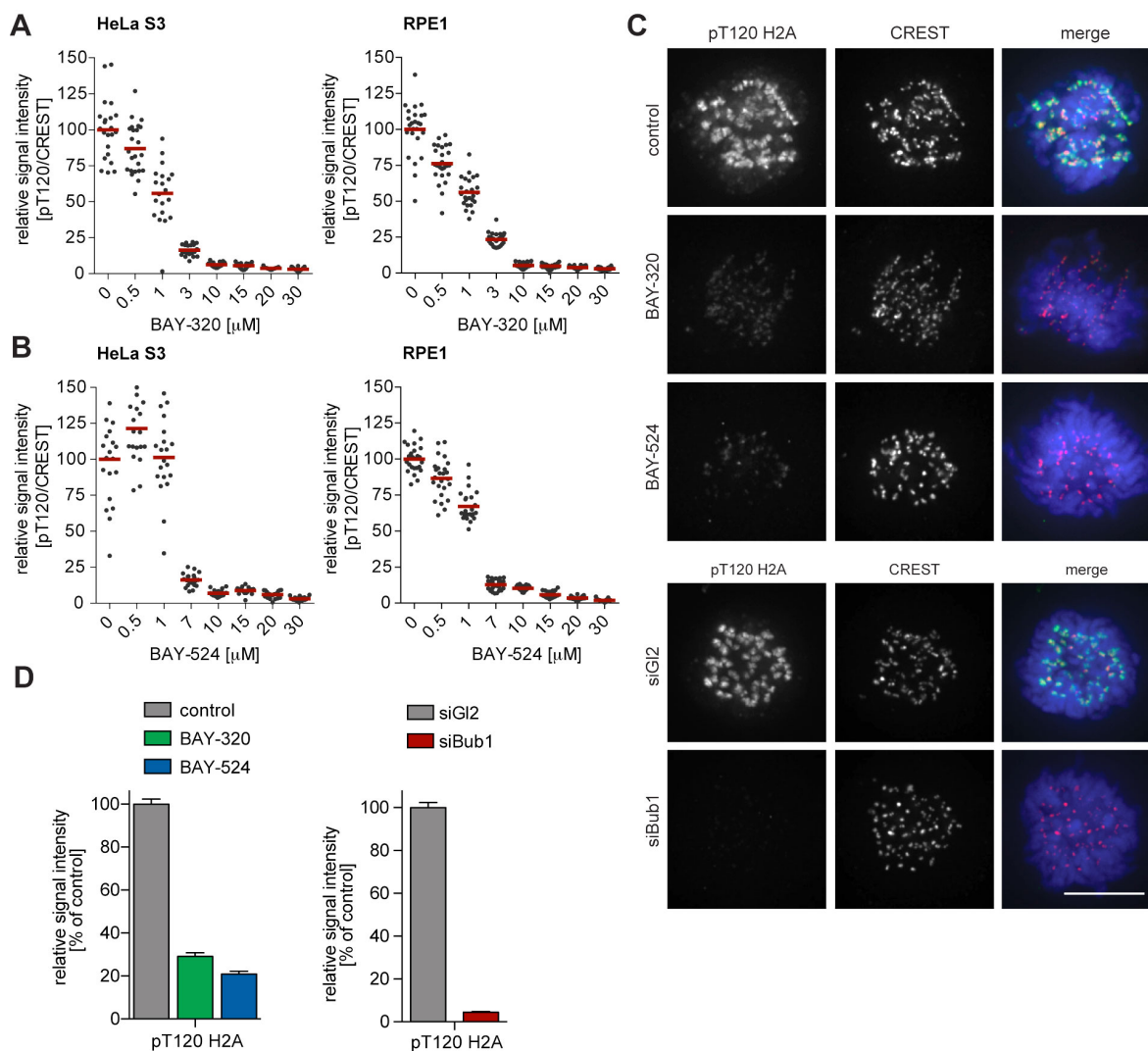


Figure 13: BAY-320 and BAY-524 inhibit Bub1 kinase *in vivo*. (A, B) Inhibition of Bub1 reduces histone H2A-T120 phosphorylation. Asynchronous cultures of HeLa S3 (left panels) and RPE1 cells (right panels) were treated with the proteasomal inhibitor MG132 for 2h, followed by the addition of 3.3 mM nocodazole and increasing doses of BAY-320 (A) or BAY-524 (B) for 1 h. Cells were fixed and analyzed by immunofluorescence microscopy (IFM). Scatter plots show centromeric levels of pT120-H2A (n=19-28 cells per condition). Bars represent mean values. (C) HeLa S3 cells were synchronized by thymidine block, released for 10 h in the presence of solvent (control), 3 μ M BAY-320 or 7 μ M BAY-524 and analyzed by quantitative IF (top panels). Cells transfected with mock (GI2) or Bub1 siRNA-oligonucleotides for 48 h were synchronized and analyzed in parallel (bottom panels) Cells were stained with antibodies raised against Bub1 and pT120-H2A. Human CREST serum was used to identify centromeres and DNA was stained with DAPI; scale bars represent 10 μ m. (D) Histograms showing the average signal intensities of centromeric pT120-H2A observed in the experiments described in (C); n=73-107 cells per condition. Error bars represent standard error of the mean (SEM). (Panel A and B by courtesy of Dr. Conrad von Schubert)

To corroborate the above immunofluorescence data, histones were purified from control and inhibitor-treated cells. Examination of histone H2A phosphorylation by Western blotting revealed that treatment of cells with either BAY-320 or BAY-524 drastically reduced Thr210 phosphorylation (Figure 14). Thus, BAY-320 and BAY-524 act as potent and selective inhibitors of Bub1 kinase *in vitro* and *in vivo* and thus constitute attractive tools to study Bub1 catalytic function during mitosis.

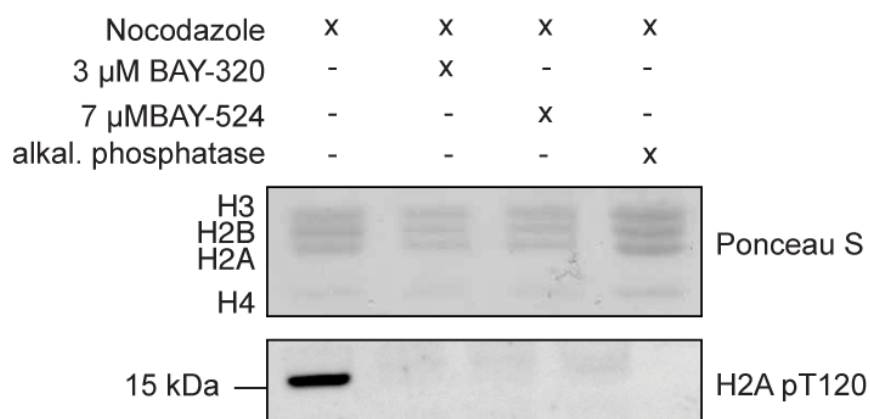


Figure 14: BAY-320 and BAY-524 reduce T120-H2A phosphorylation *in vivo*. To monitor the efficiency of Bub1 kinase inhibition *in vivo*, HeLa S3 cells were synchronized by thymidine block and released for 14 h in the presence of 3.3 μ M nocodazole as well as solvent or Bub1 inhibitors solvent as indicated. Prometaphase-arrested cells were harvested by shake-off and subsequently mitotic cell extracts were selectively treated with phosphatase inhibitor for 30 min at 30 °C. Histone isolation was followed by Western blot analysis of histone H2A T120 phosphorylation levels. Equal loading was monitored by Ponceau S staining.

3.1.4 Inhibition of Bub1 kinase activity

Next, we set out to directly compare the impact of Bub1 kinase inhibition with the previously reported consequences of siRNA-mediated Bub1 depletion (Johnson et al., 2004; Meraldi and Sorger, 2005; Boyarchuk et al., 2007) or genetic

Bub1 knock-out (Jeganathan et al., 2007; Perera et al., 2007). In a first series of experiments we used time-lapse imaging to compare progression through mitosis in asynchronously growing HeLa and RPE1 cells in response to either Bub1 inhibition or siRNA-mediated Bub1 depletion. In line with previous results (Tang et al., 2004b; Kitajima et al., 2005), depletion of Bub1 from HeLa cells significantly prolonged duration of mitosis, due to delayed chromosome alignment and transient prometa- and metaphase arrest (Figure 15B, C and D). Efficiency of siRNA-mediated depletion was monitored by Western blotting (Figure 15A).

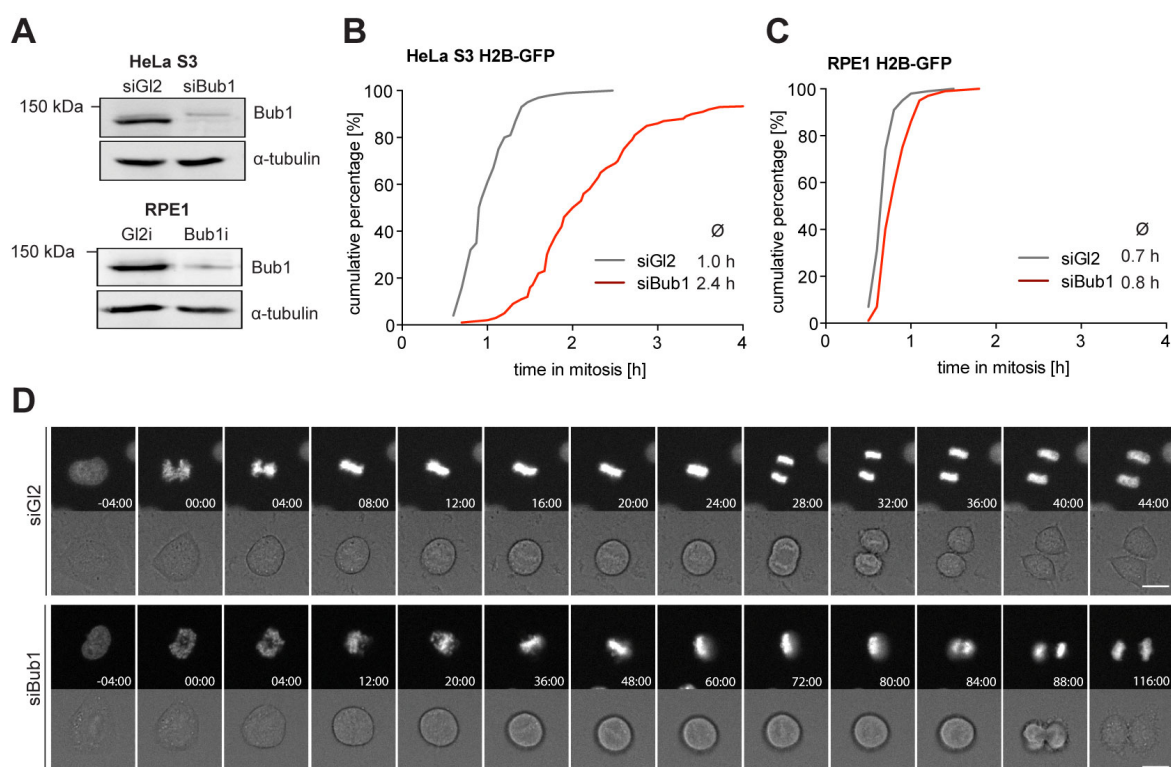


Figure 15: Bub1 depletion prolongs mitotic timing. (A) Western blots showing representative Bub1 depletion efficiencies. Asynchronous cultures of HeLa S3 or RPE1 cells were transfected with control (GL2) or Bub1 siRNA-oligos for 48 h, harvested and analyzed by Western blotting. α -tubulin served as loading control. (B) (C) Graphs show the cumulative frequency of mitotic duration determined by cell rounding/flattening. Indicated averages represent the time spent in mitosis (n=100 cells per condition). (D) Representative stills from time-lapse recordings of asynchronously growing cultures of HeLa S3 cells stably expressing GFP-tagged histone H2B. Cells were transfected with control (GL2) or Bub1 siRNA for 48 h prior to time-lapse microscopy. Scale bars represent 10 μ m.

In stark contrast, treatment with either BAY-320 or BAY-524 provoked at most minor effects on mitotic progression, marked by a short delay of anaphase onset (Figure 16). Furthermore, in contrast to aneuploid HeLa cells, diploid RPE1 cells were not significantly affected by either Bub1 inhibition or depletion (Figure 15C, Figure 16C and E).

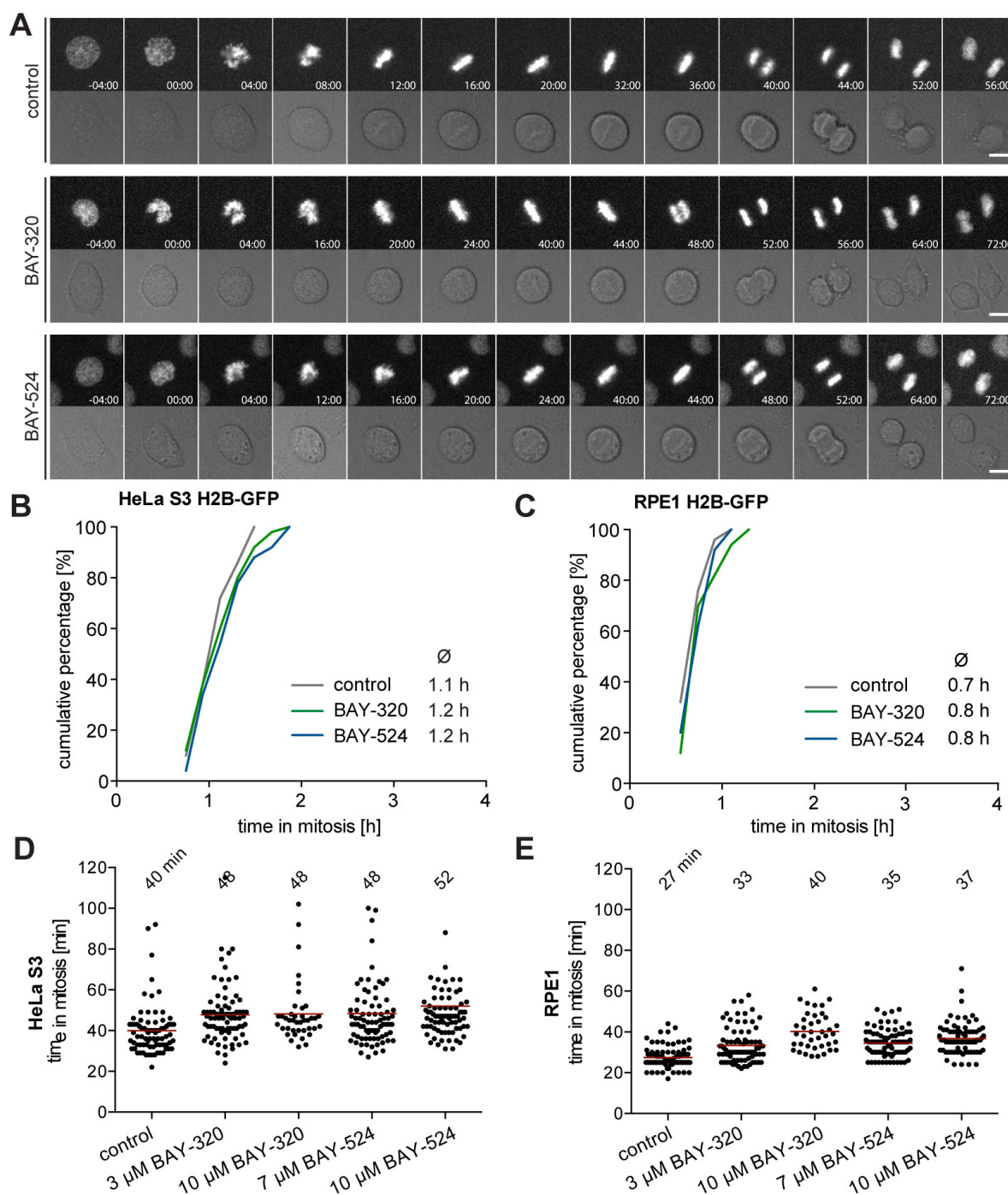


Figure 16: Inhibition of Bub1 kinase activity does not affect mitotic progression. (A) Representative stills from time-lapse recordings of asynchronously growing cultures of HeLa S3 cells stably expressing GFP-tagged histone H2B. Cells were treated with Bub1 inhibitors (3 μ M BAY-320 and 7 μ M BAY-524) prior to time-lapse microscopy. Scale bars represent 10 μ m. (B, C) Graphs show the cumulative frequency of mitotic duration determined by cell rounding/flattening. Indicated averages represent the time spent in mitosis (n=100 cells per condition). (D, E) HeLa S3 (D) or RPE1 (E) cells stably expressing GFP-H2B were treated with solvent (control) or Bub1 inhibitors at indicated doses and monitored by fluorescence time-lapse imaging. Dot plots show the time from mitotic entry to anaphase onset; bars represent mean values (n=80 cells per condition). (Panel D and E by courtesy of Dr. Conrad von Schubert)

Flow-cytometric analyses confirmed that Bub1 depletion from HeLa cells causes an increase in the G₂/M population of HeLa but not RPE-1 cells and that Bub1 inhibition by BAY-320 or BAY-524 did not detectably affect cell cycle profiles in either cell line (Figure 17). We conclude that inhibition of Bub1 kinase activity in either HeLa or RPE-1 cells produces at most subtle effects on mitotic progression, whereas Bub1 depletion exerts more profound effects, at least in HeLa cells. These results are consistent with the demonstration that Bub1 kinase activity is not required for the development and viability of mice (Ricke et al., 2012).

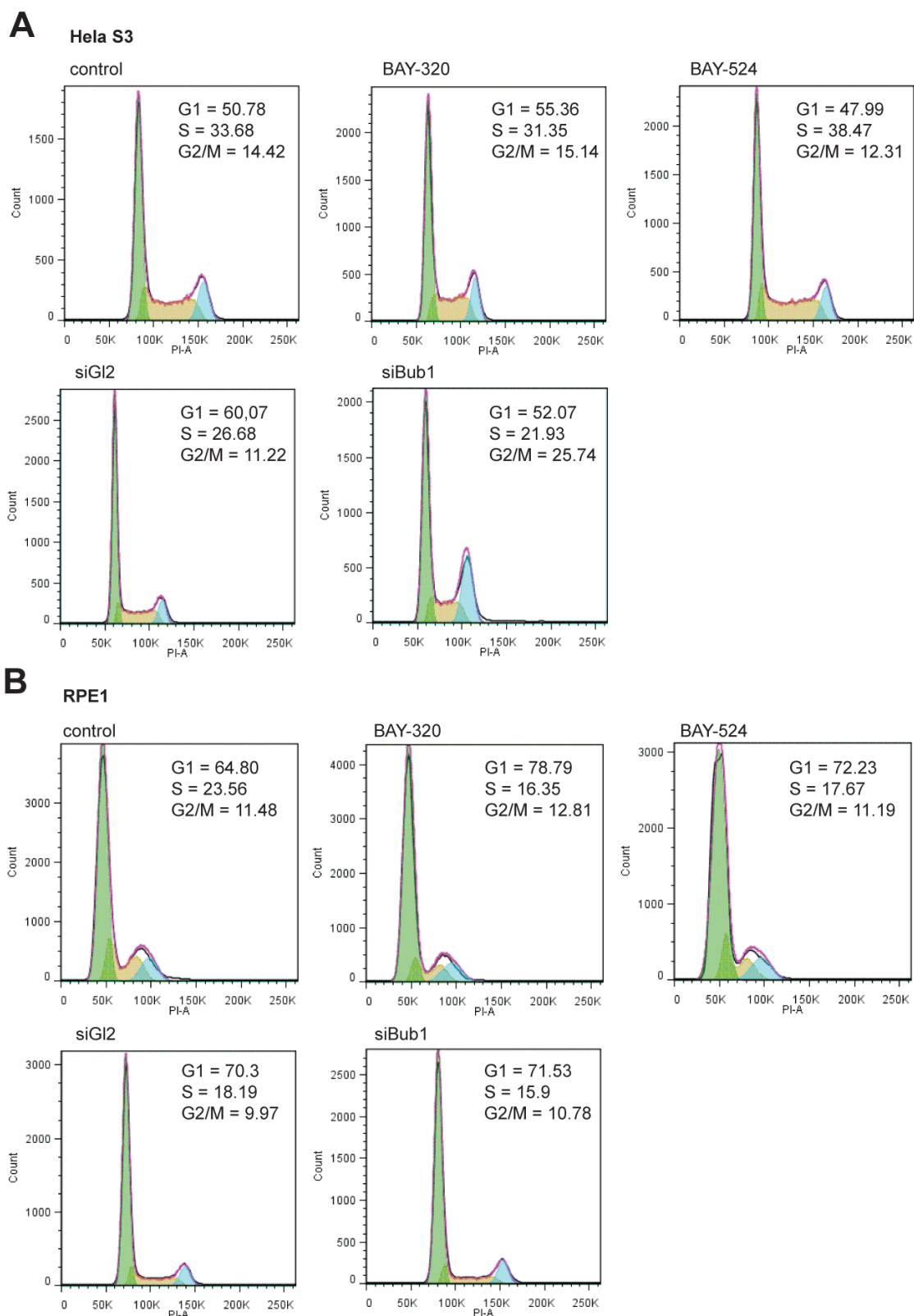


Figure 17: Bub1 depletion but not inhibition affects cell cycle distribution. (A, B) Cell cycle distribution of exponentially growing HeLa S3 (A) and RPE1 (B) cells upon treatment with solvent (control), 3 μ M BAY-320, 7 μ M BAY-524 or after Bub1 protein depletion (siGl2 served as control). After 48 h of treatment or siRNA oligo transfection cells were permeabilized and DNA was stained with propidium iodide. Cellular DNA content was determined using flow cytometry and frequencies in percentage of G1, S and G2/M phases determined.

3.1.5 Catalytic activity of Bub1 regulates Shugoshin localization and chromatid cohesion

One of the most interesting effects of Bub1 depletion described so far relates to sister chromatid cohesion (Tang et al., 2004b; Kitajima et al., 2005; Perera and Taylor, 2010; Fernius and Hardwick, 2007; Boyarchuk et al., 2007). In particular, depletion of Bub1 was shown to cause persistent arm cohesion and a redistribution of Sgo proteins from centromeres to chromosome arms (Kitajima et al., 2005). Moreover, Bub1 has been implicated in Sgo recruitment to centromeres through phosphorylation of histone H2A Thr120 (Kawashima et al., 2010; Liu et al., 2013a).

To directly demonstrate a role for Bub1 kinase activity in sister chromatid cohesion, we analyzed chromosome spreads prepared from mitotic HeLa cells or RPE1 cells after treatment with Bub1 inhibitors (Figure 18A, B and E) or Bub1-specific siRNA for comparison (Figure 18C-E). While mitotic chromosome spreads from nocodazole-treated control cells showed the expected X-shape structure, indicative of centromere cohesion, most cells treated with either Bub1 inhibitors or Bub1 siRNA showed sister chromatids whose arms remained paired (Figure 18).

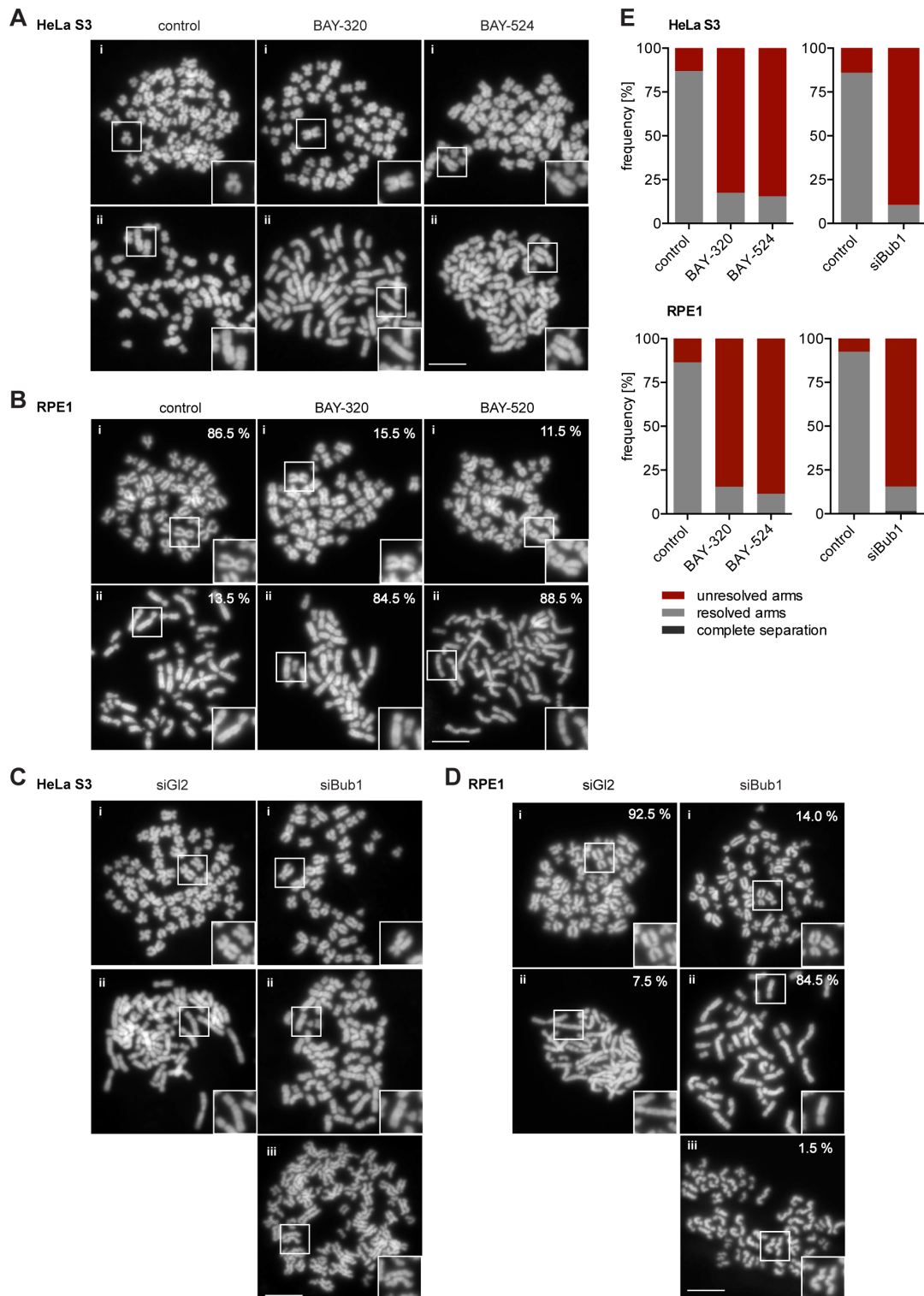


Figure 18: Catalytic activity of Bub1 defines chromatid cohesion. (A) (B) HeLa S3 (A) or RPE1 (B) cells were synchronized by thymidine block (4 mM in case of RPE1) and released for 12 h or 3 h respectively, in the presence of 3.3 mM nocodazole as well as solvent (control), 3 μ M BAY-320 or 7 μ M BAY-524. (C) (D) HeLa S3 (C) or RPE1 (D) cells were transfected with mock (Gl2) or Bub1 siRNA-oligos for 48 h were synchronized and analyzed in parallel as (A) and (B). Micrographs show representative chromosome spreads prepared from mitotic cells. Scale bars represent 10 μ m. (E) Quantitative results of the experiment described in (A) (B) (C) and (D). n= 200 cells per condition.

Moreover, centromeric levels of Sgo1 and Sgo2 were reduced to about 20% of control values in BAY-320 or BAY-524 treated cells (Figure 19A and B) and concomitantly, a significant redistribution of Sgo2 to chromosome arms could be observed (Figure 19C and D). We thus conclude that Bub1 catalytic activity contributes to the regulation of sister chromatid cohesion and the localization of Sgo proteins.

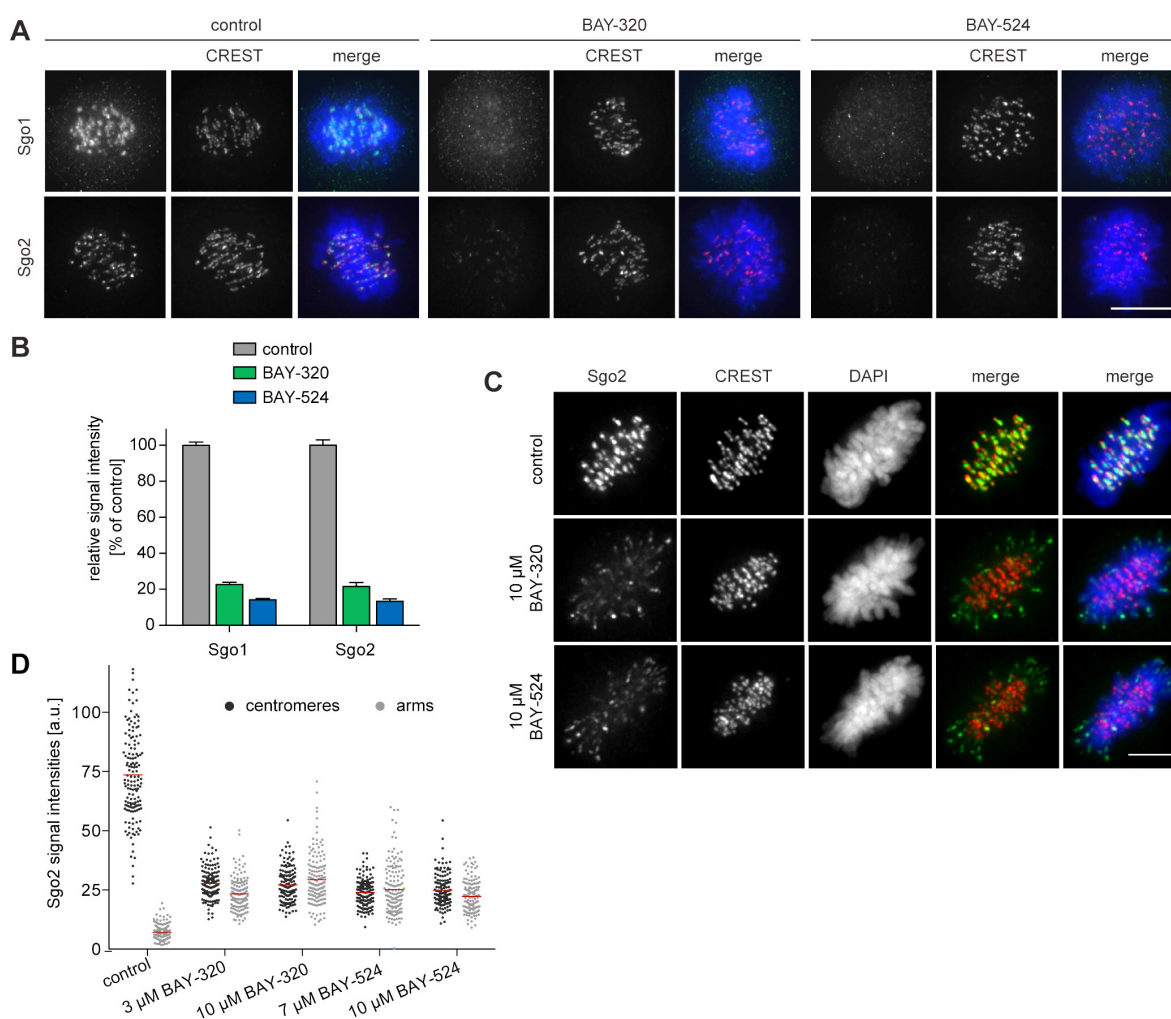


Figure 19: Catalytic activity of Bub1 defines Sgo1 and Sgo2 localization. (A) HeLa S3 cells were released from a thymidine arrest into solvent, 3 μ M BAY-320 or 7 μ M BAY-524. Cells were fixed and stained for Sgo1, Sgo2, CREST and DNA (DAPI) and analyzed by IFM. Scale bars represent 10 μ m. (B) Histogram showing average centromeric Sgo levels observed in the experiments described in (A); n=43-120 cells per condition. Error bars represent SEM. (C) Asynchronous cultures of RPE1 cells were treated with indicated doses of Bub1 inhibitors for 3 h, fixed and analyzed by IFM. Scale bar represents 5 μ m. (D) Dot plot showing the quantitative results of the experiment shown in (C). Sgo2 levels at centromeres and chromosome arms were determined in metaphase cells (n=150 centromere/arm regions from 15 different cells). Bars represent mean values. (Panel C and D by courtesy of Dr. Conrad von Schubert)

3.1.6 Bub1 inhibition affects the CPC

In addition to preserving sister chromatid cohesion, Sgo1 and Sgo2 play important roles in the recruitment of the CPC, comprising Aurora B kinase, Borealin, INCENP and Survivin (Kawashima et al., 2007; Tsukahara et al., 2010). This prompted us to investigate the impact of Bub1 inhibition on Aurora B localization and activity. Centromere recruitment of the CPC is ensured by two complementary signaling branches, which are under the control of two kinases, Bub1 and Haspin, respectively. In the first branch, Bub1-dependent phosphorylation of histone H2A-T120 (Kawashima et al., 2010; Sharp-Baker and Chen, 2001; Lin et al., 2014) triggers the centromere localization of Sgo1, which in turn recruits the CPC subunit Borealin (Kawashima et al., 2010; Tsukahara et al., 2010; Yamagishi et al., 2010). In the second branch, Haspin-dependent phosphorylation of histone H3 at T3 triggers the centromere binding of the CPC component Survivin (Du et al., 2012; Kelly et al., 2010; Wang et al., 2010). Consistent with the marked effects on centromere localization of Sgo1/2, we also observed significant effects of Bub1 inhibition on Aurora B localization. After treatment of HeLa cells with BAY-320 or BAY-524, all CPC subunits examined were displaced from centromeres (Figure 20). While Bub1 inhibition reduced centromeric levels of Aurora B, Borealin and INCENP by ~50% (Figure 20A upper panel and B left panel), depletion of Bub1 lowered centromere levels of these CPC components by ~70% (Figure 20A lower panel, and B right panel).

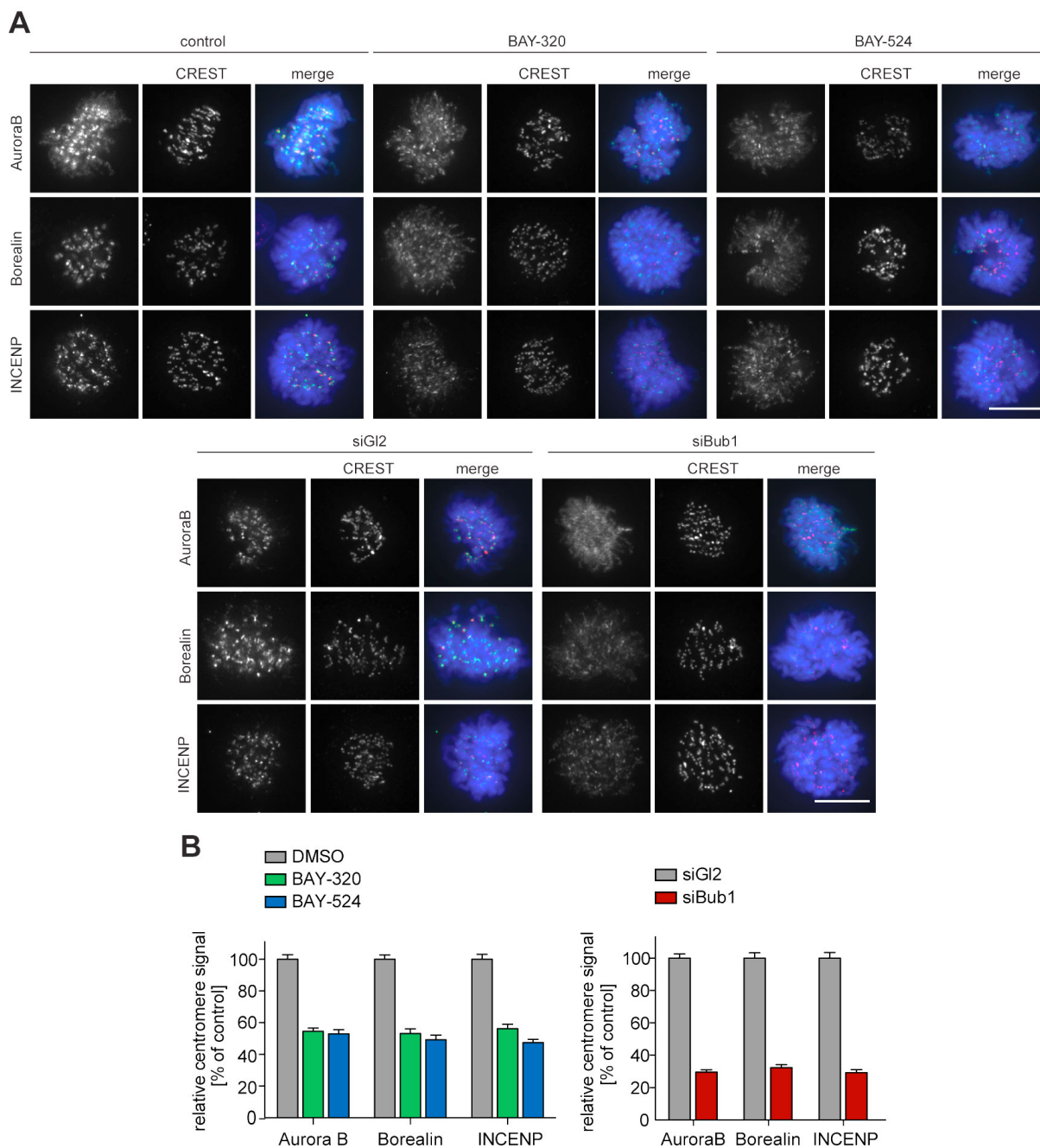


Figure 20: Bub1 inhibition affects localization and activity of the CPC. (A) Untreated or siRNA transfected (siBub1, siG12 for control) HeLa S3 cells were synchronized by thymidine block and released for 10 h, as indicated (BAY-320 was used at 3 μ M, BAY-524 at 7 μ M). Cells were fixed and stained for Aurora B, Borealin, INCENP, CREST and DNA (DAPI) and analyzed by IFM. Scale bars represent 10 μ m. **(B)** Histograms show quantitative results of the experiments described in (A). Measurements represent centromeric levels (n=63-113 cells per condition). Scale bars represent 10 μ m. Error bars represent SEM.

To examine the impact of Bub1 inhibition on the catalytic activity of Aurora B at both centromeres and chromosome arms, we next monitored phosphorylation of CENP-A Ser7 (Zeitlin et al., 2001) and histone H3 Ser10 (Hsu et al., 2000; Hirota et al., 2005), respectively. Compared to control cells, both Bub1 inhibition and depletion reduced CENP-A and histone H3 phosphorylation by ~50% and ~10-20%, respectively (Figure 21), suggesting that interference with Bub1 primarily affects Aurora B activity at centromeres. This conclusion was corroborated by showing that both inhibition and depletion of Bub1 reduced the centromere association of the Aurora B effector protein MCAK (Andrews et al., 2004) by ~50% (Figure 21).

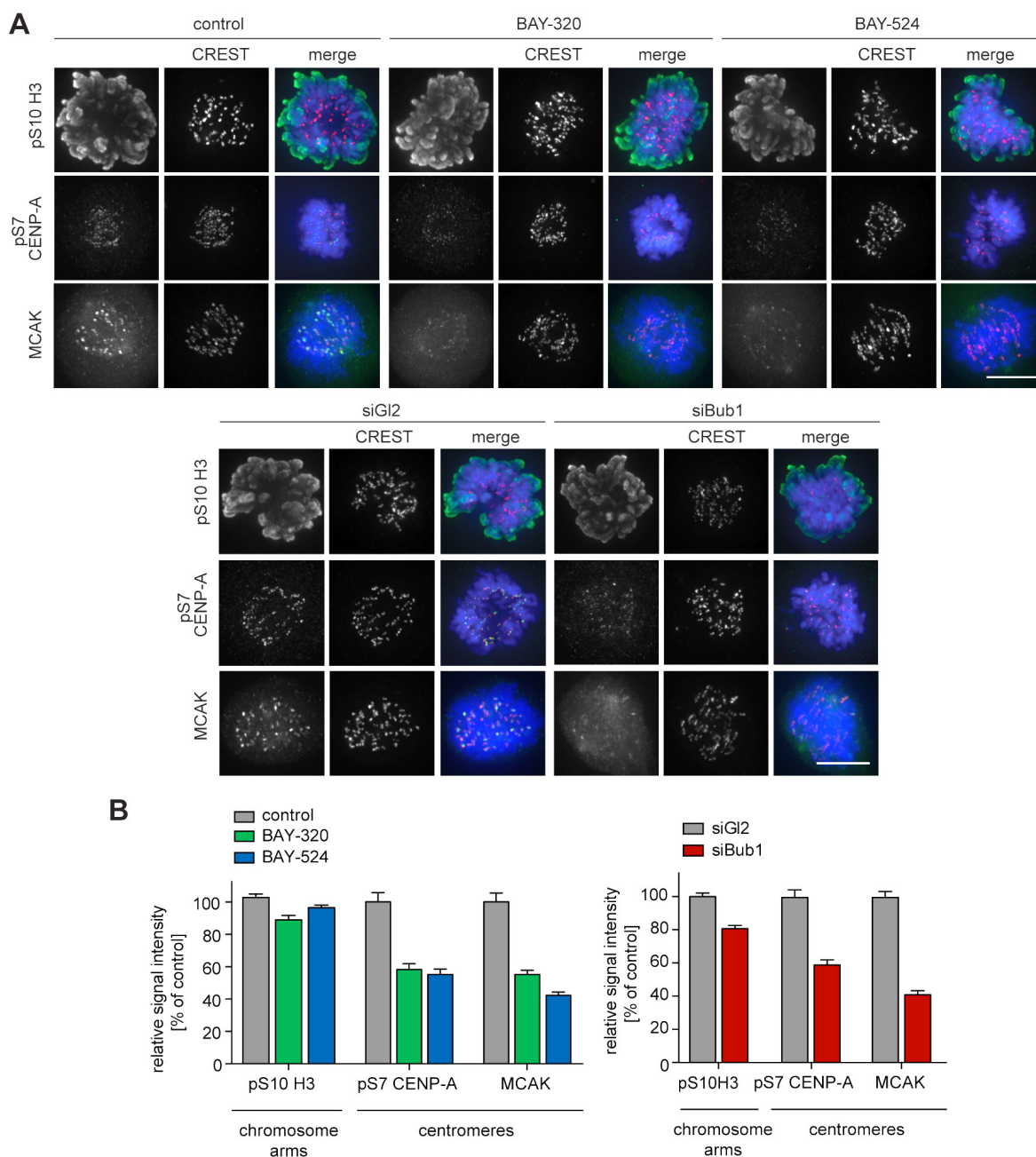


Figure 21: Bub1 inhibition affects activity of Aurora B. (A) Untreated or siRNA transfected (siBub1, siG12 for control) HeLa S3 cells were synchronized by thymidine block and released for 10 h, as indicated (BAY-320 was used at 3 μ M, BAY-524 at 7 μ M). Cells were fixed and stained for pS10-histone H3, pS7-CENP-A, MCAK, CREST and DNA (DAPI) and analyzed by IFM. Scale bars represent 10 μ m. **(B)** Histograms show quantitative results of the experiments described in (A). Measurements represent centromeric levels except for pS10-histone H3 signals, which were monitored along chromosome arms (n=40-83 cells per condition). Scale bars represent 10 μ m. Error bars represent SEM.

Furthermore, use of biosensors for Aurora B activity (Fuller et al., 2008; Wang et al., 2011) revealed a stronger reduction in fluorescence resonance energy transfer (FRET) ratios for a sensor tethered to centromeres (through fusion to histone CENP-B) than for a sensor tethered to chromosome arms (through fusion to H2B) (Figure 22). Collectively, these observations demonstrate that Bub1-dependent phosphorylation plays a major role in the regulation of Aurora B localization and activity. However, neither Bub1 inhibition nor Bub1 depletion resulted in complete removal of Aurora B from centromeres, prompting us to examine the relative contributions of Bub1 and Haspin to the process of CPC recruitment.

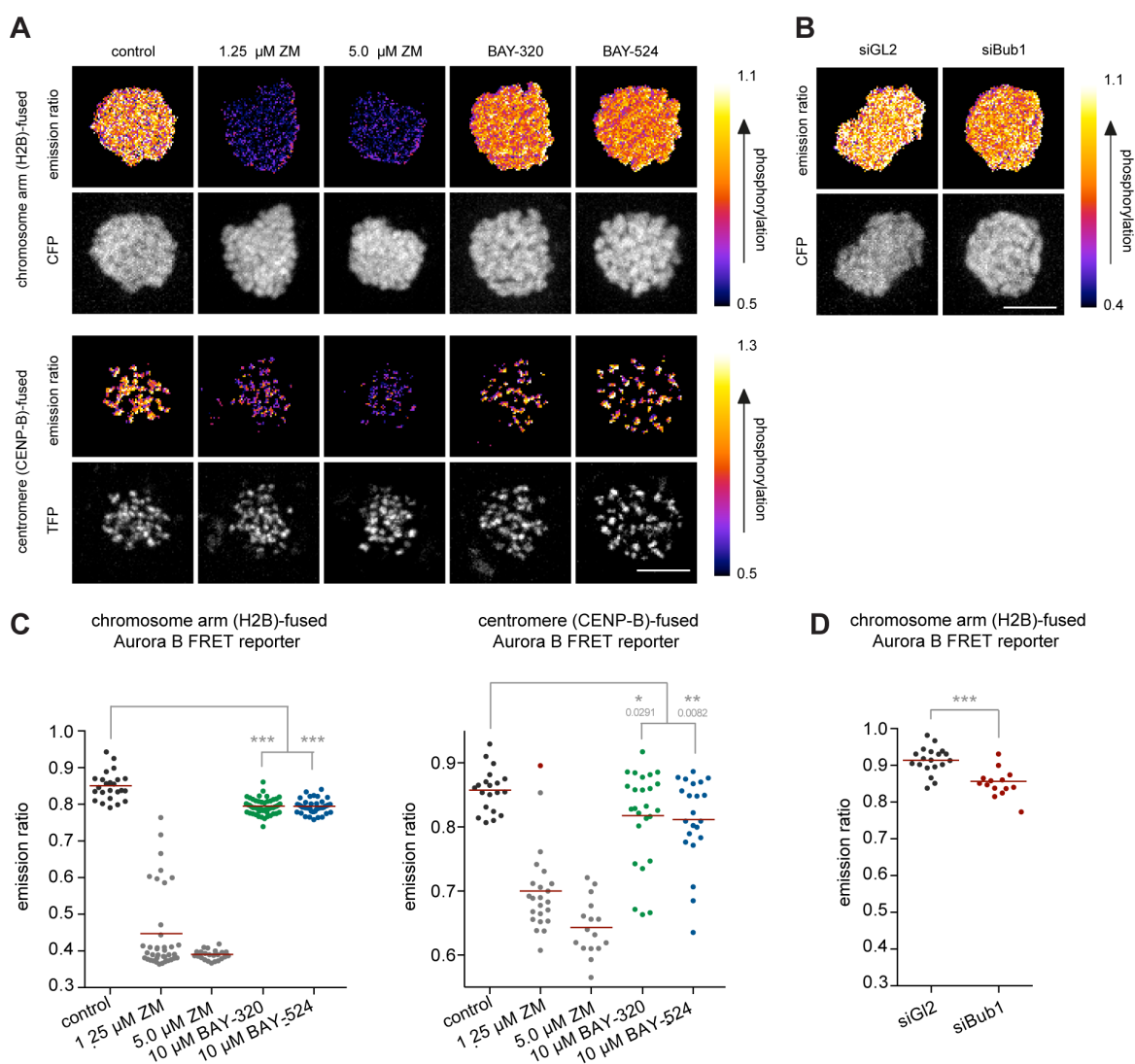


Figure 22: Bub1 inhibition affects Aurora B activity at centromeres but not at chromosome arms. (A) FRET experiments were performed on HeLa Kyoto cells stably expressing chromatin (H2B)- or centromere (CENP-B)-fused FRET reporters for Aurora B activity. Cells were synchronized in mitosis by 6 h treatment with 3.3 μ M nocodazole, before the indicated inhibitors and 10 μ M MG132 were added prior to live fluorescence microscopy. (B) HeLa Kyoto cells stably expressing the chromatin-targeted Aurora B FRET reporter were transfected with control (GL2) or Bub1 siRNA oligonucleotides for 48 h and synchronized by 6 h treatment with 3.3 μ M nocodazole, before 20 μ M MG132 were added prior to live fluorescence microscopy. (A) (B) Heat-map represents the phosphorylation status of the reporter. Scale bar represents 10 μ m. (C) Left panel: scatter plot depicts CFP/FRET emission ratios of reporter targeted to chromatin (H2B; n=23-52 cells per condition). Right panel: scatter plot depicts TFP/FRET emission ratios of reporter targeted to centromeres (CENP-B, n=16-34 cells per condition). (D) Dot plot depicts CFP/FRET emission ratios of reporter targeted to chromatin (H2B, n=14-19 cells per condition).

Bars represent mean values; ***p < 0.001 (from unpaired two-tailed Student's t-test. (Panel C and D: Data analysis with help of Dr. Conrad von Schubert)

3.1.7 Bub1 and Haspin inhibition have an additive effect on CPC recruitment to centromeres

While inhibition of Bub1 by BAY-320 or BAY-524 or inhibition of Haspin by 5-Iodotubercidin (De Antoni et al., 2012) similarly reduced centromere levels of the CPC components Aurora B, Borealin and INCENP to ~40 %, combined inhibition of both kinases resulted in a ~80 % reduction in CPC levels at centromeres (Figure 23). As an important control, treatment of cells with only BAY-320 or BAY-524 did not detectably affect the phosphorylation of the Haspin substrate histone H3 (T3), attesting to the specificity of the two Bub1 inhibitors (Figure 23). These results indicate that Bub1 and Haspin contribute to a similar extent to the recruitment of the CPC to centromeres.

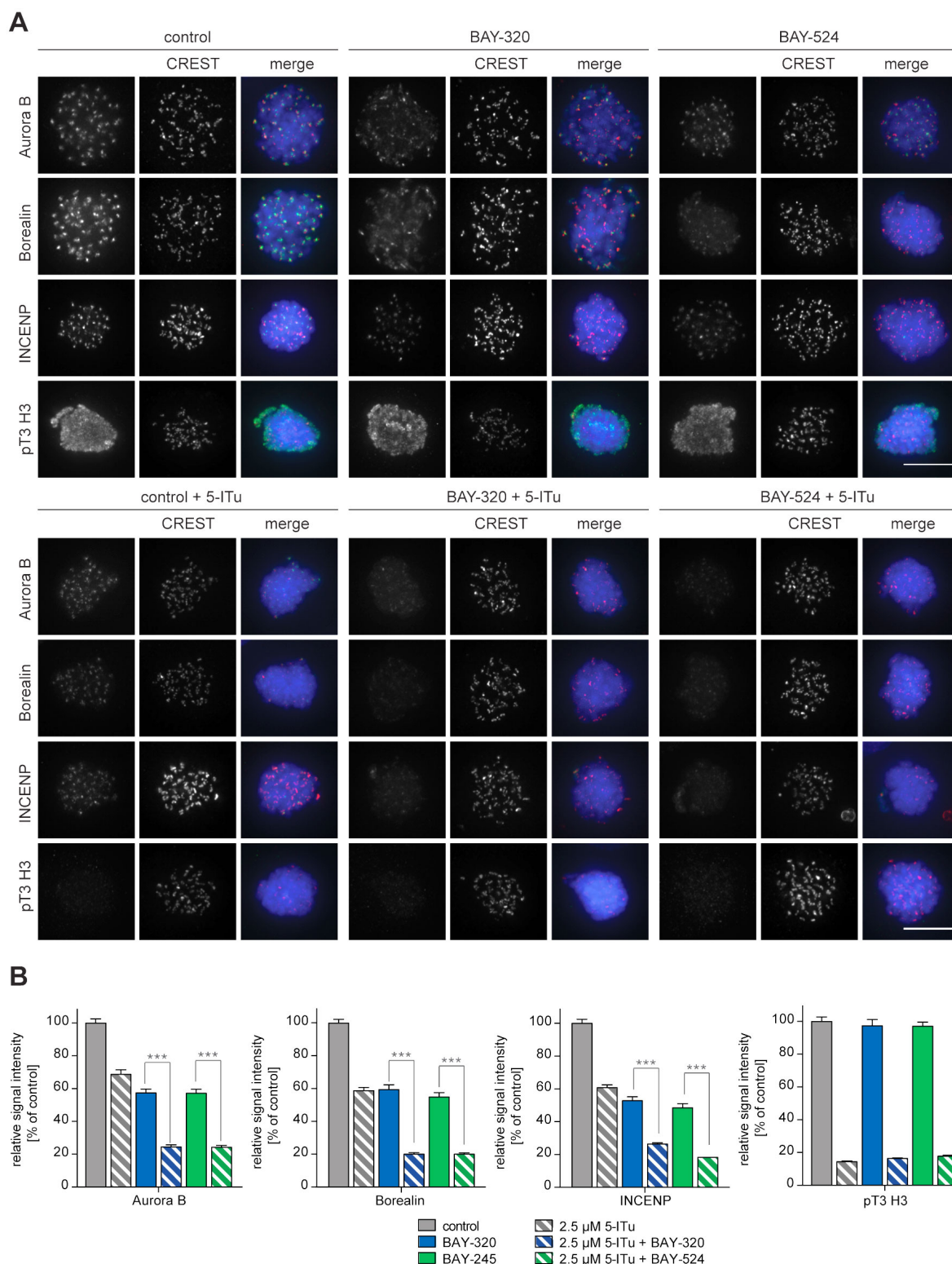


Figure 23: Bub1 and Haspin inhibition exert additive effect on centromere association of CPC. (A) HeLa S3 cells were released from a thymidine block into 3.3 μ M nocodazole, before they were additionally treated for 2 h with the proteasomal inhibitor MG132 and indicated kinase inhibitors. The Haspin inhibitor 5-iodotubercidin (5-ITu (De Antoni et al., 2012)) was used at a concentration of 2.5 μ M, BAY-320 at 3 μ M and BAY-524 at 7 μ M. Cells were fixed, stained for pT3-H3, Aurora B, Borealin, INCENP, CREST and DNA (DAPI) and analyzed by IFM. Anti-pT3-H3 antibody was used to monitor Haspin

inhibition. Scale bar represents 10 μm . **(B)** Histograms show average centromeric (AurB, Borealin, INCENP) or chromosome arm (pT3-H3) signal intensities observed in the experiments shown in (A); $n=20-100$ cells per condition. Error bars represent SEM, $***p < 0.001$ (from unpaired two-tailed Student's *t*-test).

To quantify CPC localization over chromosome arms, analysis of fixed cells proved inadequate. We therefore used an RPE1 cell line expressing one endogenous allele of Aurora B tagged with EGFP (Schubert et al., 2015b) to monitor the subcellular localization of this kinase in living cells. Following Bub1 inhibition, Aurora B-EGFP levels at chromosome arms increased approximately 2-fold, concomitant with the described reduction of Aurora B at centromeres (Figure 24A and B) (Boyarchuk et al., 2007; Ricke et al., 2012). Interestingly, this change in localization showed a strong correlation with the redistribution of Sgo2 (Figure 24C and D). In contrast, treatment of cells with the Haspin inhibitor 5-Iodotubercidin did not induce any significant redistribution of Aurora B from centromeres to chromosome arms; instead, inhibition of Haspin caused an overall reduction of EGFP signals at both centromeres and chromosome arms (Figure 24A and B). Combined inhibition of Bub1 and Haspin displaced Aurora B from both centromeres and chromosome arms (Figure 24), in line with the analysis of fixed cells described above. Taken together, these data corroborate the notion that Bub1 and Haspin cooperate in the recruitment of CPC to centromeres through phosphorylation of histone H2A-T120 and histone H3-T3, respectively. In addition, they reveal a role for Bub1 activity, but not Haspin, in the control of CPC localization to chromosome arms.

Considering the role of Aurora B kinase in the regulation of KT-MT interactions and SAC signaling, the above results raised the question of what contributions Bub1 activity might possibly make to chromosome congression and/or the SAC. Although our initial analyses had not revealed a major impact of BAY-320 or BAY-524 on the overall timing of mitotic progression (Figure 16), we considered the possibility that inhibition of Bub1 might provoke compensatory

effects on mitotic timing, notably a delay in congression and a concomitant acceleration of mitotic exit.

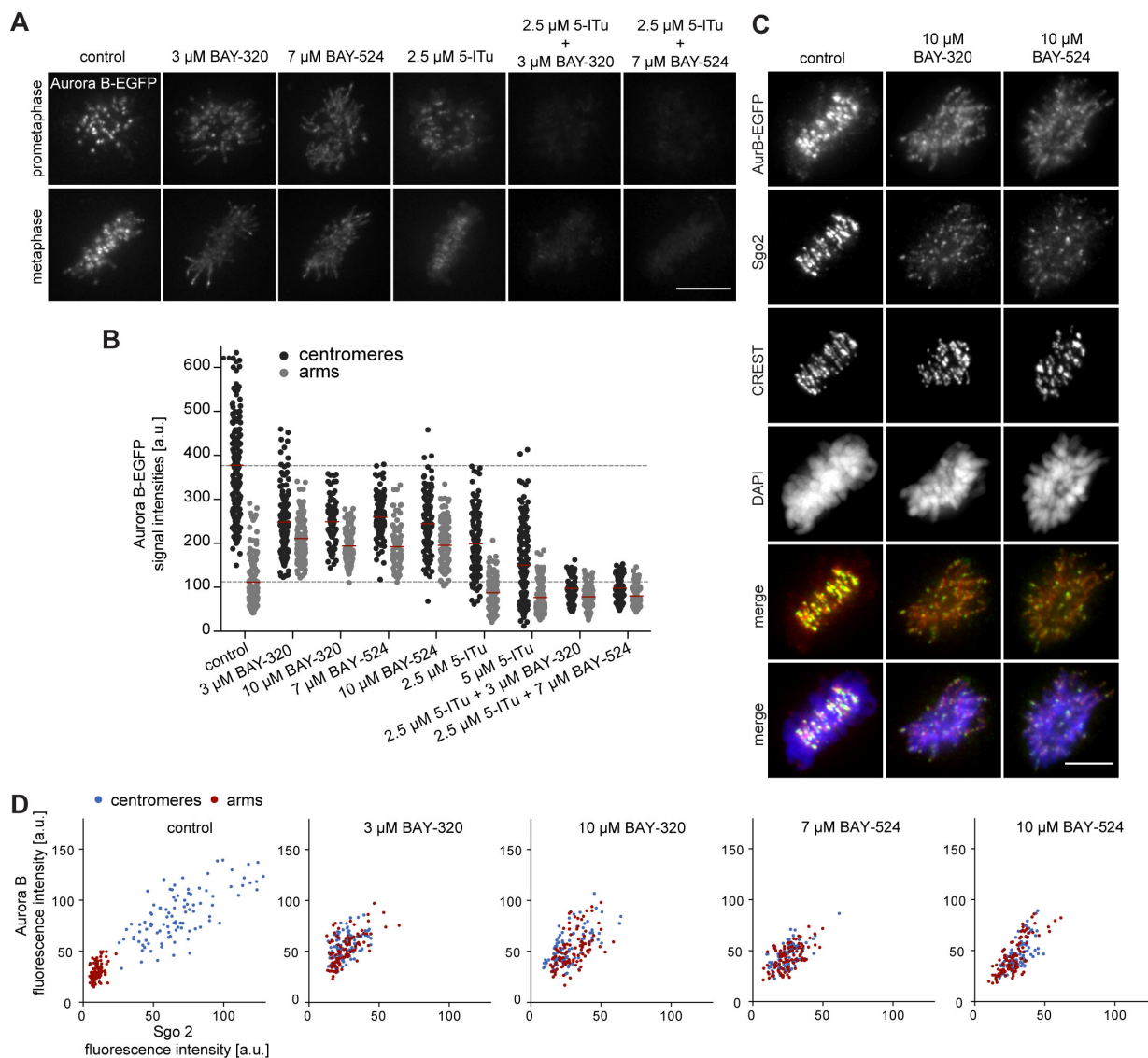


Figure 24: Aurora B localizes to chromosome arms after Bub1 inhibition. (A) RPE1 cells expressing endogenously EGFP-tagged Aurora B were incubated with the indicated drugs for several hours before EGFP signals were recorded by live fluorescence imaging. Scale bar represents 5 μ m. (B) Scatter plots depict Aurora B-EGFP signal intensities at centromeres or arms after treatment with indicated drugs (n=84-185 centromeres/arm regions from 5-6 cells per condition). Bars represent mean values. Measurements relate to the experiment shown in (A). (C) Asynchronous cultures of RPE1 cells expressing endogenously EGFP-tagged Aurora B were treated with indicated doses of Bub1 inhibitors for 3 h, fixed and analyzed by IFM. Scale bar represents 5 μ m. (D) Dot plots show the quantitative results of the experiment shown in (C). EGFP-Aurora B and Sgo2 levels at centromeres and chromosome arms were determined in metaphase cells (n=100 centromere/arm regions from 10 different cells). Bars represent mean values. (Data by courtesy of Dr. Conrad von Schubert)

According to such a scenario, effects on timing might conceivably cancel each other. In support of this possibility, we emphasize that inhibition of mitotic kinases with pleiotropic functions have previously been shown to provoke opposing phenotypes (Schubert et al., 2015b; Santaguida et al., 2011). To explore the possibility of compensatory effects of Bub1 inhibition, we thus carried out more detailed analyses of mitotic progression, notably SAC signaling and chromosome congression.

3.1.8 Bub1 inhibition produces minor effects on SAC signaling in HeLa or RPE1 cells

Depletion of Bub1 is known to weaken SAC signaling in human cells (Meraldi and Sorger, 2005; Perera et al., 2007; Klebig et al., 2009). To test the impact of Bub catalytic activity on SAC function we first analyzed KT levels of Mad1, Mad2 and BubR1 in BAY-320 or BAY-524 treated cells. With the possible exception of a very minor effect on BubR1, the localization of none of these SAC proteins was significantly affected by Bub1 inhibition (Figure 25A and C left panel). In sharp contrast, and in agreement with previous reports (Sharp-Baker and Chen, 2001; Johnson et al., 2004; Boyarchuk et al., 2007; Overlack et al., 2015), Bub1 depletion decreased KT recruitment of all three proteins by 80-90 % (Figure 25B and C right panel). Thus, the recruitment of several SAC components to KTs strongly depends on Bub1 protein, but not Bub1 kinase activity.

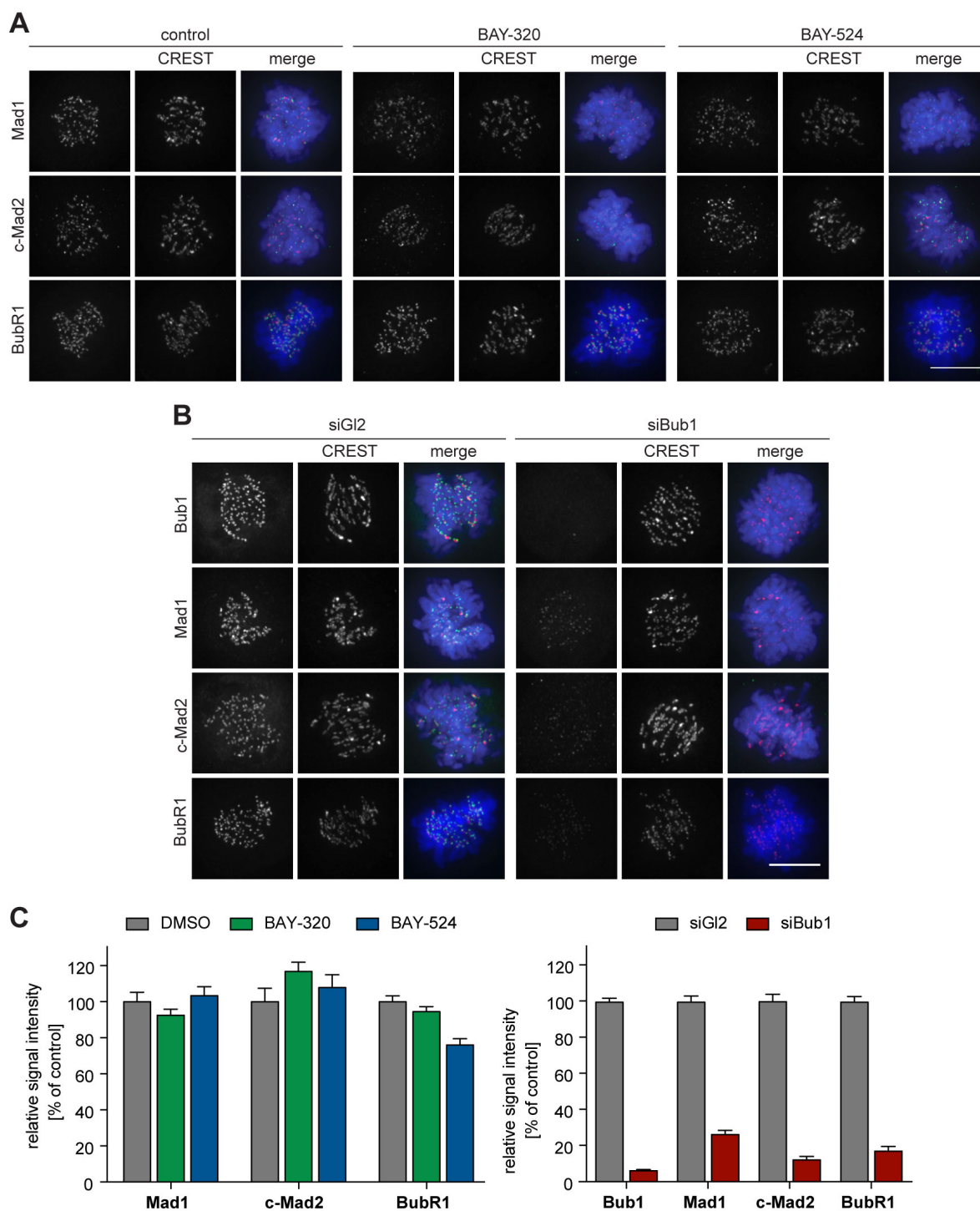


Figure 25: Inhibition of Bub1 kinase does not significantly affect recruitment of SAC effectors to unattached KTs. (A) (B). HeLa S3 cells were synchronized by thymidine block and released for 10 h in the presence of solvent (control), 3 μ M BAY-320 or 7 μ M BAY-524 (A). Cells transfected with mock (GI2) or Bub1 siRNA-oligonucleotides (B) for 48 h were synchronized and analyzed in parallel. Cells were fixed and stained for Bub1, Mad1, closed Mad2 (C-Mad2), CREST and DNA (DAPI) and analyzed by IFM. (C) Histogram shows average KT levels of indicated proteins ($n=20-50$ cells per condition) observed in the experiment shown in (A) and (B). Error bars represent SEM. Scale bar represents 10 μ m.

The association of Bub1 with unattached KTs is dynamic (Howell et al., 2004), raising the question of how Bub1 turnover at KTs is regulated. In the case of the SAC kinase Mps1, autophosphorylation constitutes a major mechanism for controlling Mps1 levels at KTs (Hewitt et al., 2010; Jelluma et al., 2010; Schubert et al., 2015b), and a recent study suggests that Bub1 turnover at KTs is also regulated by autophosphorylation (Asghar et al., 2015). To determine whether Bub1 dynamics at KTs is affected by inhibition of Bub1 activity, we made use of an RPE1 cell line harboring one allele of Bub1 tagged by EGFP at the endogenous locus (Figure 26A and B). After treatment of cells with nocodazole to assure complete MT depolymerization and full SAC activation (Yang et al., 2009; Santaguida et al., 2011), Bub1 levels and turnover at KTs were measured by immunofluorescence microscopy and fluorescence recovery after photobleaching (FRAP), respectively. In comparison to control cells, neither BAY-320 nor BAY-524 detectably affected steady-state Bub1 levels at KTs (Figure 26B-D), in line with a recent independent report (Liu et al., 2015). More importantly, FRAP experiments revealed only minor effects of Bub1 inhibition on Bub1 dynamics at KTs (Figure 26B). The extent of fluorescence recovery after FRAP was not significantly different in control cells and inhibitor treated cells, revealing an immobile fraction of ~42%, in excellent agreement with previous data (Howell et al., 2004; Asghar et al., 2015). The half-time of Bub1 recovery at KTs after FRAP was ~18 sec in controls, again in good agreement with previous data (Howell et al., 2004; Asghar et al., 2015). However, whereas Asghar and colleagues observed a ~50% reduction in the half-time of recovery of an exogenously expressed, catalytically inactive EGFP-Bub1 mutant, we found that recovery of endogenously tagged wild-type EFP-Bub1 was only marginally accelerated by Bub1 inhibition (half-time reduced from 18 seconds to 12-15 seconds) (Figure 26B). These experiments suggest that the effects of Bub1 activity on Bub1 turnover at KTs are minor, at least when compared to the striking effects of Mps1 activity on Mps1 dynamics at KTs (Hewitt et al., 2010; Jelluma et al., 2010; Schubert et al., 2015b). Since, Bub1 protein

levels at KTJs remained stable in Bub1 inhibited cells, we analyzed general Bub1 stability during mitosis. Bub1 is degraded during mitotic exit via mediated APC/C^{Cdh1} (Qi and Yu, 2007). We could not observe any difference in the degradation profile between untreated cells and cell treated with our Bub1 inhibitors, respectively (Figure 26E). Thus, the catalytic activity of Bub1 does not influence Bub1 stability during mitosis.

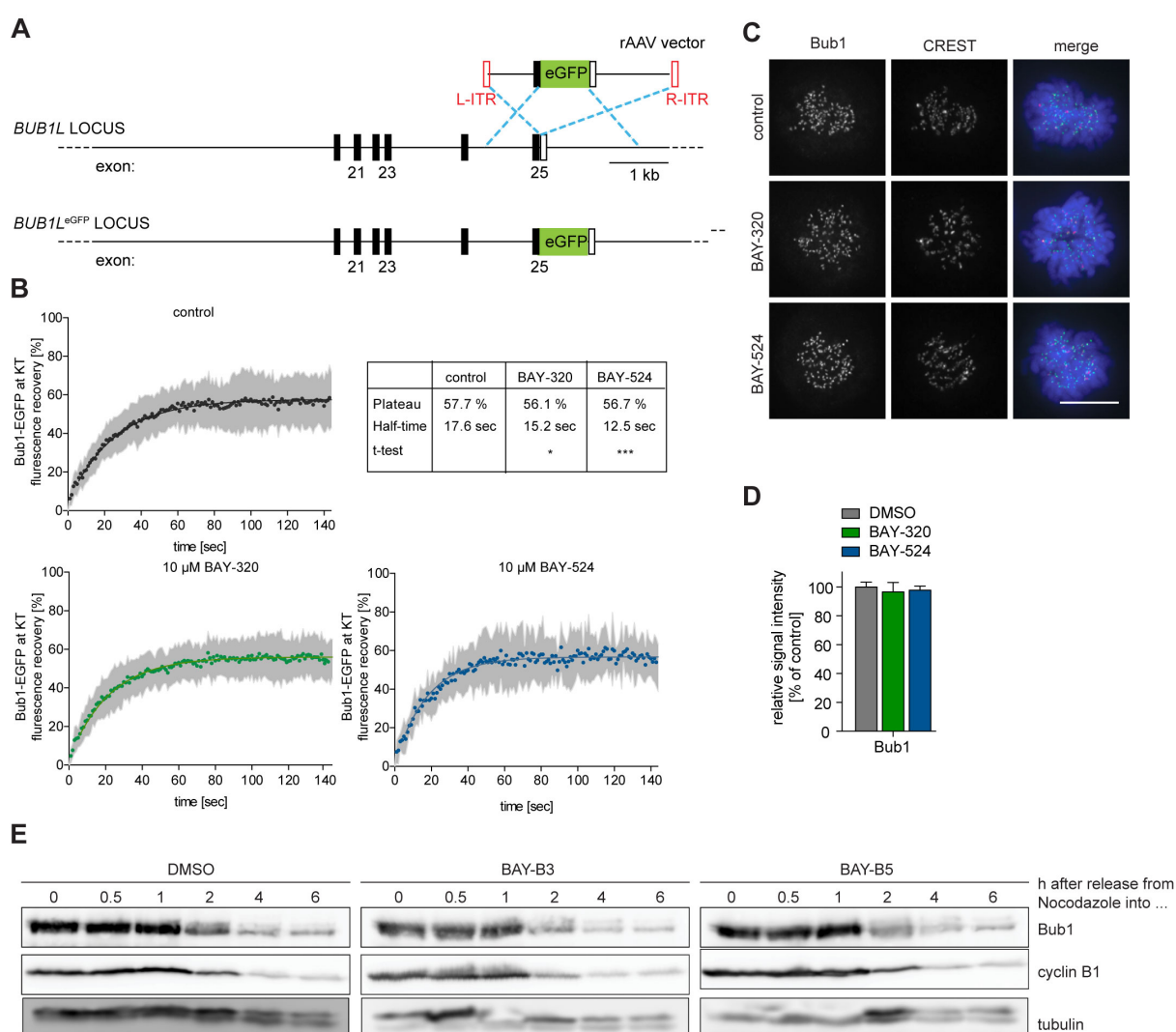


Figure 26: Bub1 inhibition does not affect protein dynamics at the unattached KT. (A) Schematic illustrating the targeting strategy used to introduce the EGFP open-reading frame into the indicated locus of RPE1 cells. The EGFP open reading frame was fused to the 3' exon of one allele of the *BUB1L* gene. **(B)** RPE1 cells expressing endogenously tagged Bub1-EGFP (Suppl. Fig. S6A) were synchronized in mitosis by overnight treatment with the Eg5 inhibitor STLC (10 μ M) and subsequently treated with 3.3 μ M nocodazole and 20 μ M MG132 as well as solvent (control), 10 mM BAY-320 or 10 mM BAY-524. Bub1-EGFP KT levels were recorded by 1 sec time-lapse microscopy. After 5 sec, a single KT

pair was bleached and fluorescence recovery was monitored. Traces illustrate average fluorescence recovery at KT pairs ($n = 10\text{--}16$ KT pairs per condition); shaded areas represent standard deviation (SD). Half-times and plateaus were determined by non-linear curve fitting based on a one-phase association. **(C)** HeLa cells were synchronized by thymidine block and released for 10 h in the presence of solvent (control), 3 μM BAY-320 or 7 μM BAY-524. Cells were fixed and stained for Bub1, CREST and DNA (DAPI) and analyzed by IFM. Scale bar represents 10 μm . **(D)** Histogram shows average Bub1 KT levels as measured in the experiment shown in (B); $n=20\text{--}22$ cells per condition. **(E)** Western blots showing Bub1 stability and degradation during mitosis and mitotic exit. HeLa cells were synchronized by thymidine block and released for 12 h in the presence of 3.3 μM Nocodazole. Mitotic cells were subsequently harvested by mitotic shake-off and replated. Those were released into fresh medium with solvent (control), 3 μM BAY-320 or 7 μM BAY-524. Cells were harvested at the indicated time points. Cell lysates were analyzed by Western blotting, probing for Bub1, cyclin B1 and tubulin as loading control. (Panel B: data analysis with the help of Dr. Conrad von Schubert)

As a further read-out for the effects of Bub1 inhibition on SAC activity, we used live cell imaging to monitor the responses of nocodazole-arrested HeLa and RPE1 cells to BAY-320 or BAY-524 and compared these to the responses seen in Bub1-depleted cells (Figure 27).

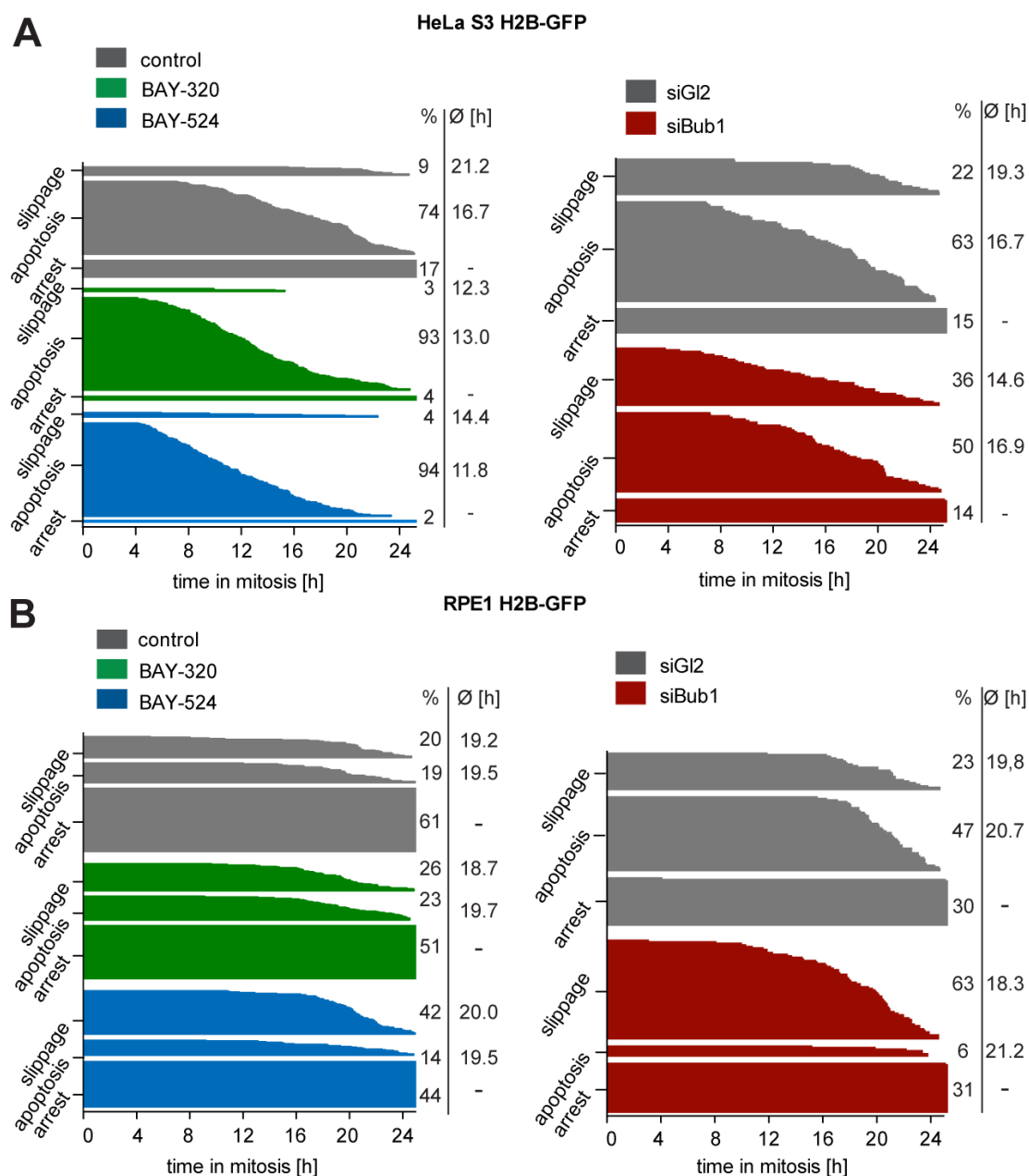


Figure 27: Bub1 inhibition in contrast to depletion, only marginally affects the spindle checkpoint. (A, B) Asynchronously growing cultures of HeLa S3 (A) or RPE1 (B) cells stably expressing GFP-tagged histone H2B were either directly treated with 3.3 μ M nocodazole and the kinase inhibitors BAY-320 (3 mM) and BAY-524 (7 mM) or transfected with control (GI2) or Bub1 siRNA for 48 h prior to addition of nocodazole. Cell fates (continued arrest, apoptosis or slippage) and duration of mitotic arrest were determined by fluorescence time-lapse imaging (n=150 cells per condition, accumulated from 3 independent experiments). Frequencies of observed cell fates as well as average times of arrest are indicated.

Over a 24 hour observation period, the percentage of HeLa cells maintaining a SAC arrest dropped from 17% in controls to 4% and 2% in response to Bub1 inhibition by BAY-320 and BAY-524, respectively. These shifts in cell fates were largely compensated by increases in the percentages of cells undergoing apoptosis, from 71% in controls to 93%-94% in Bub1-inhibited cells. In contrast, the extent of mitotic slippage remained at less than 10%, under all conditions. In RPE1 cells, maintenance of SAC arrest over 24 hours was more pronounced, but again the percentage of arrested cells dropped from 61% in controls to 51%/44% in response to Bub1-inhibition, with increasing proportions of cells undergoing apoptosis or mitotic slippage (Figure 27). For comparison, depletion of Bub1 from either HeLa or RPE1 cells resulted in a 2-3 fold increase in mitotic slippage at the expense of apoptosis, while the proportion of cells sustaining an arrest remained roughly constant (Figure 27). Collectively, these results indicate that Bub1 activity contributes to maintenance of maximal SAC activity, but that Bub1 protein levels are more important, most likely reflecting the observed role of Bub1 in the KT recruitment of SAC components (Figure 25).

Importantly, we also compared the requirements for Bub1 activity and Bub1 protein in a cellular background in which SAC activity was partially compromised by treatment of HeLa or RPE1 cells with a low dose of Reversine, a widely used inhibitor of the SAC kinase Mps1 (Santaguida et al., 2010). In agreement with the results described above, Bub1 inhibition marginally reduced the time that Reversine-treated cells remained arrested before overriding nocodazole-induced arrest (Figure 28A and B left and middle panels). Thus, we compared the impact of Bub1 inhibition on the mitotic progression of cells with a compromised SAC to cells in which a different mitotic kinase was inhibited. Addition of Aurora B or Plk1 inhibitors, used as positive controls, led to the expected shortening of the duration of mitotic arrest (Figure 28A and B middle panels) (Saurin et al., 2011; Schubert et al., 2015b). Similarly, Bub1 depletion also caused a drastic shortening of arrest (Figure 28A and B right panels). Taken

together, and considering previous studies (Perera et al., 2007; Klebig et al., 2009), these observations demonstrate that the presence of Bub1 protein is more important for SAC signaling than Bub1 catalytic activity.

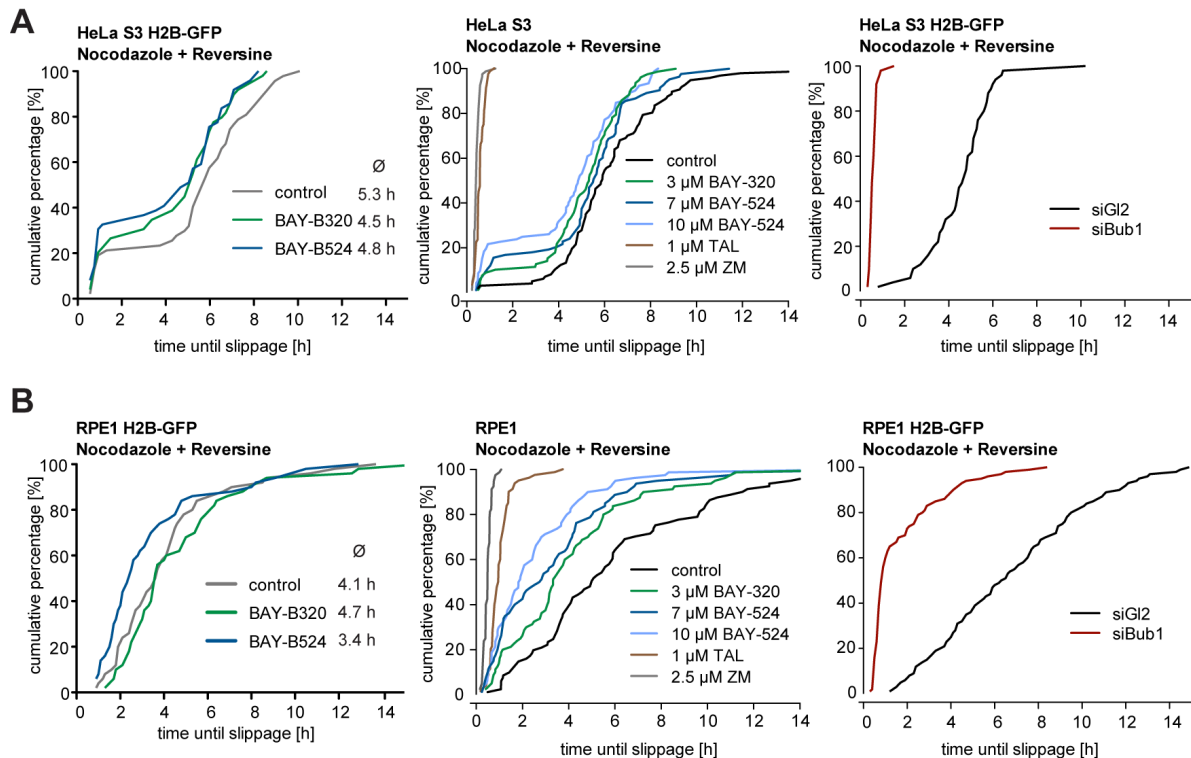


Figure 28: Bub1 inhibition marginally affects SAC signaling. (A) Asynchronously growing HeLa S3 cells or HeLa cells stably expressing GFP-tagged histone H2B were treated with 3.3 μM nocodazole and 0.5 μM of the Mps1 inhibitor Reversine as well as solvent (control), 3 and 10 μM BAY-320, 7 and 10 μM BAY-524 or 2.5 μM of the Aurora B inhibitor ZM-447439 (ZM) (left and middle panel). Alternatively, cells were transfected with control (Gl2) or Bub1 siRNA oligonucleotides for 48 h prior to addition of 3.3 μM nocodazole and 0.5 μM Reversine (right panel). Cells were monitored by fluorescence time-lapse microscopy and the time elapsed from NEBD to SAC override and mitotic slippage was determined. Traces illustrate the cumulative frequency of mitotic duration before slippage ($n=50$ cells per condition). (B) Asynchronously growing RPE1 cells stably expressing GFP-tagged histone H2B were treated and analyzed as described in (A). Scale bars represent 10 μm . (Middle panels by courtesy of Dr. Conrad von Schubert)

3.1.9 Bub1 inhibition does not significantly interfere with chromosome congression

To analyze the impact of Bub1 inhibition on chromosome alignment we treated cells with the Eg5 inhibitor Monastrol (Kapoor et al., 2000) and then monitored the restoration of KT-MT attachments during spindle bipolarization in response to drug washout (Figure 29). While nearly 28% of Bub1 depleted cells failed to completely align all chromosomes, more than 90% of Bub1 inhibited cells showed complete alignment that was indistinguishable from control cells. Inhibition of Aurora B, analyzed for control, resulted in the expected impairment of alignment (Figure 29).

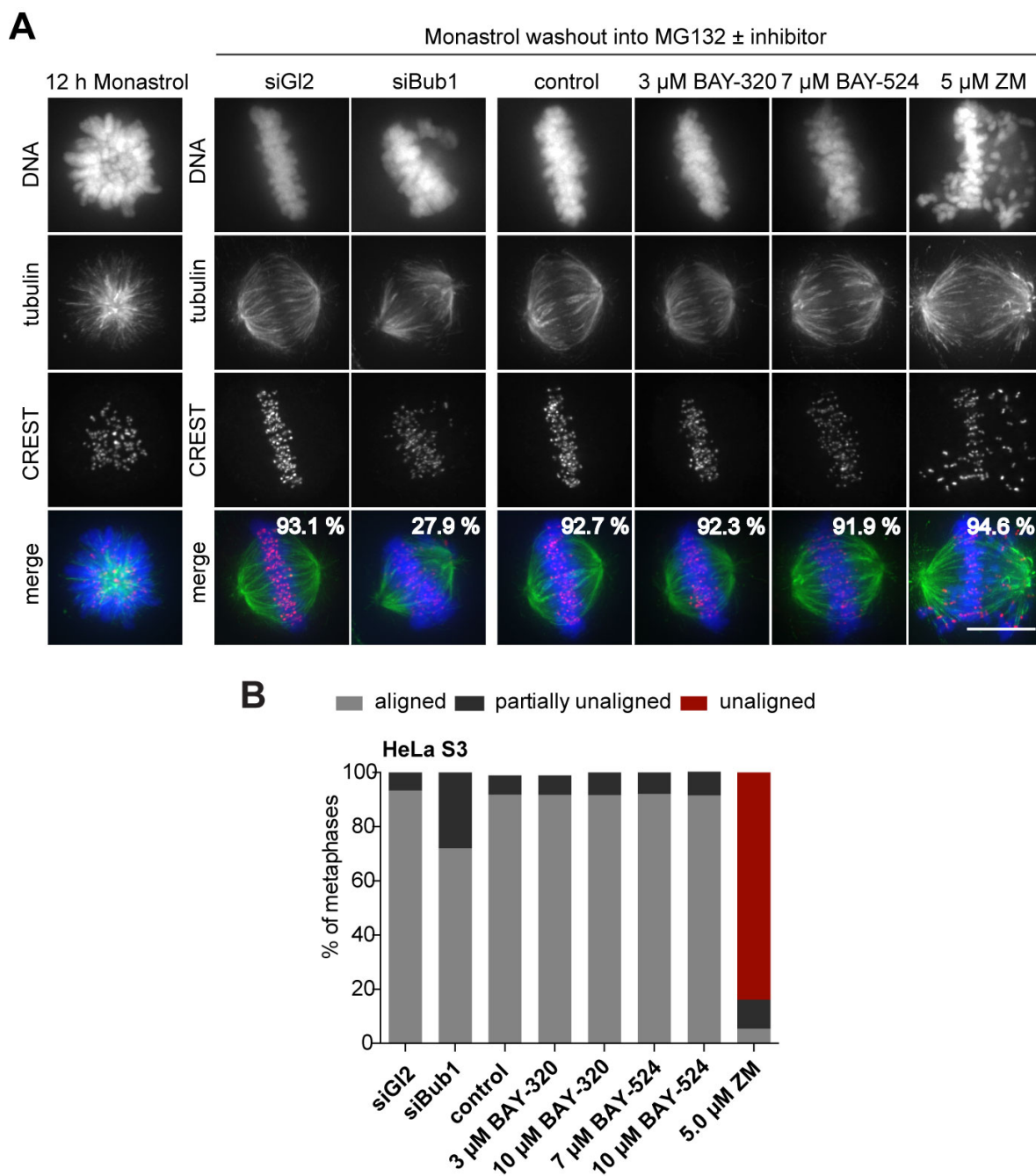


Figure 29: Bub1 inhibition does not significantly affect chromosome congression. (A) HeLa S3 cells were transfected with control (GI2) or Bub1 siRNA-oligonucleotides for 48 h, synchronized by thymidine block and released for 12 h in the presence of the Eg5 inhibitor Monastrol to induce the formation of monopolar spindles. The capacity of spindle bipolarization and metaphase plate formation was tested by Monastrol wash-out and addition of MG132 and indicated drugs for 2 h (n = 170-200 cells). Percentages indicate the frequencies of depicted spindle morphologies. **(B)** Histograms show the frequencies of full, partial (≤ 5 unaligned chromosomes) or failed metaphase chromosome alignments that were observed in the experiment shown in (A).

To complement these assays, we also used immunofluorescence microscopy to quantify the frequency of micronucleation, a read-out for chromosome segregation errors, in HeLa and RPE1 cells. While partial inhibition of Aurora B kinase provoked an increase in micronucleation in both cell lines, as expected (Gohard et al., 2014; Tao et al., 2009), Bub1 inhibition only marginally increased the frequency of micronucleation (Figure 30A). This result supports the view that Bub1 inhibition causes surprisingly mild defects in chromosome congression or segregation (Figure 16 and Figure 29). Further corroborating this conclusion, we found that BAY-320 or BAY-524 treatment exerted no significant effects on the KT recruitment of the motor protein CENP-E (Figure 30B and C, left panels). In contrast, Bub1 depletion reduced CENP-E levels at KTs by ~40 % (Figure 30B and C, right panels), in agreement with previous reports (Sharp-Baker and Chen, 2001; Johnson et al., 2004).

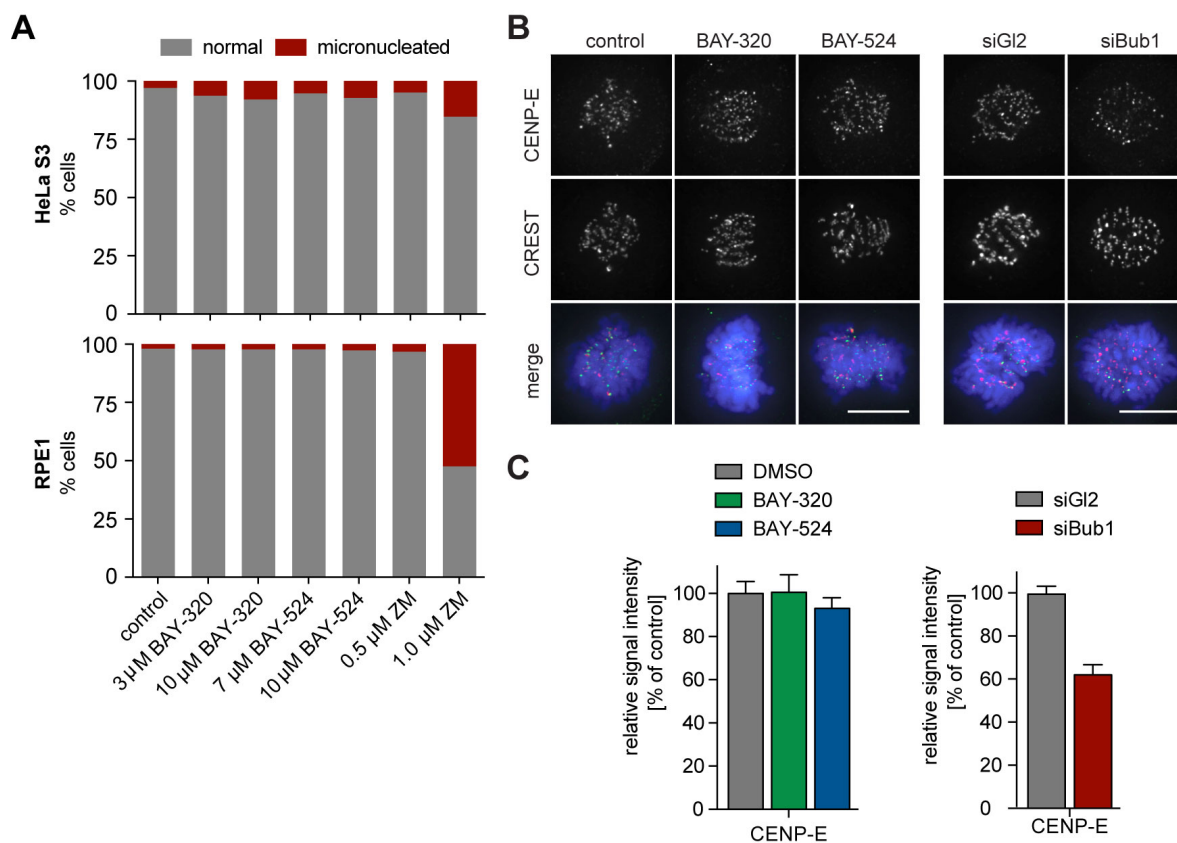


Figure 30: Bub1 inhibition does not produce micronucleation or CENP-E mislocalization. (A) HeLa S3 and RPE1 cells were treated for 16 h with the indicated drugs, fixed and analyzed by IFM. Histograms show the frequency of micronucleation among interphase cells (n=300 cells per condition). (B) Depletion but not inhibition of Bub1 kinase affects recruitment of CENP-E to unattached KT. Untreated HeLa S3 cells or cells transfected with control (Gl2) or Bub1 siRNA-oligonucleotides (for 48 h) were synchronized by thymidine block and released for 10 h in the presence or absence of 3 mM BAY-320 or 7 mM BAY-524. Cells were fixed and stained for CENP-E, CREST, DNA (DAPI) and analyzed by IFM. (C) Histograms show average CENP-E KT levels observed in prometaphase cells. Data relate to micrographs shown in (B). Error bars represent SEM. Scale bars represent 10 μ m.

Taken together, these results show that Bub1 kinase activity is largely dispensable for chromosome congression and segregation. It follows that even though Bub1 inhibition results in a marked reduction of Aurora B levels at centromeres (Figure 20), these levels are still sufficient to ensure largely faithful chromosome segregation. Conversely, Bub1 protein is clearly important for efficient chromosome congression, presumably reflecting the role of Bub1 in CENP-E recruitment to KTs.

3.1.10 Bub1 inhibition sensitizes HeLa cells to clinically relevant doses of Paclitaxel

Interference with the SAC proteins Mps1 or BubR1 was previously shown to exert synergistic effects with Paclitaxel treatment of tumor cells, significantly elevating the frequency of chromosome missegregation and lethality (Janssen et al., 2009; Lee et al., 2004). Thus, we asked how inhibition of Bub1 kinase activity by BAY-320 or BAY-524 would impact on cells in which MT dynamics was compromised by low doses of Paclitaxel. Importantly, when used at clinically relevant doses of 1-4 nM, Paclitaxel induces spindle defects and aneuploidy without delaying mitotic progression (Brito and Rieder, 2009; Janssen et al., 2009; Ikui et al., 2005; Chen and Horwitz, 2002). While single treatment with 1-4 nM Paclitaxel produced modest impairment of cell proliferation, the concomitant application of the Bub1 inhibitors, BAY-320 at 3 mM or BAY-524 at 7 or 10 mM, clearly exacerbated inhibition of proliferation. Effects were particularly drastic in aneuploid HeLa cells (Figure 31A and B, top panels), while diploid RPE1 cells were less affected (Figure 31A and B, bottom panels). For comparison, we also examined the effects of combining low dose Paclitaxel treatment with partial inhibition of Mps1 by Reversine (Janssen et al., 2009). This analysis shows that the combination of Paclitaxel with either Mps1 or Bub1 inhibition produced similar synergistic effects, albeit with cell-type specific differences (Figure 31A and B). To what extent SAC inhibition differentially affects aneuploid *versus* diploid cells will thus require further investigation (Janssen et al., 2009; Kops et al., 2004; Maia et al., 2015).

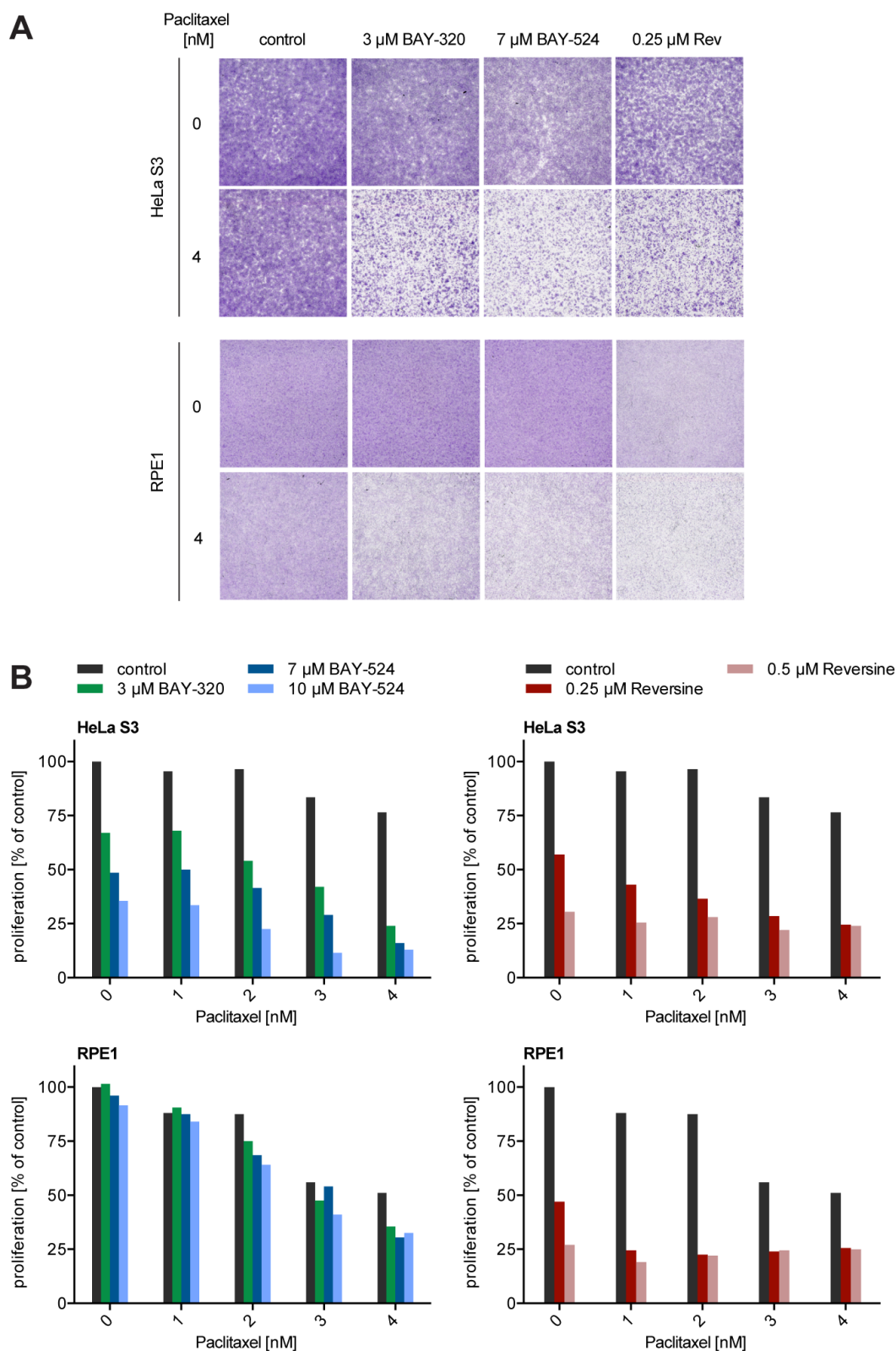


Figure 31: BAY-320 and BAY-524 treatment sensitizes cells to low doses of Paclitaxel. (A) Micrographs show colony formation of HeLa (top panel) and RPE1 cells (bottom panel) treated for 7 days with solvent (control) or the indicated kinase inhibitors in the presence or absence of 4 nM Paclitaxel. (B) Histograms quantify colony formation in HeLa (top panels) and RPE1 cells (bottom panels) treated with the indicated kinase inhibitors in the presence or absence of 1-4 nM Paclitaxel for 7 days. (Panel B by courtesy of Dr. Conrad von Schubert)

To determine whether the observed impairment of proliferation results from errors in chromosome segregation (Kops et al., 2004), we scored HeLa and RPE1 cells expressing GFP-H2B for mild and severe chromosomal defects, as illustrated in Figure 32A. Following application of the above Paclitaxel and Bub1/Mps1 inhibitor treatments, the frequencies of chromosomal defects were monitored by fluorescence time-lapse imaging and quantified (Figure 32B). Consistent with the micronucleation data described above (Figure 30A) Bub1 inhibition alone did not significantly elevate the frequency of chromosome missegregation in either HeLa or RPE1 cells (Figure 32B). For comparison, interference with the SAC by inhibition of Mps1 led to a marked increase in segregation defects in both cell lines, as expected (Figure 32B). Most importantly, HeLa cells displayed an even higher frequency of severe chromosome segregation defects when Bub1 inhibition was combined with 1-4 nM Paclitaxel, comparable to the consequences of combined Mps1 inhibition and Paclitaxel treatment (Figure 32B). In contrast, Bub1 inhibition only marginally elevated the rate of Paclitaxel -induced chromosome missegregation in RPE1 cells, while combinatorial treatment with Reversine still resulted in a high rate of mild segregation defects.

Considering the strong correlation in the data shown in Figure 29 and Figure 32, it is tempting to conclude that chromosome segregation errors constitute the most likely cause for the observed impairment of cell proliferation when Bub1 inhibition is combined with low dose Paclitaxel treatment. Thus, although inhibition of Bub1 kinase activity *per se* exerts only minor effects on SAC functionality, chromosome segregation and mitotic progression, treatment with BAY-320 or BAY-524 sensitizes cells to low, clinically relevant doses of Paclitaxel. These findings are clearly relevant for the potential therapeutic use of Bub1 inhibitors.

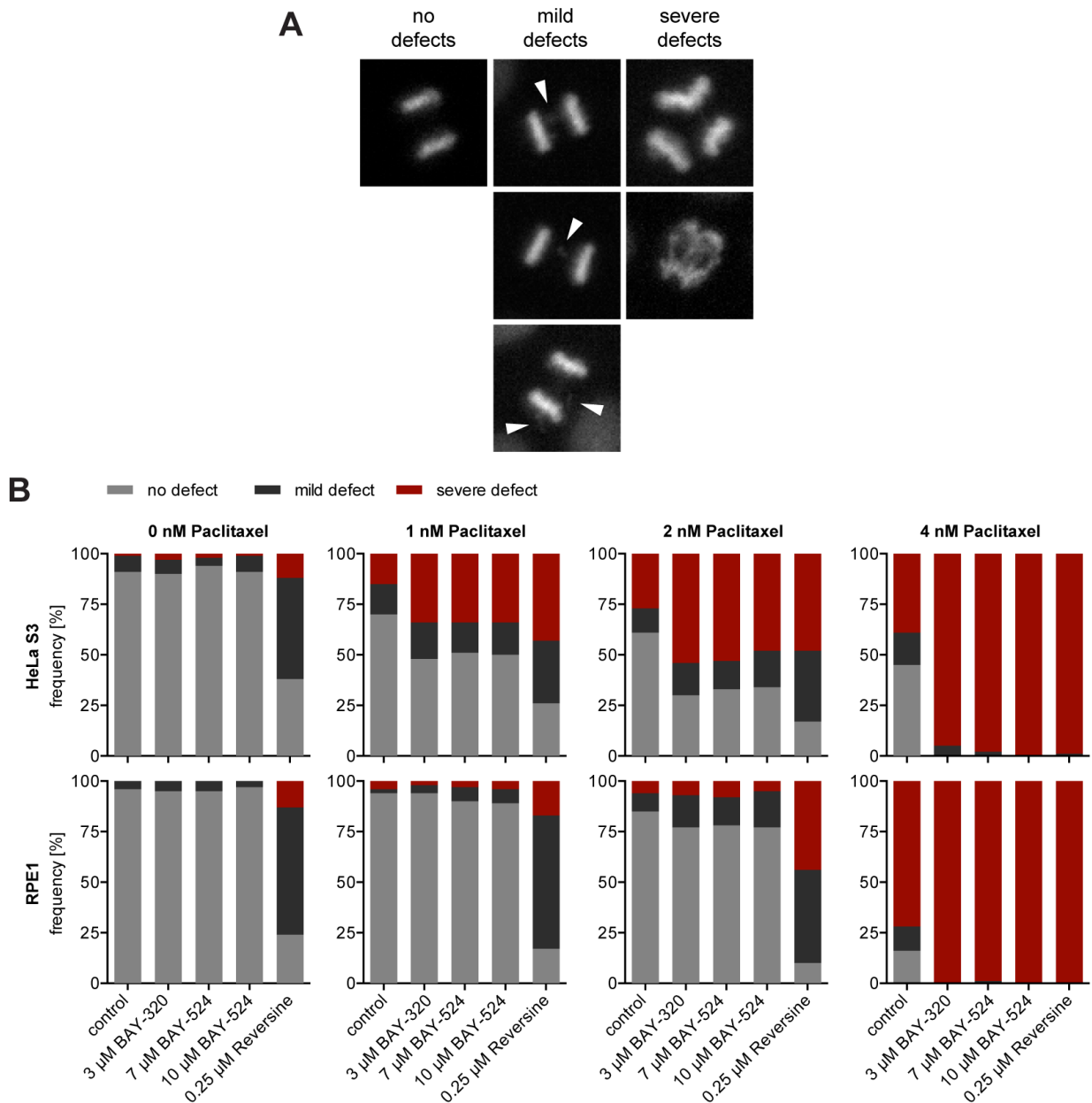


Figure 32: Bub1 inhibition in combination with Paclitaxel treatments elevates the frequency of chromosome segregation defects. (A) Time-lapse stills of HeLa cells expressing H2B-GFP illustrate chromosome segregation defects that were used to classify cell fates in the experiments described in (B); arrowheads point to chromosome bridges and lagging chromosomes. (B) HeLa (top panels) and RPE1 cells (bottom panels) stably expressing H2B-GFP were treated with solvent (control) or the indicated kinase inhibitors in the presence or absence of 1-4 nM Paclitaxel and monitored by fluorescence time-lapse imaging. Histograms show the frequencies of chromosome segregation defects, following the classification illustrated in (A) (n=100 cells per condition). (Data by courtesy of Dr. Conrad von Schubert)

3.2 Evaluation of data-dependent and –independent mass spectrometric workflows for sensitive quantification of proteins and phosphorylation sites

3.2.1 Aim of the Project

The analysis of low-abundance proteins in complex mixtures has been a long-standing challenge in the field of mass spectrometry. Proceedings in the past 10 years allow nowadays sensitive, hypothesis-driven analyses by focusing on proteins of interest. In this study the goal was to identify and develop a robust MS approach that is most suitable for the detection, identification and quantification of low abundant phosphorylated/unphosphorylated peptides in complex samples. The reason that prompted us to address this topic was the availability of different methods while their detailed comparisons with each other were lacking. In this regard the most popular MS approaches, data-dependent acquisition (DDA), directed and targeted MS, were compared and evaluated on the basis of their performance by analyzing spiked dilution curves of unmodified and phosphorylated peptides, covering several orders of magnitude in concentrations.

The chosen method was then further validated in regard of robust identification and quantification of low abundant and transient phosphorylation sites, taking the SAC protein Mad1 as a model protein.

3.2.2 Author contributions

I performed all the sample preparations, MS analyses and peptide quantifications for the modified peptides. In addition I generated the Mad1 phosphorylation site catalogue with the help of Dr. Luca Fava, Dr. Anna Santamaria and Dr. Alex Schmidt and performed Mad1 phosphorylation site

monitoring. I prepared the text regarding these analyses together with Dr. Alexander Schmidt. All sample preparations and MS analyses regarding unmodified peptides, were performed by Dr. Manuel Bauer. Dr. Erik Ahrné performed all data analyses. Dr. Manuel Bauer, Dr. Erik Ahrné and myself contributed equally to this work.

3.2.3 First-author publication

Evaluation of Data-Dependent and -Independent Mass Spectrometric Workflows for Sensitive Quantification of Proteins and Phosphorylation Sites

Manuel Bauer^{1#}, Erik Ahnér^{1#}, Anna P. Baron^{1#}, Timo Glatter, Luca L. Fava², Anna Santamaria³, Erich A. Nigg¹, and Alexander Schmidt^{1,*}

¹ Biozentrum, University of Basel, Klingelbergstrasse 50/70, CH-4056 Basel, Switzerland

² Present address: Division of Developmental Immunology Biocenter, Innsbruck Medical University, Innrain 80, 6020 Innsbruck, Austria

³ Present address: Cell cycle and mitosis laboratory, Research unit in Biomedicine and Translational Oncology, Vall Hebron Institute of Research, Psg. Vall d'Hebron 119-129, 08035 Barcelona, Spain

these authors contributed equally

*Corresponding author: Alexander Schmidt (alex.schmidt@unibas.ch)

Published in Journal of Proteome Research

Volume 13

Editors Choice

Accepted October 21, 2014

Published In Issue: December 05, 2014



Evaluation of Data-Dependent and -Independent Mass Spectrometric Workflows for Sensitive Quantification of Proteins and Phosphorylation Sites

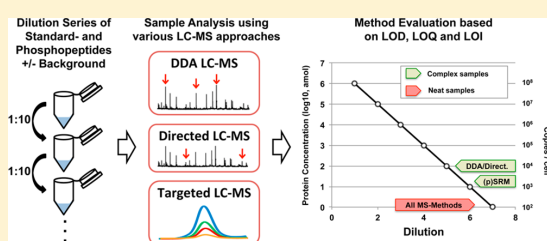
Manuel Bauer,[†] Erik Ahrné,[†] Anna P. Baron,[†] Timo Glatter, Luca L. Fava,[‡] Anna Santamaria,[§] Erich A. Nigg, and Alexander Schmidt*

Biozentrum, University of Basel, Klingelbergstrasse 50/70, CH-4056 Basel, Switzerland

Supporting Information

ABSTRACT: In recent years, directed and, particularly, targeted mass spectrometric workflows have gained momentum as alternative techniques to conventional data-dependent acquisition (DDA) LC–MS/MS approaches. By focusing on specific peptide species, these methods allow hypothesis-driven analysis of selected proteins of interest, and they have been shown to be suited to monitor low-abundance proteins within complex mixtures. Despite their growing popularity, no study has systematically evaluated these various MS strategies in terms of quantification, detection, and identification limits when they are applied to complex samples. Here, we systematically compared the performance of conventional DDA, directed, and various targeted MS approaches on two different instruments, namely, a hybrid linear ion trap–Orbitrap and a triple quadrupole instrument. We assessed the limits of identification, quantification, and detection for each method by analyzing a dilution series of 20 unmodified and 10 phosphorylated synthetic heavy-labeled reference peptides, respectively, covering 6 orders of magnitude in peptide concentration with and without a complex human cell digest background. We found that all methods performed similarly in the absence of background proteins; however, when analyzing whole-cell lysates, targeted methods were at least 5–10 times more sensitive than that of the directed or DDA method. In particular, higher stage fragmentation (MS3) of the neutral loss peak using a linear ion trap increased the dynamic quantification range of some phosphopeptides up to 100-fold. We illustrate the power of this targeted MS3 approach for phosphopeptide monitoring by successfully quantifying nine phosphorylation sites of the kinetochore and spindle assembly checkpoint component Mad1 over different cell cycle states from nonenriched pull-down samples.

KEYWORDS: Targeted mass spectrometry, directed mass spectrometry, data-dependent acquisition, peptide quantification, limit of detection, phosphorylation, MAD1, cell cycle



INTRODUCTION

The identification and precise quantification of low-abundance proteins within whole proteomes is still one of the major challenges of mass spectrometry-based proteomics.^{1–6} This can be mainly ascribed to the limited sequencing speed, sensitivity, and dynamic range of current MS instruments in combination with data-dependent acquisition (DDA) LC–MS workflows.^{7,8} The recent implementation of directed^{9–11} and targeted^{9,12,13} LC–MS workflows has tackled some of these limitations and improved the dynamic concentration range over which proteins can be detected and quantified for a selected set of proteins of interest.^{10,11,14–16}

In general, the dynamic detection range of DDA-driven workflows critically depends on the sequencing speed of the LC–MS platform employed. This is a result of the stochastic peak selection starting with the most intense precursor ions and the insufficient sequencing capabilities of current LC–MS platforms to acquire MS/MS spectra of all detectable precursor ions in the MS1 survey scans; this, in turn, hampers the

identification of low-abundance peptide ion signals when analyzing complex peptide mixtures.^{8,17,18} These problems can be largely overcome by data-independent acquisition (DIA) workflows like directed or inclusion list driven LC–MS that allow focused MS sequencing of a specific, predefined set of precursor ion masses independent of their signal intensities. The increased capability to identify low-abundance peptides and proteins of directed over DDA LC–MS has been recently demonstrated on a large scale.^{15,19} A significant advantage of directed over targeted MS approaches is the high number of peptides (up to several thousand precursor ion masses) that can be analyzed per run using current high-performance LC–MS platforms.^{20,21} On the other hand, the precursor ions have to be detected in the MS1 survey scans to trigger a MS sequencing attempt. This is challenging for low-abundance peptide species

Received: August 18, 2014

Published: October 21, 2014

within complex mixtures due to the limited intraspectral dynamic detection range.^{22,23}

Targeted LC–MS, another DIA strategy, goes one step further and overcomes this limitation by directly monitoring MS/MS product ions without the need to detect peptide precursor ions. The most popular approach is selected reaction monitoring (SRM), in which the precursor ion and fragment ion mass-to-charge (m/z) ratios as well as optimized collision energies are predefined to monitor peptides of interest.^{24,25} Once these SRM assays are set up, they can be exchanged between laboratories and instruments^{26,27} and thus represent a rich resource for the community.^{8,28} Recently, several large-scale studies have been conducted that generated SRM assays for virtually all open reading frames for a number of species and demonstrated the ability of this technique to potentially monitor any protein of a given organism.^{8,29,30} Nonetheless, accurate quantification of many low-abundance proteins within very complex protein mixtures still requires additional sample- and time-consuming fractionation/enrichment steps using current LC–MS platforms.^{2,20,22,31,32}

Pseudo-selected reaction monitoring (pSRM, also termed product ion monitoring or parallel reaction monitoring (PRM) with high-resolution/accurate mass LC–MS instruments) is another targeted MS approach, in which whole MS/MS spectra are acquired for sets of peptide ion masses of interest.^{1,6,33} These spectra can be employed for identification and, by focusing on peptide specific product ions, also quantification. With the ever increasing sequencing speed and resolution of modern Orbitrap and time-of-flight mass analyzers, high-resolution/accurate mass (HR/AM) pSRM/PRM approaches are becoming increasingly popular; because assay development efforts are reduced, fragments suitable for quantification can be selected postacquisition, and the high resolution further increases specificity and quantification confidence.^{1,6,13} Recent instruments even allow co-selection, simultaneous fragmentation, and analysis of multiple peptides per MS scan, considerably increasing peptide throughput per LC–MS analysis.¹ Considering the high popularity of the various DIA approaches, it is surprising that no systematic performance assessment, demonstrating the strengths and drawbacks of the individual approaches, has so far been reported.

Here, we present a systematic evaluation of detection, identification, and quantification limits for DDA and several popular DIA MS approaches by analyzing spiked dilution curves covering several orders of magnitude in concentrations of unmodified and phosphorylated peptides. To our knowledge, this is the first study that compares the most popular DDA and DIA approaches systematically and on a quantitative basis. Thus far, this has been done only in a semiquantitative fashion.⁷ Our assessment revealed that the high selectivity of HR/AM pSRM considerably improved analytical sensitivity for complex samples and that very sensitive phosphopeptide assays could be established using higher stage fragmentation in linear ion trap instruments. We illustrate the performance of these approaches by monitoring multiple phosphorylation sites of the mitotic spindle assembly checkpoint (SAC) protein Mad1 during different cell cycle stages.

EXPERIMENTAL PROCEDURES

Cell Culture and Sample Preparation of Human Cell Digest

HeLa S3 cells were cultured in Dulbecco's modified Eagle's medium (DMEM, Invitrogen, Carlsbad, CA) supplemented

with 10% heat-inactivated fetal calf serum (FCS) and penicillin-streptomycin (100 IU/mL and 100 μ g/mL, respectively, GIBCO) at 37 °C in a 5% CO₂ atm in a humidified incubator. Cells (10⁷) were collected by centrifugation, and cell pellets were washed twice with PBS. Cells were lysed in 200 μ L of lysis buffer (8 M urea, 0.1% RapiGest, 0.1 M ammoniumbicarbonate) using strong ultrasonication, and total protein concentration was determined by BCA assay (Thermo Scientific) according to the manufacturer's instructions. Then, proteins were reduced with 5 mM TCEP for 60 min at 37 °C and alkylated with 10 mM iodoacetamide for 30 min in the dark at 25 °C. After quenching the reactions with 12 mM *N*-acetyl-cysteine, protein samples were digested by incubation with sequencing-grade Lys-C (1:200, w/w; Wako) for 4 h at 37 °C. Samples were diluted 1:4 with 0.1 M ammoniumbicarbonate buffer to reduce urea concentration to 1.6 M, and digestion was continued by adding modified trypsin (1:50, w/w; Promega, Madison, WI) overnight at 37 °C. Subsequently, peptides were desalted on C18 reversed-phase columns according to the manufacturer's instructions (SEP-PAK Vac 3 cc 500 mg, Waters), dried under vacuum, and stored at –80 °C until further use.

Generation of Serial Dilution Mixtures

We took advantage of an ongoing parallel study aimed at the absolute quantification of centrosomal proteins and employed the chemically synthesized 20 heavy-labeled reference peptides (AQUA grade, Thermo Scientific, Table S1) as spike-in standards for our systematic quantitative evaluation of different MS approaches. In this study, for each of the 10 centrosomal proteins of interest, the two full tryptic peptides with the highest MS intensities lacking any missed cleavages were selected as reference peptides. Subsequently, a mixture comprising equal concentrations of all peptides was prepared, and a dilution series was generated using 10-fold steps starting from 0.5 pmol/ μ L to 0.5 amol/ μ L. To minimize peptide losses during pipetting and storage, low binding tips (Axygen) and glass vials (VWR International) were applied for all sample preparation steps. Next, the same dilution series was prepared adding the human cell digest sample at a concentration of 0.5 μ g/ μ L to all samples.

In a second dilution experiment, we employed a standard mixture containing 10 singly and doubly phosphorylated peptides in equal amounts (MS PhosphoMix 1 Heavy, Sigma-Aldrich, Table S1) and prepared the same two dilution series (with and without a human cell digest) as described above, starting from 50 fmol/ μ L to 0.5 amol/ μ L. Two microliters of each sample was subjected to LC–MS analysis.

Data-Dependent Acquisition (DDA) LC–MS/MS

Peptides were separated on a RP-LC column (75 μ m \times 20 cm) packed in-house with C18 resin (Magic C18 AQ 3 μ m; Michrom BioResources, Auburn, CA, USA) using a linear gradient from 95% solvent A (98% water, 2% acetonitrile, 0.15% formic acid) and 5% solvent B (98% acetonitrile, 2% water, 0.15% formic acid) to 30% solvent B over 40 min at a flow rate of 0.2 μ L/min. Each survey scan acquired in the Orbitrap at 60 000 fwhm was followed by 20 MS/MS scans of the most intense precursor ions in the linear ion trap with enabled dynamic exclusion for 20 s. Charge state screening was employed to select for ions with at least two charges and rejecting ions with undetermined charge state. The normalized collision energy was set to 32%, and one microscan was acquired for each spectrum. Collision induced dissociation was

triggered when the precursor exceeded 100 ion counts. The ion accumulation time was set to 300 ms (MS) and 50 ms (MS/MS). All samples were measured in triplicate. Phosphopeptide analysis was carried out as described above with the following modification: each survey scan was followed by 10 MS/MS scans of the most intense precursor ions in the linear ion trap with enabled multistage activation.

Directed (INL) LC–MS/MS

For directed LC–MS/MS, two inclusion mass lists comprising the calculated ion masses of the observed precursor ions of either 20 unmodified (Table S2) or 10 phosphorylated (Table S3) peptides were generated and imported as mass lists to the instrument software. LC–MS analysis was carried out using the same settings as those for DDA analysis with a few modifications: monoisotopic precursor selection was disabled, and peaks with unassigned charge states were not rejected. This helped to trigger more MS sequencing attempts. Furthermore, the ion accumulation time for MS2 scans was set to 100 ms.

Pseudo-selected Reaction Monitoring (pSRM) LC–MS/MS

PRM was carried out in the linear ion trap (LIT) (CID) and Orbitrap (HCD). For both experiments, the peptides and their modifications were imported into Skyline software (version 2.4) (<https://skyline.gs.washington.edu/labkey/wiki/home/software/Skyline/page.view?name=default>).¹⁷ The precursor ion masses were automatically calculated, and the masses of all observed precursor ions were exported as an instrument method file (Tables S2 and S3). For pSRM-CID-MS2, ion accumulation time was set to 10 ms, and the mass selection window was set to 1 Da. The collision energy was set to 35%, and the activation time was 10 ms. Fragment ions were scanned from the lowest possible m/z to 2000 Th. For pSRM-HCD, MS2 spectra were acquired at a resolution of 7500 (fwhm at 400 m/z), the ion accumulation time was 50 ms, the mass selection window was set to 2 Da, the collision energy was 35%, the activation time was 100 ms, and the measured mass range was from 100 Th to 2 times the precursor mass. Additionally, corresponding charge states were set in the instrument HCD fragmentation method. For pSRM-CID-MS3 analysis, the neutral loss masses were manually calculated and added to the pSRM-CID-MS2 instrument method. Here, to increase sensitivity, the mass selection window was set to 2 Da for MS2/MS3 ion isolation, and an ion accumulation time of 50 ms was applied.

SRM LC–MS/MS (Triple Quadrupole Instrument)

Data derived from a spectral library generated on the basis of acquired HCD spectra of the standard peptide mix from the PRM-HCD experiment were imported into the Skyline program (version 2.4) to extract the corresponding fragment ion masses and precursor ion masses (transitions). After collision energy optimization, the five most suited transitions per peptide were selected according to ref 9 and traced on a triple quadrupole mass spectrometer (QqQ, TSQ Vantage, Thermo Scientific) connected to an electrospray nano ion source and easy nano-LC system (both Thermo Scientific) using the same settings as those used for DDA LC–MS analysis. The cycle time was set to 2 s, resulting in a dwell time of 20 ms per transition. The transition lists with optimized collision energies comprising the 20 unmodified and 10 phosphopeptides are provided as Supporting Information Tables S4 and S5, respectively.

Peptide Quantification

All raw files were loaded into the Skyline software tool (version 2.4) to generate extracted ion chromatograms of the precursor (up to 5) or fragment (up to 10) ions. The mass windows were adjusted to the resolution applied in the corresponding MS method. For PRM-CID methods, a mass window of 0.4 Da was applied. To make the PRM-CID-MS3 data files readable for the Skyline software, we converted the raw files to mzXML format using MM-conversion tool (version 3.9, www.massmatrix.org) and replaced the neutral loss masses used for MS3 by the corresponding original precursor ion masses using an in-house Perl script (available upon request). All integrated peak/transitions were manually inspected and corrected or removed, if required. The integrated and quantified peak/transitions obtained for the different methods and samples are listed in Tables S6–14. Finally, we generated dilution profile correlations and applied an established algorithm¹⁹ to determine LOQ and LOD values as well as linear correlations (Pearson's correlation coefficient (R^2) from highest concentration to LOQ) for each MS method and peptide analyzed (Figures S3–S11).

Determination of Identification Limits

All raw files acquired by DDA, INL, and pSRM for the dilution curve samples of unmodified peptides were converted to mgf format using the MM-conversion tool (version 3.9, www.massmatrix.org) and searched against a decoy (consisting of forward and reverse protein sequences) human Swiss-Prot database (download date 16/05/2012) containing known contaminants, resulting in a total of 41 250 protein sequences using Mascot (Matrix Science, version 2.4). The search parameters were set as follows: full tryptic specificity was required (cleavage after lysine or arginine residues unless followed by proline); up to two missed cleavages were allowed; carbamidomethyl (C) was set as fixed modification; oxidation (M), label $^{13}\text{C}(6)^{15}\text{N}(2)$ (K), and label $^{13}\text{C}(6)^{15}\text{N}(4)$ (R) were set as variable modifications; 10 ppm precursor mass tolerance; and 0.6 (0.02) Da fragment mass tolerance for CID (HCD) tandem mass spectra. After importing the data to Scaffold software (<http://www.proteomesoftware.com>, version 4.2.1), the FDR rate was set to <1% for MS/MS spectra identifications by the Scaffold Local FDR algorithm based on the number of decoy hits. All identified MS/MS spectra in the dilution curve experiment for DDA, INL, and pSRM are available as Tables S15–S17.

Monitoring of Mad1 Phosphorylation Sites

Cell Culture, Synchronization, and Kinase Inhibitors.

HeLa S3 cells were cultured as described above. Cell cycle arrest in S-phase was induced by thymidine (2 mM, Sigma-Aldrich) treatment for 24 h. For MS analysis of mitotic cell cycle stages, cells were released from thymidine and arrested in mitosis before harvesting. Mitotic arrest in prometaphase was induced by nocodazole (0.5 $\mu\text{g}/\text{mL}$, Sigma-Aldrich) treatment for 14 h after thymidine release. Mitotic cells were collected by mitotic shake-off. Mitotic arrest in metaphase was induced by addition of the proteasome inhibitor MG132 (10 μM , Calbiochem) for 2 h, which was added 10 h after thymidine release.

Cell Extracts and Immunoprecipitations. For preparing extracts, HeLa S3 cells were washed once with ice-cold PBS and resuspended in ice-cold lysis buffer (20 mM Tris, pH 7.4, 150 mM NaCl, 0.5% IGEPAL CA-630, 1 mM DTT, 30 $\mu\text{g}/\text{mL}$ RNase, 30 $\mu\text{g}/\text{mL}$ DNase, protease inhibitor cocktail (Roche, 1

EDTA-free tablet for 10 mL of lysis buffer) and phosphatase inhibitors cocktail (cocktails 2 and 3; Sigma-Aldrich)) and incubated for 30 min on ice. After cell lysis, suspensions were cleared by centrifugation at 14 000 rpm for 15 min. Immunopurification of endogenous Mad1 was performed using 50 μ L of solid Affi-Prep protein G matrix beads (Bio-Rad Laboratories) chemically cross-linked to 1 μ g/ μ L of antibody¹² against 1 to 2 mg of clarified cell lysate for 2 h at 4 °C. Afterward, the resin was washed with lysis buffer followed by washing with HNN buffer (50 mM Hepes, pH 7.5, 150 mM NaCl, 5 mM EDTA, 50 mM NaF). Proteins were eluted with 100 mM glycine, pH 2.8, neutralized by the addition of Tris buffer (pH 8.0), reduced, alkylated, enzymatically cleaved, and prepared for MS analysis as described above. For generating a comprehensive phosphorylation site map of Mad1, immunopurified proteins obtained from 10 (S-phase) and 15 (prometaphase and metaphase) 15 cm dishes were pooled, divided in two aliquots, and subjected to the two different phosphopeptide enrichment strategies described below. For monitoring of Mad1 phosphorylation sites, sufficient protein amounts could be obtained from one (S-phase) and two (prometaphase and metaphase) 15 cm dishes. After sample preparation, the peptide samples were dissolved in 40 μ L of 0.1% formic acid containing 125 fmol/ μ L of each heavy-labeled phosphopeptide.

Western Blot. HeLa S3 cells were synchronized with thymidine and subsequently released into nocodazole for 14 h. Cells were collected by mitotic shake-off, and Mad1 and associated proteins were immunopurified from mitotic extracts. The following antibodies were used for western blot: mouse anti-Mad1,¹² rabbit anti-Mad2 (Bethyl Laboratories, cat. no. A300-301A, 1 μ g/mL), and mouse anti- α -tubulin (Sigma-Aldrich, cat. no. T9026, 0.2 μ g/mL).

Phosphopeptide Enrichment (TiO₂). Thirty microliters of titanium dioxide beads (100 mg/mL, Titansphere, GL Sciences Inc., Japan) was placed on self-made GELoader tips (Eppendorf) plugged with a piece of C8 material (Empore, 3M, 3 M Empore C8 and C18 disks, 2214-C8, Bioanalytical Technologies, St. Paul, MN). The columns were washed with water (HPLC grade, Sigma-Aldrich), methanol, and a solution of 80% ACN (Acetonitrile) and 2.5% TFA (trifluoroacetic acid) saturated with phthalic acid. Digested and dried peptides were reconstituted in 80% ACN and 2.5% TFA saturated with phthalic acid and loaded on the microcolumns. To allow maximal binding of phosphorylated peptides to the titanium dioxide beads, the peptide-bead mixture was incubated for 10 min and then slowly passed through and applied two additional times. The microcolumns were subsequently washed with a mixture of 80% ACN and 2.5% TFA saturated with phthalic acid, a mixture of 80% ACN, 20% water, and 0.1% TFA, and, finally, with 0.1% TFA. Phosphorylated peptides bound on the TiO₂ were eluted with a 0.3 M ammonium hydroxide solution. Phosphopeptide-enriched eluates were immediately acidified with 2 M HCl and 5% TFA, desalted, purified on C18 microspin columns (Harvard Apparatus), and dried in a SpeedVac concentrator.

Phosphopeptide Enrichment (IMAC). PHOS-select iron affinity gel beads (Sigma-Aldrich) and dried peptides were resuspended in 30% acetonitrile/250 mM ethanol. IMAC beads and peptides were shaken at room temperature at 1400 rpm for 2 h. Subsequently, samples were loaded three times in a constricted GELoader tip and washed four times with 30% acetonitrile/250 mM ethanol. Phosphorylated peptides were

eluted using 50 mM Na₂HPO₄/NH₃ (pH 10.0), acidified with 100% ethanol and 10% TFA (pH < 3.5), desalted, and passed to LC-MS/MS analysis.

Generation of a Mad1 Phosphorylation Site Catalogue from Phosphopeptide-Enriched Samples. One microgram of total phosphopeptides was subjected to DDA LC-MS/MS using HCD and CID with enabled multistage activation fragmentation, as specified above. Acquired raw files were database-searched using Mascot and Scaffold software, as described above, with the following parameter modification: oxidation (M), label ¹³C(6)¹⁵N(2) (K), label ¹³C(6)¹⁵N(4) (R), and phosphorylation (S, T, Y) were set as variable modifications. The identified proteins, peptides, and MS/MS spectra (Tables S18–S20) were filtered to a FDR of 1% according to the Scaffold Local FDR algorithm based on the number of decoy hits. A list of all MS/MS spectra assigned to Mad1 phosphopeptides is shown in Table S21, and a summary list comprising all identified Mad1 phosphorylation sites is illustrated in Table 1. Protein probabilities were assigned by the ProteinProphet program.³⁴ Proteins that contained similar peptides and could not be differentiated on the basis of MS/MS analysis alone were grouped to satisfy the principles of parsimony. Proteins sharing significant peptide evidence were grouped into clusters. The location of the phosphorylated residues was automatically assigned by Mascot (score >10). All annotated spectra, MS raw files, and search parameters employed have been deposited to the ProteomeXchange Consortium (<http://proteomecentral.proteomexchange.org>) via the PRIDE partner repository³⁵ with the data set identifier PXD000964 and DOI 10.6019/PXD000964.

Mad1 Phosphorylation Site Monitoring. Heavy-labeled reference peptides were synthesized for all identified phosphopeptides of Mad1. For precise quantitation of the single-serine phosphorylation sites at positions S484, S485, S486, and S490, we ordered all possible monophosphorylated versions of the corresponding heavy reference peptide (SQSSSAEQSFLFSR, Table 1). All different phosphopeptide sequences and modifications together with the identified MS/MS spectra from the previous phosphorylation catalogue experiment were imported into Skyline software (version 2.4) to set up a pSRM method to monitor all phosphopeptides. In an initial analysis, we carried out MS2- and MS3-based PRM analysis to select for the best transitions for each peptide. Because of their higher selectivity and lower noise levels, transitions originating from MS3 scans were preferred, if available. Phosphopeptides were quantified using the Skyline tool and the same parameters as described above. The quantitative results, including normalization, ratio determination, and statistical analysis, are summarized in Tables S22 and S23.

For the determination of phosphorylation site stoichiometries and to compensate variations in Mad1 concentrations, additional label-free quantification experiments of the same samples were carried out as described recently.³⁶ In brief, 1 μ g of peptides was subjected to DDA LC-MS/MS analysis using CID with enabled multistage activation fragmentation and the same LC and MS settings as specified above. LC-MS Progenesis software (version 4.1.4832.42146) in combination with the Mascot database search tool (version 2.4) was employed to identify and quantify unmodified and modified Mad1 peptides using the same database search parameters for phosphopeptides as described above. Importantly, the Progenesis software was set such that only nonconflicting peptides

with specific sequences for single proteins in the database were employed for quantification. The results were further statically validated by our in-house software tool SafeQuant (available upon request), as recently shown.³⁶ All identified and quantified peptides are listed in Table S24. Differences in Mad1 concentrations in the samples were normalized using the sum of all MS intensities generated from Mad1 peptides. The corresponding normalization factors using the first sample as base are displayed in Table S23. The data file names of LC–MS runs of all samples analyzed in this study are shown in Table S25.

RESULTS AND DISCUSSION

Experimental Overview

The general aim of this study was to assess the capabilities of three recently established LC–MS strategies in terms of sensitivity and linear relative quantification range for a variety of different peptides in the presence and absence of a complex analytical background (Figure 1). Therefore, we prepared serial dilutions of two different peptide mixtures consisting of 20 unmodified and 10 phosphorylated chemically synthesized heavy peptides (for selection criteria, see Experimental Procedures) covering a concentration range of 6 and 5 orders of magnitude, respectively (referred to as neat samples). To assess analytical performance under a more realistic scenario, we prepared the same dilution series with a complex human digest spiked into each sample (referred to as complex samples). This allowed us to precisely determine the impact of the analytical background on limit of detection (LOD), quantification (LOQ), and identification (LOI) for each peptide and MS approach applied in this study. The four dilution series were analyzed in duplicate using the following data-dependent (DDA) and -independent acquisition (DIA) MS approaches. (i) In DDA, only peptides of the highest intensities in the acquired survey scans are selected for MS sequencing, whereas many other peptides of sufficient intensity for identification pass through the instrument to remain unidentified. (ii) A directed LC–MS/MS strategy (also termed inclusion mass list driven, INL) that attempts to overcome this limitation by directing MS sequencing to the precursors of interest independent of their MS intensities using an inclusion mass list.^{10,11,14,15} Although several thousand peptides can be analyzed by this approach, a drawback is the necessity to detect the precursor ions in the MS1 survey scans to trigger fragmentation. (iii) Targeted LC–MS/MS methods (selected reaction monitoring (SRM) and pseudo-selected reaction monitoring (pSRM, like SRM, but a full MS/MS scan is acquired) that directly fragment selected peptide ions and use the corresponding fragment ions for identification and quantification. We analyzed each sample by SRM using a triple quadrupole (QqQ) MS and by pSRM using collision induced dissociation (CID, ion detection in the linear ion trap (LIT)) based fragmentation. For phosphopeptide analysis, we additionally carried out higher energy collision dissociation (HCD, ion detection in the orbitrap) and neutral loss MS2/MS3 CID fragmentation in the LIT. All peptides were quantified using Skyline,¹⁷ and fragment spectra were identified by database searching. Finally, we generated dilution profile correlations for each peptide and MS method and applied an established algorithm¹⁹ to determine linear quantification ranges as well as identification, quantification, and detection limits.

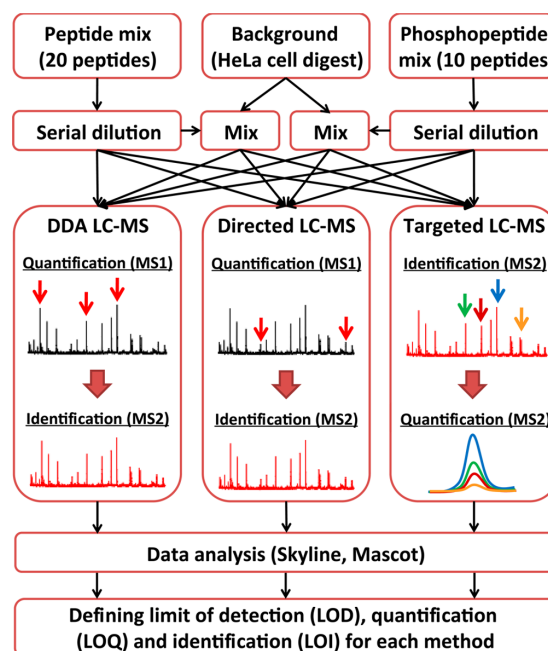


Figure 1. Experimental overview. Two dilution series were generated from two mixtures containing equal amounts of (i) 20 unmodified and (ii) 10 monophosphorylated, respectively, heavy-labeled reference peptides. Additionally, a HeLa whole-cell extract was prepared, digested with trypsin, and spiked into each dilution series sample. The mixtures were analyzed by liquid chromatography–tandem mass spectrometry using three distinct methods to quantify the peptides of interest: data-dependent acquisition (DDA), directed or inclusion list driven (INL) LC–MS, and various targeted LC–MS workflows. These include selected reaction monitoring (SRM) on a triple quadrupole instrument, pSRM on a linear ion trap (LIT) and Orbitrap instrument, and higher stage fragmentation for phosphopeptides on a LIT instrument. For all methods, peak integration and quantification were carried out using the Skyline software suite,^{17,29,30} and full MS/MS spectra were database-searched by the Mascot search engine for identification.^{2,20,22,54} From this data, limits of detection, quantification, and identification were determined for each LC–MS method and dilution series using recently established algorithms.^{1,6,19,33}

Impact of Analytical Background on Limit of Detection/Quantification of Unmodified Peptides

First, we assessed the effect of the analytical background on the dynamic detection and quantification range of the four popular MS approaches. This included data-dependent acquisition (DDA); directed, inclusion mass list driven peak quantification (INL); selected reaction monitoring (SRM) on a QqQ; and pSRM (pSRM-CID) on a LIT LC–MS platform. We determined LODs and LOQs for all peptides and every MS strategy in the presence and absence of a complex human cell digest. In general, we found a very high and linear correlation of peak intensity and analyzed peptide amounts for all MS approaches employed down to the low attomole level (Figures S3–S6). A typical example is illustrated in Figure 2A. For this peptide, LOD/LOQ were found to be in the low attomole range when analyzed by SRM (Figure 2A). However, LOD/LOQ increased by a factor of 10 when analyzing this peptide in the context of a complex human digest (Figure 2B). The observed trend of elevated LOD/LOQ values with increased

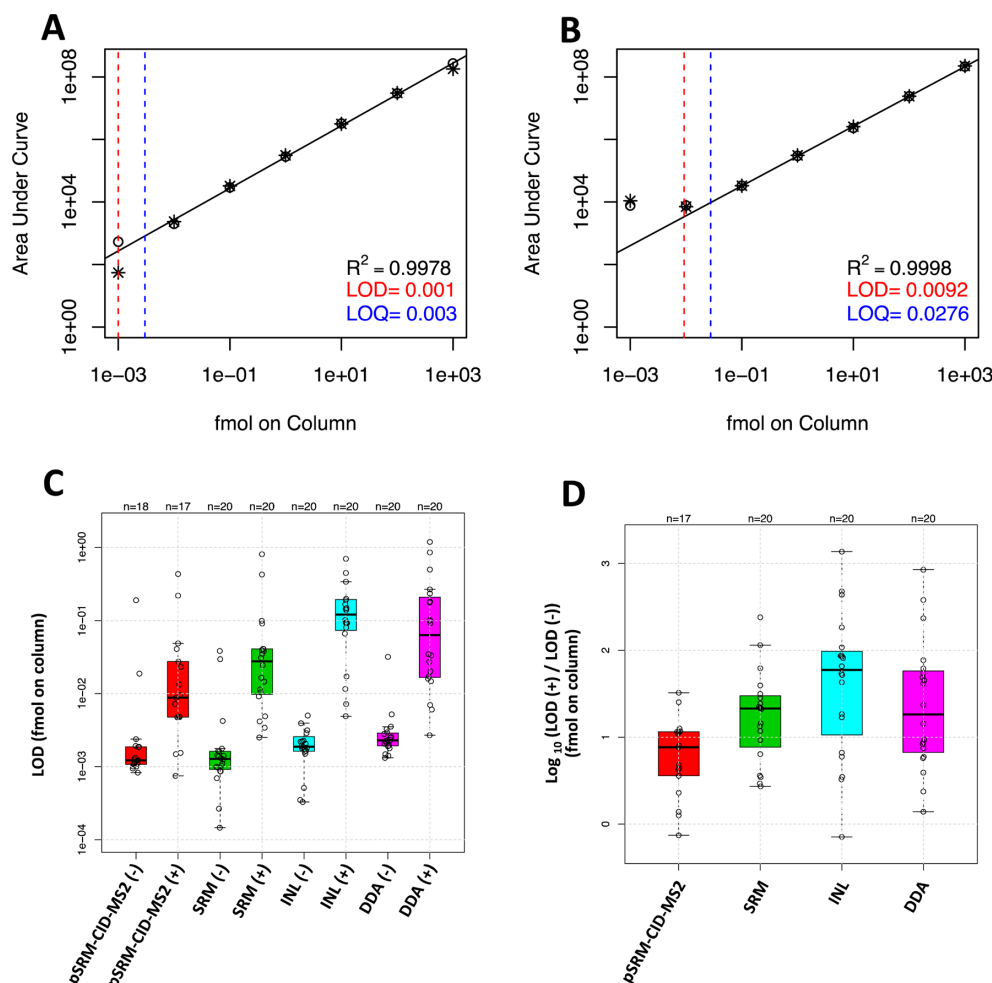


Figure 2. Defining detection and quantification limits for unmodified peptides. The peak intensities and peptide concentrations were plotted for each peptide and LC–MS method to compute linear regression (squared Pearson correlation (R^2)) from highest concentration to LOQ) as well as limit of detection (LOD) and limit of quantification (LOQ). (A) Plot of the peptide INEVLAAAK analyzed by SRM in the neat dilution series. The R^2 , LOD (red), and LOQ (blue) are indicated. (B) Similar to panel A for the same peptide analyzed in the context of complex human cell digest. (C) Box plot showing the LOD values obtained for the four different LC–MS methods applied for the neat (–) and complex (+) dilution series. The box covers the lower and higher quartiles. The median LODs are indicated as a black bar. The whiskers correspond to the maximum and the minimum values, excluding outliers. Outliers that exceed 1.5 times the lower or upper quartile were not considered and are shown as black circles. (D) Similar to panel C, showing the impact of the complex analytical background on the individual LOD values of each MS method.

sample complexity was confirmed for all peptides (Figure 2C). Although all four methods achieved similarly low LODs/LOQs with neat samples, LODs/LOQs increased in the complex samples to the mid attomole range for the targeted MS approaches and high attomole range for MS1-based quantification approaches (DDA and INL, Figure 2C). The lesser increase in LOD/LOQ of the targeted MS methods is expected, as these approaches do not need to detect the precursor ions in the MS1 survey scans and have a higher selectivity due to the double mass filtering applied. Nonetheless, the performance of targeted approaches is also affected by the analytical background present in the sample and considerably decreases the sensitivity of peptide assays by 10-fold for pSRM-CID and 20-fold for SRM. Therefore, like DDA-based analysis, reduction of complexity (e.g., by sample fractionation,²⁰ immune purifica-

tion/depletion,²² or use of longer LC columns²⁴) is an efficient way to increase the sensitivity of targeted MS assays in complex mixtures. An advantage of the pSRM approach over SRM is that less prior information is required to set up the assays (basically, the peptide ion masses are sufficient) and transition selection can be carried out after the LC–MS analysis.^{1,6} This allowed us to remove outliers and pick the most intense fragment ions for quantification postanalysis. By contrast, fragment ion masses and their fragmentation parameters have to be defined before SRM-based analysis. In line with previous studies,²⁶ popular and ubiquitous LIT–MS achieved very good sensitivities, making them a suitable alternative for targeted MS analysis in the event that QqQ instruments are not available. However, the current sequencing speed of LIT does not match the number of transitions monitored by SRM on a QqQ

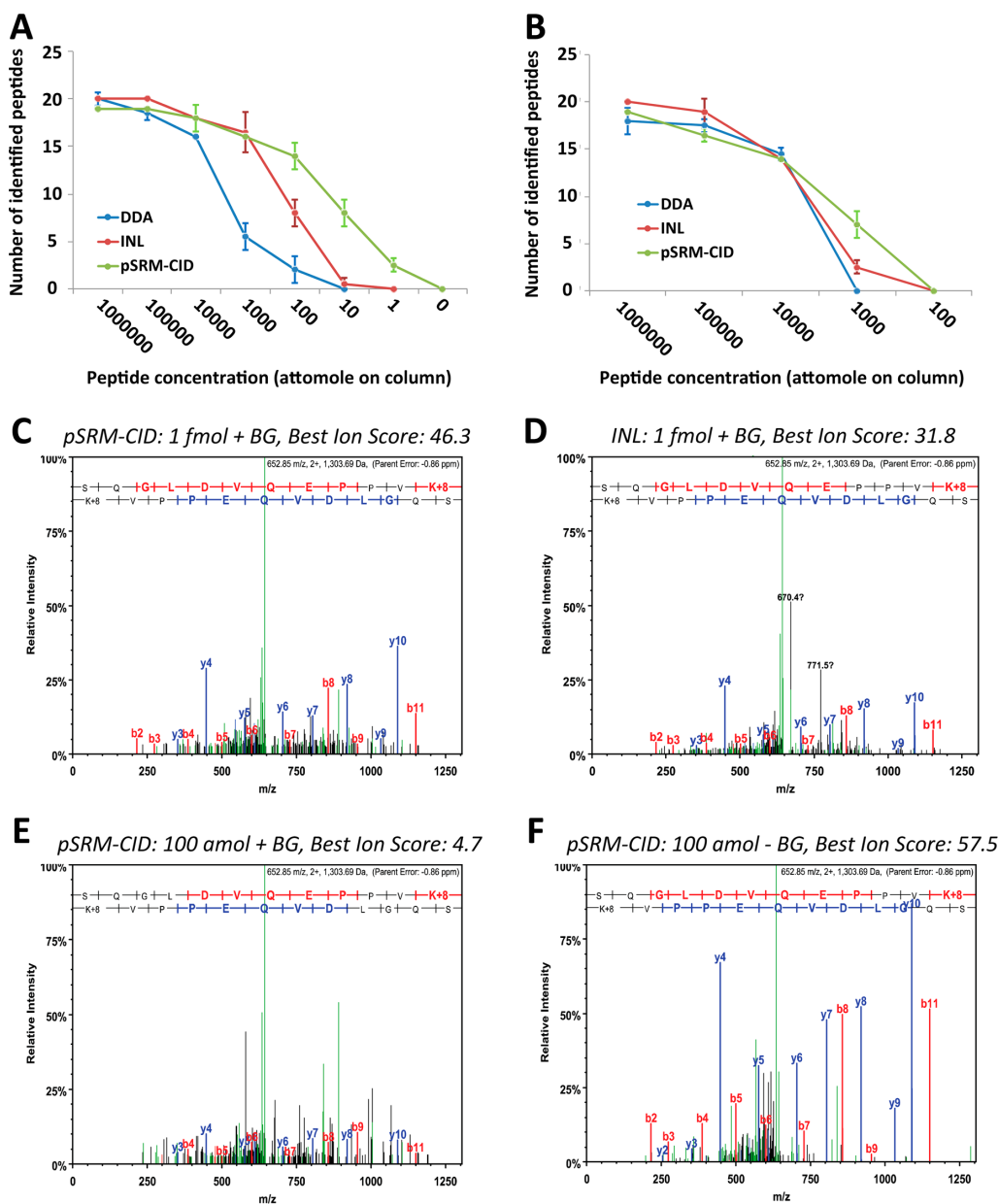


Figure 3. Defining limits of identification for unmodified peptides. (A) The graph shows the number of peptides correctly assigned by the database search tool dependent on their concentration for three different LC–MS approaches and the neat dilution series. (B) Similar to panel A, but for the complex dilution series samples. (C) MS/MS spectrum acquired by pSRM-CID having the highest Mascot ion score (46.3) for the heavy (*Lys-8) peptide SQGLDVQEPPVK* at 1 fmol concentration in the complex sample. (D) Similar to panel C, obtained by directed (INL) LC–MS at 1 fmol concentration in the complex sample. (E) Similar to panel C, but at 100 amol concentration acquired from the neat sample. (F) Similar to panel C, but acquired in the complex sample at a 10-fold lower concentration (100 amol).

instrument and therefore fewer peptides can be monitored by pSRM than by SRM. In our study, around 2.5 (5) times more peptides could be quantified by SRM (5 transitions per peptide) compared to that by pSRM-CID (HCD) in a single LC–MS run.

Naturally, since DDA and INL differed only in the way the precursor ions were picked for MS/MS analysis, both

approaches showed similar LOD/LOQ values determined from the MS1 spectra (Figure 2C). The smaller LOD/LOQ loss and the slightly lower LOD/LOQ values observed for the DDA method in the complex samples (Figure 2C,D) could be explained by the higher resolution applied for the DDA approach (60 000 at 400 m/z (fwhm)) compared to that for INL (30 000 at 400 m/z (fwhm)). Because, in a normal DDA/

INL LC–MS experiment, each peak has to be identified by MS sequencing to be assigned for analysis, these LOD and LOQ values do not represent the true dynamic range usually achieved by these methods. Therefore, defining limits of identification (LOI) will result in a more meaningful assessment and comparison of these two approaches. This will be further investigated below.

To conclude, all methods achieved similar LODs/LOQs in the low-complexity samples, and these values increased considerably with higher sample complexity. As expected, targeted methods are less affected by analytical background than that of the DDA and INL approaches. Nonetheless, the sensitivity of SRM assays will also benefit considerably from a reduction of sample complexity. On average, for complex samples, LODs/LOQs of targeted approaches were 5–10-fold lower than those of DDA/INL approaches for the peptides analyzed in this study.

Determining Limit of Identification for Unmodified Peptides

As mentioned above, LOI is a better indicator to assess the performance of the INL and DDA methods. To define LOIs, we searched all MS/MS spectra acquired with the DDA, INL, and pSRM-CID approaches against a human database and applied a peptide false discovery rate of 1% to all samples (see Experimental Procedures). When analyzing low-complexity samples, more peptides were identified at low concentrations using the INL approach compared to that using DDA (Figure 3A). In particular, in the mid concentration range at 1000 amol, almost all peptides were identified by INL, whereas DDA identified only 6 out of 20. Further zooming in on this issue, we found that, at low concentrations, many peptides were not fragmented by DDA and therefore were not identified. Apparently, disabling most peptide ion detection filters of the instrument software (see Experimental Procedures) resulted in more identifiable peptide specific MS/MS scans from the inclusion mass list for very low-intensity signals. This suggests that implementing more sophisticated peak detection algorithms for peptide ions could increase the overall sensitivity of DDA LC–MS. The lowest LOIs could be achieved by pSRM-CID, indicating that meaningful MS/MS spectra could be generated in the highly sensitive LIT even if no precursor ion was detectable in the survey scan acquired in the less sensitive Orbitrap. Therefore, to exploit the full sensitivity of an LIT in the hybrid LC–MS platform employed, a more sensitive Orbitrap would be beneficial to further improve LOIs for DDA/INL in low-complexity samples.

Compared to neat samples, LOIs increased significantly for all approaches upon higher sample complexity, and only minor differences in identification limits were observed across the three methods (Figure 3B). This indicates that limited MS/MS scan speed (tackled by the INL approach) and triggering of MS/MS spectra (overcome by the pSRM-CID approach) had only a minor impact on identification rates when analyzing complex samples. Interestingly, LOIs were, on average, 10–100-fold higher than the corresponding LODs, suggesting that many precursor ions that were easily detectable in the MS1 scan and consequently fragmented remain unidentified by database searching (Figure 2C). Therefore, we next investigated if the interpretation of these MS/MS spectra by the database search software was hampered at low peptide concentrations. A typical example is shown in Figure 3C. At a concentration of 1 fmol, the peptide could be unambiguously identified by pSRM

and INL in the complex sample with the corresponding fragment ions dominating the MS/MS spectrum (Figure 3C,D). After reducing the concentration by 10-fold, the fragment ions, albeit present, were masked by interfering peaks, which complicated the interpretation of this MS/MS spectrum and resulted in an insignificant Mascot ion score (Figure 3E). Without background, high-quality MS2 scans are obtained at this low concentration (Figure 3F). From this, one can conclude that the ratio of precursor-specific fragments to all fragment ions present in the MS/MS spectra is a far more critical parameter for the successful identification of low-abundance peptide species within complex samples than is MS/MS scan speed or dynamic detection range within the MS1 scan. As a result, the increasing prevalence of interfering peaks ultimately defines LOIs for the DDA and INL approaches evaluated in this study. This is in line with a recent publication showing that MS/MS spectra become progressively more difficult to identify if precursor ion intensity is lower than the sum of all other co-fragmenting ions within the mass selection window. The authors further report that this was the case for the large majority of MS/MS spectra acquired in a single-shot LC–MS/MS analysis.⁸ Consequently, reducing the amount of co-fragmenting peptides by applying smaller mass selection windows,⁸ using software that can identify multiple co-fragmenting peptides from the same MS2 spectra,^{31,32} extracting co-eluting peptides,^{8,37} or using fragment ion-specific search tools^{10,11,38,39} are useful approaches to extract the relevant fragment ions from noisy spectra and improve the identification rate of low-abundance peptides for these types of analyses. Furthermore, spiking in heavy reference peptides at high concentrations that are amenable to database searching is an effective way to assign the corresponding precursor/fragment ions of the endogenous peptide and considerably improve analytical sensitivity, as demonstrated for the INL approach.⁴⁰

To conclude, besides limited sequencing speed and dynamic detection range, co-fragmentation of peptides with similar ion masses and elution profiles contributed, to a large extent, to the high LOIs observed when analyzing complex samples. Smaller mass selection windows and adequate software tools that extract relevant fragment ions will be useful to lower LOIs; however, for very complex samples, co-fragmentation will remain a major challenge for single-dimension LC–MS analysis.^{8,15,16} Notably, because only correctly identified peptides are amenable to quantification in standard DDA and INL workflows, the LOIs actually define the LODs/LOQs achieved in our experimental setup for these two MS methods. With LOIs being in the low femtomole range, the actual LODs/LOQs achieved by the DDA and INL methods were therefore several fold higher than those determined solely from the precursor ions in the MS1 scans.

Impact of Analytical Background on Limit of Detection/Quantification of Phosphopeptides

Although the SRM and the corresponding pSRM methods showed the highest sensitivity for monitoring unmodified peptides within complex mixtures, we next asked if this was also the case for modified peptide species with altered fragmentation patterns. To evaluate this, we employed a commercial mix comprising 10 absolutely quantified phosphopeptides carrying single or multiple phosphorylations, as identified in a recent large-scale study using LIT-based fragmentation.^{8,18,41} To

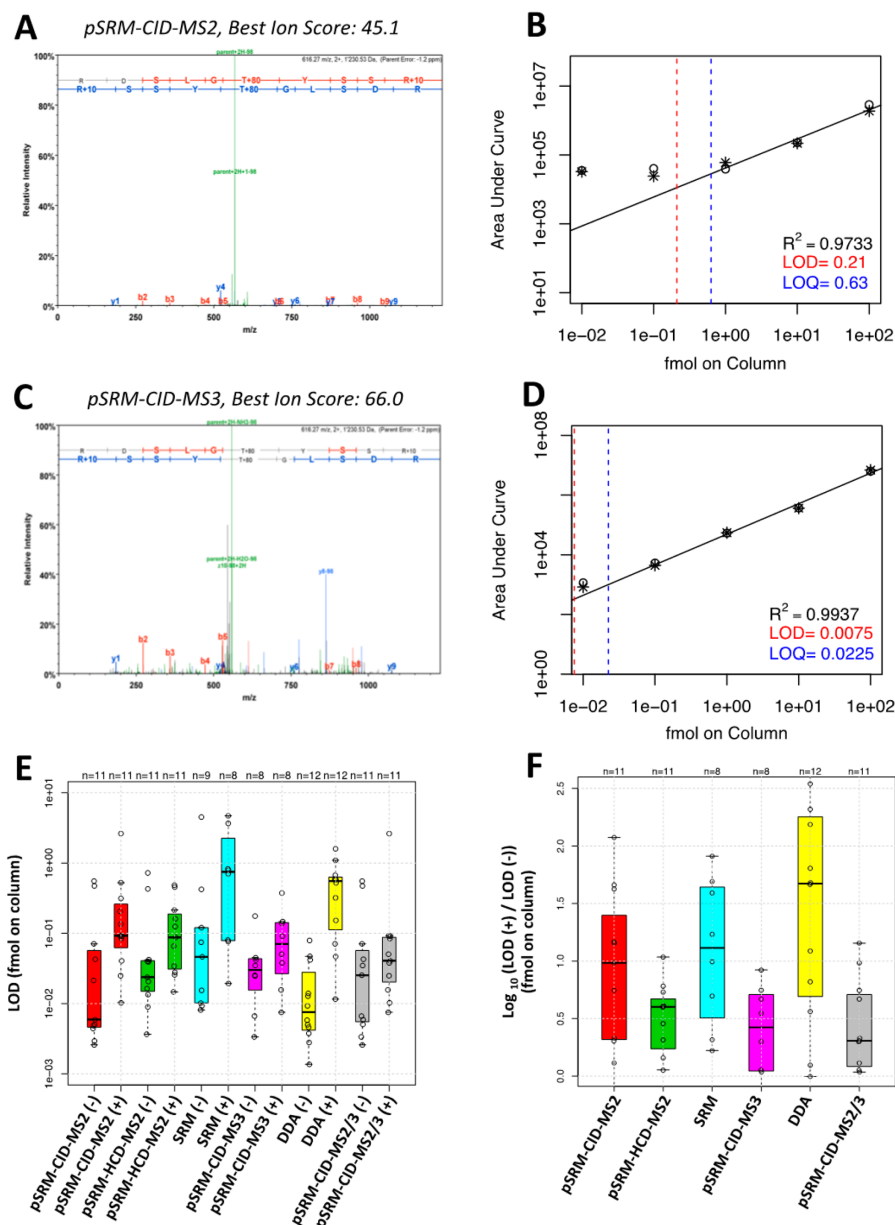


Figure 4. Defining detection and quantification limits for phosphorylated peptides. (A) MS/MS spectrum acquired by pSRM-CID-MS2 of the heavy (*Arg-10) phosphopeptide RDSLGP^{TYSSR}* in the neat sample and assigned with the highest Mascot ion score (45.1). The assigned b- (red) and y-ions (blue) as well as the neutral loss peaks (green) are indicated. (B) Plot of the peak intensities and concentrations of the heavy (*Arg-10) phosphopeptide RDSLGP^{TYSSR}* using the pSRM-CID-MS2 approach. The computed linear regression (squared Pearson correlation (R^2)) from highest concentration to LOQ as well as limits of detection (LOD) and quantification (LOQ) are shown. (C) MS3 spectrum acquired from the neutral loss peak of the same phosphopeptide having the highest ion score (66.0). The assigned b- (red) and y-ions (blue) as well as the neutral loss peaks (green) are indicated. (D) Similar to panel B, but for the pSRM-CID-MS3 method. (E) Box plot showing the LOD values obtained for the 6 different LC-MS methods applied for the neat (-) and complex (+) dilution series. The box covers the lower and higher quartiles. The median LODs are indicated as a black bar. The whiskers correspond to the maximum and the minimum values, excluding outliers. Outliers that exceed 1.5 times the lower or the upper quartile were not considered and are shown as black circles. (F) Similar to panel E, showing the impact of the complex analytical background on the individual LOD values of each MS method.

minimize sample consumption and cost, we prepared a 10-fold dilution series starting from 100 fmol down to 1 amol.

We added two more targeted MS analysis methods to our evaluation that are specifically suited for phosphopeptide analysis, namely, higher stage fragmentation (MS3)^{15,42} and

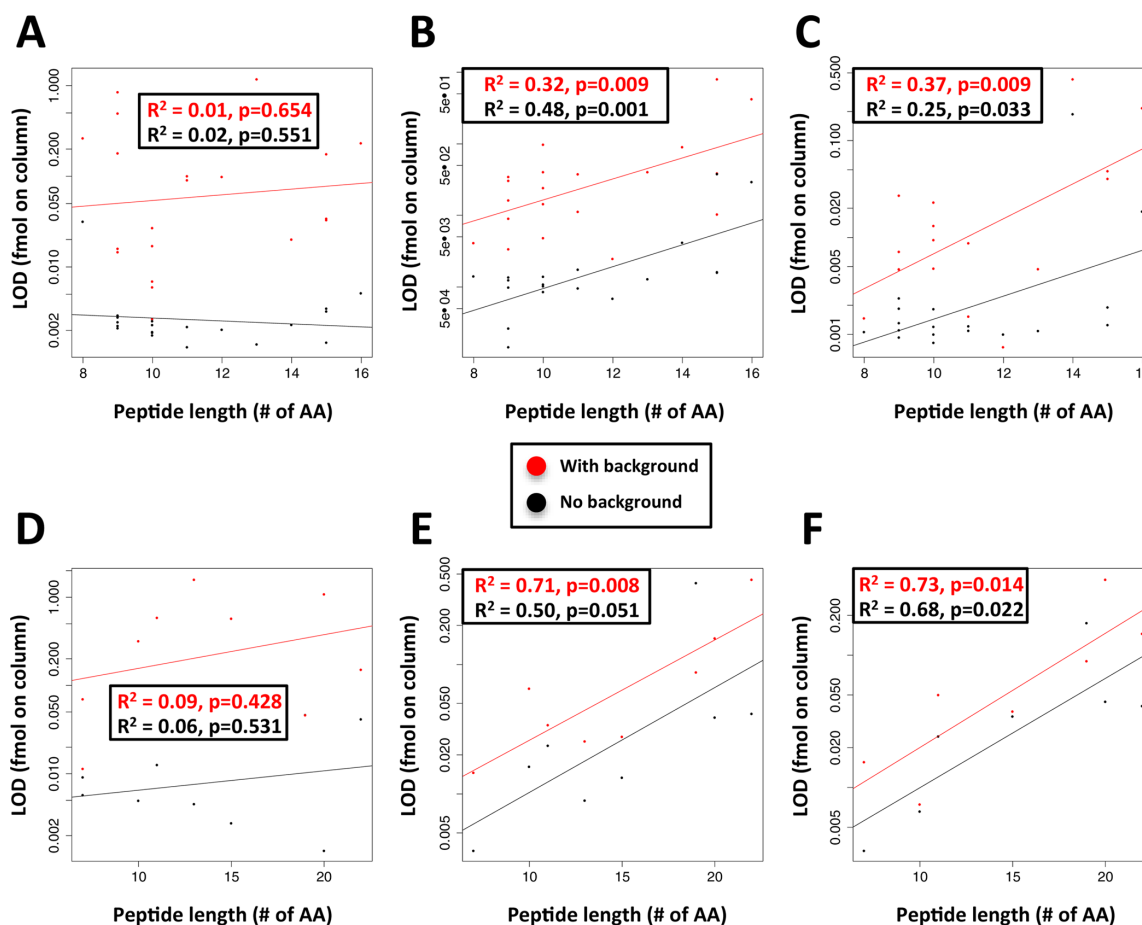


Figure 5. Dependence of peptide length on the limits of detection achieved for the different samples and best performing methods. For each peptide, the number of amino acids against the LODs achieved in the complex (red) and the neat (black) dilution series samples is shown. The plots for 20 unmodified peptides analyzed by DDA (A), SRM (B), and pSRM-CID-MS2 (C) are shown. The same plots are illustrated for the phosphopeptide dilution series analyzed by DDA (D), pSRM-HCD-MS2 (E), and pSRM-CID-MS3 (F). The trend lines and squared Pearson correlations (R^2) as well as the p -values are indicated for each plot and dilution series, respectively. We performed an ordinary least-squares regression, describing $\log(\text{LOD})$ as a function of $\log(\text{peptides length})$ (formally, $\log(\text{LOD}) = k \log(\text{PepLength}) + m$). The calculated p -value is the probability that the slope parameter k equals 0 given the observed data.

high-resolution higher energy collision dissociation (HCD).^{21,43} We performed MS3 of neutral loss peaks that frequently dominate CID spectra of serine and threonine phosphorylated peptides and thereby mask peptide-specific fragment ions required for identification and quantification.^{23,42,44} This method has been recently demonstrated to be well-suited for quantification of selected phosphopeptides by targeted MS.^{25,45} We observed neutral loss peaks in 8 of the 11 MS/MS spectra identified and generated MS3-based pSRM assays for the corresponding peptide ions. The higher selectivity gained by the additional fragmentation step can be nicely demonstrated in Figure 4. The phosphopeptide RDSLGPITYSSR showed a strong neutral loss peak in the MS2-CID spectra, which masked sequence-specific fragments amenable for quantification (Figure 4A). Conversely, the MS3 spectra of the neutral loss peak generated a concert of fragment ions suited for identification and quantification (Figure 4C). Switching from pSRM-CID-MS2 to MS3-based analysis

decreased LOD/LOQ in the complex samples for this peptide by almost 2 orders of magnitude, down to the low attomole range (Figure 4C/D). As is apparent from Figure 4D, this additional mass filter lowered LOQs without compromising the linearity of quantification. The additional fragmentation step only marginally increased the scan time of MS3 assays by 30 ms and did not compromise peptide throughput. Additionally, we quantified each phosphopeptide by high-resolution (7500 fwhm at 400 m/z (fwhm)) HCD fragmentation-based pSRM assays. Unfortunately, the instrument software did not support multistage activation-based pSRM-CID analysis^{27,42} and therefore we could not include this popular phosphopeptide analysis technique in our comparison. Because only minor performance differences were observed in the first experiments between the DDA and INL approaches, we carried out only DDA analysis for the phosphopeptide samples.

Compared to unmodified peptides, the phosphopeptides analyzed generally showed a much higher variation, and higher

Table 1. Phosphopeptides Identified for the Protein Mad1

Best Ion Score ¹	Sequence	Precursor Ion Charge	Phosphosite Position	Phosphosite Reported Previously ²	Putative Upstream Kinase(s) ³
27.71	SLNNFISQR	2+	S16	Yes	Mps1, Plk1
34.77	IQELQASQEAR	2+	S214	Yes	Mps1, Plk1, ATM kinase
33.02	DLEQKLSLQEQDAIVK	3+	S233	No	
41.78	LSLQEQDAIVK	2+	S233	No	
46.69	AILGSYDSELTPAEYSPQLTR	3+	S428	Yes	Mps1, Cdk1
54.81	AILGSYDSELTPAEYSPQLTR	2+	S428	Yes	Mps1, Cdk1
83.7	SQSSSAEQSFLFSR	2+	S484	No	
56.79	SQSSSAEQSFLFSR	2+	S485	No	
68.94	SQSSSAEQSFLFSR	2+	S486	No	
72.63	SQSSSAEQSFLFSR	2+	S490	Yes	Mps1, Plk1
31.74	SQSSSAEQSFLFSREEADTLR	3+	S494	No	
28.07	EEADTLR	2+	T500	No	
21.74	LKVEELEGERSR	3+	S513	Yes	Mps1, (Plk1)
25.55	LKVEELEGERSR	2+	S513	Yes	Mps1, (Plk1)
24.27	VEELEGERSR	2+	S513	Yes	Mps1, (Plk1)
22.61	ALQGDYDQSR	2+	S538	No	Mps1, (Plk1)
25.25	LREDHSLQQAECER	3+	S562	Yes	Mps1, (Plk1)

¹Best ion score determined by the Mascot search engine. A detailed list of all identified MS/MS spectra is shown in Tables S20 and S21. ²Obtained from www.phosphosite.org (20/05/2014). ³Predicted consensus motifs for Mps1,^{55,56} Plk1,^{57,58} Cdk1,^{58,59} and ATM/ATR^{49,60} kinases.

LOD/LOQs were determined for all methods and samples (Figure 4E). In line with the results obtained for unmodified peptides, detection limits increased in the complex samples for all methods, most dramatically by 30-fold for the DDA approach and by 10-fold for SRM and pSRM-MS2-CID, and only little impact on LOD/LOQ values was observed for HCD (4-fold increase) and MS3 (2.5-fold increase) based pSRM strategies (Figure 4F). This can be mainly ascribed to the much smaller mass windows that could be applied for fragment ion extraction with HCD/Orbitrap MS2 scans and the additional isolation/fragmentation step for MS3 that considerably reduced noise and interfering peaks in the MS spectra. Figure S1 shows a typical phosphopeptide that was analyzed by all five methods with and without the presence of a human cell digest. We observed good linearity for all methods, with the MS3 method covering the largest dynamic concentration range for analyzing this phosphopeptide within a complex sample. The improved selectivity of HCD and MS3 can be illustrated with the transitions extracted for this peptide at 1 fmol concentration within a complex analytical background. Although DDA, SRM, and pSRM-CID-MS2 all showed very high noise levels and an accumulation of interfering peaks, the small mass extraction windows applied for pSRM-HCD-MS2 and the additional fragmentation step for the pSRM-CID-MS3 method considerably increased the selectivity and facilitated accurate peak interpretation (Figure S1L,O). Because the pSRM-CID-MS3 approach was not applicable to all phosphopeptides, due to missing neutral loss peaks, we set up a combined approach of MS2 and MS3 pSRM-CID-MS2 and selected the most sensitive assay for each peptide based on the complex sample series. This hybrid pSRM-MS2/MS3 method showed the lowest decrease in sensitivity upon increased sample complexity of only 2-fold (Figure 4F) and therefore also the lowest LODs/LOQs in the complex sample (Figure 4E).

To conclude, like that for unmodified peptides, the sensitivity of phosphopeptide detection critically depends on sample complexity for most approaches. High-resolution HCD fragmentation and, in particular, higher stage fragmentation (MS3) were found to be the most sensitive MS methods that were least affected by the analytical background. To

demonstrate the power of this MS3 approach, we applied it to directly monitor phosphorylation changes in the mitotic spindle assembly checkpoint (SAC) protein Mad1 during cell cycle progression (see below).

Impact of Peptide Size on Limit of Detection/Quantification

Defining LODs/LOQs for 30 peptides allowed us to additionally evaluate the impact of general peptide properties on the sensitivity of the various MS methods tested. Interestingly, we found a strong and significant correlation between peptide length and LOD for all targeted, but not for MS1-based, DDA/INL LC-MS/MS methods. This was observed for the unmodified (Figure 5A–C) and phosphorylated (Figure 5D–F) peptides analyzed. Apparently, the higher number of fragment ions produced by longer peptides diluted the MS signal to many more ions compared to smaller peptides that generated fewer product ions. Intriguingly, no significant peptide length dependencies were found for precursor ion-based quantification methods (Figure 5A,D). This observation is further supported by a recent publication demonstrating a 3-fold loss of sensitivity when analyzing the same peptide using pSRM (fragment-based quantification) over single ion monitoring (precursor ion-based quantitation).¹ In this study, the impact of peptide size on assay sensitivity was even stronger for the peptides analyzed. On average, reducing peptide size by 8 amino acids lowered LOD for SRM and pSRM analysis by 1 order of magnitude for the unmodified and phosphorylated peptides (Figure 5). Therefore, focusing on smaller peptides could be an additional and easy to implement parameter to improve the sensitivity of MS assays for protein quantification. It is important to note that peptides selected for targeted analysis should not be too small so that a sufficient number of specific transitions is available for confident peak assignment, particularly if larger mass selection windows are applied.⁴⁶ Of note, with their high selectivity and specificity, the new HR/AM PRM approaches have demonstrated that confident peptide assignment can be achieved with as few as 3 transitions.⁶ This makes this promising MS technology particularly well suited for the targeted analysis of shorter peptides.

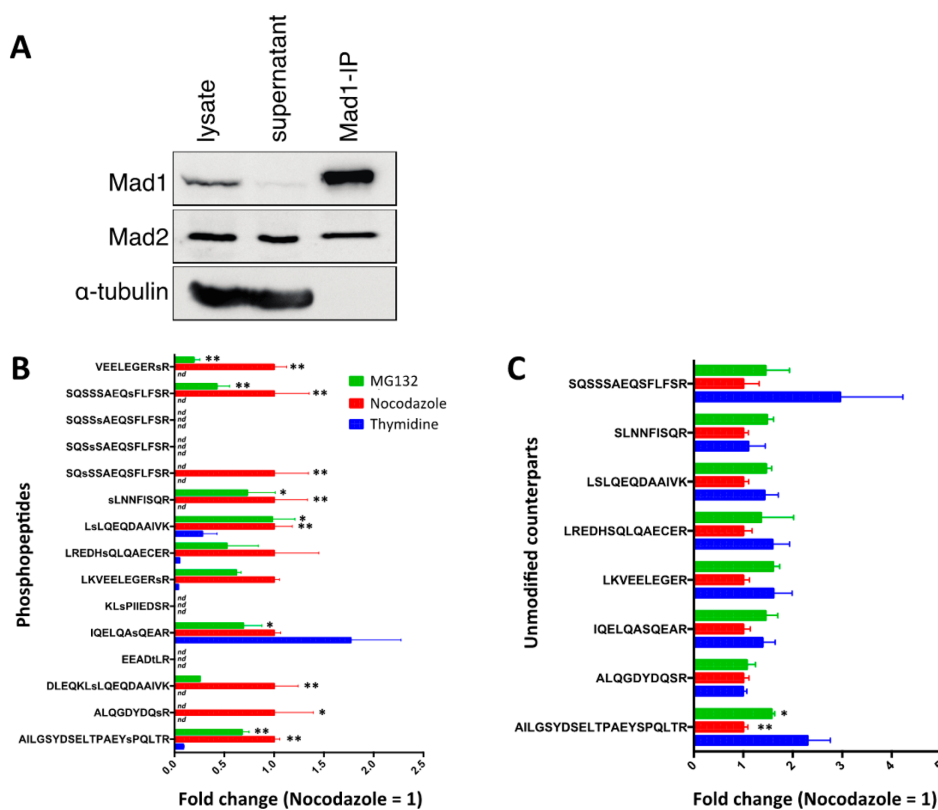


Figure 6. Quantification of all identified Mad1 phosphorylation sites across three different cell cycle stages. (A) Western blot of HeLa S3 cells synchronized with thymidine and subsequently released into nocodazole for 14 h. Cells were collected by mitotic shake-off, and Mad1 and associated proteins were immunopurified from mitotic extracts. (B) Bar chart showing the mean fold changes with error bars determined for each phosphopeptide quantified by pSRM-CID-MS2/MS3 of Mad1 immunopurified from thymidine (blue), nocodazole (red), and MG132 (green) arrested HeLa S3 cells. (C) Bar chart showing the mean abundance changes for the unmodified counterparts of the phosphopeptides monitored across the three different conditions. For clarity, the ratios for nocodazole were set to 1, and the other ratios were normalized accordingly. All experiments were carried out in triplicate. Significant changes are indicated (*, p -value < 0.05; **, p -value < 0.01; nd, no peaks detected).

Application to Mad1 Phosphorylation Site Monitoring

To demonstrate the power of the pSRM-CID-MS3 approach for sensitive phosphopeptide analysis, we applied it to monitor phosphorylation changes of the SAC protein Mad1 during cell cycle progression directly from pull-down experiments. Mad1 is one of the core proteins of the SAC, a surveillance mechanism that delays chromosome segregation until chromosome biorientation is achieved. Mad1, in complex with Mad2, transduces this wait anaphase signal at unattached kinetochores.⁴⁷ During interphase, Mad1 is located at the nucleoplasmic side of the nuclear envelope and then translocates to kinetochores after nuclear envelope breakdown (NEBD).^{47,48}

Careful mapping of Mad1 phosphorylation sites at different cell cycle stages proved to be challenging. Although immunoprecipitation of Mad1 from mitotic cells was efficient (Figure 6A), phosphorylation events on Mad1 proved to be transient and/or of low stoichiometry. Thus, preliminary experiments showed that Mad1 phosphorylation analysis was not reproducible enough to consistently quantify all identified phosphopeptides across all samples (unpublished data). In addition, the high number of cells required for efficient phosphopeptide enrichment further complicated these experi-

ments and increased the cost associated with sample preparation. Therefore, we applied the sensitive pSRM-CID-MS3 method to monitor all detectable Mad1 phosphorylation sites directly from minimal amounts of immunopurified Mad1 without phosphopeptide enrichment.

In a first step, we carried out an in-depth DDA MS analysis of phosphopeptides extracted from a pool of Mad1 immunopurifications obtained from each cell cycle state to generate an extensive catalogue of Mad1 phosphorylation sites. We identified a total of 17 unique phosphopeptide ions corresponding to 13 different phosphorylation sites, of which seven were previously unknown (Table 1). Subsequently, heavy-labeled reference peptides were synthesized for all identified phosphopeptides, and pSRM-CID-MS2/MS3 assays were generated for all phosphorylation sites as described above. No assay could be set up for S494 due to synthesis problems of the corresponding heavy reference peptide, and only the doubly charged precursor ion of the phosphopeptide AILGSYDSELT-PAEYsPQLTR covering S428 was included in the analysis. Overall, sensitive MS3-based pSRM assays could be generated for 13 of the 15 remaining phosphopeptide ions. Because several possible modification sites were in direct proximity of the peptide SQSSSAEQSFLFSR and high mascot scores were

obtained for four different sites, correct positioning of these phosphorylation sites was challenging (S484–S486 and S490, Table 1). Therefore, we first investigated whether we could obtain specific assays for each of the four phosphorylation sites. We selected specific and common fragments (Figure S2A) and analyzed them using pSRM-CID-MS3. As is apparent from Figure S2B–E, the four phosphopeptides showed different elution times and could be nearly fully resolved by the reversed-phase chromatography employed. Elution was the earlier the closer the phosphorylation was positioned to the peptide C-terminus, probably reflecting reduced interaction of the hydrophobic amino acids located at this part of the peptide with the stationary phase during LC. This allowed us to select, besides the few specific fragments, additional unspecific fragments with high MS intensities and generate sensitive, specific pSRM-CID-MS3 assays for all four phosphorylation sites (Figure S2B–E). In general, the pSRM method is particularly well-suited for localizing modifications of a particular peptide because, due to the same precursor ion mass, all possible sites can be monitored with one single MS assay.

Next, we employed these assays for extensive Mad1 phosphorylation site monitoring during three different cell cycle stages: S phase (achieved by thymidine addition), prometaphase (nocodazole treatment), where the SAC is active, and metaphase (MG132 addition), where the SAC is shut down. We could consistently detect and quantify 11 of the 15 targeted phosphopeptides (corresponding to 9 of the 13 identified phosphorylation sites) on endogenous Mad1 pulled-downs from cells in the three stages and across all biological replicates. We observed significant increases in phosphorylation for most sites after nocodazole and MG132 treatment compared to that after thymidine treatment (Figure 6B), in agreement with Mad1 function during SAC activation. According to the consensus motifs present on these phosphopeptides, Plk1, Mps1, and Cdk1 are likely candidate upstream kinases responsible for phosphorylating most of these sites in mitosis (Table 1). Interestingly, the peptide IQELQApSQEAR carrying a phosphorylation at serine 214 showed an opposite trend, namely, a clear increase during S phase (Figure 6B). Recently, this site has been shown to be phosphorylated by ATM kinase, and it has been suggested that such phosphorylation contributes to activation of the SAC.⁴⁹ In the future, it will be interesting to explore a possible role of serine 214 in the mitotic checkpoint complex assembly during interphase.

In an additional experiment, we analyzed each sample by shotgun DDA LC–MS/MS to quantify the unmodified counterparts of the phosphopeptides and define phosphorylation site stoichiometries. Here, we identified two phosphopeptides that showed a strong increase in phosphorylation occupancy of around 50% from S-phase to prometaphase and thus represent the most affected phosphorylation sites for the cell cycle stages analyzed (Figure 6C). It is important to note that with conventional DDA LC–MS/MS analysis only two phosphorylation sites of Mad1 could be identified and quantified from these pull-down samples by label-free quantification, whereas nine sites could be monitored by the more sensitive pSRM-CID-MS2/MS3 approach, increasing the coverage by 4.5-fold.

Knowing that Mad1 exerts its function mostly in the first half of mitosis and that Mad1 relocates from the nuclear envelope to unattached kinetochores,^{50–52} it is tempting to speculate that

such relocalization might depend on the phosphorylation status of Mad1.⁵³

CONCLUSIONS

This is the first study that systematically assesses the performance of the most popular DDA and DIA MS approaches currently used in proteomics. The results will help users to select the most suitable LC–MS methods for their studies, to improve their experimental design, and to define reasonable expectations for future proteomics analyses. It is important to note that different MS analyzers and detectors, which were most suited for the individual MS workflows, were used throughout this study. Because not all LC–MS platforms were available for this study (e.g., fast scanning Orbitrap or time-of-flight analyzers for parallel reaction monitoring (PRM)^{1,6}), users with a different LC–MS setup should carry out a similar method evaluation to assess the performance of their individual LC–MS platforms and workflows. Of note, a thorough comparison of the SRM (on QqQ instruments, used in this study) and PRM (on Orbitrap instruments) approaches has been described recently.^{1,6}

In our study, we observed large performance differences in particular for phosphopeptide analyses in complex samples, and high-resolution HCD and higher stage fragmentation-based pSRM approaches were identified as the most sensitive approaches. We are confident that with the increasing number of known phosphorylation sites (or other PTMs) and the relatively low cost of synthetic heavy reference peptides with modification homologues, such extensive phosphorylation site or PTM monitoring studies can be applied to any protein of interest that can be enriched from a complex protein sample without the need for modification-specific enrichment steps.

ASSOCIATED CONTENT

Supporting Information

Figure S1: Defining linearity and detection and quantification limits for the phosphopeptide RDSLGP²¹⁴TYSSR. Figure S2: Generation of specific MS assays for the different phosphorylation sites identified for the peptide SQSSSAEQSFLFSR. Figure S3: Linearity, LODs, and LOQs for 20 unmodified peptides under neat and matrix-containing conditions targeted in pSRM-CID-MS2 experiments. Figure S4: Linearity, LODs, and LOQs for 20 unmodified peptides under neat and matrix-containing conditions targeted in SRM experiments. Figure S5: Linearity, LODs, and LOQs for 20 unmodified peptides under neat and matrix-containing conditions targeted in INL experiments. Figure S6: Linearity, LODs, and LOQs for 20 unmodified peptides under neat and matrix-containing conditions targeted in DDA experiments. Figure S7: Linearity, LODs, and LOQs for 10 phosphopeptides under neat and matrix-containing conditions targeted in pSRM-CID-MS2 experiments. Figure S8: Linearity, LODs, and LOQs for 10 phosphopeptides under neat and matrix-containing conditions targeted in pSRM-HCD-MS2 experiments. Figure S9: Linearity, LODs, and LOQs for 10 phosphopeptides under neat and matrix-containing conditions targeted in SRM experiments. Figure S10: Linearity, LODs, and LOQs for 10 phosphopeptides under neat and matrix-containing conditions targeted in pSRM-CID-MS3 experiments. Figure S11: Linearity, LODs, and LOQs for 10 phosphopeptides under neat and matrix-containing conditions targeted in DDA experiments. Table S1: Peptide sequences employed for dilution curve experiments.

Table S2: Inclusion mass list used for INL-based analysis of unmodified reference peptides. Table S3: Inclusion mass list used for INL-based analysis of reference phosphopeptides. Table S4: Transition list with optimized collision energies for SRM analysis of unmodified reference peptides. Table S5: Transition list with optimized collision energies for SRM analysis of reference phosphopeptides. Table S6: Integrated peak areas determined by the Skyline software for unmodified reference peptide samples analyzed by DDA. Table S7: Integrated peak areas determined by the Skyline software for unmodified reference peptide samples analyzed by INL. Table S8: Integrated peak areas determined by the Skyline software for unmodified reference peptide samples analyzed by SRM using a QqQ instrument. Table S9: Integrated peak areas determined by the Skyline software for unmodified reference peptide samples analyzed by pSRM using a LIT instrument. Table S10: Integrated peak areas determined by the Skyline software for reference phosphopeptide samples analyzed by DDA. Table S11: Integrated peak areas determined by the Skyline software for reference phosphopeptide samples analyzed by SRM using a QqQ instrument. Table S12: Integrated peak areas determined by the Skyline software for reference phosphopeptide samples analyzed by pSRM-HCD. Table S13: Integrated peak areas determined by the Skyline software for reference phosphopeptide samples analyzed by pSRM-CID-MS2. Table S14: Integrated peak areas determined by the Skyline software for reference phosphopeptide samples analyzed by pSRM-CID-MS3. Tables S15–S17: Unmodified reference peptides identified in dilution series samples by database searching using DDA, INL, and pSRM analysis. Tables S18–S20: Identified proteins, peptides, and MS/MS spectra of a Mad1 phosphorylation site catalogue from phosphopeptide enriched samples. Table S21: List of all MS/MS spectra assigned to Mad1 phosphopeptides. Tables S22 and S23: Quantitative results of Mad1 phosphorylation site monitoring, including normalization, ratio determination, and statistical analysis. Table S24: List of All identified and quantified peptides for Mad1 phosphorylation site monitoring. Table S25: Data file names of LC–MS runs of all samples analyzed in this study. This material is available free of charge via the Internet at <http://pubs.acs.org>.

■ AUTHOR INFORMATION

Corresponding Author

*E-mail: alex.schmidt@unibas.ch. Phone: +41 61 267 20 59. Fax: +41 61 267 20 09.

Present Addresses

[‡]Division of Developmental Immunology Biocenter, Innsbruck Medical University, Innrain 80, 6020 Innsbruck, Austria.

[§]Cell Cycle and Mitosis Laboratory, Research Unit in Biomedicine and Translational Oncology, Vall Hebron Institute of Research, Psg. Vall d'Hebron 119-129, 08035 Barcelona, Spain.

Author Contributions

[†]M.B., E.A., and A.P.B. contributed equally to this work.

Notes

The authors declare no competing financial interest.

■ ACKNOWLEDGMENTS

We thank Roman Koerner (MPI for Biochemistry, Martinsried, Germany) for data sharing during the initial LC–MS

experiments on Mad1 and all members of the Biozentrum's Proteomics Core Facility and the Nigg laboratory for helpful discussions. M.B. and E.A.N. were supported by the Swiss National Science Foundation (31003A_132428 and 310030B_149641), and A.P.B., by the Fellowships for Excellence Ph.D. Program of the Werner Siemens Foundation and the University of Basel.

■ ABBREVIATIONS

DDA, data-dependent acquisition; DIA, data-independent acquisition; PRM, parallel reaction monitoring; MRM, multiple reaction monitoring; SRM, selected reaction monitoring; pSRM, pseudo-selected reaction monitoring; QqQ, triple quadrupole; HR/AM, high resolution/accurate mass; CID, collision induced dissociation; HCD, higher energy c-trap dissociation; SAC, spindle assembly checkpoint; LOD, limit of detection; LOQ, limit of quantification; LOI, limit of identification; PTM, post-translational modification; fwhm, full width at half-maximum; LIT, linear ion trap; LFQ, label-free quantification; BG, background

■ REFERENCES

- (1) Gallien, S.; Duriez, E.; Crone, C.; Kellmann, M.; Moehring, T.; Domon, B. Targeted proteomic quantification on quadrupole-orbitrap mass spectrometer. *Mol. Cell. Proteomics* **2012**, *11*, 1709–1723.
- (2) Simicevic, J.; Schmid, A. W.; Gilardoni, P. A.; Zoller, B.; Raghav, S. K.; Krier, I.; Gubelmann, C.; Lisacek, F.; Naef, F.; Moniatte, M. Absolute quantification of transcription factors during cellular differentiation using multiplexed targeted proteomics. *Nat. Methods* **2013**, *10*, 570–576.
- (3) Nagaraj, N.; Wiśniewski, J. R.; Geiger, T.; Cox, J.; Kircher, M.; Kelso, J.; Pääbo, S.; Mann, M. Deep proteome and transcriptome mapping of a human cancer cell line. *Mol. Syst. Biol.* **2011**, *7*, 548.
- (4) Beck, M.; Claassen, M.; Aebersold, R. Comprehensive proteomics. *Curr. Opin. Biotechnol.* **2011**, *22*, 3–8.
- (5) Domon, B.; Aebersold, R. Options and considerations when selecting a quantitative proteomics strategy. *Nat. Biotechnol.* **2010**, *28*, 710–721.
- (6) Peterson, A. C.; Russell, J. D.; Bailey, D. J.; Westphall, M. S.; Coon, J. J. Parallel reaction monitoring for high resolution and high mass accuracy quantitative, targeted proteomics. *Mol. Cell. Proteomics* **2012**, *11*, 1475–1488.
- (7) Sandhu, C.; Hewel, J. A.; Badis, G.; Talukder, S.; Liu, J.; Hughes, T. R.; Emili, A. Evaluation of data-dependent versus targeted shotgun proteomic approaches for monitoring transcription factor expression in breast cancer. *J. Proteome Res.* **2008**, *7*, 1529–1541.
- (8) Michalski, A.; Cox, J.; Mann, M. More than 100,000 detectable peptide species elute in single shotgun proteomics runs but the majority is inaccessible to data-dependent LC–MS/MS. *J. Proteome Res.* **2011**, *10*, 1785–1793.
- (9) Picotti, P.; Aebersold, R. Selected reaction monitoring-based proteomics: workflows, potential, pitfalls and future directions. *Nat. Methods* **2012**, *9*, 555–566.
- (10) Schmidt, A.; Gehlenborg, N.; Bodenmiller, B.; Mueller, L. N.; Campbell, D.; Mueller, M.; Aebersold, R.; Domon, B. An integrated, directed mass spectrometric approach for in-depth characterization of complex peptide mixtures. *Mol. Cell. Proteomics* **2008**, *7*, 2138–2150.
- (11) Jaffe, J. D.; Keshishian, H.; Chang, B.; Addona, T. A.; Gillette, M. A.; Carr, S. A. Accurate inclusion mass screening: a bridge from unbiased discovery to targeted assay development for biomarker verification. *Mol. Cell. Proteomics* **2008**, *7*, 1952–1962.
- (12) Fava, L. L.; Kaulich, M.; Nigg, E. A.; Santamaria, A. Probing the in vivo function of Mad1:C-Mad2 in the spindle assembly checkpoint. *EMBO J.* **2011**, *30*, 3322–3336.
- (13) Gillette, M. A.; Carr, S. A. Quantitative analysis of peptides and proteins in biomedicine by targeted mass spectrometry. *Nat. Methods* **2013**, *10*, 28–34.

- (14) Savitski, M. M.; Fischer, F.; Mathieson, T.; Sweetman, G.; Lang, M.; Bantscheff, M. Targeted data acquisition for improved reproducibility and robustness of proteomic mass spectrometry assays. *J. Am. Soc. Mass Spectrom.* **2010**, *21*, 1668–1679.
- (15) Schmidt, A.; Beck, M.; Malmstrom, J.; Lam, H.; Claassen, M.; Campbell, D.; Aebersold, R. Absolute quantification of microbial proteomes at different states by directed mass spectrometry. *Mol. Syst. Biol.* **2011**, *7*, 510.
- (16) Picotti, P.; Bodenmiller, B.; Mueller, L. N.; Domon, B.; Aebersold, R. Full dynamic range proteome analysis of *S. cerevisiae* by targeted proteomics. *Cell* **2009**, *138*, 795–806.
- (17) Maclean, B.; Tomazela, D. M.; Shulman, N.; Chambers, M.; Finney, G. L.; Frewen, B.; Kern, R.; Tabb, D. L.; Liebler, D. C.; Maccoss, M. J. Skyline: an open source document editor for creating and analyzing targeted proteomics experiments. *Bioinformatics* **2010**, *26*, 966–968.
- (18) Hebert, A. S.; Richards, A. L.; Bailey, D. J.; Ulbrich, A.; Coughlin, E. E.; Westphal, M. S.; Coon, J. J. The one hour yeast proteome. *Mol. Cell. Proteomics* **2013**, *13*, 339–347.
- (19) Anderson, D. J. Determination of the lower limit of detection. *Clin. Chem.* **1989**, *35*, 2152–2153.
- (20) Shi, T.; Fillmore, T. L.; Sun, X.; Zhao, R.; Schepmoes, A. A.; Hossain, M.; Xie, F.; Wu, S.; Kim, J.-S.; Jones, N.; et al. Antibody-free, targeted mass-spectrometric approach for quantification of proteins at low picogram per milliliter levels in human plasma/serum. *Proc. Natl. Acad. Sci. U.S.A.* **2012**, *109*, 15395–15400.
- (21) Schmidt, A.; Claassen, M.; Aebersold, R. Directed mass spectrometry: towards hypothesis-driven proteomics. *Curr. Opin. Chem. Biol.* **2009**, *13*, 510–517.
- (22) Anderson, N. L.; Anderson, N. G.; Haines, L. R.; Hardie, D. B.; Olafson, R. W.; Pearson, T. W. Mass spectrometric quantitation of peptides and proteins using stable isotope standards and capture by anti-peptide antibodies (SISCAPA). *J. Proteome Res.* **2004**, *3*, 235–244.
- (23) Makarov, A.; Denisov, E.; Lange, O.; Horning, S. Dynamic range of mass accuracy in LTQ Orbitrap hybrid mass spectrometer. *J. Am. Soc. Mass Spectrom.* **2006**, *17*, 977–982.
- (24) Burgess, M. W.; Keshishian, H.; Mani, D. R.; Gillette, M. A.; Carr, S. A. Simplified and efficient quantification of low abundance proteins at very high multiplex by targeted mass spectrometry. *Mol. Cell. Proteomics* **2014**, *13*, 1137–1149.
- (25) Lange, V.; Picotti, P.; Domon, B.; Aebersold, R. Selected reaction monitoring for quantitative proteomics: a tutorial. *Mol. Syst. Biol.* **2008**, *4*, 222.
- (26) Kulasingam, V.; Smith, C. R.; Batruch, I.; Buckler, A.; Jeffery, D. A.; Diamandis, E. P. “Product ion monitoring” assay for prostate-specific antigen in serum using a linear ion-trap. *J. Proteome Res.* **2008**, *7*, 640–647.
- (27) Addona, T. A.; Abbatello, S. E.; Schilling, B.; Skates, S. J.; Mani, D. R.; Bunk, D. M.; Spiegelman, C. H.; Zimmerman, L. J.; Ham, A.-J. L.; Keshishian, H.; et al. Multi-site assessment of the precision and reproducibility of multiple reaction monitoring-based measurements of proteins in plasma. *Nat. Biotechnol.* **2009**, *27*, 633–641.
- (28) Picotti, P.; Lam, H.; Campbell, D.; Deutsch, E. W.; Mirzaei, H.; Ranish, J.; Domon, B.; Aebersold, R. A database of mass spectrometric assays for the yeast proteome. *Nat. Methods* **2008**, *5*, 913–914.
- (29) Picotti, P.; Clément-Ziza, M.; Lam, H.; Campbell, D. S.; Schmidt, A.; Deutsch, E. W.; Röst, H.; Sun, Z.; Rinner, O.; Reiter, L.; et al. A complete mass-spectrometric map of the yeast proteome applied to quantitative trait analysis. *Nature* **2013**, *494*, 266–270.
- (30) Schubert, O. T.; Mouritsen, J.; Ludwig, C.; Röst, H. L.; Rosenberger, G.; Arthur, P. K.; Claassen, M.; Campbell, D. S.; Sun, Z.; Farrah, T.; et al. The Mtb proteome library: a resource of assays to quantify the complete proteome of *Mycobacterium tuberculosis*. *Cell Host Microbe* **2013**, *13*, 602–612.
- (31) Cox, J.; Neuhauser, N.; Michalski, A.; Scheltema, R. A.; Olsen, J. V.; Mann, M. Andromeda: a peptide search engine integrated into the MaxQuant environment. *J. Proteome Res.* **2011**, *10*, 1794–1805.
- (32) Chen, X.; Drogaris, P.; Bern, M. Identification of tandem mass spectra of mixtures of isomeric peptides. *J. Proteome Res.* **2010**, *9*, 3270–3279.
- (33) Jorge, I.; Casas, E. M.; Villar, M.; Ortega-Pérez, I.; López-Ferrer, D.; Martínez-Ruiz, A.; Carrera, M.; Marina, A.; Martínez, P.; Serrano, H.; et al. High-sensitivity analysis of specific peptides in complex samples by selected MS/MS ion monitoring and linear ion trap mass spectrometry: application to biological studies. *J. Mass Spectrom.* **2007**, *42*, 1391–1403.
- (34) Nesvizhskii, A. I.; Keller, A.; Kolker, E.; Aebersold, R. A statistical model for identifying proteins by tandem mass spectrometry. *Anal. Chem.* **2003**, *75*, 4646–4658.
- (35) Vizcaino, J. A.; Côté, R. G.; Csordas, A.; Dianes, J. A.; Fabregat, A.; Foster, J. M.; Griss, J.; Alpi, E.; Birim, M.; Contell, J.; et al. The PRoteomics IDentifications (PRIDE) database and associated tools: status in 2013. *Nucleic Acids Res.* **2013**, *41*, D1063–D1069.
- (36) Glatter, T.; Ludwig, C.; Ahn, E.; Aebersold, R.; Heck, A. J. R.; Schmidt, A. Large-scale quantitative assessment of different in-solution protein digestion protocols reveals superior cleavage efficiency of tandem Lys-C/trypsin proteolysis over trypsin digestion. *J. Proteome Res.* **2012**, *11*, 5145–5156.
- (37) Pak, H.; Nikitin, F.; Gluck, F.; Lisacek, F.; Scherl, A.; Müller, M. Clustering and filtering tandem mass spectra acquired in data-independent mode. *J. Am. Soc. Mass Spectrom.* **2013**, *24*, 1862–1871.
- (38) Reiter, L.; Rinner, O.; Picotti, P.; Hüttenhain, R.; Beck, M.; Brusniak, M.-Y.; Hengartner, M. O.; Aebersold, R. mProphet: automated data processing and statistical validation for large-scale SRM experiments. *Nat. Methods* **2011**, *8*, 430–435.
- (39) Gillet, L. C.; Navarro, P.; Tate, S.; Röst, H.; Selevsek, N.; Reiter, L.; Bonner, R.; Aebersold, R. Targeted data extraction of the MS/MS spectra generated by data-independent acquisition: a new concept for consistent and accurate proteome analysis. *Mol. Cell. Proteomics* **2012**, *11*, O111.016717.
- (40) Hanke, S.; Besir, H.; Oesterheld, D.; Mann, M. Absolute SILAC for accurate quantitation of proteins in complex mixtures down to the attomole level. *J. Proteome Res.* **2008**, *7*, 1118–1130.
- (41) Olsen, J. V.; Blagoev, B.; Gnäd, F.; Macek, B.; Kumar, C.; Mortensen, P.; Mann, M. Global, in vivo, and site-specific phosphorylation dynamics in signaling networks. *Cell* **2006**, *127*, 635–648.
- (42) Ulintz, P. J.; Yocum, A. K.; Bodenmiller, B.; Aebersold, R.; Andrews, P. C.; Nesvizhskii, A. I. Comparison of MS²-only, MSA, and MS²/MS³ methodologies for phosphopeptide identification. *J. Proteome Res.* **2009**, *8*, 887–899.
- (43) Olsen, J. V.; Macek, B.; Lange, O.; Makarov, A.; Horning, S.; Mann, M. Higher-energy C-trap dissociation for peptide modification analysis. *Nat. Methods* **2007**, *4*, 709–712.
- (44) Palumbo, A. M.; Tepe, J. J.; Reid, G. E. Mechanistic insights into the multistage gas-phase fragmentation behavior of phosphoserine- and phosphothreonine-containing peptides. *J. Proteome Res.* **2008**, *7*, 771–779.
- (45) Sherrod, S. D.; Myers, M. V.; Li, M.; Myers, J. S.; Carpenter, K. L.; Maclean, B.; Maccoss, M. J.; Liebler, D. C.; Ham, A.-J. L. Label-free quantitation of protein modifications by pseudo selected reaction monitoring with internal reference peptides. *J. Proteome Res.* **2012**, *11*, 3467–3479.
- (46) Rost, H. L.; Malmström, L.; Aebersold, R. A computational tool to detect and avoid redundancy in selected reaction monitoring. *Mol. Cell. Proteomics* **2012**, *11*, 540–549.
- (47) Foley, E. A.; Kapoor, T. M. Microtubule attachment and spindle assembly checkpoint signalling at the kinetochore. *Nat. Rev. Mol. Cell Biol.* **2013**, *14*, 25–37.
- (48) Musacchio, A.; Salmon, E. D. The spindle-assembly checkpoint in space and time. *Nat. Rev. Mol. Cell Biol.* **2007**, *8*, 379–393.
- (49) Yang, C.; Hao, J.; Kong, D.; Cui, X.; Zhang, W.; Wang, H.; Guo, X.; Ma, S.; Liu, X.; Pu, P. ATM-mediated Mad1 serine 214 phosphorylation regulates Mad1 dimerization and the spindle assembly checkpoint. *Carcinogenesis* **2014**, *35*, 2007–2013.

- (50) Campbell, M. S.; Chan, G. K.; Yen, T. J. Mitotic checkpoint proteins HsMAD1 and HsMAD2 are associated with nuclear pore complexes in interphase. *J. Cell Sci.* **2001**, *114*, 953–963.
- (51) Iouk, T.; Kerscher, O.; Scott, R. J.; Basrai, M. A.; Wozniak, R. W. The yeast nuclear pore complex functionally interacts with components of the spindle assembly checkpoint. *J. Cell Biol.* **2002**, *159*, 807–819.
- (52) Rodriguez-Bravo, V.; Maciejowski, J.; Corona, J.; Buch, H. K.; Collin, P.; Kanemaki, M. T.; Shah, J. V.; Jallepalli, P. V. Nuclear pores protect genome integrity by assembling a premitotic and mad1-dependent anaphase inhibitor. *Cell* **2014**, *156*, 1017–1031.
- (53) Funabiki, H.; Wynne, D. J. Making an effective switch at the kinetochore by phosphorylation and dephosphorylation. *Chromosoma* **2013**, *122*, 135–158.
- (54) Pappin, D. J.; Hojrup, P.; Bleasby, A. J. Rapid identification of proteins by peptide-mass fingerprinting. *Curr. Biol.* **1993**, *3*, 327–332.
- (55) Dou, Z.; von Schubert, C.; Körner, R.; Santamaria, A.; Elowe, S.; Nigg, E. A. Quantitative mass spectrometry analysis reveals similar substrate consensus motif for human Mps1 kinase and Plk1. *PLoS One* **2011**, *6*, e18793.
- (56) Hennrich, M. L.; Marino, F.; Groenewold, V.; Kops, G. J. P. L.; Mohammed, S.; Heck, A. J. R. Universal quantitative kinase assay based on diagonal SCX chromatography and stable isotope dimethyl labeling provides high-definition kinase consensus motifs for PKA and human Mps1. *J. Proteome Res.* **2013**, *12*, 2214–2224.
- (57) Santamaria, A.; Wang, B.; Elowe, S.; Malik, R.; Zhang, F.; Bauer, M.; Schmidt, A.; Silljé, H. H. W.; Körner, R.; Nigg, E. A. The Plk1-dependent phosphoproteome of the early mitotic spindle. *Mol. Cell. Proteomics* **2011**, *10*, M110.004457.
- (58) Alexander, J.; Lim, D.; Joughin, B. A.; Hegemann, B.; Hutchins, J. R. A.; Ehrenberger, T.; Ivins, F.; Sessa, F.; Hudecz, O.; Nigg, E. A.; et al. Spatial exclusivity combined with positive and negative selection of phosphorylation motifs is the basis for context-dependent mitotic signaling. *Sci. Signaling* **2011**, *4*, ra42.
- (59) Elia, A. E. H.; Cantley, L. C.; Yaffe, M. B. Proteomic screen finds pSer/pThr-binding domain localizing Plk1 to mitotic substrates. *Science* **2003**, *299*, 1228–1231.
- (60) Traven, A.; Heierhorst, J. SQ/TQ cluster domains: concentrated ATM/ATR kinase phosphorylation site regions in DNA-damage-response proteins. *BioEssays* **2005**, *27*, 397–407.

3.2.4 Supporting Information

Evaluation of data-dependent and data-independent mass spectrometric workflows for sensitive quantification of proteins and phosphorylation sites

Manuel Bauer^{1#}, Erik Ahrné^{1#}, Anna P. Baron^{1#}, Timo Glatter, Luca L. Fava², Anna Santamaria³, Erich A. Nigg¹, and Alexander Schmidt^{1,*}

these authors contributed equally

* Correspondence: alex.schmidt@unibas.ch

Content:

- Figure S1. Defining linearity and detection and quantification limits for the phosphopeptide “**RDSLGP**TYSSR”
- Figure S2. Generation of specific MS assays for the different phosphorylation sites identified for the peptide “**SQSSSAEQSFLFSR**”.
- Figure S3. Linearity, LODs and LOQs for 20 unmodified peptides under neat and matrix-containing conditions targeted in **pSRM-CID-MS2** experiments.
- Figure S4. Linearity, LODs and LOQs for 20 unmodified peptides under neat and matrix-containing conditions targeted in **SRM** experiments.
- Figure S5. Linearity, LODs and LOQs for 20 unmodified peptides under neat and matrix-containing conditions targeted in **INL** experiments.
- Figure S6. Linearity, LODs and LOQs for 20 unmodified peptides under neat and matrix-containing conditions targeted in **DDA** experiments.
- Figure S7. Linearity, LODs and LOQs for 10 phosphopeptides under neat and matrix-containing conditions targeted in **pSRM-CID-MS2** experiments.
- Figure S8. Linearity, LODs and LOQs for 10 phosphopeptides under neat and matrix-containing conditions targeted in **pSRM-HCD-MS2** experiments.

-
- Figure S9. Linearity, LODs and LOQs for 10 phosphopeptides under neat and matrix-containing conditions targeted in **SRM** experiments.
 - Figure S10. Linearity, LODs and LOQs for 10 phosphopeptides under neat and matrix-containing conditions targeted in **pSRM-CID-MS3** experiments.
 - Figure S11. Linearity, LODs and LOQs for 10 phosphopeptides under neat and matrix-containing conditions targeted in **DDA** experiments.
 - Table S1. Peptide sequences employed for dilution curve experiments.
 - Table S2. Inclusion mass list used for INL based analysis of **unmodified** reference peptides.
 - Table S3. Inclusion mass list used for INL based analysis of reference **phosphopeptides**.
 - Table S4. Transition list with optimized collision energies for SRM analysis of **unmodified** reference peptides.
 - Table S5. Transition list with optimized collision energies for SRM analysis of reference **phosphopeptides**.
 - Table S6. Integrated peak areas determined by the Skyline software for **unmodified** reference peptide samples analyzed by **DDA**.
 - Table S7. Integrated peak areas determined by the Skyline software for **unmodified** reference peptide samples analyzed by **INL**.
 - Table S8. Integrated peak areas determined by the Skyline software for **unmodified** reference peptide samples analyzed by **SRM** using a QqQ instrument.
 - Table S9. Integrated peak areas determined by the Skyline software for **unmodified** reference peptide samples analyzed by **pSRM** using a LIT instrument.
 - Table S10. Integrated peak areas determined by the Skyline software for reference **phosphopeptide** samples analyzed by **DDA**.
 - Table S11. Integrated peak areas determined by the Skyline software for reference **phosphopeptide** samples analyzed by **SRM** using a QqQ instrument.
 - Table S12. Integrated peak areas determined by the Skyline software for reference **phosphopeptide** samples analyzed by **pSRM-HCD**.

-
- Table S13. Integrated peak areas determined by the Skyline software for reference **phosphopeptide** samples analyzed by **pSRM-CID-MS2**.
 - Table S14. Integrated peak areas determined by the Skyline software for reference **phosphopeptide** samples analyzed by **pSRM-CID-MS3**.
 - Table S15. **Unmodified** reference peptides identified in dilution series samples by database searching using **DDA** analysis.
 - Table S16. **Unmodified** reference peptides identified in dilution series samples by database searching using **INL** analysis.
 - Table S17. **Unmodified** reference peptides identified in dilution series samples by database searching using **pSRM-CID-MS2** analysis.
 - Table S18. Proteins identified from phosphopeptide enriched **Mad1** immunopurified samples using Mascot/Scaffold software.
 - Table S19. Peptides identified from phosphopeptide enriched **Mad1** immunopurified samples using Mascot/Scaffold software.
 - Table S20. Peptide spectrum matches from phosphopeptide enriched **Mad1** immunopurified samples using Mascot/Scaffold software.
 - Table S21. **Mad1** phosphorylation sites identified from phosphopeptide enriched Mad1 immunopurified samples using Mascot/Scaffold software.
 - Table S22. Phosphopeptide ratios to spiked in heavy reference peptides obtained from all identified **Mad1** phosphorylation sites using **pSRM-CID-MS2/MS3** and Skyline analysis.
 - Table S23. Normalization and **statistical analysis** of quantified Mad1 phosphopeptides.
 - Table S24. **Label-free quantification** results of the same Mad1 pull-down samples employed for pSRM-CID-MS2/MS3 analysis.
 - Table S25. List of **all sample and file names** employed in this study.

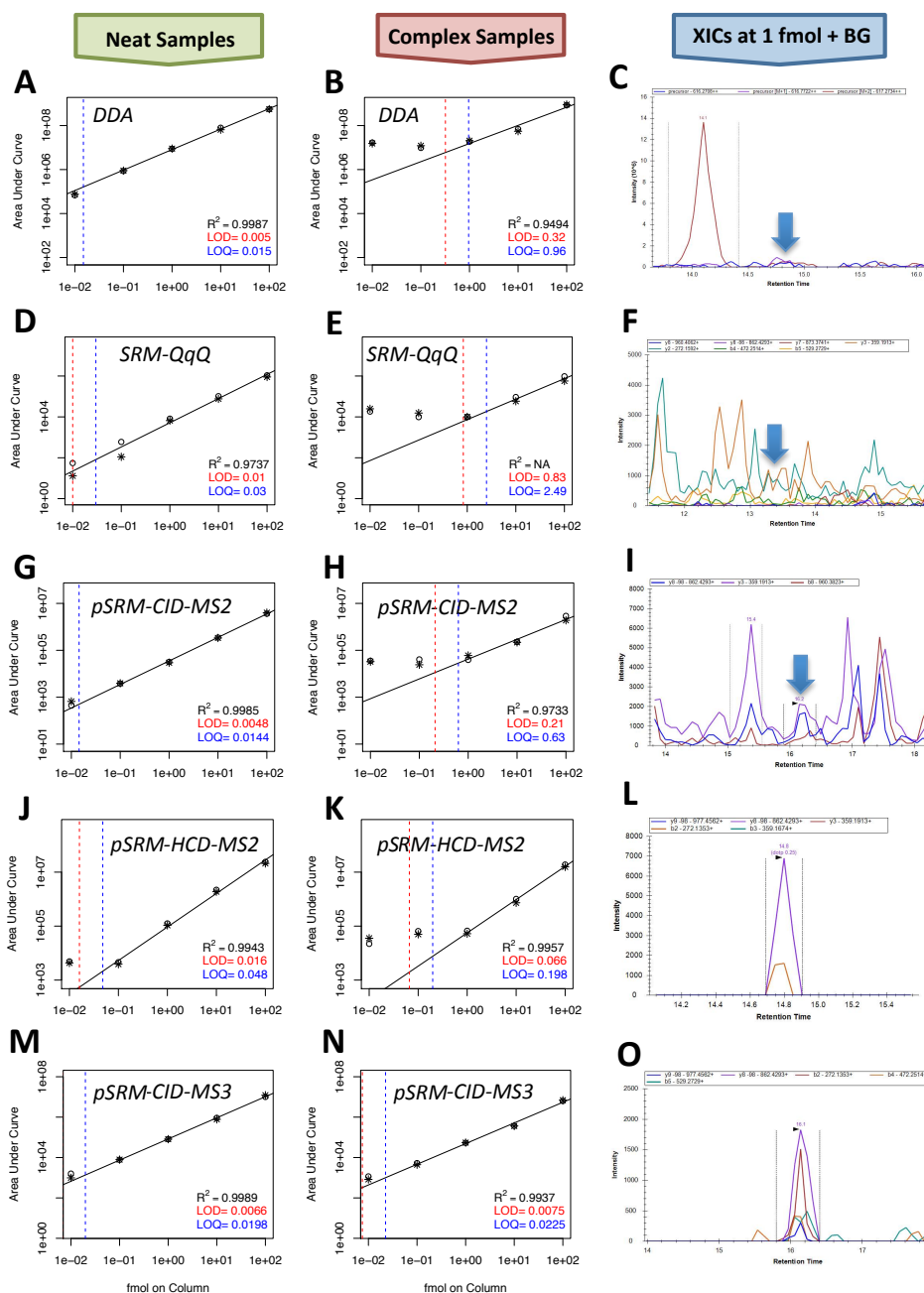


Figure S1. Defining linearity and detection and quantification limits for the phosphopeptide “RDSLGP TYSSR”. The peak intensities and peptide concentrations were plotted for each LC-MS method to compute linear regression (squared Pearson Correlation (R^2) from highest concentration to LOQ) as well as limit of detection (LOD) and limit of quantification (LOQ), respectively. The plots for neat (A, D, G, J, M) and complex samples (B, E, H, K, N) are illustrated. (C, F, I, L, O) Extracted ion chromatograms (XICs) of precursor ions (DDA) and transitions (SRM+pSRM) obtained by the different MS-methods when analyzing 1 fmol of the phosphopeptide in the complex samples using Skyline. For clarification, the elution time of transition/precursor ion XICs for low intense peaks are indicated (blue arrow). (BG, background)

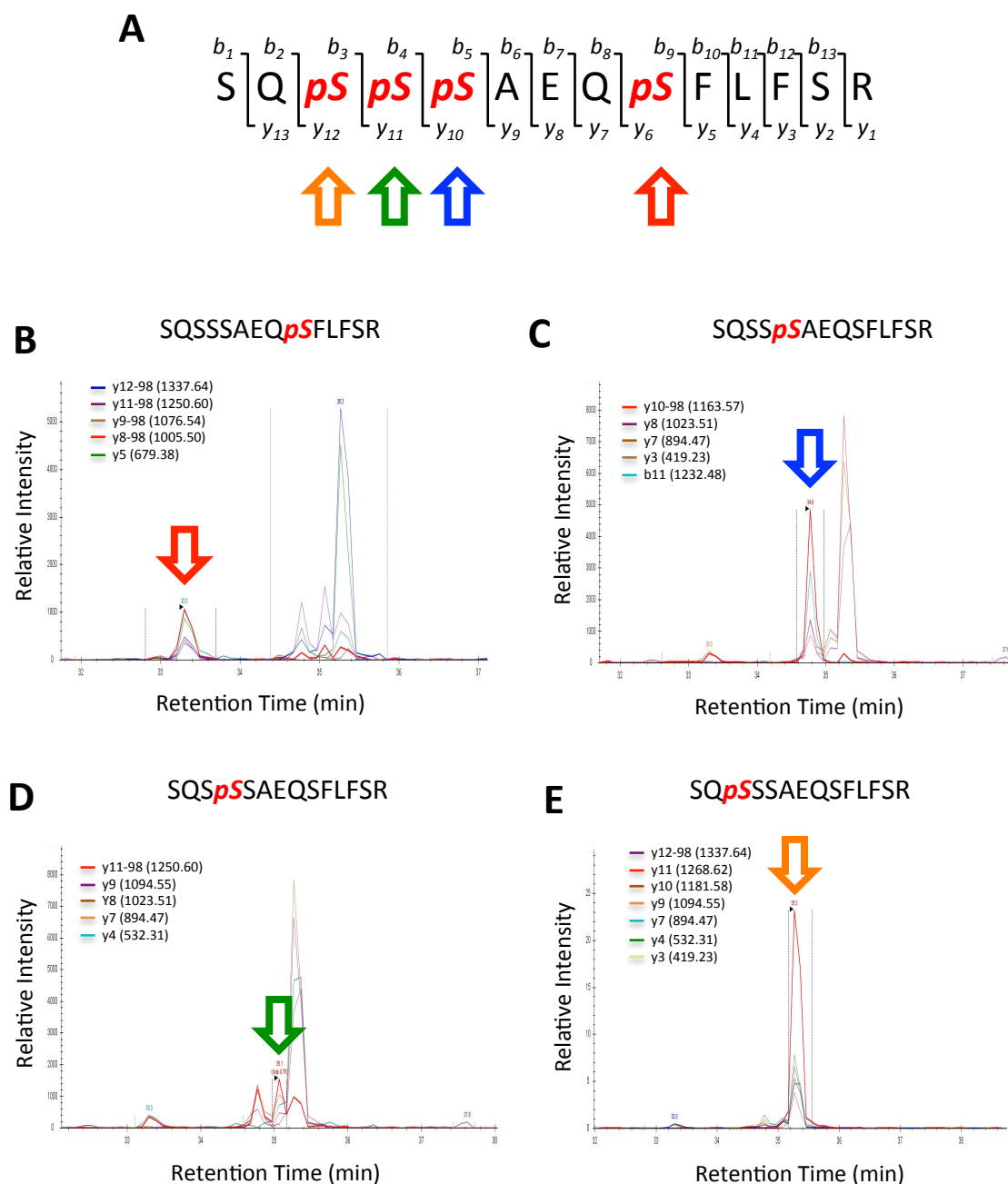


Figure S2. Generation of specific MS assays for the different phosphorylation sites identified for the peptide “SQSSSAEQSFLFSR”. Four heavy reference peptides carrying one phosphorylation at the identified serine residues, respectively, were synthesized and used for MS assay generation. **(A)** Sequence of the peptide indicating the location of four phosphorylation sites on serine residues with the corresponding b- and y-ions identified by discovery LC-MS/MS. **(B-E)** Most intense transitions obtained for **(B)** “SQSSAEQpSFLFSR” (red arrow), **(C)** “SQSSpSAEQSFLFSR” (blue arrow), **(D)** “SQSpSSAEQSFLFSR” (green arrow) and **(E)** “SQpSSSAEQSFLFSR” (orange arrow). The peak displaying the most intense phosphorylation site-specific transition is indicated in red for each chromatogram and phosphorylation site, respectively.

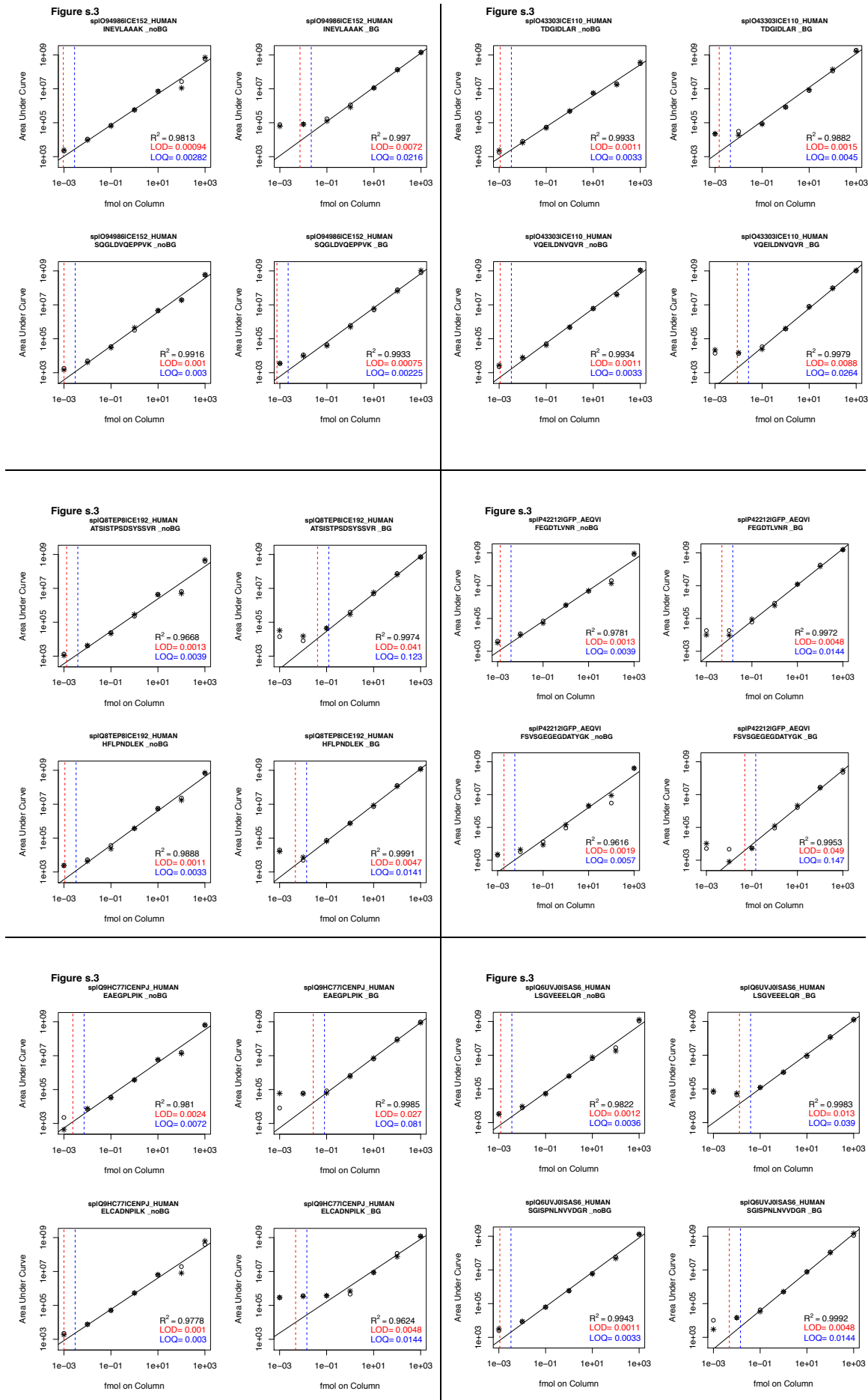


Figure s.3

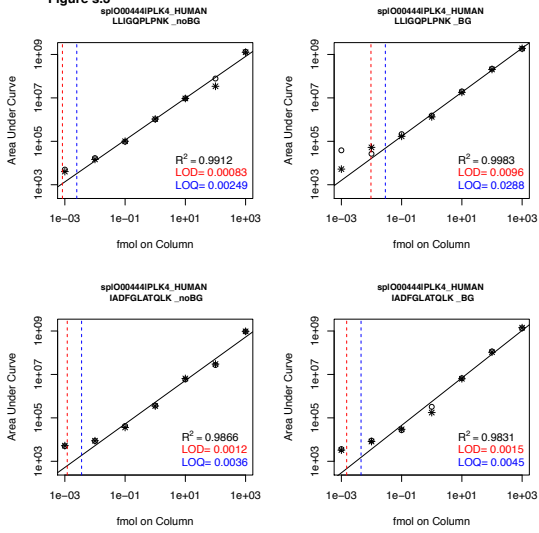


Figure s.3

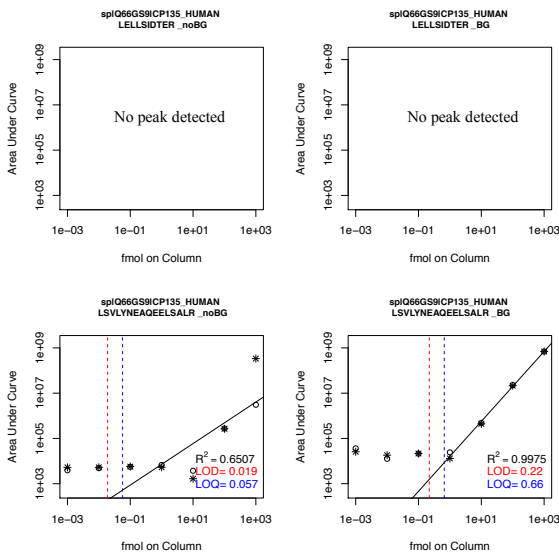
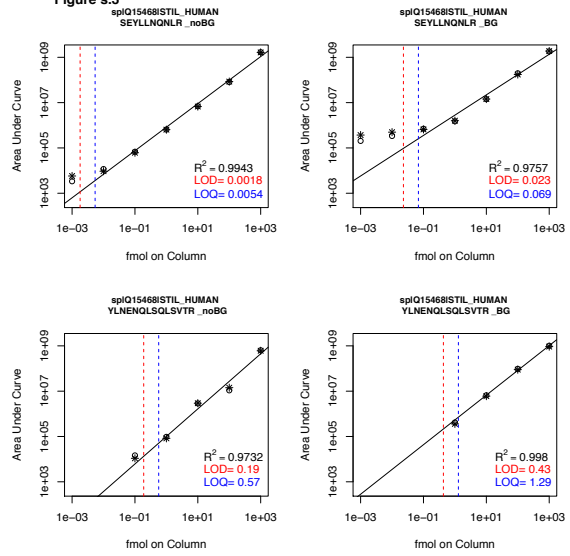


Figure s.4

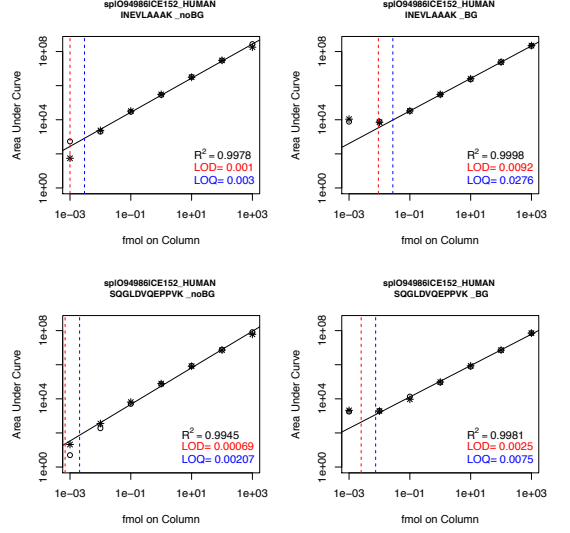


Figure s.4

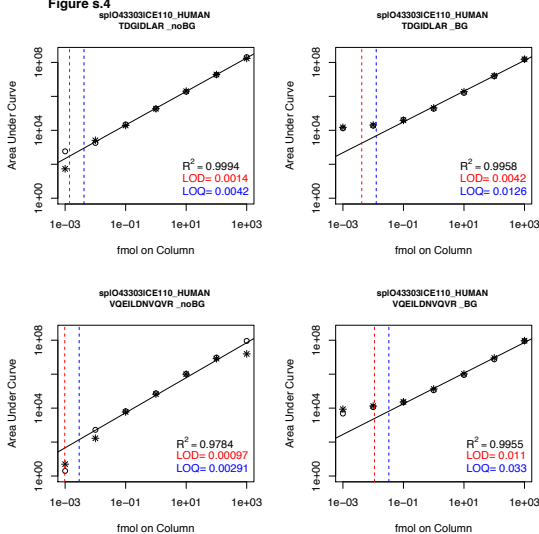
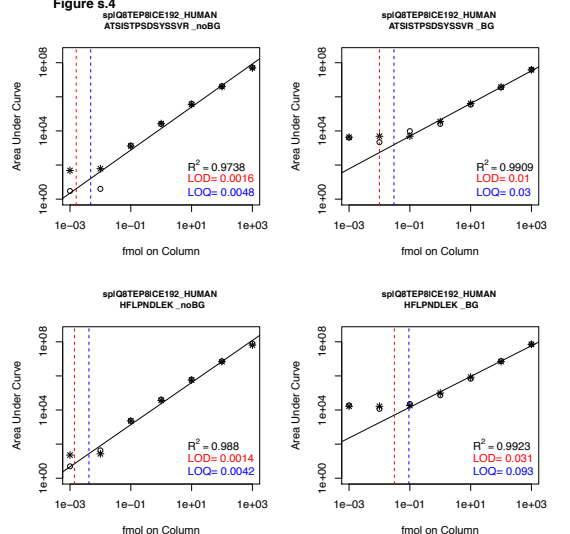


Figure s.4



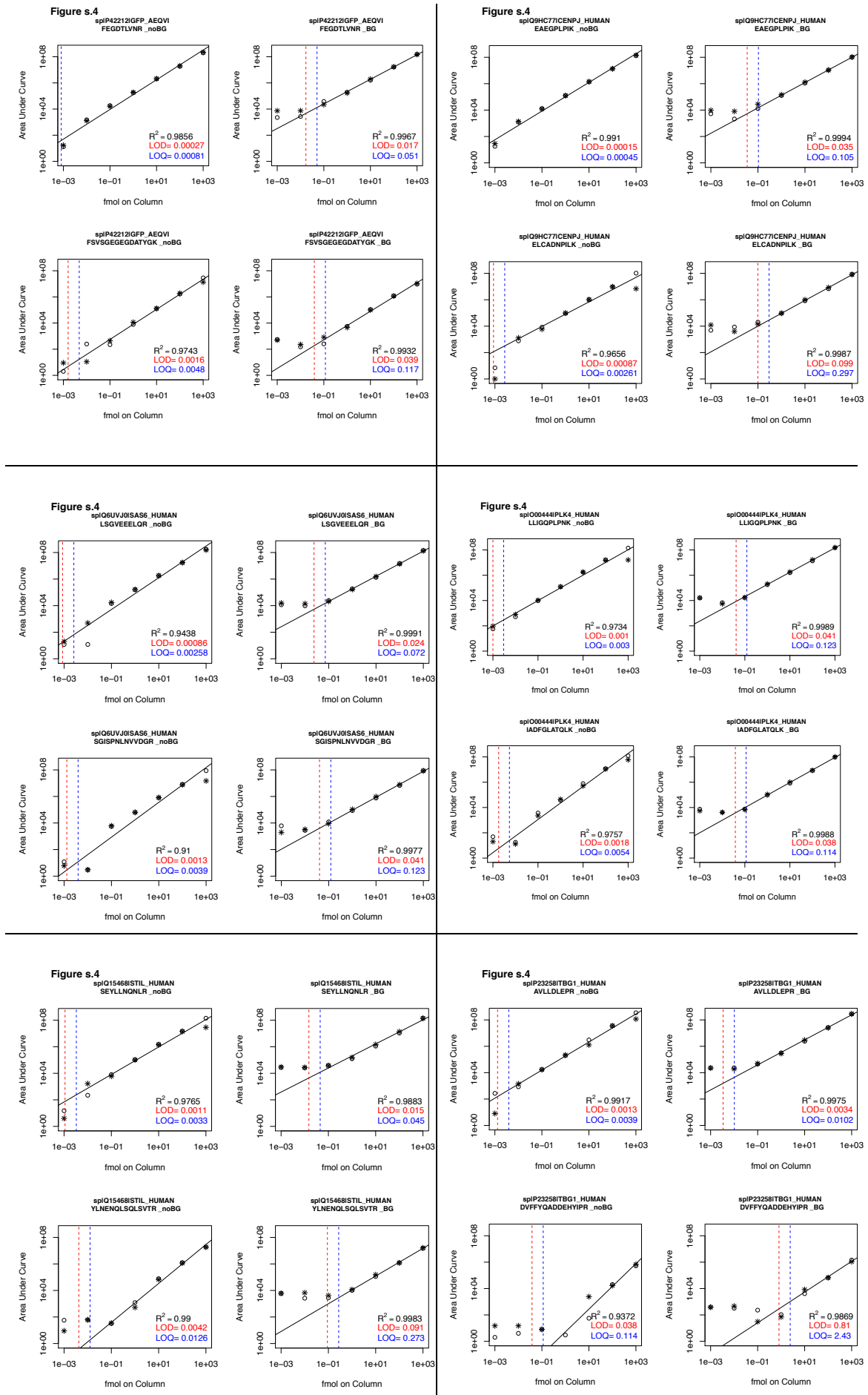


Figure s.4

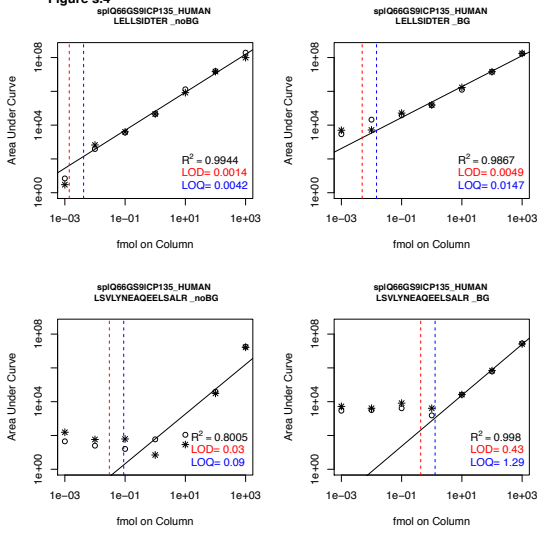


Figure s.5

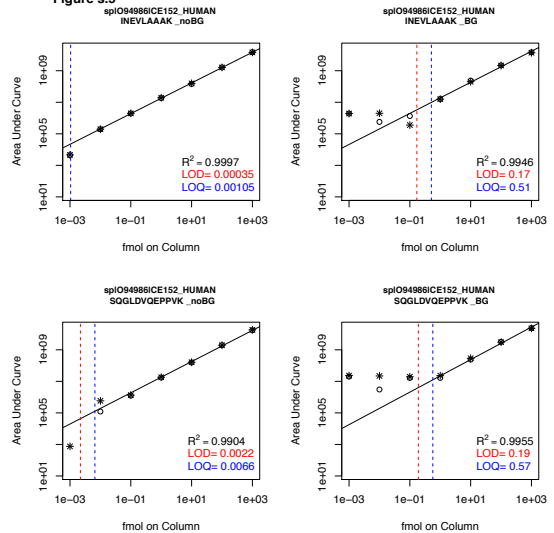


Figure s.5

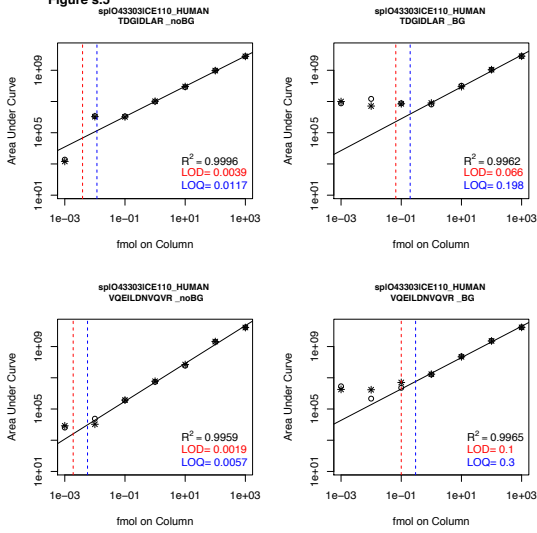


Figure s.5

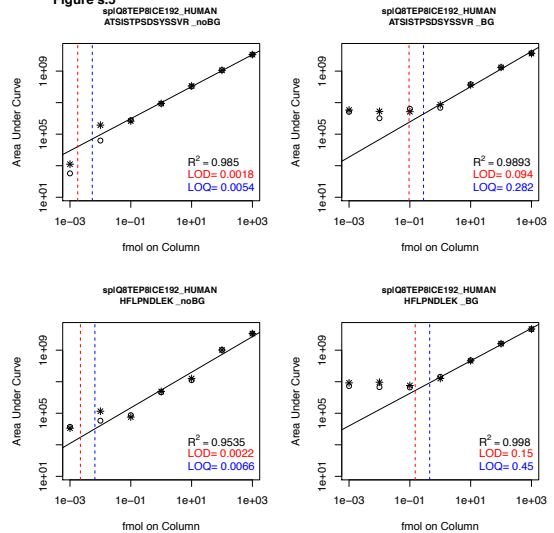


Figure s.5

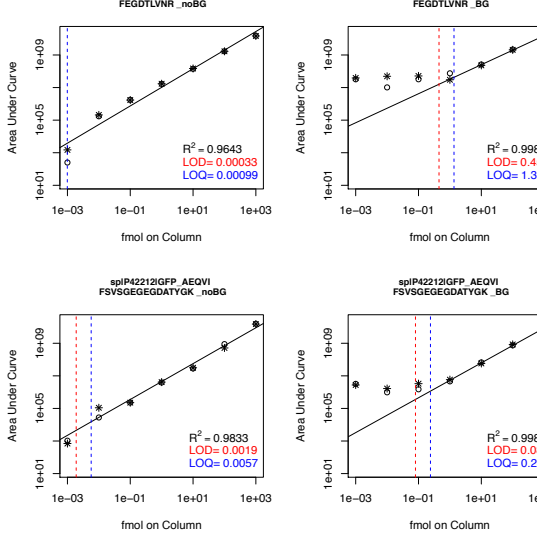
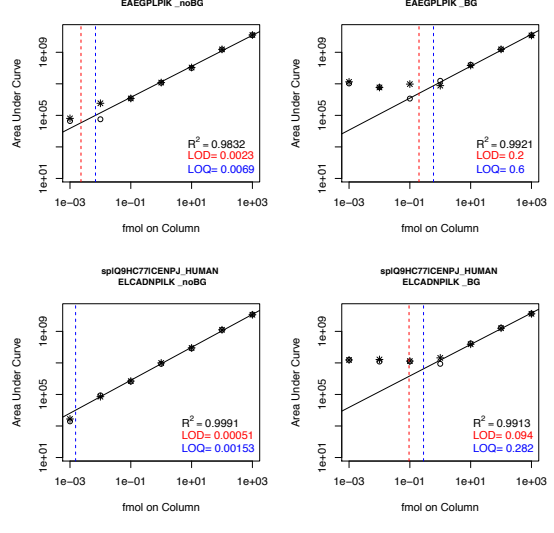
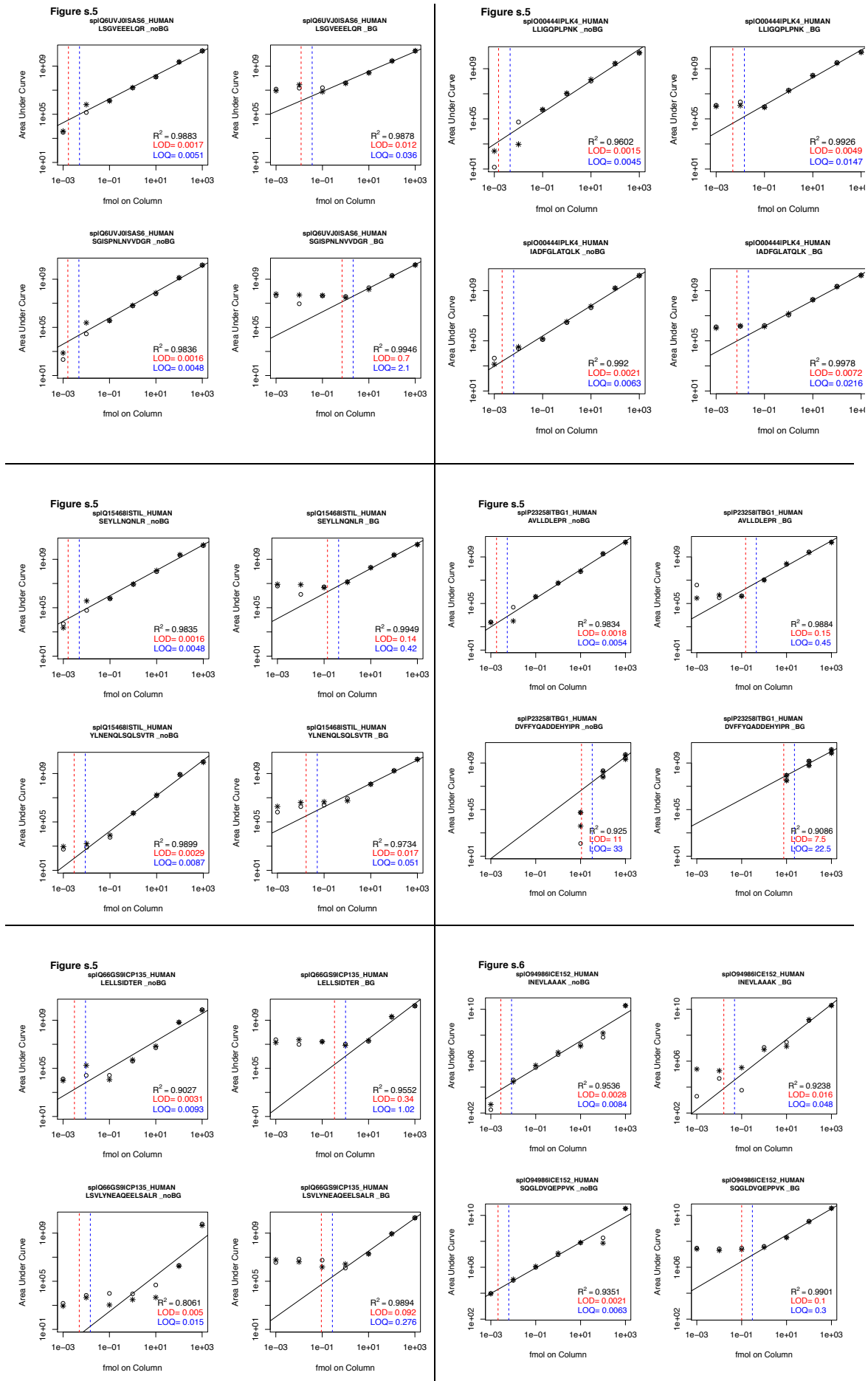
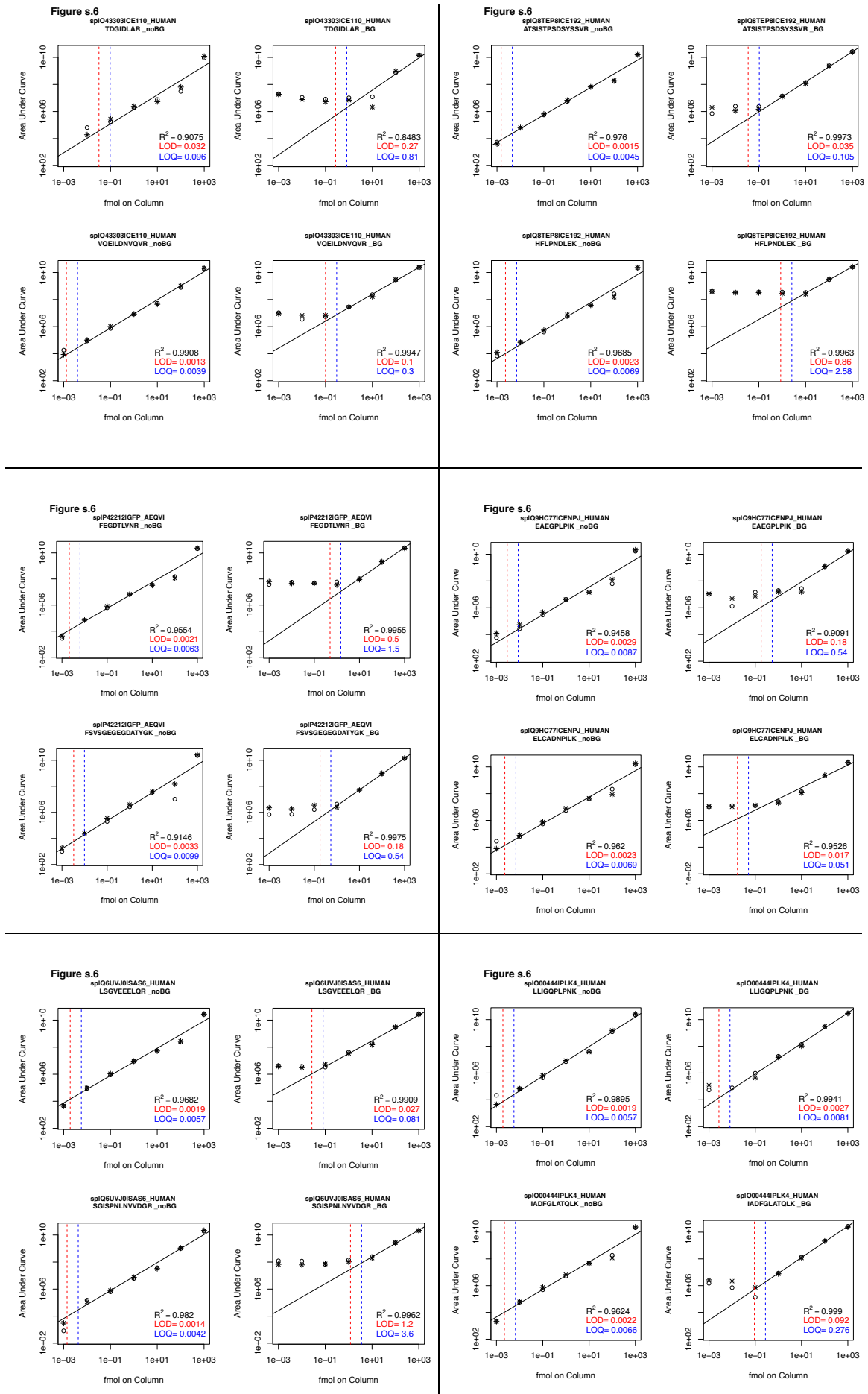


Figure s.5







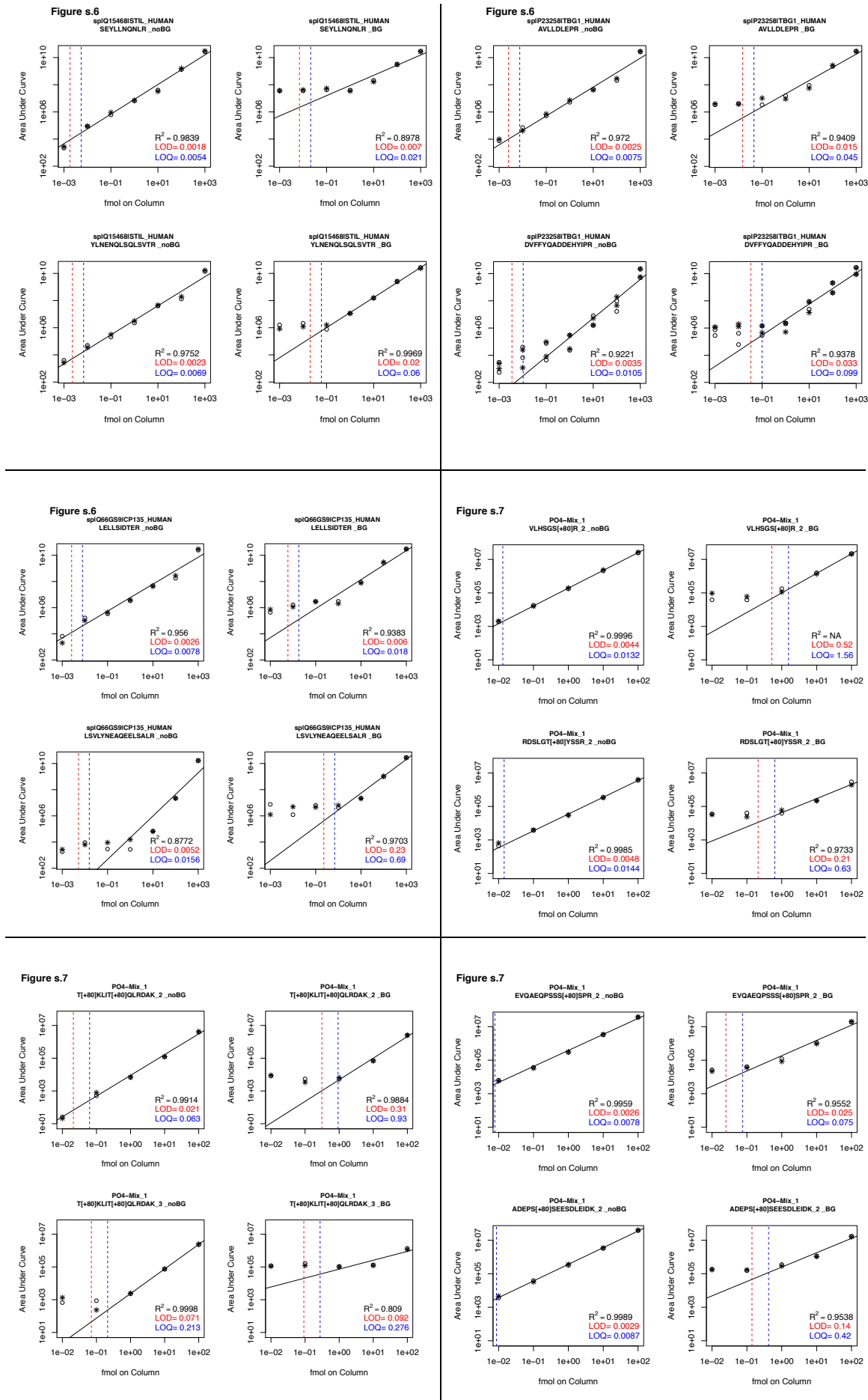


Figure s.7

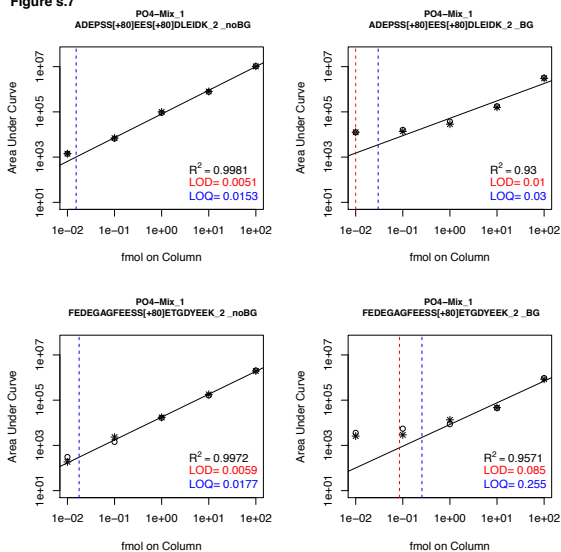


Figure s.7

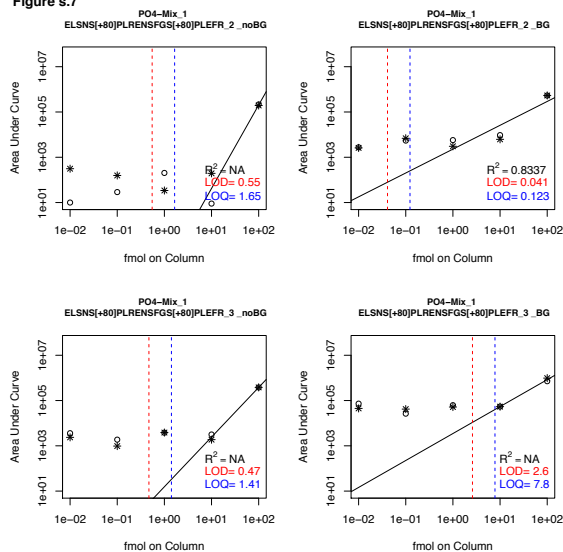


Figure s.7

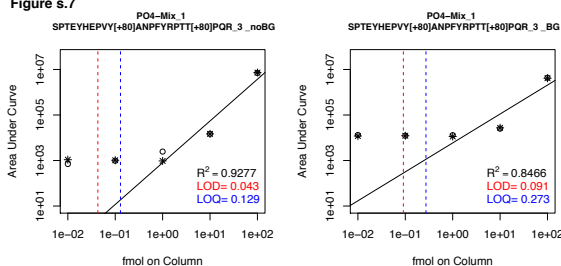


Figure s.8

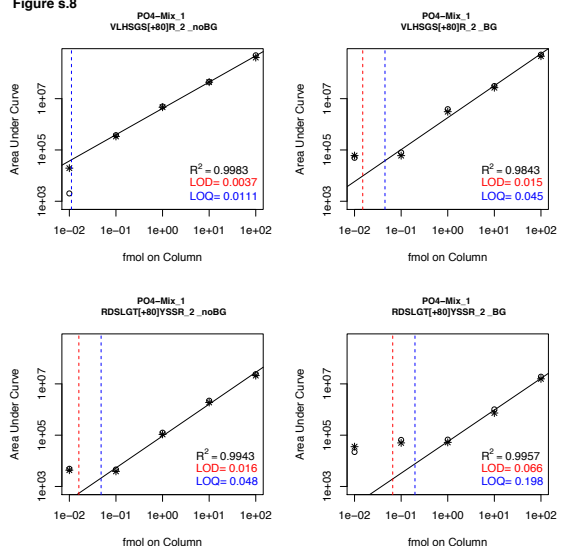


Figure s.8

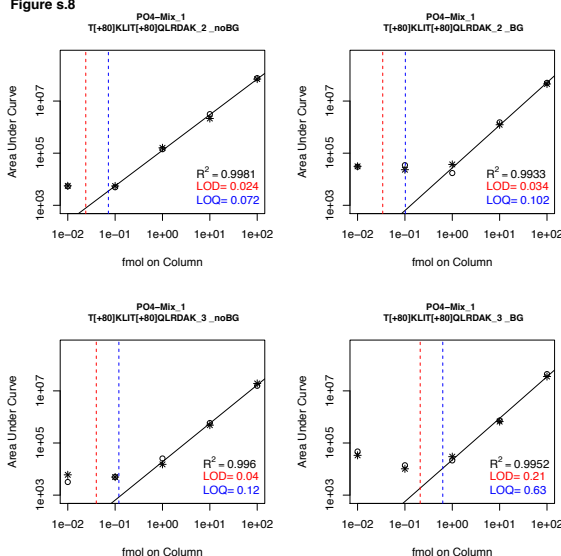


Figure s.8

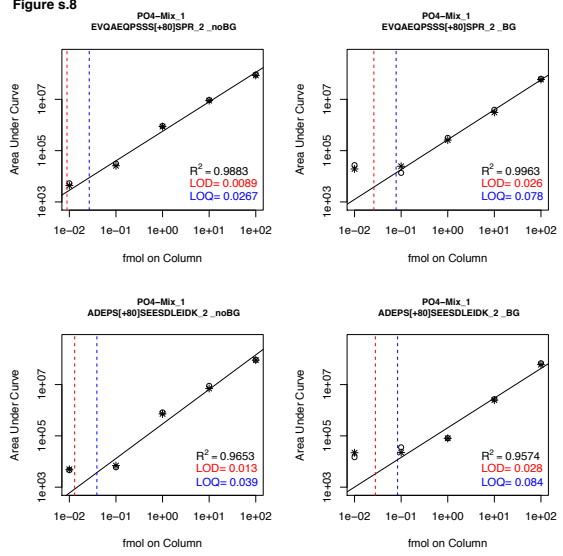


Figure s.8

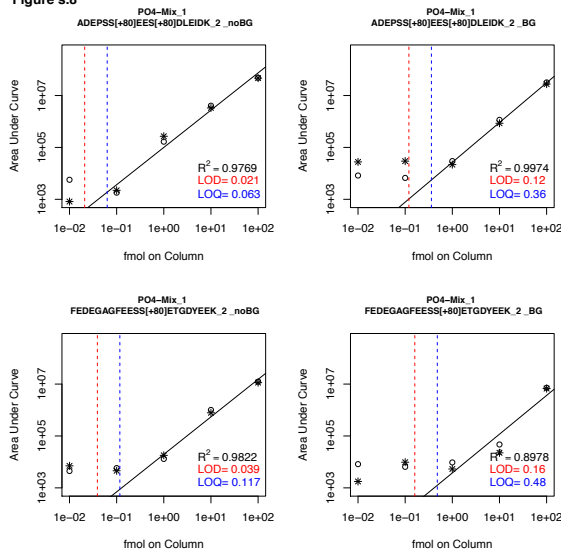


Figure s.8

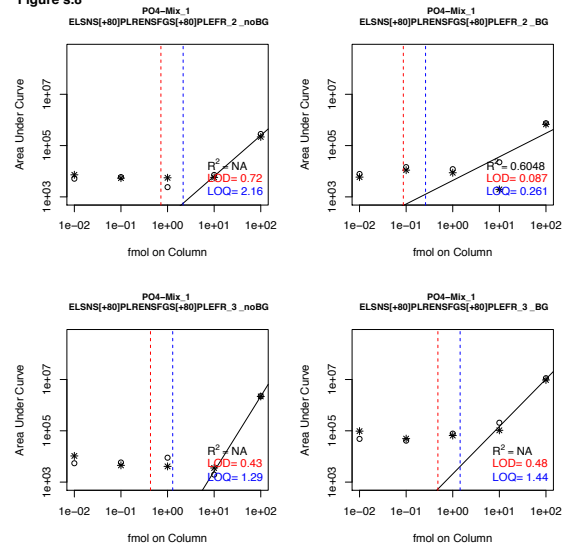


Figure s.8

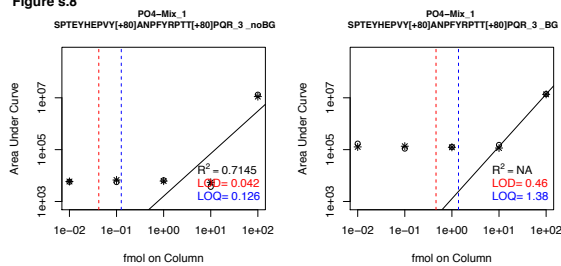


Figure s.9

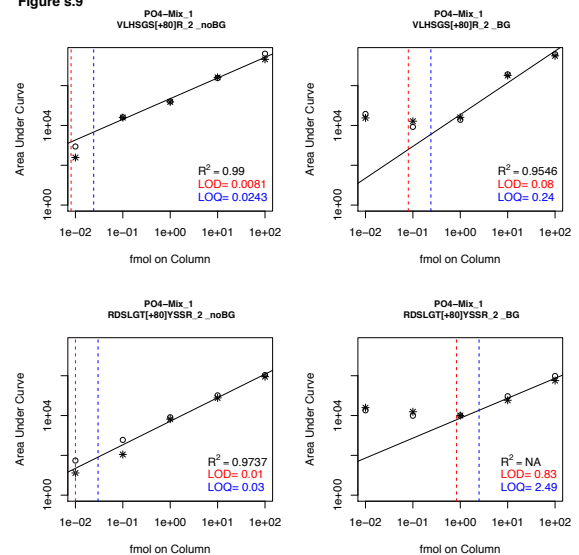


Figure s.9

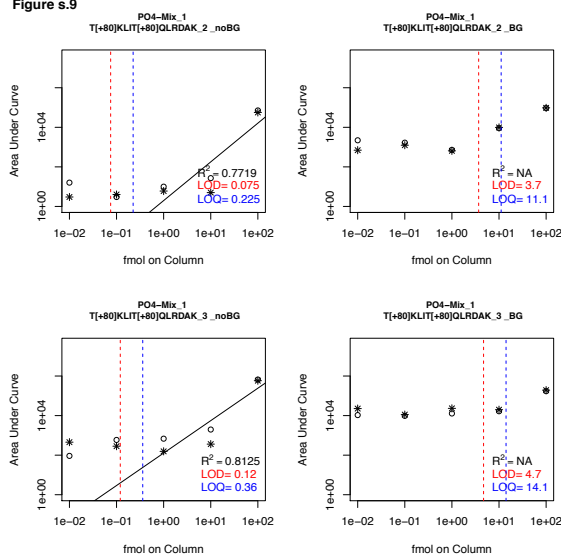


Figure s.9

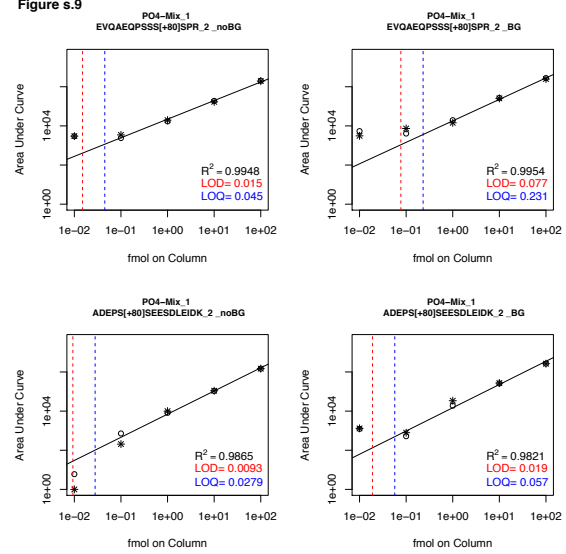


Figure s.9

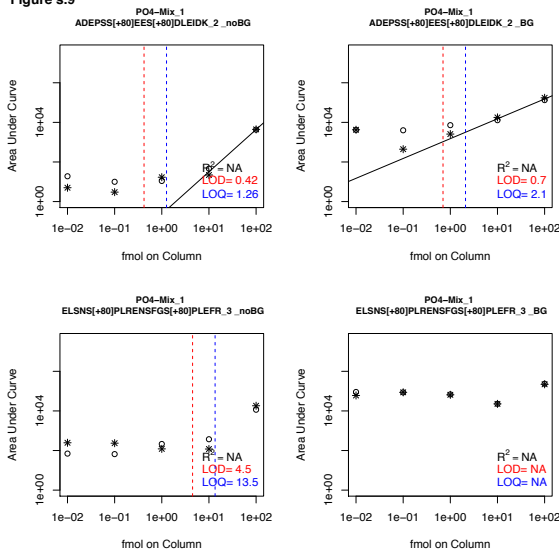


Figure s.9

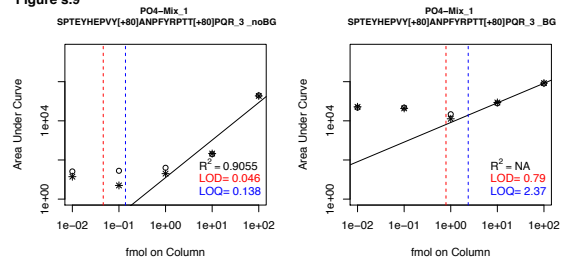


Figure s.10

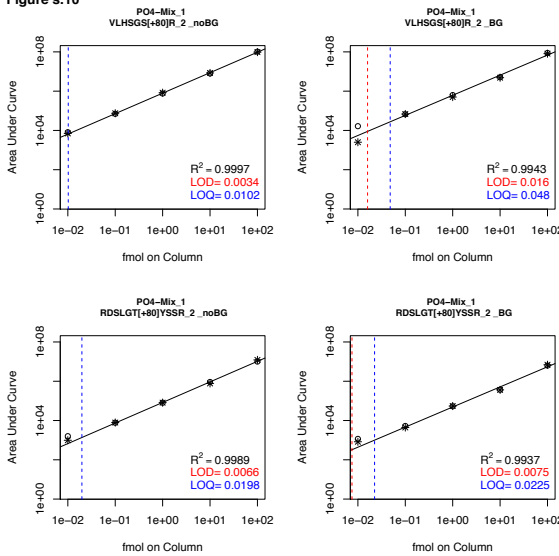


Figure s.10

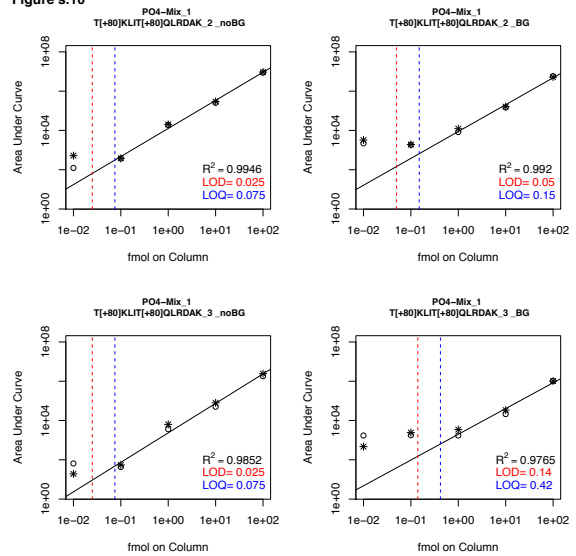


Figure s.10

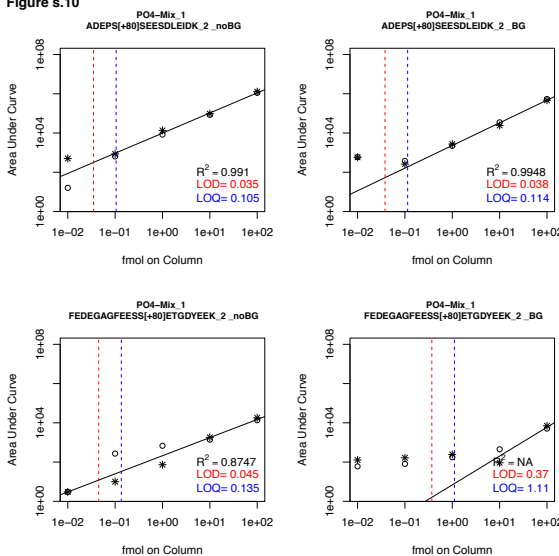


Figure s.10

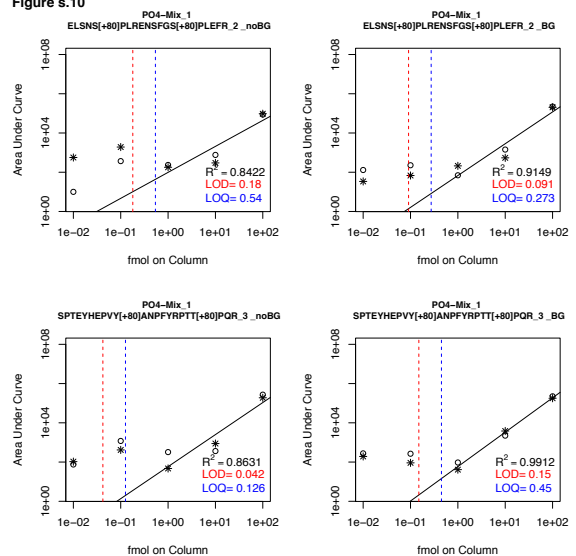


Figure s.11

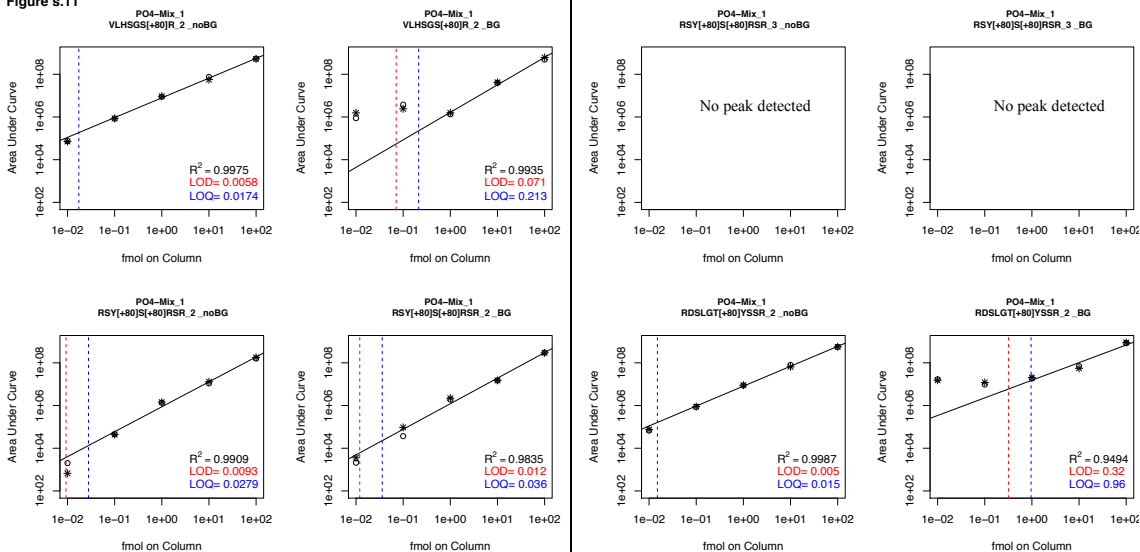


Figure s.11

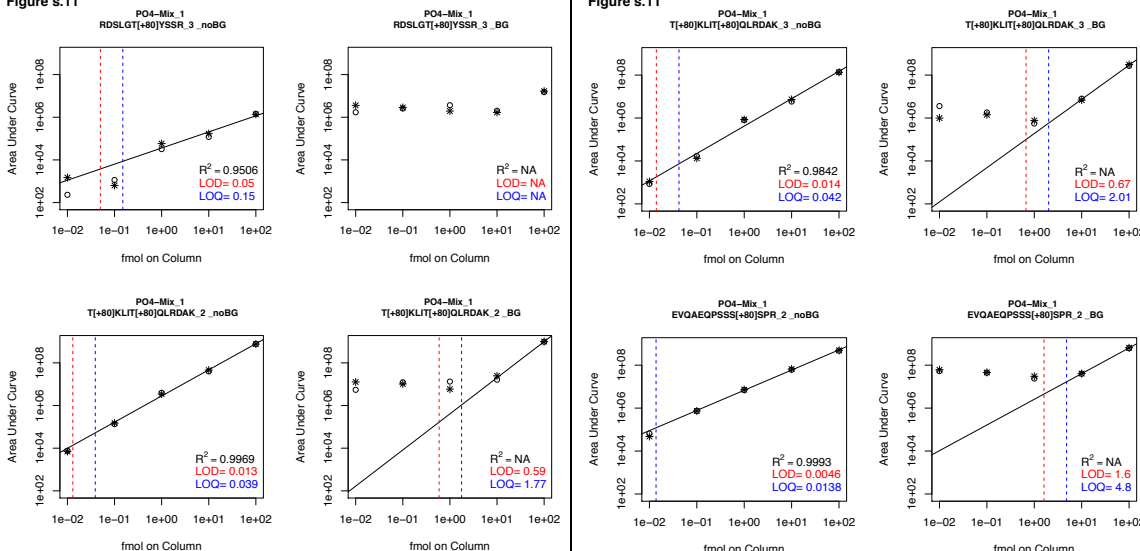


Figure s.11

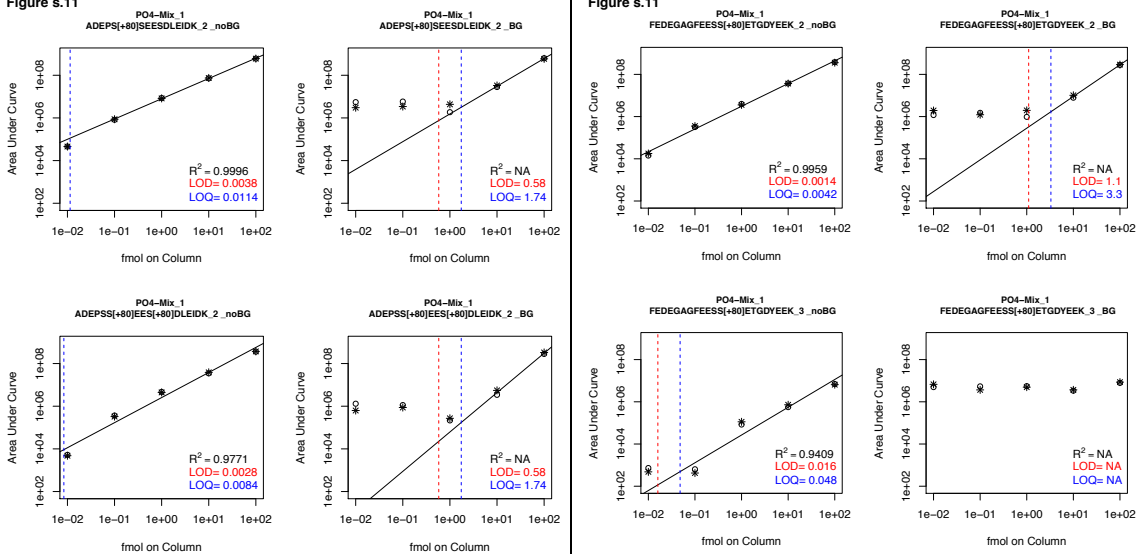


Figure s.11

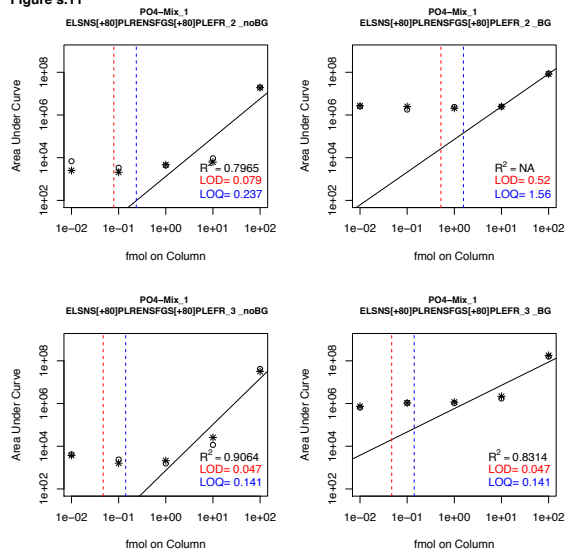
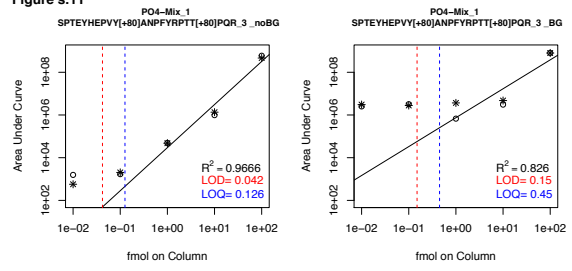


Figure s.11



4. General Discussion & Outlook

4.1 BAY-320 and BAY-524: novel tools to probe Bub1 function

Bub1 is a serine/threonine kinase that is recruited to unattached KTs at a very early stage during mitosis (Jablonski et al., 1998). Indeed, it has been shown that Bub1 plays a central role in chromosome congression and the fidelity of chromosome segregation in species from yeast to vertebrates (Elowe, 2011; Funabiki and Wynne, 2013). Ever since, Bub1 was identified, the requirement of its catalytic activity for all its functions has been a matter of debate.

Here, we have characterized two novel small molecule ATP-competitive inhibitors of Bub1, BAY-320 and BAY-524. We have used these inhibitors to get further insight into the mitotic functions of Bub1 kinase activity and set out to differentiate between scaffolding and catalytic function of Bub1. In detail, we compared cell fates provoked by Bub1 inhibition with those that were due to siRNA-mediated Bub1 protein depletion. According to that we conclude that Bub1 exerts its functions mostly through its ability to act as a scaffold. We show that Bub1 kinase inhibition influences chromosome arm cohesion and the localization of Sgo pools. Moreover, Bub1 inhibition seems to have minor effects on mitotic progression as well as the establishment of a SAC response due to spindle defects. Also the efficiency of chromosome alignment is not impaired by inhibition of Bub1. On the contrary, there is a striking synergy between Bub1 kinase inhibition and Paclitaxel-induced interference with MT dynamics. Bub1 inhibited cells are sensitized to clinically relevant doses of Paclitaxel, displayed by a marked increase in chromosome segregation errors and drastically reduced cell proliferation. The results of this study thus give insight into the role of Bub1 catalytic activity during mitotic progression and elaborate on the potential use of Bub1 inhibitors in therapeutic applications.

4.1.1 Validation of BAY-320 and BAY-524 as Bub1 inhibitors

Elucidating the role of Bub1 catalytic activity in dividing cells has been a long standing question. So far, this question has been mostly addressed by introducing Bub1 kinase-dead mutants into cells (Klebig et al., 2009) or by the development of Bub1-KD mice (Ricke et al., 2012). However, these approaches are most often accompanied by technical challenges, high variability and low temporal resolution. The availability of small-molecule inhibitors is a big advantage, since they can overcome the described drawbacks. However, no specific Bub1 inhibitor has been available so far. The only previously described inhibitor of Bub1 is the bulky ATP analog 2OH-BNPP1 (Kang et al., 2008; Krenn et al., 2012; Liu et al., 2015; Nyati et al., 2015), however a detailed characterization of its specificity and efficacy in intact cells has been missing.

Here, two novel small molecule inhibitors for Bub1 are introduced, BAY-320 and BAY-524, developed at BAYER Pharma AG. BAY-320 and BAY-524 have proved to be useful tools as they both efficiently inhibit Bub1 kinase in intact cells and *in vitro*. Ideally, small molecule inhibitors should be both potent and selective, to enable complete inhibition of the target kinase and minimize the potential for off-target effects in cells. Both compounds were able to specifically inhibit T120-H2A phosphorylation (Kawashima et al., 2010). In addition, BAY-320 and BAY-524 caused a persistence of chromosome arm cohesion, a phenotype that has already been accounted to Bub1 (Kitajima et al., 2005; Kawashima et al., 2010; Liu et al., 2015). Moreover, *in vitro* assays performed on a large panel of kinases showed that inhibition of off-target substrates required at least 20x higher concentrations of BAY-320 than inhibition of Bub1. One potential and relevant off target identified is the kinase Haspin. However BAY-320 and BAY-524 failed to inhibit intracellular Haspin activity at concentrations used in our assays illustrated by the phosphorylation of histone H3 on threonine 3 (Figure 23, Table 3). Thus, we are confident that BAY-320 and BAY-524 constitute highly effective and specific tools to explore the role of Bub1 kinase activity during mitotic progression.

4.1.2 Impact of Bub1 inhibition on mitotic progression

One striking phenotype that results from the inhibition of Bub1 is the persistent chromosome arm cohesion during prometaphase. Both Sgo2 and Aurora B are not focused at centromeres and relocalize to chromosome arms when Bub1 is inhibited, most likely due to the dephosphorylation of T120-H2A. Phosphorylation of Sgo2 by Aurora B promotes Sgo2 interaction with protein phosphatase 2A (PP2A) (Tanno et al., 2010), and PP2A in turn enforces the protection of cohesin proteins against phosphorylation from Plk1 (Kitajima et al., 2006; Riedel et al., 2006). Thus, colocalization of Sgo2 and Aurora B in Bub1-inhibited cells provides a straightforward explanation for the observed persistence of arm cohesion (Perera and Taylor, 2010; Perera et al., 2007; Kitajima et al., 2005). However, alternative mechanisms should not be excluded and it might be rewarding to explore a possible connection between Bub1 kinase and the Sororin-Wapl pathway (Peters and Nishiyama, 2012). The establishment of cohesion during S phase and its maintenance throughout mitosis is governed by Sororin. Sororin mediates sister-chromatid cohesion by antagonizing Wapl and its ability to release DNA from cohesin (Nishiyama et al., 2010). Moreover Aurora B and Cdk1 further promote the release of cohesion by phosphorylating Sororin and thereby disturbing the interaction with its binding partner Pds5 (Nishiyama et al., 2013). Since we could show that the kinase activity of the chromatin-associated fraction of Aurora B was not affected after Bub1 inhibition, it is tempting to speculate whether Bub1 kinase contributes to Wapl localization at chromatid arms.

Furthermore, inhibition of Bub1 results in the clear reduction of CPC levels from the centromeric region. Borealin gets recruited to the centromere via interaction with Sgo1 (Kawashima et al., 2010; Tsukahara et al., 2010; Yamagishi et al., 2010). Thus there is a direct relationship between pT20-H2A level reduction, followed by impaired Sgo recruitment and thus impaired CPC recruitment. With

at least Sgo2 being redistributed to chromosome arms, a relocalization of Sgos in general is likely to foster also the localization of the CPC to arms. Comparably, mutant mice that lack Bub1 kinase activity fail at localizing Aurora B at the centromere (Ricke et al., 2012). CPC levels at KTs are further reduced upon simultaneous inhibition of Bub1 and Haspin, in line with the established roles of these kinases in the phosphorylation of histones H2A-T120 and H3-T3, respectively (Yamagishi et al., 2010; Wang et al., 2011).

Surprisingly, persistent chromosome arm cohesion, observed in Bub1 inhibited cells did not markedly prolong mitotic timing (Figure 16). But it is very interesting to mention that depletion of Wapl also causes persistent cohesion without significantly affecting mitotic progression (Lara-Gonzalez and Taylor, 2012). In contrast to Bub1 inhibition, depletion of Bub1 markedly extended mitotic timing (Figure 15). One straightforward explanation for this observation is that Bub1 depletion, but not Bub1 inhibition, caused the displacement of CENP-E from KTs, a motor protein required for efficient chromosome congression (Putkey et al., 2002; Tanudji et al., 2004; Bancroft et al., 2015). A mechanism centered on CENP-E may also explain the observation that Bub1 depletion exerted a more extensive mitotic delay in the hypertriploid HeLa cells than in diploid RPE1 cells.

Considering the important role of Aurora B in the regulation of KT-MT interactions (Carmena et al., 2012; Funabiki and Wynne, 2013), it is remarkable that the observed reduction of KT-associated CPC caused by Bub1 inhibition did not exert a more profound effect on the fidelity of chromosome segregation. Bub1 inhibition using BAY-320 and BAY-524 also significantly reduced centromeric Aurora B activity however leaving Aurora B activity at chromosome arms unaffected. This suggests that the remaining levels of the CPC are sufficient for correct chromosome segregation. Moreover, partial impairment of CPC recruitment to centromeres did not abolish viability or trigger extensive defects in chromosome segregation in budding yeast or chicken DT40 cells (Campbell and Desai, 2013; Yue et al., 2008).

Further support for BAY-320 and BAY-524 validity as Bub1 inhibitors comes from the observation that inhibitor-treated cells behaved similar to cells in which endogenous Bub1 was replaced with an exogenous KD mutant form of the kinase or in studies using Bub1-KD mice in several important respects (Klebig et al., 2009; Ricke et al., 2012).

Bub1 is an established member of the signaling network comprising the SAC (Lara-Gonzalez et al., 2012; Elowe, 2011). Inhibition of Bub1 kinase activity did not significantly reduce the KT recruitment of Mad1, Mad2 and BubR1 and barely affected the ability of nocodazole-treated cells to maintain a SAC arrest. Even when SAC activity was compromised by partial inhibition of the SAC kinase Mps1, Bub1 inhibition triggered only minor weakening of SAC signaling. In striking contrast, Bub1 depletion produced a drastic weakening of the SAC in this sensitized background. For comparison, combined inhibition of Mps1 and either Plk1 or Aurora B resulted in a complete SAC shutdown and immediate mitotic exit, in line with previous results (Saurin et al., 2011; Schubert et al., 2015b). Recently it has been shown that Plk1 strengthens SAC establishment and maintenance during prolonged mitotic arrest (Schubert et al., 2015b). Collectively these findings confirm that mitotic functions of Bub1 depend primarily on Bub1 protein rather than kinase activity. In the future, it will be interesting to explore whether Bub1 activity contributes to purported non-mitotic functions of Bub1 (Yang et al., 2012; Nyati et al., 2015).

The major conclusion emerging from the present study is that the overall impact of Bub1 inhibition on mitotic progression is surprisingly mild, clearly less severe than the impact of Bub1 depletion. This strengthens the notion that Bub1 is required during chromosome congression and segregation primarily via its scaffolding function (Sharp-Baker and Chen, 2001; Fernius and Hardwick, 2007; Rischitor et al., 2007; Klebig et al., 2009). It is difficult to say whether a small portion of Bub1 catalytic activity is not responsive to inhibition and hence able to sustain Bub1 functionality. However, the genetic elimination of Bub1 kinase

activity is compatible with mouse development in contrast to complete Bub1 elimination (Ricke et al., 2012; Perera et al., 2007). This argues against a fundamental role of Bub1 kinase activity for mitotic progression. Thus, inhibitor studies and genetic data concur to indicate that lack of Bub1 kinase activity produces only mild disturbances of mitotic progression.

4.1.3 Bub1 inhibition and its potential therapeutic influence

The principle of cancer chemotherapy is the killing of cells that divide rapidly, usually by chemical substances that are thus cytotoxic (Malhotra and Perry, 2003). It is probably ironic that the most effective cancer fighting strategies involves the induction of abnormal mitoses, thereby triggering programmed cell death (apoptosis) and therefore the elimination of malignant cells. Anti-mitotic agents are a vastly used element in cancer chemotherapy, mostly MT poisons such as taxanes (Gascoigne and Taylor, 2009). The inhibition of SAC kinases has emerged as a potentially attractive strategy to kill tumor cells (Janssen et al., 2009; Salmela and Kallio, 2013). Several inhibitors of the SAC kinase Mps1 have shown to exert anti-tumor effects in mouse models (Colombo et al., 2010; Tardif et al., 2011; Tannous et al., 2013; Kusakabe et al., 2015), but toxicity associated with single agent therapy remains a concern (Martinez et al., 2015). Paclitaxel is a widely used anti-mitotic drug, which induces a mitotic checkpoint-dependent delay at high dose by inhibiting MT dynamics (Gascoigne and Taylor, 2008; Brito and Rieder, 2006). The combination of SAC-inhibiting compounds together with MT poisons seems to represent a more advantageous policy (Maia et al., 2015; Jemaà et al., 2013; Janssen et al., 2009). Here, we have made use of the combination of Bub1 inhibitors BAY-320 and BAY-524 together with Paclitaxel. Our data suggests that this combinatorial treatment might be beneficial for cancer therapy. BAY-320 and BAY-524 had comparatively little effect on mitotic progression when

used as single agents. However, in combination with therapeutic doses of Paclitaxel, a substantial increase in anti-proliferative activity along with an increase in chromosome segregation errors could be observed. Paclitaxel increases KT-MT attachments errors at low doses that are usually corrected by Aurora B/CPC. However in this setting, the combination of Paclitaxel and Bub1 inhibition induces KT-MT attachment errors that cannot be efficiently corrected by Aurora B/CPC anymore, due to their displacement from the kinetochore/centromeric region. In our setup as well, these synergistic effects were substantially more pronounced in aneuploid HeLa cells than in near-diploid RPE1 cells. This result is very exciting in terms of cancer therapy. It shows a great potential in targeting specifically cancer cells while leaving healthy cells spared. Also another study, has shown that untransformed fibroblasts with reduced Mps1 levels were not sensitive to low doses of paclitaxel, compared to tumor cell with lowered Mps1 levels (Janssen et al., 2009). Thus, targeting members of the SAC that are also involved in chromosome alignment, in combination with clinically relevant doses of Paclitaxel, might constitute a selective approach to fight uncontrolled cell proliferation.

Whether Bub1 inhibitors will prove valuable for pharmacological intervention in anti-tumor therapy remains to be seen. The findings described in this thesis clearly encourage further exploration of the potential use of Bub1 inhibitors for therapeutic applications.

4.1.4 Future prospects

According to this study, inhibition of Bub1 catalytic activity seems to have only a mild impact on mitotic progression. This is probably why it is not very surprising that only few substrates of Bub1 kinase have been described so far. The best characterized substrate of Bub1 is T120-H2A (Kawashima et al., 2010), as

already mentioned. Another substrate of Bub1 that has been described so far, is Cdc20 (Tang et al., 2004a). This phosphorylation is supposed to exert an inhibitory function on the APC/C. However, this phosphorylation event has only been shown to happen *in vitro* (Tang et al., 2004a; Kang et al., 2008). Thus, the identification of Cdc20 as a physiological substrate of Bub1 kinase is still awaited. However, considering the very mild effect of Bub1 kinase inhibition on SAC signaling, it is tempting to speculate that Bub1-mediated Cdc20 phosphorylation is an artifact or of very low significance. However, we can still not rule out that a small portion of Bub1 is not affected by BAY-320 and BAY-524. Besides, no further substrates of Bub1 are known. Hence it would be beneficial to investigate the Bub1-dependent phosphoproteome in mitotic cells, using the described Bub1 inhibitors in combination with mass spectrometry. Considering the mild effects on mitotic progression by Bub1 inhibition, it is debatable whether and how many substrates are awaiting their identification.

4.2 The evolution of phospho-peptide quantification

Another major goal in this study was to evaluate the most popular MS approaches for quantification of proteins and for changes in PTMs.

During our initial proof-of-principle experiments we analyzed several phospho-peptides spiked at increasing concentrations into a cell lysate digest. Especially for phospho-peptides analyses in complex samples, huge variations in terms of quantification, detection and identification limits were obtained. We were able to identify high-resolution HCD and higher stage fragmentation-based pSRM methods as the most sensitive approaches, since they allow in depth analysis of MS spectra that are usually poor of information, due to neutral loss peaks.

However, phospho-proteomics in mass spectrometry is a fast evolving field with a constant development in more sensitive and specific LC-MS setups as well

as MS-workflows and quantification approaches. Hence, this kind of comparison that we have described in this thesis has to be repeated as new methods and devices are available. One of these newly emerging approaches is SWATH-MS (Gillet et al., 2012).

SWATH-MS is a DIA strategy that combines advantages of DDA with those of SRM. This means that high throughput can be achieved together with high reproducibility and consistency. In detail, SWATH-MS enables quantitative MS/MS data for every peptide or protein in a sample, meaning unbiased, reproducible quantitation with no sample-specific method development. During data acquisition, all analytes within a given m/z precursor range, are detected by repeatedly cycling through a series of fixed precursor isolation windows (swaths) (Gillet et al., 2012; SCIEX, 2012). During each cycle, all precursors from the isolation window are fragmented and their complete and highly accurate fragment ion spectra are recorded. The same precursor isolation window is further fragmented during each cycle, thus generating a time-resolved recording of the fragment ions of all peptide precursors that elute on the LC. The window size is chosen in such a way that the cycle time is short enough to allow each peptide to be fragmented ~8–10 times across its chromatographic elution profile (Schubert et al., 2015a).

Post-acquisition, a data extraction strategy is applied that uses information from spectral ion libraries to identify proteins and peptides of interest. The fragment ion signals, their relative intensities, chromatographic concurrence and other information accessible from spectral libraries help to search the acquired data for constellations of signals that precisely correlate with the known coordinates of a targeted peptide (Gillet et al., 2012). Matching combinations allow specific identification. Only the increasing availability of proteome-wide spectral libraries allows this targeted data extraction analysis. However, the quality of the quantitative data is highly dependent on the quality of the spectral library (Zi et al., 2014). Moreover, this approach allows the generation of a

permanent digital archive for every sample. Those can retrospectively be reanalyzed when new hypothesis arise, without running the sample again.

Taken together, SWATH-MS offers a new advantage of analyzing multiple samples in a global fashion, without the usual constraints and bias of DDA-MS, thereby combining high throughput with specificity and sensitivity.

This MS approach is so far only applicable with the fast, high resolution quadrupole time-of-flight (triple TOF) instruments or qOrbitrap systems, which is why we did not include this approach in our comparison, since these instruments were not available to us at the time of our study.

5. Material and Methods

5.1 Preparation of BAY-320 and BAY-524 inhibitors

BAY-320 and BAY-524 were synthesized as described in (Hitchcock et al., 2013). Synthesis was performed by Bayer Pharma AG, Global Drug Discovery, Muellerstrasse 178, Berlin, 13342 Germany. For *in vitro* and *in vivo* experiments BAY-320 and BAY-524 were used from stock solutions (5 mM) in dimethyl sulfoxide (DMSO). Working concentration of Bub1 inhibitors are depicted in Figures and Figure legends, respectively.

5.2 Determination of IC₅₀-concentrations

Inhibitory activities BAY-320 and BAY-524 towards Bub1 in presence of 2 mM ATP were quantified as previously published (Hitchcock et al., 2013). A time-resolved fluorescence energy transfer (TR-FRET) kinase assay was used to measure phosphorylation of the synthetic peptide Biotin-Ahx-VLLPKKSFAEPG (C-terminus in amide form, Biosyntan, Berlin, Germany) by the recombinant catalytic domain of human Bub1 (amino acids 704-1085). Recombinant human Bub1 (704-1085) was expressed in Hi5 insect cells with an N-terminal His6-tag and purified by affinity- (Ni-NTA) and size exclusion chromatography.

5.3 Kinase selectivity profiling

BAY-320 was counter screened against a panel of 222 kinases using the Eurofins kinase profiler screen (Millipore) at 10 μ M and 10 μ M ATP. Screen was performed by Bayer Pharma AG, Global Drug Discovery, Muellerstrasse 178, Berlin, 13342 Germany.

5.4 In vitro kinase assay

HEK 293T cells were transfected with plasmids coding for LAP-tagged Bub1 wild-type (WT) or the K821R kinase-dead (KD) mutant (kindly provided by G. Kops, Utrecht, Netherlands) (Suijkerbuijk et al., 2012b). After induction of mitotic arrest (18 hours incubation with 1 μ g/ml of nocodazole), cells were harvested and

lysed in kinase lysis buffer (50mM HEPES pH7.5, 150mM NaCl, 5mM EDTA, 0.5% NP-40, 1mM Na₃VO₄, 1mM β-glycerophosphate, 1mM NaF and complete protease inhibitor (Roche)). Lysates were cleared by centrifugation for 15 minutes at 21,000 g, 4°C, and LAP-Bub1 proteins isolated by a 2 hour incubation with S-protein-agarose (Novagen, EMD Chemical, CA, USA). Beads were washed 6 times in lysis buffer containing increasing concentrations of NaCl (150 mM, 200 mM, 300 mM, 400 mM, 500 mM and 600mM) and 3 times in kinase buffer (20 mM HEPES pH7.5, 100 mM KCl, 10 mM MgCl, 1mM Na₃VO₄, 1mM β-glycerophosphate, 1mM NaF, 1mM DTT). The bead-bound LAP-Bub1 was then aliquoted and used for kinase assays in 30 µl reaction volumes. Kinase reactions were carried out at 30°C in kinase buffer in presence of 100 µM ATP, 5 µCi γ-³²P-ATP, 1 µg recombinant histone H2A (NEB, Frankfurt am Main, Germany) as substrate, and serial dilutions of Bub1 inhibitors. Reactions were stopped after 30 min by addition of sample buffer and heating to 95°C. Samples were then resolved by SDS-PAGE and visualized by autoradiography and Western blotting.

5.5 Cell Culture

HeLa S3 cells, HeLa S3 cells expressing histone H2B-GFP (Silljé et al., 2006), HeLa Kyoto cells expressing a FRET reporter for Aurora B fused to histone H2B (van der Waal et al., 2012) and HEK293T cells were grown under standard conditions in DMEM-Glutamax medium (Invitrogen, CA, USA), supplemented with 10% heat-inactivated fetal calf serum (FCS) (PAN Biotech, Aidenbach, Germany) and penicillin-streptomycin (Pen-Strep; 100 IU/ml and 100 mg/ml respectively, Gibco Life Technologies, Zug, Switzerland). hTERT-RPE1 cells and hTERT-RPE1 cells expressing histone H2B-GFP (kind gift of Stephen Taylor, University of Manchester, UK) were cultured in F12 DMEM nutrient mixture F-12 HAM (Sigma Aldrich, MO, USA) supplemented with 10% heat-inactivated FCS, , L-glutamine (2 mM; PAN Biotech, Aidenbach, Germany), sodium bicarbonate (0.35 %; Sigma-Aldrich, MO, USA) and Pen-Strep. Thymidine arrest was

performed for 24h and cells were either released into fresh medium for 10 h or into medium supplemented with Nocodazole for 12-14 h. Thymidine (Sigma-Aldrich, MO, USA) was used at 2 mM, Nocodazole (Sigma-Aldrich, MO, USA) at 3.3 μ M if not otherwise stated, RO-3306 at 10 μ M (Calbiochem), Paclitaxel (Taxol, Merck Milipore) at 1-4 nM, Reversine (Enzo Life Sciences, Lausen, Switzerland) at 0.25 and 0.5 μ M, 5-Iodotubercidin (5'ITU, Santa Cruz, Biotechnology, TX, US) at 2.5 μ M, Monastrol (Enzo Life Sciences, Lausen, Switzerland) at 150 μ M and MG132 (Calbiochem, Darmstadt, Germany) at 10 μ M.

5.6 Transient plasmid transfection and siRNA-mediated protein depletion

Transient transfections of HEK293T cells with plasmids and small interfering RNA (siRNA) duplexes were performed using TransIT-LT1 transfection reagent (Mirus Bio, Madison, WI) and Oligofectamine (Invitrogen, CA, USA), respectively, according to manufacturers protocols. The following siRNA duplex oligonucleotides were used: siG12 CGTACGCGGAATACTTCGA (Elbashir et al., 2001), siBub1 CCAGGCTGAACCCAGAGAGTT (Tang 2004). All siRNA duplex oligonucleotides were ordered from Qiagen, Hilden, Germany.

5.7 Fluorescence-activated cell sorting

HeLa S3 or RPE1 cells were incubated with kinase inhibitors or depleted of the indicated proteins for 48 h. Cell suspensions were then fixed with 70% ice cold ethanol and incubated with 0.2 mg/ml RNase (Sigma-Aldrich, MO, USA) and 5 μ g/ml propidium iodide (Sigma-Aldrich, MO, USA). Cellular DNA content was determined by flow cytometry using FACSCanto II (BD Biosciences Clontech, San Jose, CA, USA) and FlowJo (Treestar, Ashland, OR, USA) instruments.

5.8 Cell extracts and sample preparation for Western blot analysis

Cells extracts were prepared on ice for 30 min in Tris lysis buffer (20 mM

Tris, pH 7.4, 150 mM NaCl, 0.5 % IGEPAL CA-630, 30 µg/ml RNase, 30 µg/ml DNase, 1 mM DTT, protease inhibitors cocktail (Roche, Basel, Switzerland) and phosphatase inhibitor cocktails (cocktails 2 and 3, Sigma-Aldrich, MO, USA). Lysates were cleared by centrifugation for 15 minutes at 21,000 g, 4°C, and proteins were resolved by SDS-PAGE and analyzed by Western blotting.

5.9 Histone Isolation

HeLa S3 cells were as described above and mitotic cells were collected by shake-off. Cells were washed with cold PBS and lysed at 4°C for 30 min using histone lysis buffer (50 mM Tris pH 7.8, 300 mM NaCl, 1% IGEPAL CA-630). Nuclei were collected by centrifugation (110 g, 4°C, 10 min) and washed three times with histone lysis buffer. After an additional wash with Tris-EDTA (100 mM Tris, 1 mM EDTA) the nuclear pellet was incubated for 2 h in 0.4 M HCl at 4°C. After high-speed centrifugation of the sample, 6 volumes of acetone were added to the supernatant, followed by overnight incubation at -20 °C. Histones were collected by centrifugation, washed with acetone, air-dried and resolved by SDS-PAGE.

5.10 Antibodies

Antibodies used for Western blotting: anti-Bub1 ((Hanisch et al., 2006b) or ab9000, Abcam, Cambridge, UK), anti-pT120H2A (Active Motif, Carlsbad, CA, USA), anti-cyclinB1 (Merck Millipore) and anti- α -tubulin (DM1A, Sigma-Aldrich, MO, USA). Antibodies used for immunofluorescence microscopy: anti-Mad1 (clone 117-468 (Fava et al., 2011)), anti-cMad2 (clone 107-276 (Fava et al., 2011)) anti-Borealin (Klein et al., 2006), anti-INCENP (clone 58-217, ab23956, Abcam, Cambridge, UK), anti-Bub1 (antibody against Bub1 hybridoma (clone 62-406) was produced after mice were injected with Bub1 recombinant protein spanning residues 1-318, anti-Bub1 (ab9000, Abcam), CREST anti-human auto-immune serum (Immunovision, Springdale, AR, USA), anti-Aurora B (AIM-1, BD

Biosciences, San Jose, CA, USA), anti-Bub1 (ab9000, Abcam, Cambridge, UK), anti-CENP-E (1H12, Abcam, Cambridge, UK), anti-Mad2 (A300-301A, Bethyl Laboratories, Montgomery, TX, USA), anti-Sgo1 (Abnova, Taipei, Taiwan), anti-Sgo2 (Bethyl Laboratories, Montgomery, TX, USA), anti-pT120H2A (Active Motif, Carlsbad, CA, USA), anti-pS7CENP-A (clone NL41, Merck Millipore, Billerica, MA, USA), anti-pT3H3 (clone 9714, Cell Signaling Technology, Danvers, MA, USA) and anti-pS10H3 (Millipore, Billerica, MA, USA). The polyclonal MCAK (R120) antibody was raised in rabbits by immunization with bacterially expressed His-MCAK_{aa588-725}. For immunofluorescence experiments, all primary antibodies were detected with AlexaRed-594-, AlexaRed-564-, and AlexaGreen-488-labeled secondary anti-mouse and anti-rabbit antibodies (Invitrogen, Carlsbad, CA, USA) or Cy5-conjugated donkey antibodies (Dianova, Hamburg, Germany). For Western blotting, signals were detected using HRP-conjugated anti-mouse or anti-rabbit antibodies (Pierce, Rockford, IL, USA).

5.11 Immunofluorescence microscopy, image processing, quantification and live cell imaging

For fluorescence microscopy cells were grown on coverslips and fixed in PTEMF buffer (20 mM PIPES, pH 6.8, 0.2% Triton X-100, 10 mM EGTA, 1 mM MgCl₂, 4% formaldehyde) or methanol at -20°C (for CENP-A pS7) respectively. Images of randomly selected cell were acquired as z-stacks using a DeltaVision microscope (GE Healthcare) on an Olympus IX71 base (Applied Precision, WA, USA), equipped with a Plan Aplanachromat N 60x/NA1.42 oil immersion objective (Olympus) and a CoolSNAP HQ2 camera (Photometrics). Serial optical sections were deconvolved and projected using SoftWorx software (GE Healthcare). Images were quantified as previously described (Schubert et al., 2015b) using automated pipelines run by Cell Profiler software (Carpenter et al., 2006). Results from 2-3 independent experiments were pooled and statistical analysis was done

with GraphPad Prism software. Error bars on histograms illustrate SEM. Scale bars represent 10 μM .

For time-lapse imaging, cells were imaged using a Nikon ECLIPSE Ti microscope equipped with a CoolLED pE-1 illumination system and a 20x/NA0.75 air Plan Apochromat objective (Nikon) in a climate-controlled environment. Images were acquired at multiple positions at indicated time intervals. MetaMorph 7.7 software (MDS Analytical Technologies, Sunnyvale, CA, USA) was used for acquisition and processing of data. FRET, FRAP and high sensitivity microscopy (monitoring endogenously EGFP-tagged proteins) experiments were carried out using a spinning disk confocal system (Intelligent Imaging Innovations) based on a Zeiss Axio Observer stand equipped with a Photometric Evolve 512 back-illuminated EMCCD camera, 63x/NA1.4 plan apochromat objective and diode lasers and run by SlideBook software. FRET analyses were carried out by excitation with a 440 nm diode laser and by recording of CFP (CFP signal) and YFP (FRET signal) fluorescence emission in z-stacks. Background-corrected FRET ratios (CFP signal/FRET signal) were calculated in ImageJ using the Ratio Plus plugin. FRAP analysis of EGFP-Bub1 was performed with a 488 diode laser on one KT pair per cell. Overall bleaching was corrected using the signal intensities at a cytoplasmic region not targeted for photobleaching (average of the first 4 frames). Fluorescence recovery half-times and plateaus were determined by non-linear curve fitting based on a one-phase association in Prism software (GraphPad).

5.12 Colony Formation Assay

Asynchronous cell cultures (50,000/well) were plated on 6-well plates (Falcon). After 7 days of growth in the presence of the indicated drugs, cells were fixed with ice-cold Methanol at -20°C and stained with 0.1 % cresyl violet dH₂O according to standard procedures. Cell densities were measured using ImageJ after black-and-white-conversion and inversion of the images.

5.13 rAAV-mediated gene targeting

For gene targeting, homology arms to human Bub1 (*BUB1*) gene were amplified from RPE1 cell genomic DNA. Targeting constructs allowing the insertion of an EGFP tag C-terminal to Bub1 were assembled by 4-piece ligation in a NotI-digested pAAV vector. Recombinant adenovirus-associated virus (rAAV) particles were generated as previously described (Berdougo et al., 2009). RPE1 cells were infected with 3 ml of viral supernatant for 48h and then expanded into fresh medium for an additional 48h. FACS sorting was used to select EGFP-positive cells, as previously described (Collin et al., 2013). To facilitate detection of fluorescence at mitotic stages, cells were synchronized with RO-3306 (10mM) for 18h and released into nocodazole (50nM) for 2 hours, before they were trypsinized and subjected to sorting in the continued presence of nocodazole (10nM). Infected or uninfected cells were filtered (30 mm, Partec) and EGFP-positive cells (488 excitation, 514/30 emission filter) were isolated on an Aria IIIu (BD) cell sorter by selecting the 514/30 channel against a 585/42 filter detecting cellular autofluorescence. Single cells were sorted into 96-well plates filled with conditioned medium and positive clones screened for by fluorescence microscopy. Generation of the stable RPE1 EGFP-Bub1 cell line was performed by Dr. Fabien Cubizolles.

6. Appendix

6.1 Abbreviations

All units are abbreviated according to the International Unit System

aa	amino acid
APC/C	anaphase promoting complex/cyclosome
ATP	adenosine 5'-triphosphate
Bub1	budding uninhibited by benzimidazole 1
BubR1	budding uninhibited by benzimidazole related 1
Cdk	cyclin-dependent kinase
CID	collision-induced dissociation
CIN	numerical chromosomal aberration
CPC	chromosomal passenger complex
Da	dalton
DAPI	4'6'-diamidino-2-phenylindole
DDA	data dependent acquisition
DHB	2,5 dihydroxy benzoic acid
DIA	data independent acquisition
DMSO	dimethyl sulfoxide
DNA	deoxyribonucleic acid
DTT	dithiothreitol
EDTA	ethylenediaminetetraacetic acid
FCS	fetal calf serum
FRAP	fluorescence recovery after photobleaching
FRET	fluorescence resonance energy transfer
GEF	guanine nucleotid exchange factor
GLEBS	Gle2-binding domain
HCD	higher-energy collisional dissociation
HCl	hydrochloric acid

HEK	human embryonic kidney
HEPES	N-2-hydroxyethylpiperazine-N'-2-ethane sulfonic acid
IFM	immunofluorescence microscopy
IMAC	immobilized metal affinity chromatography
IP	immunoprecipitation
KD	kinase dead
KT	kinetochore
KT-MT	kinetochore-microtubule
LC	liquid chromatography
LOD	limit of detection
Mad	mitotic arrest deficiency
MCC	mitotic checkpoint complex
Mps1	monopolar-spindle 1
MS	mass spectrometry
MSA	multi stage activation
MT	microtubule
MTOC	microtubule organizing center
m/z	mass to charge ratio
NEBD	nuclear envelope breakdown
PBD	polo-box domain
Plk1	Polo-like kinase 1
PMSF	phenylmethylsulfonyl fluoride
PTM	post-translational modification
SA	stromal antigen
SAC	spindle assembly checkpoint
SD	standard deviation
SDS-PAGE	sodium dodecylsulfate polyacrylamide gelelectrophoresis
SEM	standard error of the mean
Sgo	Shugoshin

SILAC	stable isotope labeling by/with amino acids in cell culture
siRNA	small interference ribonucleic acid
SRM	selected reaction monitoring
pSRM	pseudo selected reaction monitoring
TAL	ZK-Thiazolidinone
TPR	tetratricopeptide repeat
WB	Western blot
WT	wild type
XIC	extracted ion chromatograph

7. References

- Alberts, B., A. Johnson, J. Lewis, D. Morgan, M. Raff, K. Roberts, and P. Walter. 2014. *Molecular Biology of the Cell*, Sixth Edition. Garland Science. 1 pp.
- Alberts, B., D. Bray, K. Hopkin, A. Johnson, J. Lewis, M. Raff, K. Roberts, and P. Walter. 2013. *Essential Cell Biology*, Fourth Edition. Garland Science. 1 pp.
- Allan, L.A., and P.R. Clarke. 2007. Phosphorylation of caspase-9 by CDK1/cyclin B1 protects mitotic cells against apoptosis. *Molecular Cell*. 26:301–310. doi:10.1016/j.molcel.2007.03.019.
- Anderson, D.E., A. Losada, H.P. Erickson, and T. Hirano. 2002. Condensin and cohesin display different arm conformations with characteristic hinge angles. *The Journal of Cell Biology*. 156:419–424. doi:10.1083/jcb.200111002.
- Andrews, P.D., Y. Ovechkina, N. Morrice, M. Wagenbach, K. Duncan, L. Wordeman, and J.R. Swedlow. 2004. Aurora B regulates MCAK at the mitotic centromere. *Developmental Cell*. 6:253–268.
- Asghar, A., A. Lajeunesse, K. Dulla, G. Combes, P. Thebault, E.A. Nigg, and S. Elowe. 2015. Bub1 autophosphorylation feeds back to regulate kinetochore docking and promote localized substrate phosphorylation. *Nat Commun*. 6:8364. doi:10.1038/ncomms9364.
- Bancroft, J., P. Auckland, C.P. Samora, and A.D. McAinsh. 2015. Chromosome congression is promoted by CENP-Q- and CENP-E-dependent pathways. *Journal of Cell Science*. 128:171–184. doi:10.1242/jcs.163659.
- Bantscheff, M., M. Schirle, G. Sweetman, J. Rick, and B. Kuster. 2007. Quantitative mass spectrometry in proteomics: a critical review. *Anal Bioanal Chem*. 389:1017–1031. doi:10.1007/s00216-007-1486-6.
- Barr, F.A., and U. Gruneberg. 2007. Cytokinesis: placing and making the final cut. *Cell*. 131:847–860. doi:10.1016/j.cell.2007.11.011.
- Berdougo, E., M.-E. Terret, and P.V. Jallepalli. 2009. Functional dissection of mitotic regulators through gene targeting in human somatic cells. *Methods Mol Biol*. 545:21–37. doi:10.1007/978-1-60327-993-2_2.
- Berg, J.M., L. Stryer, and J.L. Tymoczko. 2015. *Stryer Biochemie*. Springer-Verlag. 1 pp.
- Bertoli, C., J.M. Skotheim, and R.A.M. de Bruin. 2013. Control of cell cycle transcription during G1 and S phases. *Nat. Rev. Mol. Cell Biol*. 14:518–528. doi:10.1038/nrm3629.
- Blackburn, K., and M.B. Goshe. 2009. Challenges and strategies for targeted

- phosphorylation site identification and quantification using mass spectrometry analysis. *Brief Funct Genomic Proteomic*. 8:90–103. doi:10.1093/bfgp/eln051.
- Boersema, P.J., S. Mohammed, and A.J.R. Heck. 2009. Phosphopeptide fragmentation and analysis by mass spectrometry. *J Mass Spectrom*. 44:861–878. doi:10.1002/jms.1599.
- Bolanos-Garcia, V.M., and T.L. Blundell. 2011. BUB1 and BUBR1: multifaceted kinases of the cell cycle. *Trends in Biochemical Sciences*. 36:141–150. doi:10.1016/j.tibs.2010.08.004.
- Boyarchuk, Y., A. Salic, M. Dasso, and A. Arnaoutov. 2007. Bub1 is essential for assembly of the functional inner centromere. *The Journal of Cell Biology*. 176:919–928. doi:10.1083/jcb.200609044.
- Brito, D.A., and C.L. Rieder. 2006. Mitotic checkpoint slippage in humans occurs via cyclin B destruction in the presence of an active checkpoint. *Current Biology*. 16:1194–1200. doi:10.1016/j.cub.2006.04.043.
- Brito, D.A., and C.L. Rieder. 2009. The ability to survive mitosis in the presence of microtubule poisons differs significantly between human nontransformed (RPE-1) and cancer (U2OS, HeLa) cells. *Cell Motil. Cytoskeleton*. 66:437–447. doi:10.1002/cm.20316.
- Buschhorn, B.A., G. Petzold, M. Galova, P. Dube, C. Kraft, F. Herzog, H. Stark, and J.-M. Peters. 2011. Substrate binding on the APC/C occurs between the coactivator Cdh1 and the processivity factor Doc1. *Nat. Struct. Mol. Biol*. 18:6–13. doi:10.1038/nsmb.1979.
- Campbell, C.S., and A. Desai. 2013. Tension sensing by Aurora B kinase is independent of survivin-based centromere localization. *Nature*. 497:118–121. doi:10.1038/nature12057.
- Carmena, M., M. Wheelock, H. Funabiki, and W.C. Earnshaw. 2012. The chromosomal passenger complex (CPC): from easy rider to the godfather of mitosis. *Nat. Rev. Mol. Cell Biol*. 13:789–803. doi:10.1038/nrm3474.
- Carpenter, A.E., T.R. Jones, M.R. Lamprecht, C. Clarke, I.H. Kang, O. Friman, D.A. Guertin, J.H. Chang, R.A. Lindquist, J. Moffat, P. Golland, and D.M. Sabatini. 2006. CellProfiler: image analysis software for identifying and quantifying cell phenotypes. *Genome Biol*. 7:R100. doi:10.1186/gb-2006-7-10-r100.
- Chang, L., and D. Barford. 2014. Insights into the anaphase-promoting complex: a molecular machine that regulates mitosis. *Curr. Opin. Struct. Biol*. 29:1–9. doi:10.1016/j.sbi.2014.08.003.

- Chao, W.C.H., K. Kulkarni, Z. Zhang, E.H. Kong, and D. Barford. 2012. Structure of the mitotic checkpoint complex. *Nature*. 484:208–213. doi:10.1038/nature10896.
- Cheeseman, I.M., and A. Desai. 2008. Molecular architecture of the kinetochore-microtubule interface. *Nat. Rev. Mol. Cell Biol.* 9:33–46. doi:10.1038/nrm2310.
- Cheeseman, I.M., J.S. Chappie, E.M. Wilson-Kubalek, and A. Desai. 2006. The conserved KMN network constitutes the core microtubule-binding site of the kinetochore. *Cell*. 127:983–997. doi:10.1016/j.cell.2006.09.039.
- Chen, J.-G., and S.B. Horwitz. 2002. Differential mitotic responses to microtubule-stabilizing and -destabilizing drugs. *Cancer Research*. 62:1935–1938.
- Chen, X., S. Wei, Y. Ji, X. Guo, and F. Yang. 2015. Quantitative proteomics using SILAC: Principles, applications, and developments. *Proteomics*. 15:3175–3192. doi:10.1002/pmic.201500108.
- Ciferri, C., S. Pasqualato, E. Screpanti, G. Varetto, S. Santaguida, G. Dos Reis, A. Maiolica, J. Polka, J.G. De Luca, P. De Wulf, M. Salek, J. Rappsilber, C.A. Moores, E.D. Salmon, and A. Musacchio. 2008. Implications for kinetochore-microtubule attachment from the structure of an engineered Ndc80 complex. *Cell*. 133:427–439. doi:10.1016/j.cell.2008.03.020.
- Cleveland, D.W., Y. Mao, and K.F. Sullivan. 2003. Centromeres and kinetochores: from epigenetics to mitotic checkpoint signaling. *Cell*. 112:407–421.
- Cohen, P. 2002. The origins of protein phosphorylation. *Nature Cell Biology*. 4:E127–30. doi:10.1038/ncb0502-e127.
- Collin, P., O. Nashchekina, R. Walker, and J. Pines. 2013. The spindle assembly checkpoint works like a rheostat rather than a toggle switch. *Nature Cell Biology*. 15:1378–1385. doi:10.1038/ncb2855.
- Colombo, R., M. Caldarelli, M. Mennecozi, M.L. Giorgini, F. Sola, P. Cappella, C. Perrera, S.R. Depaolini, L. Rusconi, U. Cucchi, N. Avanzi, J.A. Bertrand, R.T. Bossi, E. Pesenti, A. Galvani, A. Isacchi, F. Colotta, D. Donati, and J. Moll. 2010. Targeting the mitotic checkpoint for cancer therapy with NMS-P715, an inhibitor of MPS1 kinase. *Cancer Research*. 70:10255–10264. doi:10.1158/0008-5472.CAN-10-2101.
- Cooper, G.M., and R.E. Hausman. 2013. *The Cell*. Sinauer Associates Incorporated. 1 pp.
- CSLS, The University of Tokyo. 2011. A comprehensive approach to life science. <http://csls-text.c.u-tokyo.ac.jp/active.html>.

- da Fonseca, P.C.A., E.H. Kong, Z. Zhang, A. Schreiber, M.A. Williams, E.P. Morris, and D. Barford. 2011. Structures of APC/C(Cdh1) with substrates identify Cdh1 and Apc10 as the D-box co-receptor. *Nature*. 470:274–278. doi:10.1038/nature09625.
- Davenport, J., L.D. Harris, and R. Goorha. 2006. Spindle checkpoint function requires Mad2-dependent Cdc20 binding to the Mad3 homology domain of BubR1. *Experimental Cell Research*. 312:1831–1842. doi:10.1016/j.yexcr.2006.02.018.
- De Antoni, A., C.G. Pearson, D. Cimini, J.C. Canman, V. Sala, L. Nezi, M. Mapelli, L. Sironi, M. Faretta, E.D. Salmon, and A. Musacchio. 2005. The Mad1/Mad2 complex as a template for Mad2 activation in the spindle assembly checkpoint. *Current Biology*. 15:214–225. doi:10.1016/j.cub.2005.01.038.
- De Antoni, A., S. Maffini, S. Knapp, A. Musacchio, and S. Santaguida. 2012. A small-molecule inhibitor of Haspin alters the kinetochore functions of Aurora B. *The Journal of Cell Biology*. 199:269–284. doi:10.1083/jcb.201205119.
- DeLuca, J.G., W.E. Gall, C. Ciferri, D. Cimini, A. Musacchio, and E.D. Salmon. 2006. Kinetochore microtubule dynamics and attachment stability are regulated by Hec1. *Cell*. 127:969–982. doi:10.1016/j.cell.2006.09.047.
- Dephoure, N., K.L. Gould, S.P. Gygi, and D.R. Kellogg. 2013. Mapping and analysis of phosphorylation sites: a quick guide for cell biologists. *Mol. Biol. Cell*. 24:535–542. doi:10.1091/mbc.E12-09-0677.
- Dick, A.E., and D.W. Gerlich. 2013. Kinetic framework of spindle assembly checkpoint signalling. *Nature Cell Biology*. 15:1370–1377. doi:10.1038/ncb2842.
- Ditchfield, C., V.L. Johnson, A. Tighe, R. Ellston, C. Haworth, T. Johnson, A. Mortlock, N. Keen, and S.S. Taylor. 2003. Aurora B couples chromosome alignment with anaphase by targeting BubR1, Mad2, and Cenp-E to kinetochores. *The Journal of Cell Biology*. 161:267–280. doi:10.1083/jcb.200208091.
- Domon, B., and R. Aebersold. 2010. Options and considerations when selecting a quantitative proteomics strategy. *Nat. Biotechnol.* 28:710–721. doi:10.1038/nbt.1661.
- Donzelli, M., and G.F. Draetta. 2003. Regulating mammalian checkpoints through Cdc25 inactivation. *EMBO Rep*. 4:671–677. doi:10.1038/sj.embor.embor887.
- Dou, Z., C. von Schubert, R. Körner, A. Santamaria, S. Elowe, and E.A. Nigg. 2011. Quantitative mass spectrometry analysis reveals similar substrate consensus motif for human Mps1 kinase and Plk1. *PLoS ONE*. 6:e18793. doi:10.1371/journal.pone.0018793.

- Du, J., A.E. Kelly, H. Funabiki, and D.J. Patel. 2012. Structural basis for recognition of H3T3ph and Smac/DIABLO N-terminal peptides by human Survivin. *Structure*. 20:185–195. doi:10.1016/j.str.2011.12.001.
- Elbashir, S.M., J. Harborth, W. Lendeckel, A. Yalcin, K. Weber, and T. Tuschl. 2001. Duplexes of 21-nucleotide RNAs mediate RNA interference in cultured mammalian cells. *Nature*. 411:494–498. doi:10.1038/35078107.
- Elia, A.E.H., L.C. Cantley, and M.B. Yaffe. 2003. Proteomic screen finds pSer/pThr-binding domain localizing Plk1 to mitotic substrates. *Science*. 299:1228–1231. doi:10.1126/science.1079079.
- Elmore, S. 2007. Apoptosis: a review of programmed cell death. *Toxicol Pathol*. 35:495–516. doi:10.1080/01926230701320337.
- Elowe, S. 2011. Bub1 and BubR1: at the interface between chromosome attachment and the spindle checkpoint. *Molecular and Cellular Biology*. 31:3085–3093. doi:10.1128/MCB.05326-11.
- Emanuele, M.J., W. Lan, M. Jwa, S.A. Miller, C.S.M. Chan, and P.T. Stukenberg. 2008. Aurora B kinase and protein phosphatase 1 have opposing roles in modulating kinetochore assembly. *The Journal of Cell Biology*. 181:241–254. doi:10.1083/jcb.200710019.
- Espeut, J., P. Lara-Gonzalez, M. Sassine, A.K. Shiau, A. Desai, and A. Abrieu. 2015. Natural Loss of Mps1 Kinase in Nematodes Uncovers a Role for Polo-like Kinase 1 in Spindle Checkpoint Initiation. *Cell Rep*. doi:10.1016/j.celrep.2015.05.039.
- Fang, G. 2002. Checkpoint protein BubR1 acts synergistically with Mad2 to inhibit anaphase-promoting complex. *Mol. Biol. Cell*. 13:755–766. doi:10.1091/mbc.01-09-0437.
- Farr, K.A., and M.A. Hoyt. 1998. Bub1p kinase activates the *Saccharomyces cerevisiae* spindle assembly checkpoint. *Molecular and Cellular Biology*. 18:2738–2747.
- Fava, L.L., M. Kaulich, E.A. Nigg, and A. Santamaria. 2011. Probing the in vivo function of Mad1:C-Mad2 in the spindle assembly checkpoint. *The EMBO Journal*. 30:3322–3336. doi:10.1038/emboj.2011.239.
- Fernius, J., and K.G. Hardwick. 2007. Bub1 kinase targets Sgo1 to ensure efficient chromosome biorientation in budding yeast mitosis. *PLoS Genet*. 3:e213. doi:10.1371/journal.pgen.0030213.
- Figuroa-Masot, X.A., M. Hetman, M.J. Higgins, N. Kokot, and Z. Xia. 2001. Taxol

- induces apoptosis in cortical neurons by a mechanism independent of Bcl-2 phosphorylation. *J. Neurosci.* 21:4657–4667.
- Fíla, J., and D. Honys. 2012. Enrichment techniques employed in phosphoproteomics. *Amino Acids.* 43:1025–1047. doi:10.1007/s00726-011-1111-z.
- Foley, E.A., and T.M. Kapoor. 2013. Microtubule attachment and spindle assembly checkpoint signalling at the kinetochore. *Nat. Rev. Mol. Cell Biol.* 14:25–37. doi:10.1038/nrm3494.
- Foley, E.A., M. Maldonado, and T.M. Kapoor. 2011. Formation of stable attachments between kinetochores and microtubules depends on the B56-PP2A phosphatase. *Nature Cell Biology.* 13:1265–1271. doi:10.1038/ncb2327.
- Fuller, B.G., M.A. Lampson, E.A. Foley, S. Rosasco-Nitcher, K.V. Le, P. Tobelmann, D.L. Brautigan, P.T. Stukenberg, and T.M. Kapoor. 2008. Midzone activation of aurora B in anaphase produces an intracellular phosphorylation gradient. *Nature.* 453:1132–1136. doi:10.1038/nature06923.
- Funabiki, H., and D.J. Wynne. 2013. Making an effective switch at the kinetochore by phosphorylation and dephosphorylation. *Chromosoma.* 122:135–158. doi:10.1007/s00412-013-0401-5.
- Gallien, S., E. Duriez, C. Crone, M. Kellmann, T. Moehring, and B. Domon. 2012. Targeted proteomic quantification on quadrupole-orbitrap mass spectrometer. *Mol. Cell Proteomics.* 11:1709–1723. doi:10.1074/mcp.O112.019802.
- Gandhi, R., P.J. Gillespie, and T. Hirano. 2006. Human Wapl is a cohesin-binding protein that promotes sister-chromatid resolution in mitotic prophase. *Current Biology.* 16:2406–2417. doi:10.1016/j.cub.2006.10.061.
- Gascoigne, K.E., and S.S. Taylor. 2008. Cancer cells display profound intra- and interline variation following prolonged exposure to antimetabolic drugs. *Cancer Cell.* 14:111–122. doi:10.1016/j.ccr.2008.07.002.
- Gascoigne, K.E., and S.S. Taylor. 2009. How do anti-mitotic drugs kill cancer cells? *Journal of Cell Science.* 122:2579–2585. doi:10.1242/jcs.039719.
- Gassmann, R., A.J. Holland, D. Varma, X. Wan, F. Civril, D.W. Cleveland, K. Oegema, E.D. Salmon, and A. Desai. 2010. Removal of Spindly from microtubule-attached kinetochores controls spindle checkpoint silencing in human cells. *Genes & Development.* 24:957–971. doi:10.1101/gad.1886810.
- Gillet, L.C., P. Navarro, S. Tate, H. Röst, N. Selevsek, L. Reiter, R. Bonner, and R. Aebersold. 2012. Targeted data extraction of the MS/MS spectra generated by data-independent acquisition: a new concept for consistent and accurate

-
- proteome analysis. *Mol. Cell Proteomics*. 11:O111.016717–O111.016717. doi:10.1074/mcp.O111.016717.
- Gillette, M.A., and S.A. Carr. 2013. Quantitative analysis of peptides and proteins in biomedicine by targeted mass spectrometry. *Nature Methods*. 10:28–34. doi:10.1038/nmeth.2309.
- Gohard, F.H., D.J. St-Cyr, M. Tyers, and W.C. Earnshaw. 2014. Targeting the INCENP IN-box-Aurora B interaction to inhibit CPC activity in vivo. *Open Biol*. 4:140163–140163. doi:10.1098/rsob.140163.
- Gregan, J., S. Polakova, L. Zhang, I.M. Tolić-Nørrelykke, and D. Cimini. 2011. Merotelic kinetochore attachment: causes and effects. *Trends in Cell Biology*. 21:374–381. doi:10.1016/j.tcb.2011.01.003.
- Gruber, S., C.H. Haering, and K. Nasmyth. 2003. Chromosomal cohesin forms a ring. *Cell*. 112:765–777.
- Guimaraes, G.J., Y. Dong, B.F. McEwen, and J.G. DeLuca. 2008. Kinetochore-microtubule attachment relies on the disordered N-terminal tail domain of Hec1. *Current Biology*. 18:1778–1784. doi:10.1016/j.cub.2008.08.012.
- Guo, Y., C. Kim, and Y. Mao. 2013. New insights into the mechanism for chromosome alignment in metaphase. *Int Rev Cell Mol Biol*. 303:237–262. doi:10.1016/B978-0-12-407697-6.00006-4.
- Haarhuis, J.H.I., A.M.O. Elbatsh, and B.D. Rowland. 2014. Cohesin and Its Regulation: On the Logic of X-Shaped Chromosomes. *Developmental Cell*. 31:7–18.
- Haering, C.H., A.-M. Farcas, P. Arumugam, J. Metson, and K. Nasmyth. 2008. The cohesin ring concatenates sister DNA molecules. *Nature*. 454:297–301. doi:10.1038/nature07098.
- Haering, C.H., J. Löwe, A. Hochwagen, and K. Nasmyth. 2002. Molecular architecture of SMC proteins and the yeast cohesin complex. *Molecular Cell*. 9:773–788.
- Hanisch, A., A. Wehner, E.A. Nigg, and H.H.W. Silljé. 2006a. Different Plk1 functions show distinct dependencies on Polo-Box domain-mediated targeting. *Mol. Biol. Cell*. 17:448–459. doi:10.1091/mbc.E05-08-0801.
- Hanisch, A., H.H.W. Silljé, and E.A. Nigg. 2006b. Timely anaphase onset requires a novel spindle and kinetochore complex comprising Ska1 and Ska2. *The EMBO Journal*. 25:5504–5515. doi:10.1038/sj.emboj.7601426.
-

- Hardwick, K.G., R.C. Johnston, D.L. Smith, and A.W. Murray. 2000. MAD3 encodes a novel component of the spindle checkpoint which interacts with Bub3p, Cdc20p, and Mad2p. *The Journal of Cell Biology*. 148:871–882.
- Hartwell, L.H., and T.A. Weinert. 1989. Checkpoints: controls that ensure the order of cell cycle events. *Science*.
- Hauf, S., I.C. Waizenegger, and J.M. Peters. 2001. Cohesin cleavage by separase required for anaphase and cytokinesis in human cells. *Science*. 293:1320–1323. doi:10.1126/science.1061376.
- Hauf, S., R.W. Cole, S. LaTerra, C. Zimmer, G. Schnapp, R. Walter, A. Heckel, J. van Meel, C.L. Rieder, and J.-M. Peters. 2003. The small molecule Hesperadin reveals a role for Aurora B in correcting kinetochore-microtubule attachment and in maintaining the spindle assembly checkpoint. *The Journal of Cell Biology*. 161:281–294. doi:10.1083/jcb.200208092.
- Heald, R., R. Tournebise, T. Blank, R. Sandaltzopoulos, P. Becker, A. Hyman, and E. Karsenti. 1996. Self-organization of microtubules into bipolar spindles around artificial chromosomes in *Xenopus* egg extracts. *Nature*. 382:420–425. doi:10.1038/382420a0.
- Hewitt, L., A. Tighe, S. Santaguida, A.M. White, C.D. Jones, A. Musacchio, S. Green, and S.S. Taylor. 2010. Sustained Mps1 activity is required in mitosis to recruit O-Mad2 to the Mad1-C-Mad2 core complex. *The Journal of Cell Biology*. 190:25–34. doi:10.1083/jcb.201002133.
- Hirota, T., J.J. Lipp, B.-H. Toh, and J.-M. Peters. 2005. Histone H3 serine 10 phosphorylation by Aurora B causes HP1 dissociation from heterochromatin. *Nature*. 438:1176–1180. doi:10.1038/nature04254.
- Hitchcock, M., A. Mengel, A. Richter, H. Briem, K. Eis, V. Pütter, G. Siemeister, S. Prechtel, A.E. Fernandez-Montalvan, C. Stegmann, S. Holton, M.J. Gnoth, and C. Preusse. 2013. Substituted benzylpyrazoles WO2013092512.
- Holland, A.J., and D.W. Cleveland. 2009. Boveri revisited: chromosomal instability, aneuploidy and tumorigenesis. *Nat. Rev. Mol. Cell Biol.* 10:478–487. doi:10.1038/nrm2718.
- Honda, R., R. Körner, and E.A. Nigg. 2003. Exploring the functional interactions between Aurora B, INCENP, and survivin in mitosis. *Mol. Biol. Cell*. 14:3325–3341. doi:10.1091/mbc.E02-11-0769.
- Howell, B.J., B. Moree, E.M. Farrar, S. Stewart, G. Fang, and E.D. Salmon. 2004. Spindle checkpoint protein dynamics at kinetochores in living cells. *Current Biology*. 14:953–964. doi:10.1016/j.cub.2004.05.053.

- Howell, B.J., B.F. McEwen, J.C. Canman, D.B. Hoffman, E.M. Farrar, C.L. Rieder, and E.D. Salmon. 2001. Cytoplasmic dynein/dynactin drives kinetochore protein transport to the spindle poles and has a role in mitotic spindle checkpoint inactivation. *The Journal of Cell Biology*. 155:1159–1172. doi:10.1083/jcb.200105093.
- Hoyt, M.A., L. Totis, and B.T. Roberts. 1991. *S. cerevisiae* genes required for cell cycle arrest in response to loss of microtubule function. *Cell*. 66:507–517.
- Hsu, J.Y., Z.W. Sun, X. Li, M. Reuben, K. Tatchell, D.K. Bishop, J.M. Grushcow, C.J. Brame, J.A. Caldwell, D.F. Hunt, R. Lin, M.M. Smith, and C.D. Allis. 2000. Mitotic phosphorylation of histone H3 is governed by Ipl1/aurora kinase and Glc7/PP1 phosphatase in budding yeast and nematodes. *Cell*. 102:279–291.
- Ibarrola, N., D.E. Kalume, M. Gronborg, A. Iwahori, and A. Pandey. 2003. A proteomic approach for quantitation of phosphorylation using stable isotope labeling in cell culture. *Anal. Chem*. 75:6043–6049. doi:10.1021/ac034931f.
- Iemura, K., and K. Tanaka. 2015. Chromokinesin Kid and kinetochore kinesin CENP-E differentially support chromosome congression without end-on attachment to microtubules. *Nat Commun*. 6:6447. doi:10.1038/ncomms7447.
- Ikui, A.E., C.-P.H. Yang, T. Matsumoto, and S.B. Horwitz. 2005. Low concentrations of taxol cause mitotic delay followed by premature dissociation of p55CDC from Mad2 and BubR1 and abrogation of the spindle checkpoint, leading to aneuploidy. *Cell Cycle*. 4:1385–1388.
- Ivanov, D., and K. Nasmyth. 2005. A topological interaction between cohesin rings and a circular minichromosome. *Cell*. 122:849–860. doi:10.1016/j.cell.2005.07.018.
- Jablonski, S.A., G.K. Chan, C.A. Cooke, W.C. Earnshaw, and T.J. Yen. 1998. The hBUB1 and hBUBR1 kinases sequentially assemble onto kinetochores during prophase with hBUBR1 concentrating at the kinetochore plates in mitosis. *Chromosoma*. 107:386–396.
- Jaffe, J.D., H. Keshishian, B. Chang, T.A. Addona, M.A. Gillette, and S.A. Carr. 2008. Accurate inclusion mass screening: a bridge from unbiased discovery to targeted assay development for biomarker verification. *Mol. Cell Proteomics*. 7:1952–1962. doi:10.1074/mcp.M800218-MCP200.
- Janssen, A., G.J.P.L. Kops, and R.H. Medema. 2009. Elevating the frequency of chromosome mis-segregation as a strategy to kill tumor cells. *Proc. Natl. Acad. Sci. U.S.A.* 106:19108–19113. doi:10.1073/pnas.0904343106.
- Jeganathan, K., L. Malureanu, D.J. Baker, S.C. Abraham, and J.M. van Deursen.

2007. Bub1 mediates cell death in response to chromosome missegregation and acts to suppress spontaneous tumorigenesis. *The Journal of Cell Biology*. 179:255–267. doi:10.1083/jcb.200706015.
- Jelluma, N., A.B. Brenkman, N.J.F. van den Broek, C.W.A. Cruijsen, M.H.J. van Osch, S.M.A. Lens, R.H. Medema, and G.J.P.L. Kops. 2008. Mps1 phosphorylates Borealin to control Aurora B activity and chromosome alignment. *Cell*. 132:233–246. doi:10.1016/j.cell.2007.11.046.
- Jelluma, N., T.B. Dansen, T. Sliedrecht, N.P. Kwiatkowski, and G.J.P.L. Kops. 2010. Release of Mps1 from kinetochores is crucial for timely anaphase onset. *The Journal of Cell Biology*. 191:281–290. doi:10.1083/jcb.201003038.
- Jemaà, M., L. Galluzzi, O. Kepp, L. Senovilla, M. Brands, U. Boemer, M. Koppitz, P. Lienau, S. Prechtel, V. Schulze, G. Siemeister, A.M. Wengner, D. Mumberg, K. Ziegelbauer, A. Abrieu, M. Castedo, I. Vitale, and G. Kroemer. 2013. Characterization of novel MPS1 inhibitors with preclinical anticancer activity. *Cell Death Differ*. 20:1532–1545. doi:10.1038/cdd.2013.105.
- Jia, L., B. Li, R.T. Warrington, X. Hao, S. Wang, and H. Yu. 2011. Defining pathways of spindle checkpoint silencing: functional redundancy between Cdc20 ubiquitination and p31(comet). *Mol. Biol. Cell*. 22:4227–4235. doi:10.1091/mbc.E11-05-0389.
- Johnson, V.L., M.I.F. Scott, S.V. Holt, D. Hussein, and S.S. Taylor. 2004. Bub1 is required for kinetochore localization of BubR1, Cenp-E, Cenp-F and Mad2, and chromosome congression. *Journal of Cell Science*. 117:1577–1589. doi:10.1242/jcs.01006.
- Kang, J., M. Yang, B. Li, W. Qi, C. Zhang, K.M. Shokat, D.R. Tomchick, M. Machius, and H. Yu. 2008. Structure and substrate recruitment of the human spindle checkpoint kinase Bub1. *Molecular Cell*. 32:394–405. doi:10.1016/j.molcel.2008.09.017.
- Kapoor, T.M., M.A. Lampson, P. Hergert, L. Cameron, D. Cimini, E.D. Salmon, B.F. McEwen, and A. Khodjakov. 2006. Chromosomes can congress to the metaphase plate before biorientation. *Science*. 311:388–391. doi:10.1126/science.1122142.
- Kapoor, T.M., T.U. Mayer, M.L. Coughlin, and T.J. Mitchison. 2000. Probing spindle assembly mechanisms with monastrol, a small molecule inhibitor of the mitotic kinesin, Eg5. *The Journal of Cell Biology*. 150:975–988. doi:10.1038/35036012.
- Kawashima, S.A., T. Tsukahara, M. Langeegger, S. Hauf, T.S. Kitajima, and Y.

- Watanabe. 2007. Shugoshin enables tension-generating attachment of kinetochores by loading Aurora to centromeres. *Genes & Development*. 21:420–435. doi:10.1101/gad.1497307.
- Kawashima, S.A., Y. Yamagishi, T. Honda, K.-I. Ishiguro, and Y. Watanabe. 2010. Phosphorylation of H2A by Bub1 prevents chromosomal instability through localizing shugoshin. *Science*. 327:172–177. doi:10.1126/science.1180189.
- Kelly, A.E., C. Ghenoiu, J.Z. Xue, C. Zierhut, H. Kimura, and H. Funabiki. 2010. Survivin reads phosphorylated histone H3 threonine 3 to activate the mitotic kinase Aurora B. *Science*. 330:235–239. doi:10.1126/science.1189505.
- Kim, Y., A.J. Holland, W. Lan, and D.W. Cleveland. 2010. Aurora kinases and protein phosphatase 1 mediate chromosome congression through regulation of CENP-E. *Cell*. 142:444–455. doi:10.1016/j.cell.2010.06.039.
- Kirschner, M.W., and T. Mitchison. 1986. Microtubule dynamics. *Nature*. 324:621–621. doi:10.1038/324621a0.
- Kishi, K., M.A.T.M. van Vugt, K.-I. Okamoto, Y. Hayashi, and M.B. Yaffe. 2009. Functional dynamics of Polo-like kinase 1 at the centrosome. *Molecular and Cellular Biology*. 29:3134–3150. doi:10.1128/MCB.01663-08.
- Kitajima, T.S., S. Hauf, M. Ohsugi, T. Yamamoto, and Y. Watanabe. 2005. Human Bub1 defines the persistent cohesion site along the mitotic chromosome by affecting Shugoshin localization. *Current Biology*. 15:353–359. doi:10.1016/j.cub.2004.12.044.
- Kitajima, T.S., T. Sakuno, K.-I. Ishiguro, S.-I. Iemura, T. Natsume, S.A. Kawashima, and Y. Watanabe. 2006. Shugoshin collaborates with protein phosphatase 2A to protect cohesin. *Nature*. 441:46–52. doi:10.1038/nature04663.
- Kiyomitsu, T., H. Murakami, and M. Yanagida. 2011. Protein interaction domain mapping of human kinetochore protein Blinkin reveals a consensus motif for binding of spindle assembly checkpoint proteins Bub1 and BubR1. *Molecular and Cellular Biology*. 31:998–1011. doi:10.1128/MCB.00815-10.
- Klebig, C., D. Korinth, and P. Meraldi. 2009. Bub1 regulates chromosome segregation in a kinetochore-independent manner. *The Journal of Cell Biology*. 185:841–858. doi:10.1083/jcb.200902128.
- Klein, U.R., E.A. Nigg, and U. Gruneberg. 2006. Centromere targeting of the chromosomal passenger complex requires a ternary subcomplex of Borealin, Survivin, and the N-terminal domain of INCENP. *Mol. Biol. Cell*. 17:2547–2558. doi:10.1091/mbc.E05-12-1133.

- Knowlton, A.L., W. Lan, and P.T. Stukenberg. 2006. Aurora B is enriched at merotelic attachment sites, where it regulates MCAK. *Current Biology*. 16:1705–1710. doi:10.1016/j.cub.2006.07.057.
- Kolodner, R.D., D.W. Cleveland, and C.D. Putnam. 2011. Cancer. Aneuploidy drives a mutator phenotype in cancer. *Science*. 333:942–943. doi:10.1126/science.1211154.
- Kops, G.J.P.L., A.T. Saurin, and P. Meraldi. 2010. Finding the middle ground: how kinetochores power chromosome congression. *Cell. Mol. Life Sci*. 67:2145–2161. doi:10.1007/s00018-010-0321-y.
- Kops, G.J.P.L., D.R. Foltz, and D.W. Cleveland. 2004. Lethality to human cancer cells through massive chromosome loss by inhibition of the mitotic checkpoint. *Proc. Natl. Acad. Sci. U.S.A.* 101:8699–8704. doi:10.1073/pnas.0401142101.
- Krenn, V., A. Wehenkel, X. Li, S. Santaguida, and A. Musacchio. 2012. Structural analysis reveals features of the spindle checkpoint kinase Bub1-kinetochore subunit Knl1 interaction. *The Journal of Cell Biology*. 196:451–467. doi:10.1083/jcb.201110013.
- Krenn, V., K. Overlack, I. Primorac, S. van Gerwen, and A. Musacchio. 2014. KI motifs of human Knl1 enhance assembly of comprehensive spindle checkpoint complexes around MELT repeats. *Curr. Biol*. 24:29–39. doi:10.1016/j.cub.2013.11.046.
- Kruse, T., G. Zhang, M.S.Y. Larsen, T. Lischetti, W. Streicher, T. Kragh Nielsen, S.P. Bjørn, and J. Nilsson. 2013. Direct binding between BubR1 and B56-PP2A phosphatase complexes regulate mitotic progression. *Journal of Cell Science*. 126:1086–1092. doi:10.1242/jcs.122481.
- Kueng, S., B. Hegemann, B.H. Peters, J.J. Lipp, A. Schleiffer, K. Mechtler, and J.-M. Peters. 2006. Wapl controls the dynamic association of cohesin with chromatin. *Cell*. 127:955–967. doi:10.1016/j.cell.2006.09.040.
- Kulukian, A., J.S. Han, and D.W. Cleveland. 2009. Unattached kinetochores catalyze production of an anaphase inhibitor that requires a Mad2 template to prime Cdc20 for BubR1 binding. *Developmental Cell*. 16:105–117. doi:10.1016/j.devcel.2008.11.005.
- Kusakabe, K.-I., N. Ide, Y. Daigo, T. Itoh, T. Yamamoto, H. Hashizume, K. Nozu, H. Yoshida, G. Tadano, S. Tagashira, K. Higashino, Y. Okano, Y. Sato, M. Inoue, M. Iguchi, T. Kanazawa, Y. Ishioka, K. Dohi, Y. Kido, S. Sakamoto, S. Ando, M. Maeda, M. Higaki, Y. Baba, and Y. Nakamura. 2015. Discovery of imidazo[1,2-b]pyridazine derivatives: selective and orally available Mps1

- (TTK) kinase inhibitors exhibiting remarkable antiproliferative activity. *J. Med. Chem.* 58:1760–1775. doi:10.1021/jm501599u.
- Lampson, M.A., and I.M. Cheeseman. 2011. Sensing centromere tension: Aurora B and the regulation of kinetochore function. *Trends in Cell Biology.* 21:133–140. doi:10.1016/j.tcb.2010.10.007.
- Lampson, M.A., K. Renduchitala, A. Khodjakov, and T.M. Kapoor. 2004. Correcting improper chromosome-spindle attachments during cell division. *Nature Cell Biology.* 6:232–237. doi:10.1038/ncb1102.
- Lan, W., and D.W. Cleveland. 2010. A chemical tool box defines mitotic and interphase roles for Mps1 kinase. *The Journal of Cell Biology.* 190:21–24. doi:10.1083/jcb.201006080.
- Lan, W., X. Zhang, S.L. Kline-Smith, S.E. Rosasco, G.A. Barrett-Wilt, J. Shabanowitz, D.F. Hunt, C.E. Walczak, and P.T. Stukenberg. 2004. Aurora B phosphorylates centromeric MCAK and regulates its localization and microtubule depolymerization activity. *Current Biology.* 14:273–286. doi:10.1016/j.cub.2004.01.055.
- Lange, V., P. Picotti, B. Domon, and R. Aebersold. 2008. Selected reaction monitoring for quantitative proteomics: a tutorial. *Molecular Systems Biology.* 4:222. doi:10.1038/msb.2008.61.
- Lara-Gonzalez, P., and S.S. Taylor. 2012. Cohesion fatigue explains why pharmacological inhibition of the APC/C induces a spindle checkpoint-dependent mitotic arrest. *PLoS ONE.* 7:e49041. doi:10.1371/journal.pone.0049041.
- Lara-Gonzalez, P., F.G. Westhorpe, and S.S. Taylor. 2012. The spindle assembly checkpoint. *Curr. Biol.* 22:R966–80. doi:10.1016/j.cub.2012.10.006.
- Larsen, M.R., T.E. Thingholm, O.N. Jensen, P. Roepstorff, and T.J.D. Jørgensen. 2005. Highly selective enrichment of phosphorylated peptides from peptide mixtures using titanium dioxide microcolumns. *Mol. Cell Proteomics.* 4:873–886. doi:10.1074/mcp.T500007-MCP200.
- Larsen, N.A., and S.C. Harrison. 2004. Crystal structure of the spindle assembly checkpoint protein Bub3. *J. Mol. Biol.* 344:885–892. doi:10.1016/j.jmb.2004.09.094.
- Larsen, N.A., J. Al-Bassam, R.R. Wei, and S.C. Harrison. 2007. Structural analysis of Bub3 interactions in the mitotic spindle checkpoint. *Proc. Natl. Acad. Sci. U.S.A.* 104:1201–1206. doi:10.1073/pnas.0610358104.

- Lee, E.A., M.K. Keutmann, M.L. Dowling, E. Harris, G. Chan, and G.D. Kao. 2004. Inactivation of the mitotic checkpoint as a determinant of the efficacy of microtubule-targeted drugs in killing human cancer cells. *Mol. Cancer Ther.* 3:661–669.
- Lenart, P., M. Petronczki, M. Steegmaier, B. Di Fiore, J.J. Lipp, M. Hoffmann, W.J. Rettig, N. Kraut, and J.-M. Peters. 2007. The small-molecule inhibitor BI 2536 reveals novel insights into mitotic roles of polo-like kinase 1. *Current Biology.* 17:304–315. doi:10.1016/j.cub.2006.12.046.
- Li, H.Y., D. Wirtz, and Y. Zheng. 2003. A mechanism of coupling RCC1 mobility to RanGTP production on the chromatin in vivo. *The Journal of Cell Biology.* 160:635–644. doi:10.1083/jcb.200211004.
- Li, R., and A.W. Murray. 1991. Feedback control of mitosis in budding yeast. *Cell.* 66:519–531.
- Li, X., and R.B. Nicklas. 1995. Mitotic forces control a cell-cycle checkpoint. *Nature.* 373:630–632. doi:10.1038/373630a0.
- Lin, Z., L. Jia, D.R. Tomchick, X. Luo, and H. Yu. 2014. Substrate-specific activation of the mitotic kinase Bub1 through intramolecular autophosphorylation and kinetochore targeting. *Structure.* 22:1616–1627. doi:10.1016/j.str.2014.08.020.
- Liu, D., G. Vader, M.J.M. Vromans, M.A. Lampson, and S.M.A. Lens. 2009. Sensing chromosome bi-orientation by spatial separation of aurora B kinase from kinetochore substrates. *Science.* 323:1350–1353. doi:10.1126/science.1167000.
- Liu, D., M. Vleugel, C.B. Backer, T. Hori, T. Fukagawa, I.M. Cheeseman, and M.A. Lampson. 2010. Regulated targeting of protein phosphatase 1 to the outer kinetochore by KNL1 opposes Aurora B kinase. *The Journal of Cell Biology.* 188:809–820. doi:10.1083/jcb.201001006.
- Liu, H., L. Jia, and H. Yu. 2013a. Phospho-H2A and cohesin specify distinct tension-regulated Sgo1 pools at kinetochores and inner centromeres. *Curr. Biol.* 23:1927–1933. doi:10.1016/j.cub.2013.07.078.
- Liu, H., Q. Qu, R. Warrington, A. Rice, N. Cheng, and H. Yu. 2015. Mitotic Transcription Installs Sgo1 at Centromeres to Coordinate Chromosome Segregation. *Molecular Cell.* 59:426–436. doi:10.1016/j.molcel.2015.06.018.
- Liu, H., S. Rankin, and H. Yu. 2013b. Phosphorylation-enabled binding of SGO1-PP2A to cohesin protects sororin and centromeric cohesion during mitosis. *Nature Cell Biology.* 15:40–49. doi:10.1038/ncb2637.

- Liu, S.-T., G.K.T. Chan, J.C. Hittle, G. Fujii, E. Lees, and T.J. Yen. 2003. Human MPS1 kinase is required for mitotic arrest induced by the loss of CENP-E from kinetochores. *Mol. Biol. Cell.* 14:1638–1651. doi:10.1091/mbc.02-05-0074.
- Liu, X., and M. Winey. 2012. The MPS1 family of protein kinases. *Annu. Rev. Biochem.* 81:561–585. doi:10.1146/annurev-biochem-061611-090435.
- Lodish, H., A. Berk, C.A. Kaiser, M. Krieger, M.P. Scott, A. Bretscher, H. Ploegh, and P. Matsudaira. 2012. *Molecular Cell Biology*. Macmillan Higher Education.
- London, N., and S. Biggins. 2014. Mad1 kinetochore recruitment by Mps1-mediated phosphorylation of Bub1 signals the spindle checkpoint. *Genes & Development.* 28:140–152. doi:10.1101/gad.233700.113.
- London, N., S. Ceto, J.A. Ranish, and S. Biggins. 2012. Phosphoregulation of Spc105 by Mps1 and PP1 regulates Bub1 localization to kinetochores. *Curr. Biol.* 22:900–906. doi:10.1016/j.cub.2012.03.052.
- Losada, A. 2014. Cohesin in cancer: chromosome segregation and beyond. *Nat. Rev. Cancer.* 14:389–393. doi:10.1038/nrc3743.
- Maciejowski, J., K.A. George, M.-E. Terret, C. Zhang, K.M. Shokat, and P.V. Jallepalli. 2010. Mps1 directs the assembly of Cdc20 inhibitory complexes during interphase and mitosis to control M phase timing and spindle checkpoint signaling. *The Journal of Cell Biology.* 190:89–100. doi:10.1083/jcb.201001050.
- Maia, A.R.R., J. de Man, U. Boon, A. Janssen, J.-Y. Song, M. Omerzu, J.G. Sterrenburg, M.B.W. Prinsen, N. Willemsen-Seegers, J.A.D.M. de Roos, A.M. van Doornmalen, J.C.M. Uitdehaag, G.J.P.L. Kops, J. Jonkers, R.C. Buijsman, G.J.R. Zaman, and R.H. Medema. 2015. Inhibition of the spindle assembly checkpoint kinase TTK enhances the efficacy of docetaxel in a triple-negative breast cancer model. *Ann. Oncol.* mdv293. doi:10.1093/annonc/mdv293.
- Malhotra, V., and M.C. Perry. 2003. Classical chemotherapy: mechanisms, toxicities and the therapeutic window. *Cancer Biol. Ther.* 2:S2–4.
- Malumbres, M., and M. Barbacid. 2009. Cell cycle, CDKs and cancer: a changing paradigm. *Nat. Rev. Cancer.* 9:153–166. doi:10.1038/nrc2602.
- Mapelli, M., F.V. Filipp, G. Rancati, L. Massimiliano, L. Nezi, G. Stier, R.S. Hagan, S. Confalonieri, S. Piatti, M. Sattler, and A. Musacchio. 2006. Determinants of conformational dimerization of Mad2 and its inhibition by p31comet. *The EMBO Journal.* 25:1273–1284. doi:10.1038/sj.emboj.7601033.

- Mapelli, M., L. Massimiliano, S. Santaguida, and A. Musacchio. 2007. The Mad2 conformational dimer: structure and implications for the spindle assembly checkpoint. *Cell*. 131:730–743. doi:10.1016/j.cell.2007.08.049.
- Martinez, R., A. Blasina, J.F. Hallin, W. Hu, I. Rymer, J. Fan, R.L. Hoffman, S. Murphy, M. Marx, G. Yanochko, D. Trajkovic, D. Dinh, S. Timofeevski, Z. Zhu, P. Sun, P.B. Lappin, and B.W. Murray. 2015. Mitotic Checkpoint Kinase Mps1 Has a Role in Normal Physiology which Impacts Clinical Utility. *PLoS ONE*. 10:e0138616. doi:10.1371/journal.pone.0138616.
- McEwen, B.F., G.K. Chan, B. Zubrowski, M.S. Savoian, M.T. Sauer, and T.J. Yen. 2001. CENP-E is essential for reliable bioriented spindle attachment, but chromosome alignment can be achieved via redundant mechanisms in mammalian cells. *Mol. Biol. Cell*. 12:2776–2789.
- Meraldi, P., and P.K. Sorger. 2005. A dual role for Bub1 in the spindle checkpoint and chromosome congression. *The EMBO Journal*. 24:1621–1633. doi:10.1038/sj.emboj.7600641.
- Meraldi, P., V.M. Draviam, and P.K. Sorger. 2004. Timing and checkpoints in the regulation of mitotic progression. *Developmental Cell*. 7:45–60. doi:10.1016/j.devcel.2004.06.006.
- Michalski, A., J. Cox, and M. Mann. 2011. More than 100,000 detectable peptide species elute in single shotgun proteomics runs but the majority is inaccessible to data-dependent LC-MS/MS. *J. Proteome Res.* 10:1785–1793. doi:10.1021/pr101060v.
- Michel, L., E. Diaz-Rodriguez, G. Narayan, E. Hernando, V.V.V.S. Murty, and R. Benezra. 2004. Complete loss of the tumor suppressor MAD2 causes premature cyclin B degradation and mitotic failure in human somatic cells. *Proc. Natl. Acad. Sci. U.S.A.* 101:4459–4464. doi:10.1073/pnas.0306069101.
- Morgan, D.O. 2007. *The Cell Cycle: Principles of Control*. New Science Press Ltd., London.
- Morrow, C.J., A. Tighe, V.L. Johnson, M.I.F. Scott, C. Ditchfield, and S.S. Taylor. 2005. Bub1 and aurora B cooperate to maintain BubR1-mediated inhibition of APC/CCdc20. *Journal of Cell Science*. 118:3639–3652. doi:10.1242/jcs.02487.
- Moyle, M.W., T. Kim, N. Hattersley, J. Espeut, D.K. Cheerambathur, K. Oegema, and A. Desai. 2014. A Bub1-Mad1 interaction targets the Mad1-Mad2 complex to unattached kinetochores to initiate the spindle checkpoint. *The Journal of Cell Biology*. 204:647–657. doi:10.1083/jcb.201311015.
- Musacchio, A. 2011. Spindle assembly checkpoint: the third decade. *Philos. Trans.*

- R. Soc. Lond., B, Biol. Sci.* 366:3595–3604. doi:10.1098/rstb.2011.0072.
- Musacchio, A., and E.D. Salmon. 2007. The spindle-assembly checkpoint in space and time. *Nat. Rev. Mol. Cell Biol.* 8:379–393. doi:10.1038/nrm2163.
- Musacchio, A., and K.G. Hardwick. 2002. The spindle checkpoint: structural insights into dynamic signalling. *Nat. Rev. Mol. Cell Biol.* 3:731–741. doi:10.1038/nrm929.
- Nagahara, H., R.R. Latek, S.A. Ezhevsky, and S.F. Dowdy. 1999. 2-D phosphopeptide mapping. *Methods Mol. Biol.* 112:271–279.
- Nasmyth, K. 2001. A prize for proliferation. *Cell.* 107:689–701.
- Nasmyth, K., and C.H. Haering. 2009. Cohesin: its roles and mechanisms. *Annu. Rev. Genet.* 43:525–558. doi:10.1146/annurev-genet-102108-134233.
- Nasmyth, K., J.M. Peters, and F. Uhlmann. 2000. Splitting the chromosome: cutting the ties that bind sister chromatids. *Science.* 288:1379–1385.
- Nezi, L., and A. Musacchio. 2009. Sister chromatid tension and the spindle assembly checkpoint. *Curr. Opin. Cell Biol.* 21:785–795. doi:10.1016/j.ceb.2009.09.007.
- Nigg, E.A. 2001. Mitotic kinases as regulators of cell division and its checkpoints. *Nat. Rev. Mol. Cell Biol.* 2:21–32. doi:10.1038/35048096.
- Nijenhuis, W., E. von Castelmur, D. Littler, V. De Marco, E. Tromer, M. Vleugel, M.H.J. van Osch, B. Snel, A. Perrakis, and G.J.P.L. Kops. 2013. A TPR domain-containing N-terminal module of MPS1 is required for its kinetochore localization by Aurora B. *The Journal of Cell Biology.* 201:217–231. doi:10.1083/jcb.201210033.
- Nilsson, J., M. Yekezare, J. Minshull, and J. Pines. 2008. The APC/C maintains the spindle assembly checkpoint by targeting Cdc20 for destruction. *Nature Cell Biology.* 10:1411–1420. doi:10.1038/ncb1799.
- Nishiyama, T., M.M. Sykora, P.J. Huis in 't Veld, K. Mechtler, and J.-M. Peters. 2013. Aurora B and Cdk1 mediate Wapl activation and release of acetylated cohesin from chromosomes by phosphorylating Sororin. *Proc. Natl. Acad. Sci. U.S.A.* 110:13404–13409. doi:10.1073/pnas.1305020110.
- Nishiyama, T., R. Ladurner, J. Schmitz, E. Kreidl, A. Schleiffer, V. Bhaskara, M. Bando, K. Shirahige, A.A. Hyman, K. Mechtler, and J.-M. Peters. 2010. Sororin mediates sister chromatid cohesion by antagonizing Wapl. *Cell.* 143:737–749. doi:10.1016/j.cell.2010.10.031.

-
- Nyati, S., K. Schinske-Sebolt, S. Pitchiaya, K. Chekhovskiy, A. Chator, N. Chaudhry, J. Dosch, M.E. Van Dort, S. Varambally, C. Kumar-Sinha, M.K. Nyati, D. Ray, N.G. Walter, H. Yu, B.D. Ross, and A. Rehemtulla. 2015. The kinase activity of the Ser/Thr kinase BUB1 promotes TGF- β signaling. *Sci Signal*. 8:ra1–ra1. doi:10.1126/scisignal.2005379.
- Olsen, J.V., B. Macek, O. Lange, A. Makarov, S. Horning, and M. Mann. 2007. Higher-energy C-trap dissociation for peptide modification analysis. *Nature Methods*. 4:709–712. doi:10.1038/nmeth1060.
- Ong, S.-E., L.J. Foster, and M. Mann. 2003. Mass spectrometric-based approaches in quantitative proteomics. *Methods*. 29:124–130.
- Overlack, K., I. Primorac, M. Vleugel, V. Krenn, S. Maffini, I. Hoffmann, G.J.P.L. Kops, and A. Musacchio. 2015. A molecular basis for the differential roles of Bub1 and BubR1 in the spindle assembly checkpoint. *eLife*. 4:e05269. doi:10.7554/eLife.05269.
- Ozlu, N., B. Akten, W. Timm, N. Haseley, H. Steen, and J.A.J. Steen. 2010. Phosphoproteomics. *Wiley Interdiscip Rev Syst Biol Med*. 2:255–276. doi:10.1002/wsbm.41.
- Palumbo, A.M., J.J. Tepe, and G.E. Reid. 2008. Mechanistic insights into the multistage gas-phase fragmentation behavior of phosphoserine- and phosphothreonine-containing peptides. *J. Proteome Res*. 7:771–779. doi:10.1021/pr0705136.
- Paweletz, N. 2001. Walther Flemming: pioneer of mitosis research. 2. Nature Publishing Group. 4 pp.
- Perdiguero, E., and A.R. Nebreda. 2004. Regulation of Cdc25C activity during the meiotic G2/M transition. *Cell Cycle*. 3:733–737.
- Perera, D., and S.S. Taylor. 2010. Sgo1 establishes the centromeric cohesion protection mechanism in G2 before subsequent Bub1-dependent recruitment in mitosis. *Journal of Cell Science*. 123:653–659. doi:10.1242/jcs.059501.
- Perera, D., V. Tilston, J.A. Hopwood, M. Barchi, R.P. Boot-Handford, and S.S. Taylor. 2007. Bub1 maintains centromeric cohesion by activation of the spindle checkpoint. *Developmental Cell*. 13:566–579. doi:10.1016/j.devcel.2007.08.008.
- Peters, J.-M., and T. Nishiyama. 2012. Sister chromatid cohesion. *Cold Spring Harb Perspect Biol*. 4:a011130–a011130. doi:10.1101/cshperspect.a011130.
- Peters, J.M. 1999. Subunits and substrates of the anaphase-promoting complex. *Experimental Cell Research*. 248:339–349. doi:10.1006/excr.1999.4443.
-

- Peterson, A.C., J.D. Russell, D.J. Bailey, M.S. Westphall, and J.J. Coon. 2012. Parallel reaction monitoring for high resolution and high mass accuracy quantitative, targeted proteomics. *Mol. Cell Proteomics*. 11:1475–1488. doi:10.1074/mcp.O112.020131.
- Petronczki, M., P. Lenart, and J.-M. Peters. 2008. Polo on the Rise—from Mitotic Entry to Cytokinesis with Plk1. *Developmental Cell*. 14:646–659. doi:10.1016/j.devcel.2008.04.014.
- Picotti, P., B. Bodenmiller, L.N. Mueller, B. Domon, and R. Aebersold. 2009. Full Dynamic Range Proteome Analysis of *S. cerevisiae* by Targeted Proteomics. *Cell*. 138:795–806. doi:10.1016/j.cell.2009.05.051.
- Pines, J. 2006. Mitosis: a matter of getting rid of the right protein at the right time. *Trends in Cell Biology*. 16:55–63. doi:10.1016/j.tcb.2005.11.006.
- Pines, J. 2011. Cubism and the cell cycle: the many faces of the APC/C. *Nat. Rev. Mol. Cell Biol.* 12:427–438. doi:10.1038/nrm3132.
- Pines, J., and C.L. Rieder. 2001. Re-staging mitosis: a contemporary view of mitotic progression. *Nature Cell Biology*. 3:E3–6. doi:10.1038/35050676.
- Pinsky, B.A., and S. Biggins. 2005. The spindle checkpoint: tension versus attachment. *Trends in Cell Biology*. 15:486–493. doi:10.1016/j.tcb.2005.07.005.
- Primorac, I., J.R. Weir, E. Chiroli, F. Gross, I. Hoffmann, S. van Gerwen, A. Ciliberto, and A. Musacchio. 2013. Bub3 reads phosphorylated MELT repeats to promote spindle assembly checkpoint signaling. *eLife*. 2:e01030. doi:10.7554/eLife.01030.
- Putkey, F.R., T. Cramer, M.K. Morpew, A.D. Silk, R.S. Johnson, J.R. McIntosh, and D.W. Cleveland. 2002. Unstable kinetochore-microtubule capture and chromosomal instability following deletion of CENP-E. *Developmental Cell*. 3:351–365.
- Qi, W., and H. Yu. 2007. KEN-box-dependent degradation of the Bub1 spindle checkpoint kinase by the anaphase-promoting complex/cyclosome. *J. Biol. Chem.* 282:3672–3679. doi:10.1074/jbc.M609376200.
- Ricke, R.M., and J.M. van Deursen. 2011. Aurora B hyperactivation by Bub1 overexpression promotes chromosome missegregation. *Cell Cycle*. 10:3645–3651. doi:10.4161/cc.10.21.18156.
- Ricke, R.M., K.B. Jeganathan, L. Malureanu, A.M. Harrison, and J.M. van Deursen. 2012. Bub1 kinase activity drives error correction and mitotic checkpoint control but not tumor suppression. *The Journal of Cell Biology*. 199:931–949.

doi:10.1083/jcb.201205115.

- Riedel, C.G., V.L. Katis, Y. Katou, S. Mori, T. Itoh, W. Helmhart, M. Galova, M. Petronczki, J. Gregan, B. Cetin, I. Mudrak, E. Ogris, K. Mechtler, L. Pelletier, F. Buchholz, K. Shirahige, and K. Nasmyth. 2006. Protein phosphatase 2A protects centromeric sister chromatid cohesion during meiosis I. *Nature*. 441:53–61. doi:10.1038/nature04664.
- Rieder, C.L., R.W. Cole, A. Khodjakov, and G. Sluder. 1995. The checkpoint delaying anaphase in response to chromosome monoorientation is mediated by an inhibitory signal produced by unattached kinetochores. *The Journal of Cell Biology*. 130:941–948.
- Rischitor, P.E., K.M. May, and K.G. Hardwick. 2007. Bub1 is a fission yeast kinetochore scaffold protein, and is sufficient to recruit other spindle checkpoint proteins to ectopic sites on chromosomes. *PLoS ONE*. 2:e1342. doi:10.1371/journal.pone.0001342.
- Roberts, B.T., K.A. Farr, and M.A. Hoyt. 1994. The *Saccharomyces cerevisiae* checkpoint gene BUB1 encodes a novel protein kinase. *Molecular and Cellular Biology*. 14:8282–8291.
- Rodriguez-Bravo, V., J. Maciejowski, J. Corona, H.K. Buch, P. Collin, M.T. Kanemaki, J.V. Shah, and P.V. Jallepalli. 2014. Nuclear pores protect genome integrity by assembling a premitotic and Mad1-dependent anaphase inhibitor. *Cell*. 156:1017–1031. doi:10.1016/j.cell.2014.01.010.
- Rogers, L.D., and L.J. Foster. 2009. Phosphoproteomics—finally fulfilling the promise? *Molecular BioSystems*. 5:1122–1129. doi:10.1039/B905580K.
- Sacristan, C., and G.J.P.L. Kops. 2015. Joined at the hip: kinetochores, microtubules, and spindle assembly checkpoint signaling. *Trends in Cell Biology*. 25:21–28. doi:10.1016/j.tcb.2014.08.006.
- Salmela, A.-L., and M.J. Kallio. 2013. Mitosis as an anti-cancer drug target. *Chromosoma*. 122:431–449. doi:10.1007/s00412-013-0419-8.
- Sandhu, C., J.A. Hewel, G. Badis, S. Talukder, J. Liu, T.R. Hughes, and A. Emili. 2008. Evaluation of data-dependent versus targeted shotgun proteomic approaches for monitoring transcription factor expression in breast cancer. *J. Proteome Res.* 7:1529–1541. doi:10.1021/pr700836q.
- Santaguida, S., A. Tighe, A.M. D'Alise, S.S. Taylor, and A. Musacchio. 2010. Dissecting the role of MPS1 in chromosome biorientation and the spindle checkpoint through the small molecule inhibitor reversine. *The Journal of Cell Biology*. 190:73–87. doi:10.1083/jcb.201001036.

- Santaguida, S., and A. Musacchio. 2009. The life and miracles of kinetochores. *The EMBO Journal*. 28:2511–2531. doi:10.1038/emboj.2009.173.
- Santaguida, S., C. Vernieri, F. Villa, A. Ciliberto, and A. Musacchio. 2011. Evidence that Aurora B is implicated in spindle checkpoint signalling independently of error correction. *The EMBO Journal*. 30:1508–1519. doi:10.1038/emboj.2011.70.
- Santamaria, A., B. Wang, S. Elowe, R. Malik, F. Zhang, M. Bauer, A. Schmidt, H.H.W. Silljé, R. Körner, and E.A. Nigg. 2011. The Plk1-dependent phosphoproteome of the early mitotic spindle. *Mol. Cell Proteomics*. 10:M110.004457–M110.004457. doi:10.1074/mcp.M110.004457.
- Santamaria, A., R. Neef, U. Eberspächer, K. Eis, M. Husemann, D. Mumberg, S. Prechtel, V. Schulze, G. Siemeister, L. Wortmann, F.A. Barr, and E.A. Nigg. 2007. Use of the novel Plk1 inhibitor ZK-thiazolidinone to elucidate functions of Plk1 in early and late stages of mitosis. *Mol. Biol. Cell*. 18:4024–4036. doi:10.1091/mbc.E07-05-0517.
- Saurin, A.T., M.S. van der Waal, R.H. Medema, S.M.A. Lens, and G.J.P.L. Kops. 2011. Aurora B potentiates Mps1 activation to ensure rapid checkpoint establishment at the onset of mitosis. *Nat Commun*. 2:316. doi:10.1038/ncomms1319.
- Savitski, M.M., F. Fischer, T. Mathieson, G. Sweetman, M. Lang, and M. Bantscheff. 2010. Targeted data acquisition for improved reproducibility and robustness of proteomic mass spectrometry assays. *J. Am. Soc. Mass Spectrom*. 21:1668–1679. doi:10.1016/j.jasms.2010.01.012.
- Schaar, B.T., G.K. Chan, P. Maddox, E.D. Salmon, and T.J. Yen. 1997. CENP-E function at kinetochores is essential for chromosome alignment. *The Journal of Cell Biology*. 139:1373–1382.
- Schmidt, A., M. Claassen, and R. Aebersold. 2009. Directed mass spectrometry: towards hypothesis-driven proteomics. *Curr Opin Chem Biol*. 13:510–517. doi:10.1016/j.cbpa.2009.08.016.
- Schmidt, A., N. Gehlenborg, B. Bodenmiller, L.N. Mueller, D. Campbell, M. Mueller, R. Aebersold, and B. Domon. 2008. An integrated, directed mass spectrometric approach for in-depth characterization of complex peptide mixtures. *Mol. Cell Proteomics*. 7:2138–2150. doi:10.1074/mcp.M700498-MCP200.
- Schmit, T.L., and N. Ahmad. 2007. Regulation of mitosis via mitotic kinases: new opportunities for cancer management. *Mol. Cancer Ther*. 6:1920–1931. doi:10.1158/1535-7163.MCT-06-0781.
- Schmitz, J., E. Watrin, P. Lenart, K. Mechtler, and J.-M. Peters. 2007. Sororin Is

- Required for Stable Binding of Cohesin to Chromatin and for Sister Chromatid Cohesion in Interphase. *Current Biology*. 17:630–636. doi:10.1016/j.cub.2007.02.029.
- Scholey, J.M., I. Brust-Mascher, and A. Mogilner. 2003. Cell division. *Nature*. 422:746–752. doi:10.1038/nature01599.
- Schubert, O.T., L.C. Gillet, B.C. Collins, P. Navarro, G. Rosenberger, W.E. Wolski, H. Lam, D. Amodei, P. Mallick, B. MacLean, and R. Aebersold. 2015a. Building high-quality assay libraries for targeted analysis of SWATH MS data. *Nat Protoc*. 10:426–441. doi:10.1038/nprot.2015.015.
- Schubert, von, C., and E.A. Nigg. 2013. Polo-like kinases. *Curr. Biol*. 23:R225–7. doi:10.1016/j.cub.2013.01.066.
- Schubert, von, C., F. Cubizolles, J.M. Bracher, T. Sliedrecht, G.J.P.L. Kops, and E.A. Nigg. 2015b. Plk1 and Mps1 Cooperatively Regulate the Spindle Assembly Checkpoint in Human Cells. *Cell Rep*. doi:10.1016/j.celrep.2015.06.007.
- SCIEX. 2012. MS/MS ALL with SWATH Acquisition. <https://www.youtube.com/watch?v=VZAZtAqEbg>.
- Sebastian, B., A. Kakizuka, and T. Hunter. 1993. Cdc25M2 activation of cyclin-dependent kinases by dephosphorylation of threonine-14 and tyrosine-15. *Proc. Natl. Acad. Sci. U.S.A.* 90:3521–3524. doi:10.1073/pnas.90.8.3521.
- Sharp-Baker, H., and R.H. Chen. 2001. Spindle checkpoint protein Bub1 is required for kinetochore localization of Mad1, Mad2, Bub3, and CENP-E, independently of its kinase activity. *The Journal of Cell Biology*. 153:1239–1250.
- Shepperd, L.A., J.C. Meadows, A.M. Sochaj, T.C. Lancaster, J. Zou, G.J. Buttrick, J. Rappsilber, K.G. Hardwick, and J.B.A. Millar. 2012. Phosphodependent recruitment of Bub1 and Bub3 to Spc7/KNL1 by Mph1 kinase maintains the spindle checkpoint. *Curr. Biol*. 22:891–899. doi:10.1016/j.cub.2012.03.051.
- Sherrod, S.D., M.V. Myers, M. Li, J.S. Myers, K.L. Carpenter, B. MacLean, M.J. MacCoss, D.C. Liebler, and A.-J.L. Ham. 2012. Label-free quantitation of protein modifications by pseudo selected reaction monitoring with internal reference peptides. *J. Proteome Res*. 11:3467–3479. doi:10.1021/pr201240a.
- Silljé, H.H.W., S. Nagel, R. Körner, and E.A. Nigg. 2006. HURP is a Ran-importin beta-regulated protein that stabilizes kinetochore microtubules in the vicinity of chromosomes. *Current Biology*. 16:731–742. doi:10.1016/j.cub.2006.02.070.
- Skotheim, J.M., S. Di Talia, E.D. Siggia, and F.R. Cross. 2008. Positive feedback of G1 cyclins ensures coherent cell cycle entry. *Nature*. 454:291–296.

doi:10.1038/nature07118.

- Sliedrecht, T., C. Zhang, K.M. Shokat, and G.J.P.L. Kops. 2010. Chemical genetic inhibition of Mps1 in stable human cell lines reveals novel aspects of Mps1 function in mitosis. *PLoS ONE*. 5:e10251. doi:10.1371/journal.pone.0010251.
- Steen, H., J.A. Jebanathirajah, J. Rush, N. Morrice, and M.W. Kirschner. 2006. Phosphorylation analysis by mass spectrometry: myths, facts, and the consequences for qualitative and quantitative measurements. *Mol. Cell Proteomics*. 5:172–181. doi:10.1074/mcp.M500135-MCP200.
- Stucke, V.M., H.H.W. Silljé, L. Arnaud, and E.A. Nigg. 2002. Human Mps1 kinase is required for the spindle assembly checkpoint but not for centrosome duplication. *The EMBO Journal*. 21:1723–1732. doi:10.1093/emboj/21.7.1723.
- Sudakin, V., G.K. Chan, and T.J. Yen. 2001. Checkpoint inhibition of the APC/C in HeLa cells is mediated by a complex of BUBR1, BUB3, CDC20, and MAD2. *The Journal of Cell Biology*. 154:925–936. doi:10.1083/jcb.200102093.
- Suijkerbuijk, S.J.E., M. Vleugel, A. Teixeira, and G.J.P.L. Kops. 2012a. Integration of kinase and phosphatase activities by BUBR1 ensures formation of stable kinetochore-microtubule attachments. *Developmental Cell*. 23:745–755. doi:10.1016/j.devcel.2012.09.005.
- Suijkerbuijk, S.J.E., T.J.P. van Dam, G.E. Karagöz, E. von Castelmur, N.C. Hubner, A.M.S. Duarte, M. Vleugel, A. Perrakis, S.G.D. Rüdiger, B. Snel, and G.J.P.L. Kops. 2012b. The vertebrate mitotic checkpoint protein BUBR1 is an unusual pseudokinase. *Developmental Cell*. 22:1321–1329. doi:10.1016/j.devcel.2012.03.009.
- Sumara, I., E. Vorlaufer, P.T. Stukenberg, O. Kelm, N. Redemann, E.A. Nigg, and J.-M. Peters. 2002. The dissociation of cohesin from chromosomes in prophase is regulated by Polo-like kinase. *Molecular Cell*. 9:515–525.
- Tang, Z., H. Shu, D. Oncel, S. Chen, and H. Yu. 2004a. Phosphorylation of Cdc20 by Bub1 provides a catalytic mechanism for APC/C inhibition by the spindle checkpoint. *Molecular Cell*. 16:387–397. doi:10.1016/j.molcel.2004.09.031.
- Tang, Z., H. Shu, W. Qi, N.A. Mahmood, M.C. Mumby, and H. Yu. 2006. PP2A is required for centromeric localization of Sgo1 and proper chromosome segregation. *Developmental Cell*. 10:575–585. doi:10.1016/j.devcel.2006.03.010.
- Tang, Z., Y. Sun, S.E. Harley, H. Zou, and H. Yu. 2004b. Human Bub1 protects centromeric sister-chromatid cohesion through Shugoshin during mitosis. *Proc. Natl. Acad. Sci. U.S.A.* 101:18012–18017. doi:10.1073/pnas.0408600102.

- Tanno, Y., T.S. Kitajima, T. Honda, Y. Ando, K.-I. Ishiguro, and Y. Watanabe. 2010. Phosphorylation of mammalian Sgo2 by Aurora B recruits PP2A and MCAK to centromeres. *Genes & Development*. 24:2169–2179. doi:10.1101/gad.1945310.
- Tannous, B.A., M. Kerami, P.M. Van der Stoop, N. Kwiatkowski, J. Wang, W. Zhou, A.F. Kessler, G. Lewandrowski, L. Hiddingh, N. Sol, T. Lagerweij, L. Wedekind, J.M. Niers, M. Barazas, R.J.A. Nilsson, D. Geerts, P.C. De Witt Hamer, C. Hagemann, W.P. Vandertop, O. Van Tellingen, D.P. Noske, N.S. Gray, and T. Würdinger. 2013. Effects of the selective MPS1 inhibitor MPS1-IN-3 on glioblastoma sensitivity to antimetabolic drugs. *J. Natl. Cancer Inst.* 105:1322–1331. doi:10.1093/jnci/djt168.
- Tanudji, M., J. Shoemaker, L. L'Italien, L. Russell, G. Chin, and X.M. Schebye. 2004. Gene silencing of CENP-E by small interfering RNA in HeLa cells leads to missegregation of chromosomes after a mitotic delay. *Mol. Biol. Cell*. 15:3771–3781. doi:10.1091/mbc.E03-07-0482.
- Tao, Y., C. Leteur, J. Calderaro, F. Girdler, P. Zhang, V. Frascogna, M. Varna, P. Opolon, M. Castedo, J. Bourhis, G. Kroemer, and E. Deutsch. 2009. The aurora B kinase inhibitor AZD1152 sensitizes cancer cells to fractionated irradiation and induces mitotic catastrophe. *Cell Cycle*. 8:3172–3181.
- Tardif, K.D., A. Rogers, J. Cassiano, B.L. Roth, D.M. Cimborra, R. McKinnon, A. Peterson, T.B. Douce, R. Robinson, I. Dorweiler, T. Davis, M.A. Hess, K. Ostanin, D.I. Papac, V. Baichwal, I. McAlexander, J.A. Willardsen, M. Saunders, H. Christophe, D.V. Kumar, D.A. Wettstein, R.O. Carlson, and B.L. Williams. 2011. Characterization of the cellular and antitumor effects of MPI-0479605, a small-molecule inhibitor of the mitotic kinase Mps1. *Mol. Cancer Ther.* 10:2267–2275. doi:10.1158/1535-7163.MCT-11-0453.
- Taylor, S., and J.-M. Peters. 2008. Polo and Aurora kinases—lessons derived from chemical biology. *Curr. Opin. Cell Biol.* 20:77–84. doi:10.1016/j.ceb.2007.11.008.
- Taylor, S.S., and F. McKeon. 1997. Kinetochore localization of murine Bub1 is required for normal mitotic timing and checkpoint response to spindle damage. *Cell*. 89:727–735.
- Taylor, S.S., E. Ha, and F. McKeon. 1998. The human homologue of Bub3 is required for kinetochore localization of Bub1 and a Mad3/Bub1-related protein kinase. *The Journal of Cell Biology*. 142:1–11.
- Thingholm, T.E., and M.R. Larsen. 2009. The use of titanium dioxide micro-columns to selectively isolate phosphopeptides from proteolytic digests. *Methods Mol. Biol.* 527:57–66– xi. doi:10.1007/978-1-60327-834-8_5.

-
- Tighe, A., O. Staples, and S. Taylor. 2008. Mps1 kinase activity restrains anaphase during an unperturbed mitosis and targets Mad2 to kinetochores. *The Journal of Cell Biology*. 181:893–901. doi:10.1083/jcb.200712028.
- Trost, B., and A. Kusalik. 2011. Computational prediction of eukaryotic phosphorylation sites. *Bioinformatics*. 27:2927–2935. doi:10.1093/bioinformatics/btr525.
- Tsukahara, T., Y. Tanno, and Y. Watanabe. 2010. Phosphorylation of the CPC by Cdk1 promotes chromosome bi-orientation. *Nature*. 467:719–723. doi:10.1038/nature09390.
- Ulintz, P.J., A.K. Yocum, B. Bodenmiller, R. Aebersold, P.C. Andrews, and A.I. Nesvizhskii. 2009. Comparison of MS(2)-only, MSA, and MS(2)/MS(3) methodologies for phosphopeptide identification. *J. Proteome Res.* 8:887–899. doi:10.1021/pr800535h.
- van der Geer, P., and T. Hunter. 1994. Phosphopeptide mapping and phosphoamino acid analysis by electrophoresis and chromatography on thin-layer cellulose plates. *Electrophoresis*. 15:544–554.
- van der Waal, M.S., A.T. Saurin, M.J.M. Vromans, M. Vleugel, C. Wurzenberger, D.W. Gerlich, R.H. Medema, G.J.P.L. Kops, and S.M.A. Lens. 2012. Mps1 promotes rapid centromere accumulation of Aurora B. *Nature Publishing Group*. 13:847–854. doi:10.1038/embor.2012.93.
- Vassilev, L.T., C. Tovar, S. Chen, D. Knezevic, X. Zhao, H. Sun, D.C. Heimbrook, and L. Chen. 2006. Selective small-molecule inhibitor reveals critical mitotic functions of human CDK1. *Proc. Natl. Acad. Sci. U.S.A.* 103:10660–10665. doi:10.1073/pnas.0600447103.
- Vermeulen, K., D.R. Van Bockstaele, and Z.N. Berneman. 2003. The cell cycle: a review of regulation, deregulation and therapeutic targets in cancer. *Cell Prolif.* 36:131–149.
- Villén, J., S.A. Beausoleil, and S.P. Gygi. 2008. Evaluation of the utility of neutral-loss-dependent MS3 strategies in large-scale phosphorylation analysis. *Proteomics*. 8:4444–4452. doi:10.1002/pmic.200800283.
- Vitale, I., L. Galluzzi, M. Castedo, and G. Kroemer. 2011. Mitotic catastrophe: a mechanism for avoiding genomic instability. *Nat. Rev. Mol. Cell Biol.* 12:385–392. doi:10.1038/nrm3115.
- Vleugel, M., E. Hoogendoorn, B. Snel, and G.J.P.L. Kops. 2012. Evolution and function of the mitotic checkpoint. *Developmental Cell*. 23:239–250. doi:10.1016/j.devcel.2012.06.013.
-

- Vleugel, M., E. Tromer, M. Omerzu, V. Groenewold, W. Nijenhuis, B. Snel, and G.J.P.L. Kops. 2013. Arrayed BUB recruitment modules in the kinetochore scaffold KNL1 promote accurate chromosome segregation. *The Journal of Cell Biology*. 203:943–955. doi:10.1083/jcb.201307016.
- Waizenegger, I.C., S. Hauf, A. Meinke, and J.M. Peters. 2000. Two distinct pathways remove mammalian cohesin from chromosome arms in prophase and from centromeres in anaphase. *Cell*. 103:399–410.
- Walczak, C.E., S. Cai, and A. Khodjakov. 2010. Mechanisms of chromosome behaviour during mitosis. *Nat. Rev. Mol. Cell Biol.* 11:91–102. doi:10.1038/nrm2832.
- Wang, F., J. Dai, J.R. Daum, E. Niedzialkowska, B. Banerjee, P.T. Stukenberg, G.J. Gorbsky, and J.M.G. Higgins. 2010. Histone H3 Thr-3 phosphorylation by Haspin positions Aurora B at centromeres in mitosis. *Science*. 330:231–235. doi:10.1126/science.1189435.
- Wang, F., N.P. Ulyanova, M.S. van der Waal, D. Patnaik, S.M.A. Lens, and J.M.G. Higgins. 2011. A positive feedback loop involving Haspin and Aurora B promotes CPC accumulation at centromeres in mitosis. *Curr. Biol.* 21:1061–1069. doi:10.1016/j.cub.2011.05.016.
- Warren, C.D., D.M. Brady, R.C. Johnston, J.S. Hanna, K.G. Hardwick, and F.A. Spencer. 2002. Distinct chromosome segregation roles for spindle checkpoint proteins. *Mol. Biol. Cell*. 13:3029–3041. doi:10.1091/mbc.E02-04-0203.
- Weaver, B.A.A., and D.W. Cleveland. 2006. Does aneuploidy cause cancer? *Curr. Opin. Cell Biol.* 18:658–667. doi:10.1016/j.ceb.2006.10.002.
- Westhorpe, F.G., A. Tighe, P. Lara-Gonzalez, and S.S. Taylor. 2011. p31comet-mediated extraction of Mad2 from the MCC promotes efficient mitotic exit. *Journal of Cell Science*. 124:3905–3916. doi:10.1242/jcs.093286.
- Windecker, H., M. Langegger, S. Heinrich, and S. Hauf. 2009. Bub1 and Bub3 promote the conversion from monopolar to bipolar chromosome attachment independently of shugoshin. *Nature Publishing Group*. 10:1022–1028. doi:10.1038/embor.2009.183.
- Wollman, R., E.N. Cytrynbaum, J.T. Jones, T. Meyer, J.M. Scholey, and A. Mogilner. 2005. Efficient chromosome capture requires a bias in the “search-and-capture” process during mitotic-spindle assembly. *Current Biology*. 15:828–832. doi:10.1016/j.cub.2005.03.019.
- Wong, J.W.H., and G. Cagney. 2010. An overview of label-free quantitation methods in proteomics by mass spectrometry. *Methods Mol. Biol.* 604:273–283.

doi:10.1007/978-1-60761-444-9_18.

- Wurzenberger, C., and D.W. Gerlich. 2011. Phosphatases: providing safe passage through mitotic exit. *Nat. Rev. Mol. Cell Biol.* 12:469–482. doi:10.1038/nrm3149.
- Xu, P., E.A. Raetz, M. Kitagawa, D.M. Virshup, and S.H. Lee. 2013. BUBR1 recruits PP2A via the B56 family of targeting subunits to promote chromosome congression. *Biol Open.* 2:479–486. doi:10.1242/bio.20134051.
- Yamagishi, Y., C.-H. Yang, Y. Tanno, and Y. Watanabe. 2012. MPS1/Mph1 phosphorylates the kinetochore protein KNL1/Spc7 to recruit SAC components. *Nature Cell Biology.* 14:746–752. doi:10.1038/ncb2515.
- Yamagishi, Y., T. Honda, Y. Tanno, and Y. Watanabe. 2010. Two histone marks establish the inner centromere and chromosome bi-orientation. *Science.* 330:239–243. doi:10.1126/science.1194498.
- Yamaguchi, S., A. Decottignies, and P. Nurse. 2003. Function of Cdc2p-dependent Bub1p phosphorylation and Bub1p kinase activity in the mitotic and meiotic spindle checkpoint. *The EMBO Journal.* 22:1075–1087. doi:10.1093/emboj/cdg100.
- Yang, C., H. Wang, Y. Xu, K.L. Brinkman, H. Ishiyama, S.T.C. Wong, and B. Xu. 2012. The kinetochore protein Bub1 participates in the DNA damage response. *DNA Repair (Amst.).* 11:185–191. doi:10.1016/j.dnarep.2011.10.018.
- Yang, Z., A.E. Kenny, D.A. Brito, and C.L. Rieder. 2009. Cells satisfy the mitotic checkpoint in Taxol, and do so faster in concentrations that stabilize syntelic attachments. *The Journal of Cell Biology.* 186:675–684. doi:10.1083/jcb.200906150.
- Yang, Z., U.S. Tulu, P. Wadsworth, and C.L. Rieder. 2007. Kinetochore dynein is required for chromosome motion and congression independent of the spindle checkpoint. *Current Biology.* 17:973–980. doi:10.1016/j.cub.2007.04.056.
- Yue, Z., A. Carvalho, Z. Xu, X. Yuan, S. Cardinale, S. Ribeiro, F. Lai, H. Ogawa, E. Gudmundsdottir, R. Gassmann, C.G. Morrison, S. Ruchaud, and W.C. Earnshaw. 2008. Deconstructing Survivin: comprehensive genetic analysis of Survivin function by conditional knockout in a vertebrate cell line. *The Journal of Cell Biology.* 183:279–296. doi:10.1083/jcb.200806118.
- Zeitlin, S.G., R.D. Shelby, and K.F. Sullivan. 2001. CENP-A is phosphorylated by Aurora B kinase and plays an unexpected role in completion of cytokinesis. *The Journal of Cell Biology.* 155:1147–1157. doi:10.1083/jcb.200108125.
- Zhang, G., T. Lischetti, and J. Nilsson. 2014. A minimal number of MELT repeats supports all the functions of KNL1 in chromosome segregation. *Journal of Cell*

Science. 127:871–884. doi:10.1242/jcs.139725.

Zhang, J., X. Shi, Y. Li, B.-J. Kim, J. Jia, Z. Huang, T. Yang, X. Fu, S.Y. Jung, Y. Wang, P. Zhang, S.-T. Kim, X. Pan, and J. Qin. 2008. Acetylation of Smc3 by Eco1 is required for S phase sister chromatid cohesion in both human and yeast. *Molecular Cell*. 31:143–151. doi:10.1016/j.molcel.2008.06.006.

Zhang, X., W. Lan, S.C. Ems-McClung, P.T. Stukenberg, and C.E. Walczak. 2007. Aurora B phosphorylates multiple sites on mitotic centromere-associated kinesin to spatially and temporally regulate its function. *Mol. Biol. Cell*. 18:3264–3276. doi:10.1091/mbc.E07-01-0086.

Zi, J., S. Zhang, R. Zhou, B. Zhou, S. Xu, G. Hou, F. Tan, B. Wen, Q. Wang, L. Lin, and S. Liu. 2014. Expansion of the ion library for mining SWATH-MS data through fractionation proteomics. *Anal. Chem.* 86:7242–7246. doi:10.1021/ac501828a.

Curriculum Vitae

Anna Pauline Baron

Email anna.baron@gmx.ch
Date of birth March 6th, 1987
Nationality German

Professional Experience

- 03/2012 – 12/2015 Researcher in the field of cell biology
Biozentrum, University of Basel, Switzerland, Laboratory of Prof. Dr. Erich A. Nigg
- Field of research: molecular biology and cell biology
 - understanding of cell proliferation regulatory mechanisms, essential processes deregulated in cancer, with a particular focus on chromosome segregation
- 2010-2011 Research Fellow (Postgraduate)
Biozentrum, University of Basel, Switzerland, Laboratory of Prof. Dr. Erich A. Nigg
- Field of research: molecular biology and cell biology
 - introduction into the analysis of the cell proteome using mass spectrometry

Education

- 05/2012 – 12/2015 Doctor of Philosophy in Cell Biology
Fellowships for Excellence International PhD Program
Biozentrum, University of Basel, Switzerland
Thesis Title: On the Regulation of Chromosome Segregation in Human Cells – Implications of Bub1 Kinase Inhibition During Cell Division
- 09/2010 – 11/2011 Master of Science in Cell Biology
Biozentrum, University of Basel, Switzerland
Thesis Title: Elucidating the role of Mad1 Phosphorylation in the context of the spindle assembly checkpoint
- 10/2006 – 07/2009 Bachelor of Science in Biology, Major in Molecular Biology
University of Basel, Switzerland
- 09/2003-07/2006 German University Entrance Qualification, Abitur
Ernährungswissenschaftliches Gymnasium, Lörrach, Germany
Focus on biochemistry, physiology and molecular biology

Extracurricular Activities

05/2012 – 07/2015	PhD Student Representative board member Secretary of PhD Student Representative board Organization of PhD Talk series
02/2015	Project-Management – An introduction 2-day course by SPOL AG
05/2015	Project Management 3-day course organized by RUPPLI + PARTNER AG and Advanced Studies of the University of Basel
06/2013 – 06/2014	Fellowships for Excellence Symposium 2014 Basel, Switzerland Organizing Committee Member
2012	Swiss Proteomics Society – PhD Student Symposium 2012 Basel, Switzerland Organizing Committee Member

Award & Scholarship

2012 – 2015	Selected Fellow of the <i>Fellowships for Excellence</i> International PhD Program - providing support in terms of travel grants, access to scientific and soft skill workshops and salary
-------------	--

Publications

2015	<u>Baron AP.</u> , von Schubert C., Cubizolles F., Siemeister G., Hitchcock M., Mengel A., Schröder J., Fernández-Montalvan A., von Nussbaum F., Mumberg D., Nigg EA. <i>Probing the catalytic functions of Bub1 kinase using the small molecule inhibitors BAY-320 and BAY-524.</i> – Under revision in eLife
2015	Bauer M.*, Ahrné E.*, <u>Baron A.P.*</u> , Glatter T., Fava L.L., Santamaria, S., Nigg E.A., Schmidt A. <i>Assessment of current mass spectrometric workflows for the quantification of low abundant proteins and phosphorylation sites.</i> – Data in Brief *These authors contributed equally to this work
2014	Bauer M.*, Ahrné E.*, <u>Baron A.P.*</u> , Glatter T., Fava L.L., Santamaria, S., Nigg E.A., Schmidt A. <i>Evaluation of data-dependent and data-independent mass spectrometric workflows for sensitive quantification of proteins and phosphorylation sites.</i> – Journal of Proteome Research *These authors contributed equally to this work

Acknowledgements

This work would not have been possible without the guidance, help and support of several individuals, who in one way or another contributed in the preparation and completion of this study.

I would like to thank Prof. Erich Nigg for giving me the opportunity to be a member of his laboratory and to work in such a stimulating research context. I also thank him for his guidance, input, patience and the freedom he gave me in conducting scientific research.

I am grateful to Prof. Christoph Handschin and Prof. Michel Steinmetz for taking part in my PhD Advisory Committee and for their input.

Very special thanks go to Dr. Conrad von Schubert. You have been a great supervisor and a constant source of help. Thank you for all your help while preparing the Bub1 manuscript. To all the past and present members of the lab, especially the 'mitosis lab': Ana Amaro-Meyer, Cristina Viganó, Patrick Redli, Conrad von Schubert and Anna Santamaria. Thanks for sharing all the challenges that have been faced while working with the 'spindle assembly checkpoint' and all the discussions we have had. Also to the other members of the lab: Elena Nigg, Dominik Schnerch, Christian Arquint, Anna-Maria Gabryjonczyk, Fabien Cubizolles, Olivier Ganier, Agathe Morand, Nadine Iberl, Lukas Cajanek, Manuel Bauer and Katharina Sonnen. It was a pleasure to work with all of you.

Thanks to all the members of the Proteomics Core Facility, especially Alexander Schmidt. Thanks for all the data analysis and for your patient explanations. It was much appreciated.

Moreover, I am grateful to the *Fellowships for Excellence* program and the *Werner von Siemens Foundation* for funding and for providing so many opportunities to network.

I would also thank all people at BAYER Pharma AG that were involved in the -Bub1 inhibitor project-, especially Dr. Gerhard Siemeister for a successful

collaboration.

My dearest gratitude goes to my family and friends. I would like to thank my parents, my sister Agi, Timon, Ilaria, Stefan, Loïc, Anjana, Anna, Daniele, Vanja, Pavlina and Mario. You have been a constant source of support and encouragement throughout my studies. Thank you for all the fun moments, for sharing the 'ups and downs' of a PhD life and for your confidence in me! You are great!

